Leveraging RNA-sequencing data to obtain insights about mRNA splicing: from daily rhythms to secretory adaptations and cryptic splice sites

Inaugural-Dissertation

to obtain the academic degree

Doctor rerum naturalium (Dr. rer. nat.)

submitted to the Department of Biology, Chemistry and Pharmacy

of Freie Universität Berlin

by

Alexander Neumann

2019

Declaration

This work was carried out in the period of July 2015 to June 2019 under the supervision of Prof. Dr. Florian Heyd at the Institute of Chemistry and Biochemistry, Freie Universität Berlin, Germany.

First reviewer:

Prof. Dr. Florian Heyd
Institute for Chemistry and Biochemistry
Laboratory of RNA Biochemistry
Freie Universität Berlin
Takustraße 6
14195 Berlin, Germany

Second reviewer:

Prof. Sutapa Chakrabarti, PhD
Institute for Chemistry and Biochemistry
Laboratory of mRNA metabolism
Freie Universität Berlin
Takustraße 6
14195 Berlin, Germany

Date of defense: 06.12.2019

Selbstständigkeitserklärung

Gem. § 7 Abs. 4 der Promotionsordnung basierend auf den Mitteilungen im Amtsblatt der Freien Universität Berlin Nr. 52/2007 vom 04.09.2007 und Nr. 04/2008 vom 07.02.2008 und Nr. 02/2012 vom 18.02. 2012.

Hierdurch versichere ich, dass ich die vorliegende Dissertation selbstständig und ohne unerlaubte Hilfe angefertigt habe.

Hierdurch versichere ich, dass meine Dissertation nicht auf meiner Masterarbeit aufbaut bzw. nicht daraus erwachsen ist.

Hierdurch versichere ich, dass ich meine Dissertation im Einvernehmen mit meinem Betreuer Prof. Dr. Florian Heyd in Teilen veröffentlicht habe. Die Publikationen sind Bestandteil der kumulativen Dissertation.

“Gagagagaga - Baum - Ball - Rattarattarattaratta”

Leonie Neumann

Acknowledgements

First of all I want to thank Florian Heyd. Thank you for giving me the opportunity of conducting my thesis in your lab. These past years were extremely productive with many highs and only few lows. You gave me the freedom to grow as a scientist and the impetus needed to succeed.

Secondly, my thanks goes to Sutapa Chakrabarti, not only for acting as second reviewer but also for our insightful and encouraging talks when we met while preparing tea.

I acknowledge Bernd Timmermann for conducting RNA sequencing, Annette Schürmann for providing RNA samples of human adipocytes and the DFG and CRC958 for funding.

I thank all former and current members of the Heyd group. We had a fantastic working environment that consisted of hard work, but did not neglect having a beer afterwards. I cherish the barbecues, playing football, chess or table tennis. I will particularly miss discussing science with Marco, getting scolded by our lab mother Olga, getting supplied with Berliner Luft by Magdalena and the conspiratorial winter meetings with Tom.

My appreciation also goes to Karin, Antje, Simone and Carola for all their administrative help.

Lastly, my family always gave enormous support. My deepest gratitude goes to my parents, Jürgen, Lisa, Elisabeth, Ludger, Johannes and finally Theresa. Theresa, you are the second best thing that happened to me. The best thing was a present you gave me last year. It is currently making us stay up at nights and read the same 6-page, 8-sentence book over and over.

Abstract

Pre-mRNA splicing is a highly regulated process that generates the mature mRNA which can then be translated into a protein. Alternative splicing (AS) allows creation of multiple mature mRNA isoforms from the same pre-mRNA, which dramatically increases the proteomic diversity and fine-tunes numerous cellular processes. With the advent of Next-Generation Sequencing (NGS) and its ever-falling costs in the last two decades, high-throughput quantification of all transcripts of a biological sample became first viable and nowadays routine.

The studies presented in this dissertation combine biochemical and bioinformatical methods to elucidate how AS is regulated by exogenous and endogenous factors. They demonstrate how the nearly 30 petabytes of publicly available NGS data can be leveraged to identify global patterns, to perform highly integrative analyses and to deepen our understanding of disease-causing mutations.

We identified AS to be controlled by body temperature in mammals, first for a single target and then globally for numerous examples. Since body temperature of mammals varies depending on their circadian rhythm, these isoforms are generated in a circadian-like fashion. In addition, we found Cdc-like kinase and temperature-dependent SR protein phosphorylation to be the driving force behind this mechanism. We then discovered that the nonsense-mediated decay pathway is often triggered by temperature-dependent isoforms. This leads to cycling expression of the affected genes, a phenomenon that was previously described but poorly understood.

Furthermore, we discovered dramatically altered early secretory pathway capacities depending on Sec16a AS. We followed this up with a thorough bioinformatical analysis to identify further isoforms that influence transport processes. Indeed, we found hundreds of AS events that modulate the whole secretory pathway. An effect of these targets on membrane trafficking was validated *in vivo*. We demonstrated that these adaptations of the secretory pathway are highly tissue-specific and often induced in dynamic differentiation and activation processes.

Finally, we interrogated two disease associated mutations in the (RNA binding) splicing factor U2AF35. Although these mutations have been annotated to be missense mutations and only change one amino acid, we determined that one of them leads to the creation of a cryptic splice site and therefore a four amino acid deletion. We investigated these mutant proteins in detail and could describe unique RNA binding characteristics. Lastly, we confirmed usage of the cryptic splice site and an effect of the resulting protein in patients carrying this specific mutation.

All these findings heavily relied on the use of RNA-sequencing data analysis. Such studies illustrate the power of using NGS datasets and integrating them into biochemical research. Using complementary and interdisciplinary approaches like the ones presented here accelerates research, saves time and money and allows to gain novel insights unimaginable a decade ago.

Zusammenfassung

Prä-mRNA Spleißen ist ein stark regulierter Prozess, der die reife mRNA produziert welche dann zu einem Protein translatiert werden kann. Alternatives Spleißen (AS) ermöglicht die Erstellung von mehreren mRNA Isoformen aus der gleichen prä-mRNA und erhöht so die proteomische Vielfalt und optimiert viele zelluläre Prozesse. Mit der Etablierung von *Next-Generation Sequencing* (NGS) und den ständig sinkenden Kosten wurde die Hochdurchsatzquantifizierung von allen Transkripten einer biologischen Probe zunächst möglich und heutzutage Routine.

Die in dieser Dissertation vorgestellten Studien verbinden biochemische und bioinformatische Methoden, um die Regulation von AS durch exogene und endogene Faktoren zu untersuchen. Sie zeigen, wie die fast 30 Petabyte öffentlich verfügbarer NGS Daten genutzt werden können, um globale Muster zu identifizieren, hochgradig integrative Analysen durchzuführen und unser Verständnis von krankheitsverursachenden Mutationen zu vertiefen.

Wir haben Körpertemperatur-abhängiges AS in Säugetieren für zahlreiche Beispiele gezeigt. Da die Körpertemperatur von Säugetieren abhängig von ihrem zirkadianen Rhythmus variiert, werden diese Isoformen tageszeitabhängig generiert. Wir haben außerdem *Cdc-like* Kinasen und temperaturabhängige SR Protein Phosphorylierung als die treibende Kraft hinter diesem Mechanismus identifiziert. Danach fanden wir heraus, dass durch temperaturabhängiges Spleißen oft *nonsense-mediated decay* Isoformen gebildet werden. Dies führt zu zyklischer Genexpression, ein Phänomen, welches vorher beschrieben aber unzureichend verstanden wurde.

Des Weiteren haben wir dramatisch veränderte Kapazitäten des frühen sekretorischen Weges in Abhängigkeit von Sec16a AS entdeckt. Darauf aufbauend haben wir eine gründliche bioinformatische Analyse durchgeführt, um weitere Isoformen zu finden welche Transportprozesse beeinflussen. Wir haben hunderte Spleißereignisse gefunden, die den ganzen sekretorischen Weg modulieren und ein Effekt dieser Isoformen auf den Membrantransport wurde *in vivo* validiert. Schließlich zeigten wir, dass diese Adaptionen des sekretorischen Weges stark gewebsspezifisch sind und oft durch dynamische Differenzierungs- und Aktivierungsprozesse induziert werden.

Zuletzt haben wir zwei krankheitsassoziierte Mutationen in dem (RNA bindenden) Spleißfaktor U2AF35 untersucht. Obwohl diese als Missense-Mutationen, welche nur eine Aminosäure verändern, annotiert wurden haben wir gezeigt, dass eine von ihnen zur Bildung einer kryptischen Spleißstelle und damit zu einer Deletion von vier Aminosäuren führt. Wir haben diese mutierten Proteine im Detail untersucht und konnten einzigartige RNA Bindecharakteristika beschreiben. Abschließend haben wir die Verwendung der kryptischen Spleißstelle und einen Effekt des daraus resultierenden Proteins in Patienten mit der zugehörigen Mutation bestätigt.

All diese Ergebnisse basieren stark auf der Analyse von RNA Sequenzierungsdaten. Solche Studien verdeutlichen das Potential der Verwendung von NGS Datensätzen und deren Integration in die eigene Forschung. Die Nutzung von komplementären und interdisziplinären Ansätzen wie sie hier beschrieben sind beschleunigt die Forschung, spart Zeit und Geld und ermöglicht es neue Erkenntnisse zu gewinnen, die so vor einem Jahrzehnt noch unvorstellbar waren.

Table of Contents

List of publications

This cumulative dissertation is based on the following publications. First or co-first author publications are marked with an asterisk. The list is sorted in chronological order.

Wilhelmi I, Kanski R, **Neumann A**, Herdt O, Hoff F, Jacob R, Preußner M, Heyd F. Sec16 alternative splicing dynamically controls COPII transport efficiency. Nat Commun. 2016 Aug 5;7:12347. doi: 10.1038/ncomms12347.

AN performed microscopy assays during revision of the manuscript. He performed αSEC24C stainings of HEK293 wild-type and HEK293 SEC16A ΔE29 cells, imaged the slides and analysed the obtained images.

Preußner M, Goldammer G, **Neumann A**, Haltenhof T, Rautenstrauch P, Müller-McNicoll M, Heyd F. Body Temperature Cycles Control Rhythmic Alternative Splicing in Mammals. Mol Cell. 2017 Aug 3;67(3):433-446.e4. doi: 10.1016/j.molcel.2017.06.006.

AN analysed RNA-sequencing data to identify cold-responsive alternative splicing events and performed meta-analysis on the resulting list of events.

***** Herdt O, **Neumann A**, Timmermann B, Heyd F. The cancer-associated U2AF35 470A>G (Q157R) mutation creates an in-frame alternative 5' splice site that impacts splicing regulation in Q157R patients. RNA. 2017 Dec;23(12):1796-1806. doi: 10.1261/rna.061432.117.

AN analysed RNA-sequencing data to elucidate the rescue capabilities and individual 3’ splice site binding preferences of different U2AF35 mutant proteins (corresponding to proteins potentially produced in patients with the U2AF35 Q157R or Q157P mutations). This included the creation of a custom annotation to incorporate novel splicing targets in the MISO analysis. Furthermore, AN queried public datasets to find RNA-sequencing data of patients with these mutations and quantified mutation-induced mis-splicing, verifying production of a deleterious protein formed in

the Q157R patients. AN compared alternative splicing in these patients and 3' splice site binding preferences, suggesting an effect of the deletion protein variant on splicing regulation.

Goldammer G, **Neumann A**, Strauch M, Müller-McNicoll M, Heyd F, Preußner M. Characterization of cis-acting elements that control oscillating alternative splicing. RNA Biol. 2018;15(8):1081-1092. doi: 10.1080/15476286.2018.1502587.

AN analysed RNA-sequencing data to identify temperature-responsive, circadian-like alternative splicing events and performed meta-analysis on the resulting list of events.

*** Neumann A**, Schindler M, Olofsson D, Wilhelmi I, Schürmann A, Heyd F. Genome-wide identification of alternative splicing events that regulate protein transport across the secretory pathway. JCS. 2019 Apr 25;132(8). pii: jcs230201. doi: 10.1242/jcs.230201.

AN analysed RNA-sequencing data to identify secretion-related alternative splicing events and performed meta-analyses on the resulting set. AN established the RUSH system to quantify transport efficiencies, including a custom tool for semi-automated analysis. AN and MS performed experiments to manipulate alternative splicing (using Morpholinos and CRISPR/Cas9) and validate a transport deficiency for four of the secretion-related alternative splicing events. AN showed a global tissue-, differentiation- and activation-specificity of the events using public RNA-sequencing data of human tissues, T cells and adipocytes. AN and FH conceptualised the work and wrote the manuscript.

* **Neumann A**, Meinke S, Goldammer G, Strauch M, Timmermann B, Heyd F, Preußner M. Rhythmic gene expression is controlled by evolutionary conserved temperature regulated alternative splicing triggering nonsense mediated decay. In preparation.

AN analysed mouse hepatocyte and liver RNA-sequencing data to *de-novo* identify alternative splicing events that trigger the nonsense-mediated decay pathway. To this end, published analysis tools were combined with custom scripts and analysis pipelines. AN characterised these events using several meta-analysis methods (molecular function, sequence conservation) and compared

the findings with previous studies. AN also analysed public RNA-sequencing data from Arabidopsis thaliana in different temperature conditions to transfer the findings in mouse to plants. AN and MP designed the study, planned experiments, analysed data and wrote the manuscript with help from SM and FH.

The following works were also published during the time in the Heyd lab, but are not part of the cumulative work:

De Bortoli F, **Neumann A**, Kotte A, Timmermann B, Schüler T, Wahl MC, Loll B, Heyd F. Increased versatility despite reduced molecular complexity: evolution, structure and function of metazoan splicing factor PRPF39. Nucleic Acids Res. 2019 Jun 20;47(11):5867-5879. doi: 10.1093/nar/gkz243.

Bose D, **Neumann A**, Timmermann B, Meinke S, Heyd F. Differential IL2 transcription kinetics render mouse but not human T cells vulnerable to splicing inhibition early after activation. Mol Cell Biol. 2019 Jun 3. pii: MCB.00035-19. doi: 10.1128/MCB.00035-19.

Chapter 1. Introduction

1.1 Post-transcriptional control of mRNAs

According to the central dogma of biology, sequence information in a cell is passed from genomic (desoxyribonucleic acid – DNA) to transcriptomic (ribonucleic acid – RNA) to proteomic (protein) level (CRICK, 1958). Although challenged by findings of retrograde information transfer from RNA to DNA (for example during reverse transcription by retroviruses) (Temin and Mizutani, 1970), this dogma still stands in its general form, as genetic information has not yet been shown to be passed from protein to nucleic acid. In eukaryotic cells, protein expression is achieved by transcription of DNA to precursor messenger RNA (pre-mRNA), which is later translated into a protein. In order to be translated, the pre-mRNA molecule needs to be processed into a mature mRNA in three steps: addition of a 7-methylguanosine residue to the 5' terminal phosphate (5' capping), addition of a poly-adenosine (poly-A) tail to the 3' end (polyadenylation) and pre-mRNA splicing (Figure 1.1-1). The first two modifications are vital for mRNA stability, nuclear export and subsequent translation initiation (Shatkin, 1976; Colgan and Manley, 1997; Wilusz, Wormington and Peltz, 2001). Furthermore, alternative polyadenylation (APA) has been identified as an important factor for controlling gene expression (GE) and regulating the interaction of RNA-binding proteins (RBPs) and micro RNAs (Di Giammartino et al. 2011; Tian & Manley 2017). The third processing step, pre-mRNA splicing, will be introduced in the following subchapters.

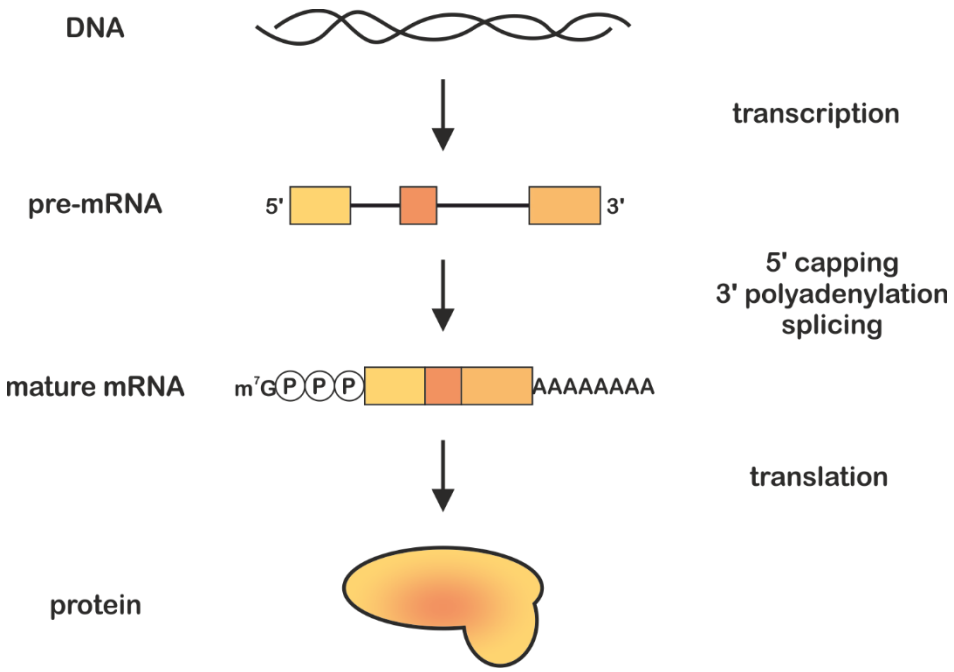

Figure 1.1-1: From DNA to protein. DNA is transcribed to a pre-mRNA, which consists of protein-coding exons (boxes) and non-coding introns (lines). The pre-mRNA is then processed in three steps to yield the mature mRNA, which is translated into a protein. m7G: 7-Methylguanosine, circled P: phosphate, A: adenosine.

1.1.1 pre-mRNA splicing

Most unspliced eukaryotic mRNAs consist of protein-coding exons intervened by non-coding introns. During pre-mRNA splicing, introns are excised from the mRNA and exons are joined together. The boundaries between introns and exons are marked by splice sites (ss) at the intron-exon junction. The branch point (BP, an adenosine) and a polypyrimidine tract, which both lie within the intron, are additional crucial sequences for the splicing process. Excision of an intron and ligation of the adjacent exons is achieved by two nucleophilic transesterification reactions of the SN2 type: Initially, the 2’ hydroxyl group of the BP adenosine attacks the phosphate group at the 5’ splice site (Krämer, 1996), releasing the upstream exon. This results in a free hydroxyl group at the 5’ ss of the upstream exon, which attacks the phosphate at the 3’ ss of the downstream exon. After this second reaction, the exons are ligated, while the intron is released in a so-called lariat structure (Figure 1.1-2).

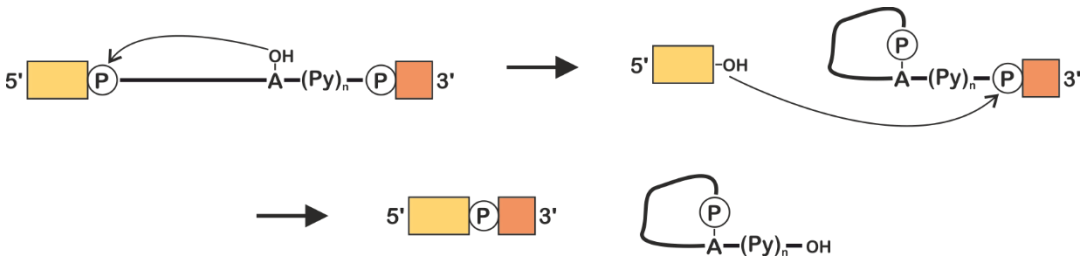

Figure 1.1-2: Schematic chemical depiction of a splicing reaction. Shown are the two nucleophilic reactions that lead to excision of an intron and ligation of the adjacent exons. Exons are shown as boxes, the intron as a line. Circled P: phosphate, A: branch point adenosine, $(Py)_n$: polypyrimidine tract.

The splicing process is catalysed by the spliceosome, a large and highly dynamic RNA-protein machinery. The spliceosome consists of five small nuclear ribonucleoprotein particles (snRNPs) – called U1, U2, U4, U5 and U6 – which are assembled at the pre-mRNA in a stepwise manner. Splicing is initiated via recognition and binding of the upstream 5' ss by the U1 snRNP, the downstream 3' ss by the U2 auxiliary factor (U2AF) and of the branch point by the splicing factor 1 (SF1), in total forming the E complex. In the next step, the U2 snRNP replaces SF1 at the BP, forming the A complex. Thereafter the catalytically inactive (pre-catalytic) B complex is formed by recruitment of the pre-assembled U4/U6●U5 tri-snRNP complex. This complex is remodelled and thereby activated to catalyse the first transesterification reaction. During remodelling, the U1 and U4 snRNPs are released, resulting in the C complex. After another rearrangement of the snRNPs, the C complex is activated and catalyses the second splicing reaction, joining the exons and releasing the intron lariat as well as the U2, U5 and U6 snRNPs (Wahl, Will and Lührmann, 2009; Will and Lührmann, 2011) (Figure 1.1-3).

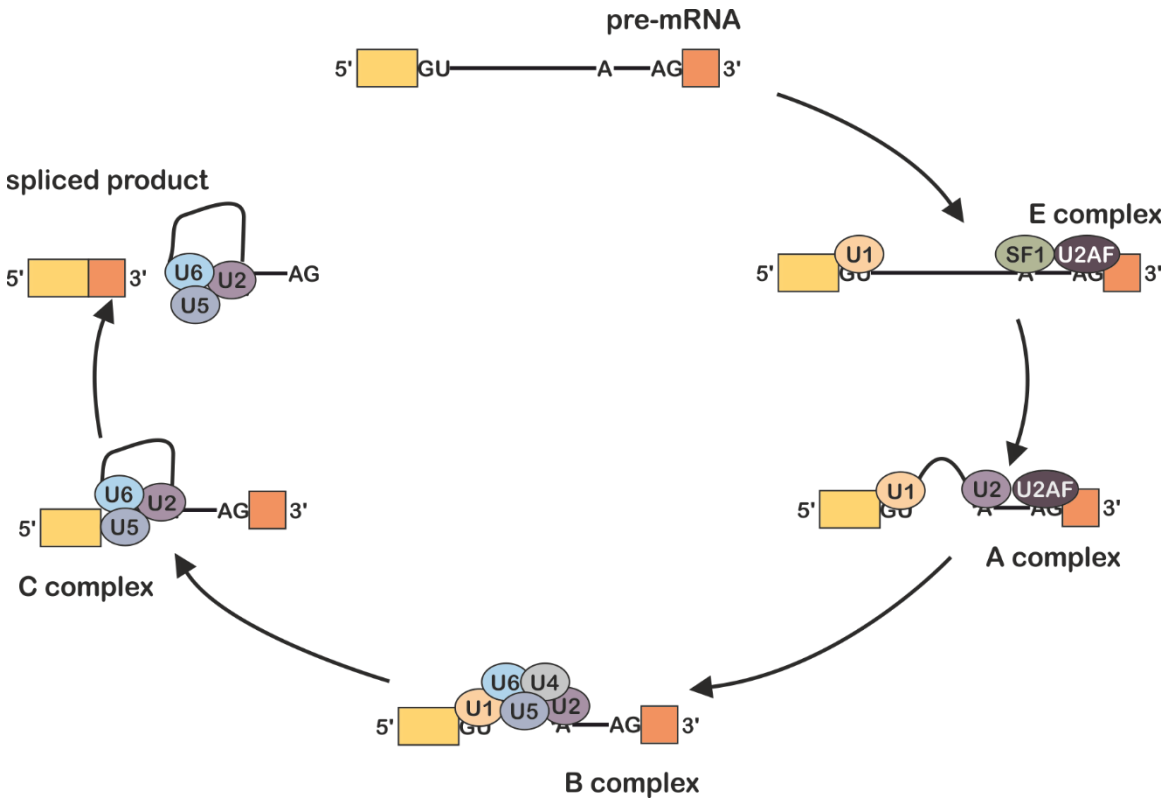

Figure 1.1-3: A simplified spliceosome-mediated splicing reaction. Exons are depicted by boxes, the intron as a line. Proteins are shown in circles with their names indicated. GU: consensus 5' splice site, A: branch point adenosine, AG: consensus 3' splice site. Adopted from Wahl, Will and Lührmann, 2009.

1.1.2 Alternative splicing

Over 95% of human multiexon genes can be spliced in a way that multiple different mature mRNAs are created (Pan *et al.*, 2008; Barbosa-Morais *et al.*, 2012; Merkin *et al.*, 2012). In contrast to constitutive splicing, where only one mRNA isoform is created from a gene, this process is called alternative splicing (AS). AS can be classified into five major categories: shortening of an exon by using an alternative 5' or 3' splice site (A5ss/ A3ss), skipping of a cassette exon (SE), skipping of

either one of two consecutive exons and simultaneous inclusion of the other (mutually exclusive exons, MXE) or retaining of an intron (RI) (Figure 1.1-4).

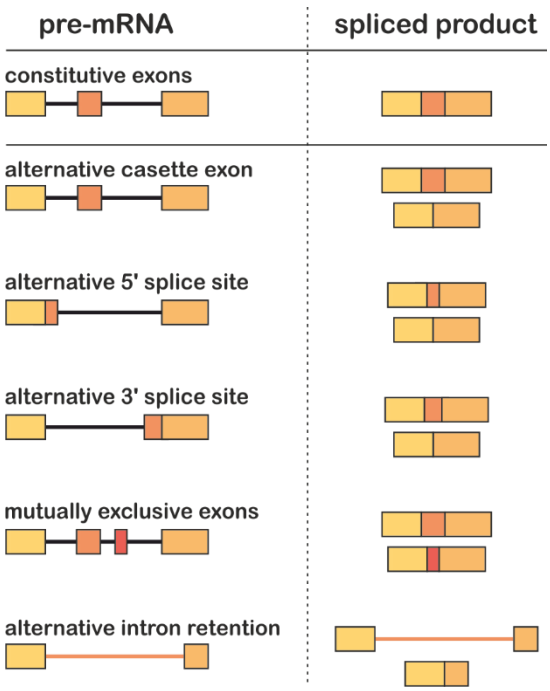

Figure 1.1-4: Modes of alternative splicing. Shown are the pre-mRNA (left) and corresponding spliced products (right) for constitutive splicing and five types of AS. Exons are depicted as boxes, introns as lines.

AS leads to an immense increase in proteomic diversity since the different mRNAs usually code for different proteins (Liu *et al.*, 2017). These different protein isoforms have been shown to often behave like distinct proteins, in many cases exhibiting completely independent interaction profiles (Yang *et al.*, 2016). Apart from different proteins, AS can also influence mRNA stability, decay and translation efficiency, thereby regulating protein levels (Mockenhaupt and Makeyev, 2015) (Figure 1.1-5). One example of AS events controlling mRNA levels and thereby protein levels are highly conserved exons in a class of proteins called serine-arginine-rich (SR) proteins (see below). These exons, when included into the transcript, lead to degradation of the mRNA via the nonsense-

mediated decay (NMD) pathway. These exons are therefore termed “poison exons” (Lareau *et al.*, 2007) (see also Neumann *et al.*, 2019 below for further information).

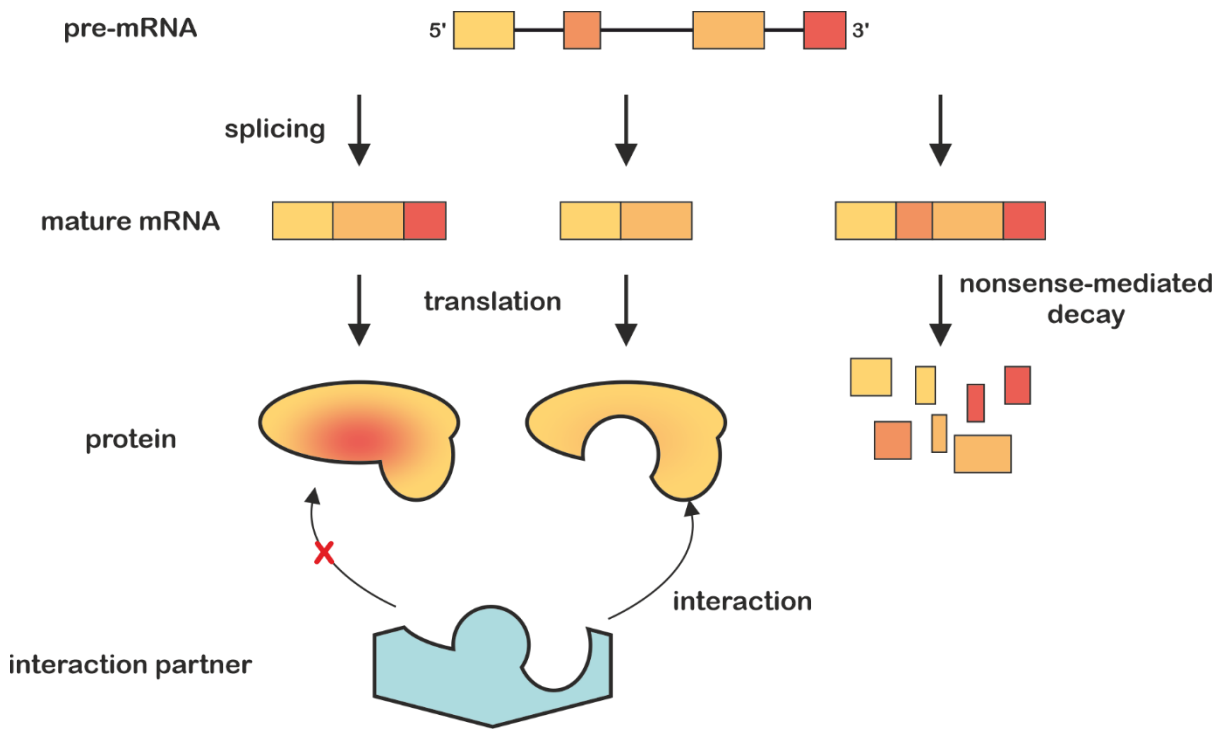

Figure 1.1-5: Possible consequences of alternative splicing. AS can lead to different protein isoforms, which often have distinct interaction partners. Furthermore, AS can lead to changes of mRNA levels (via NMD or by changing mRNA stability) and protein levels (by changing the translation efficiency, not shown).

Alternative splicing factors regulate AS by interacting with the spliceosome machinery and can either promote or repress the usage of a particular splice site. These *trans*-acting protein factors bind the pre-mRNA at *cis*-regulatory elements within its sequence. *Cis*-regulatory elements can be divided into four categories based on their position and type of regulation: intronic splicing enhancers (ISE), exonic splicing enhancers (ESE, both promote ss usage), intronic splicing silencers (ISS) and exonic splicing silencers (ESS, both repress ss usage) (Black, 2003). The most prominent *trans*-acting regulators of AS belong either to the SR or heterogeneous nuclear ribonucleoprotein particle (hnRNP) protein families. These bind to *cis*-regulatory elements and either promote or repress ss usage. SR proteins contain serine-arginine repeat domains and are mainly described to promote ss usage by recruitment of spliceosomal components or auxiliary

factors. hnRNPs on the contrary are mostly described to repress ss usage by a variety of mechanisms (Busch and Hertel, 2012; Fu and Ares, 2014). These and several more splicing factors often have an impact on the same target, constituting a regulatory network to yield the final transcript (Figure 1.1-6). Furthermore, the influence of the RBP on ss usage can depend on binding position (Fu and Ares, 2014; Hamid and Makeyev, 2017). It should be mentioned that AS is additionally regulated by other factors such as secondary structures (McManus and Graveley, 2011; Kornblihtt, 2015; Taliaferro *et al.*, 2016) and transcription speed (Naftelberg *et al.*, 2015).

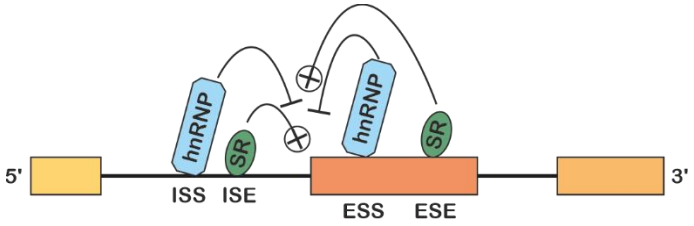

Figure 1.1-6: AS regulation by RNA-binding proteins. In general, hnRNPs bind to intronic or exonic splicing silencer sites (ISS/ ESS) and repress splice site usage. In contrast, SR proteins bind to splicing enhancers (ISE/ ESE) and promote splice site usage.

AS is highly tissue-specific and often changes during dynamic processes such as cell differentiation or activation (Heyd and Lynch, 2011; Merkin *et al.*, 2012). Since AS regulation is a very fast process and downstream of transcriptional regulation, it is an ideal mechanism to quickly adapt cells to changing requirements.

1.1.3 High-throughput quantification using Next-Generation Sequencing techniques

Quantification of alternative splicing has been classically performed using reverse transcription (RT) coupled to a target-specific and splicing-sensitive polymerase chain reaction (PCR). This method yields accurate results but allows quantification of only few targets (<100) in a reasonable time frame. With the advent of Next-Generation Sequencing (NGS) technologies, quantification of virtually all transcripts at once can be achieved. Using NGS it is possible to quickly and accurately read the nucleotide sequences of millions of DNA or RNA molecules in parallel. This enables

transcriptomic analyses at an unprecedented scale and resolution, profoundly impacting biomedical research with applications in academic, pharmaceutical and clinical settings (Mardis, 2011, 2013; Levy and Myers, 2016).

High-throughput RNA-sequencing (RNA-seq) in its simplest form allows both quantification of GE levels and AS ratios of a sample. Numerous tools have been developed to process the output generated by NGS machines (reads in fastq format) and enable these quantifications as well as comparisons between samples (Trapnell, Pachter and Salzberg, 2009; Katz *et al.*, 2010; Trapnell *et al.*, 2012; Dobin *et al.*, 2013; Love, Huber and Anders, 2014; Shen *et al.*, 2014; Bray *et al.*, 2016; Patro *et al.*, 2017; Sterne-Weiler *et al.*, 2018). After quality control, an RNA-seq analysis workflow comparing two conditions consists of three main parts: read alignment, differential analysis and meta-analysis.

Reads represent short nucleotide sequences from the input mRNA (currently usually 50-150 nucleotides). These need to be aligned to a reference genome or transcriptome to identify the region they originally stem from. Typical aligners, also called read mappers, are Tophat, STAR, Kallisto and Salmon (Trapnell, Pachter and Salzberg, 2009; Dobin *et al.*, 2013; Bray *et al.*, 2016; Patro *et al.*, 2017). Mapping is computationally challenging, since mRNA reads often consist of sequences from multiple exons. As exons are intervened by introns, these reads do not naturally align to the genomic reference. To achieve proper alignment, they need to be split into smaller parts during mapping. As the correct position for splitting the read is not known beforehand, several fragmentations need to be tested to yield optimal results. This computationally expensive method has been revolutionised by the recent introduction of quasi-mappers that make efficient use of special data structures to improve mapping speed (Bray *et al.*, 2016; Srivastava *et al.*, 2016; Patro *et al.*, 2017). The downside of quasi-mappers is that the output usually only reports which transcript the read belongs to, but not to which specific genomic position.

For differential analysis of GE or AS, expression levels and inclusion ratios are first calculated on a per-sample basis. This quantification is dependent on the initial read alignment step. Samples from the same condition are then aggregated and differential analysis between conditions is

achieved applying advanced statistical methods (Katz *et al.*, 2010; Love, Huber and Anders, 2014; Shen *et al.*, 2014; Bray *et al.*, 2016; Patro *et al.*, 2017; Sterne-Weiler *et al.*, 2018).

Finally, meta-analysis interprets and visualises the results from the alignment and differential analysis steps. There is a plethora of applications that can cater to very generic but also extremely specific needs. Some of the most common operations to gain initial biological insight from the differential analysis are gene ontology and gene set enrichment applications (Ashburner *et al.*, 2000; Subramanian *et al.*, 2005; Mi, Muruganujan and Thomas, 2013). Clustering of samples using a principal component analysis, heatmaps and Sashimi plots for AS representation are common visualisation techniques (Katz *et al.*, 2014; Love, Huber and Anders, 2014). For further discussion about advantages and disadvantages of true read mappers, quasi-aligners and the available software suites for differential analysis, see chapter 3.3.

The adoption rate of NGS technology has been greatly accelerated by a significant drop in sequencing costs that has occurred over the last decades. As an example, the cost of sequencing a human genome has decreased from almost 100 million dollars in 2001 to just over 1000 dollars in 2017 due to incremental technical improvements (according to data from the National Human Genome Research Institute, https://www.genome.gov/about-genomics/fact-sheets/DNA-Sequencing-Costs-Data, accessed 29th of July 2019) (Figure 1.1-7, left). To date, there are over 1.5 million RNA-sequencing samples stored for public access in the Short Read Archive of the National Center for Biotechnology Information (accessed 29th of July 2019) and this number is steadily increasing (Figure 1.1-7, right). Harnessing the power of these data and applying big data

analytics to them lead to the description of "the splicing code" (Barash *et al.*, 2010), which strives to predict tissue-dependent AS outcomes based on hundreds of RNA features.

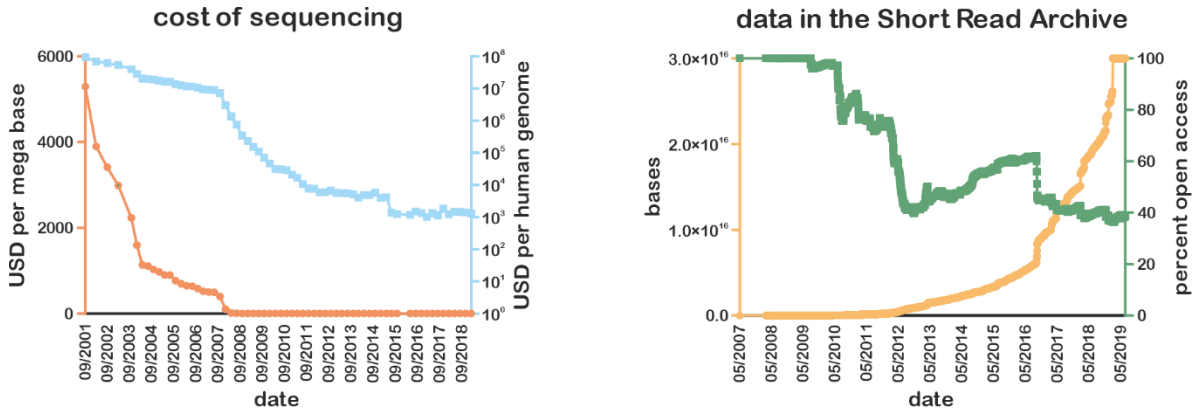

Figure 1.1-7: Next-Generation Sequencing technologies accelerate data production. Left: Shown are the cost of sequencing per mega base (orange) and per human genome (blue) in US$ between 2001 and 2019. Right: Shown is the amount of data stored in the Short Read Archive in bases (yellow) and the proportion of this data that is stored as open access (green) since its establishment in 2007 until 2019.

1.2 Biological rhythms

Since emergence of the last universal common ancestor, virtually all organisms on this planet experienced diurnal changes of their environment – namely day and night – as well as other rhythmic cues such as the seasons or the lunar phase (Neumann, 1966; Yanovsky and Kay, 2002; Brunner and Schafmeier, 2006; Glansdorff, Xu and Labedan, 2008; Harmer, 2009; Edgar *et al.*, 2012; Kaiser *et al.*, 2016). Organisms that were able to adapt to or even predict these oscillations had an evolutionary advantage (Panda, Hogenesch and Kay, 2002). This is why almost all organisms living today display biological oscillations in some form (Bhadra *et al.*, 2017; Dunlap and Loros, 2017) to adjust to predictable environmental cues such as the time of the day or simply changes of external temperature (Diernfellner *et al.*, 2005; Low *et al.*, 2008; Koike *et al.*, 2012; Haupt, Bennett and Oosthuizen, 2017). These cell autonomous oscillations are mediated by internal pacemakers (or clocks), which are regulated by genetic circuits (Bell-Pedersen *et al.*, 2005; Dibner, Schibler and Albrecht, 2010). Some examples of such rhythms in evolutionary distant organisms are explained in the following subchapters, both on organismal as well as on molecular level.

1.2.1 The circadian clock from lower to higher organisms

As stated above, nearly all organisms exhibit rhythmic phenotypes, even the archaeal organism *Halobacterium salinarum* NRC-1 was shown to have oscillations in peroxiredoxin oxidation activity (Edgar *et al.*, 2012). The cyanobacterium *Synechococcus elongates* PCC 7942 is well-studied regarding its clock gene regulation mechanisms. These bacteria can perform photosynthesis and nitrogen fixation. However, oxygen – the by-product from photosynthesis – inhibits enzymes that are involved in nitrogen fixation. As it is not possible to spatially separate both processes for the bacteria, they temporally separate them: photosynthesis happens during the day, while nitrogen fixation occurs in the night. This diurnal behaviour is preserved even in constant light conditions, although temperature modulates the behaviour to some extent. The molecular basis for this rhythm are multiple highly interconnected negative feedback loops that regulate transcription, translation, phosphorylation and stability of the involved players (Ishiura *et al.*, 1998).

Plants display several obvious time of the day-dependent adaptations, such as leaf position, germination, flower opening, photosynthetic activity or fragrance emission (Cumming and Wagner, 1968). *Arabidopsis thaliana* (*A. thaliana*) is described to exhibit three major feedback

loops on transcriptional level to predict and adapt to circadian changes: The CIRCADIAN AND CLOCK ASSOCIATED1 (CCA1) and LATE ELONGATED HYPOCOTYL (LHY) proteins repress expression of the TIMING OF CAB EXPRESSION (TOC1) gene, while TOC1 indirectly induces CCA1 and LHY transcription (Glossop *et al.*, 1999). CCA1/LHY at the same time promote transcription of the PSEUDO-RESPONSE REGULATOR (PRR) proteins PRR7 and PRR9, which in turn repress CCA1/LHY expression (Farré *et al.*, 2005; Nakamichi *et al.*, 2010). Finally, there is another undiscovered protein that is thought to promote TOC1 transcription. Expression of this protein is negatively influenced by TOC1, CCA1 and LHY (Figure 1.2-1, left). It should be noted however, that existence of the third loop was challenged based on computational modelling. Based on the new model, TOC1 might be a negative instead of a positive regulator of CCA1/LHY transcription (Pokhilko *et al.*, 2012). Nevertheless, these loops lead to the following expression pattern: At dawn, expression of CCA1/LHY is at its peak. This directly and indirectly leads to reduced levels of TOC1 but increasing PRR7/PRR9 levels. Due to reduced levels of TOC1 and increasing levels of PRR7/PRR9, transcription of CCA1/LHY is reduced over time, which leads to higher TOC1 expression. TOC1 expression peaks at the end of the day, when CCA1/LHY expression is at its lowest. During the night, high TOC1 expression yields higher transcription rates of CCA1/LHY and lower transcription of TOC1 itself, which leads to a new circadian cycle (Más and Yanovsky, 2009) (Figure 1.2-1, right). Aside from each other, CCA1, LHY and TOC1 induce transcription of various other genes, thereby regulating numerous cellular pathways (Harmer *et al.*, 2000). Light is the main *zeitgeber* that synchronises time setting across the plant. This is achieved by several photoreceptors, mainly of the cryptochrome and phytochrome classes, that relay detailed information about the intensity and wavelengths of incoming light to the circadian oscillators and regulate their expression (Oakenfull and Davis, 2017).

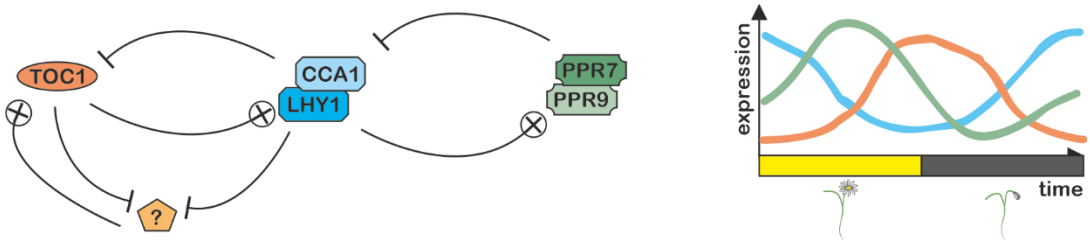

Figure 1.2-1: The molecular circadian clock of *A. thaliana*. The proposed feedback loops with negative and positive regulation (left) and resulting expression levels of the players (right, approximated) are shown. Arrows with + signs at the tip represent transcriptional promotion, a | at the tip represents transcriptional repression. Yellow and black bars represent day and night, respectively.

The circadian clock of *Drosophila melanogaster* (*D. melanogaster*) controls behaviour and perception of the fly, for example locomotion and olfactory sensing (Shaw *et al.*, 2000; Chatterjee *et al.*, 2010). It consists of two interconnected transcriptional negative feedback loops: In the first, period (per) and timeless (tim) gene transcription is promoted during the day by binding of the Drosophila CLOCK (dCLK) and CYCLE (CYC) transcription factor proteins. The transcriptional regulation is mediated by binding to the so-called E-box (or clock-box) regulatory element within the per and tim promoters (Hao, Allen and Hardin, 1997; Darlington *et al.*, 1998). PER protein in the cytoplasm is bound by DOUBLE-TIME (DBT), phosphorylated and then degraded (Kloss *et al.*, 2001). In the evening, once TIM is abundantly present in the cytoplasm, it interacts with PER, preventing phosphorylation and thus degradation. TIM is itself phosphorylated by SHAGGY (SGG) upon which the TIM/PER/DBT multimer is translocated into the nucleus. TIM detaches from the nuclear complex, which enables PER/DBT to repress dCLK/CYC binding to the E-box and thus per and tim expression. At the same time, PER is phosphorylated and degraded since it is no longer stabilised by TIM (Kloss *et al.*, 2001). Both degradation and reduced transcription lead to higher dCLK/CYC activity, enabling the beginning of another circadian cycle. The second cycle is much simpler: dClk transcription is repressed by its protein product and (indirectly) promoted by PER, yielding cycling protein levels (Lee, Bae and Edery, 1998; Glossop, Lyons and Hardin, 1999) (Figure 1.2-2). A third feedback loop has been suggested, in which the transcription factor vrille is required for oscillating per and tim expression (Blau and Young, 1999). The *D. melanogaster* circadian clock is light entrained similar as it is the case in plants. Light information is acquired by photoreceptors in the eye and transmitted to the rest of the body via so-called pacemaker neurons. The main circadian photoreceptor is cryptochrome (cry), although the rhodopsin rh7 was recently identified to take part in this process as well (Stanewsky *et al.*, 1998; Helfrich-Förster *et al.*, 2001; Ozturk *et al.*, 2011; Ni *et al.*, 2017).

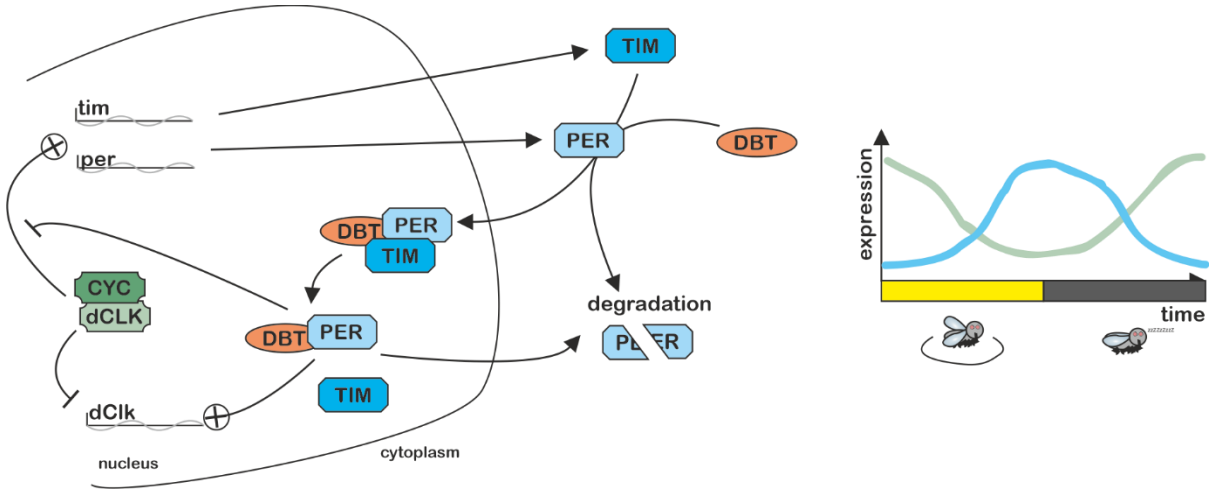

Figure 1.2-2: A simplified molecular circadian clock of *D. melanogaster*. The proposed main feedback loops (left) and resulting expression levels of the involved proteins (right, approximated) are shown. Arrows with + signs at the tip represent transcriptional promotion, a | at the tip represents transcriptional repression or inhibition. Yellow and black bars represent day and night, respectively.

1.2.2 The mammalian circadian clock

The core mechanisms and many players described above for *D. melanogaster* are conserved in mammals with only minor differences in function (Table 1.2-1).

Table 1.2-1: Putative orthologues between fly and mammalian circadian clock genes. Adopted from Panda, Hogenesch and Kay, 2002.

***D. melanogaster* circadian clock genes**	**Mammalian circadian clock genes**
period (per)	Period1 (Per1), Period2 (Per2), Period3 (Per3)
timeless (tim)	Timeless (Tim)
dClock (dClk)	Circadian locomotor output cycle kaput (Clock)
cycle (cyc)	Brain and Muscle ARNT-Like 1 (Bmal1)
double-time (dbt)	Casein kinase Iε (CKIε)
vrille (vri)	Nuclear factor, interleukin 3 regulated (Nfil3)
shaggy (sgg)	?
cryptochrome (cry)	Cryptochrome1 (Cry1), Cryptochrome2 (Cry2)

In short, Per and Cry transcription is positively regulated by the CLOCK/BMAL1 dimer. PER is degraded after CKIε mediated phosphorylation but stabilised by CRY binding. The PER/CKIε/CRY complex is translocated into the nucleus, where it dissociates. CRY represses CLOCK/BMAL1 activity, while PER promotes Bmal1 transcription before it is degraded. Bmal1 transcription is repressed by its protein product (Panda, Hogenesch and Kay, 2002) (Figure 1.2-3, left). In mice, this leads to the following cycling pattern: Bmal1 expression is highest at dawn and decreases during the day. It is lowest around dusk and then rises again during the night. Per and Cry expression inversely mirror the Bmal1 cycle (G. Yang *et al.*, 2016) (Figure 1.2-3, right). In mammals, signals of the external *zeitgeber* light are forwarded from the eye to the suprachiasmatic nucleus (SCN), where the central clock resides. The entrained central clock then synchronises the peripheral clocks in other parts of the body (Reppert and Weaver, 1997).

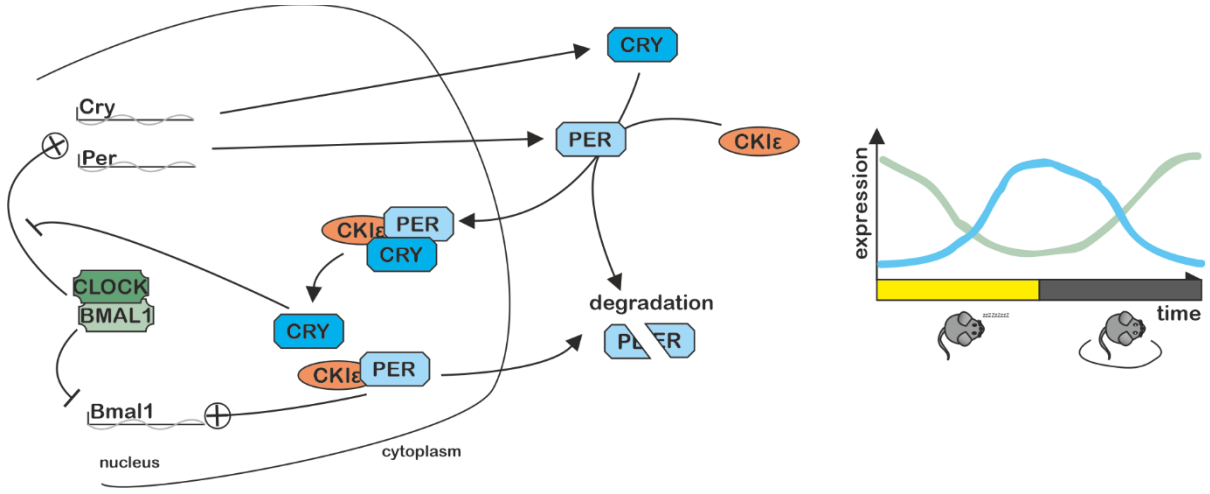

Figure 1.2-3: A simplified mammalian molecular circadian clock. The main feedback loops (left) and resulting expression levels of the involved proteins (right, approximated for mouse) are shown. Arrows with + signs at the tip represent transcriptional promotion, a | at the tip represents transcriptional repression or inhibition. Yellow and black bars represent day and night, respectively.

The main circadian feedback loops are therefore highly conserved between fly and mammals. However, while dClk expression cycles in the fly, mammalian Clock does not, but instead the cyc orthologue Bmal1. Furthermore, while PER has roles in both feedback loops in *D. melanogaster* (blocking of CYC/dCLK activity and transcriptional upregulation of dClk), it only regulates Bmal1 transcription in mammals. The task of blocking CLOCK/BMAL1 binding is performed by CRY in

this case. Finally, TIM is not involved in the main circadian feedback loops and its role is taken over by CRY. Mammalian Timeless possibly is not involved in circadian function at all but rather in embryonic development (Gotter *et al.*, 2000; Gotter, 2006). Instead, a circadian and light inducible splice isoform of U2af26 was shown to specifically interact with and regulate stability of PER1 via a Timeless homology domain (Preußner *et al.*, 2014).

1.2.3 Temperature and biological rhythms

The circadian clock is commonly described to be entrained by light signals. Furthermore, there are several examples that show how the period length is temperature compensated, rendering it robust even in heat fluctuations (Salomé, Weigel and McClung, 2010; Bodenstein, Heiland and Schuster, 2012; Kidd, Young and Siggia, 2015; Shinohara *et al.*, 2017). Nevertheless, temperature plays a role in diurnal adaptations to some extent. The clock of the Neurospora fungus is both light and temperature-dependent. In natural environments, light corresponds to higher and darkness to lower temperature. When this is inversed in experimental conditions (light is paired with colder and darkness with higher temperature), temperature is the dominant signal for entrainment (Bhadra *et al.*, 2017).

Similar as in unicellular organisms, internal temperature is mostly controlled by external heat sources in plants and poikilothermic animals. This can lead to drastic body temperature changes during the course of the day. Temperature-dependent transcriptional activity is well studied in plants and has been implicated both in daily and seasonal adaptations of circadian clock output (Jung *et al.*, 2016; Cortijo *et al.*, 2017; Webb *et al.*, 2019).

Mammals are endotherm organisms that do not drastically change their body temperature in response to external conditions. They however show cycling body temperature that correlates with their circadian rhythm: higher temperatures are exhibited when awake and lower temperatures when asleep. These temperature changes have an amplitude of up to 4°C (Refinetti and Menaker, 1992; Nabenishi and Yamazaki, 2017). Temperature rhythms in this range have not yet been reported to trigger major molecular or organismal reactions, even though it is known that temperature is able to control protein levels, for example of the cold inducible RNA binding protein Cirbp (Nishiyama *et al.*, 1997).

1.3 The secretory pathway

After synthesis at the (ribosome-containing) rough endoplasmic reticulum (ER), most proteins are transported to another compartment of the cell by the secretory pathway, usually by vesicular membrane trafficking (Lippincott-Schwartz, Roberts and Hirschberg, 2000; Borgese, 2016). This pathway is divided into the early and late secretory pathway. The early stage represents transport between the ER, ER-Golgi intermediate compartment (ERGIC) and the Golgi apparatus and the late stage signifies post-Golgi transport. The anterograde transport from ER to the ERGIC is mainly mediated by coat protein II complex (COPII) vesicles, while the corresponding retrograde transport from ERGIC to ER is accomplished by COPI vesicle trafficking. Trafficking between ERGIC and Golgi apparatus is mostly mediated by COPI vesicles (Szul and Sztul, 2011). Post-Golgi trafficking is mediated by clathrin-coated vesicles, which transport cargo between Golgi apparatus, early endosome, late endosome, lysosome and plasma membrane (PM) (Kirchhausen, Owen and Harrison, 2014) (Figure 1.3-1).

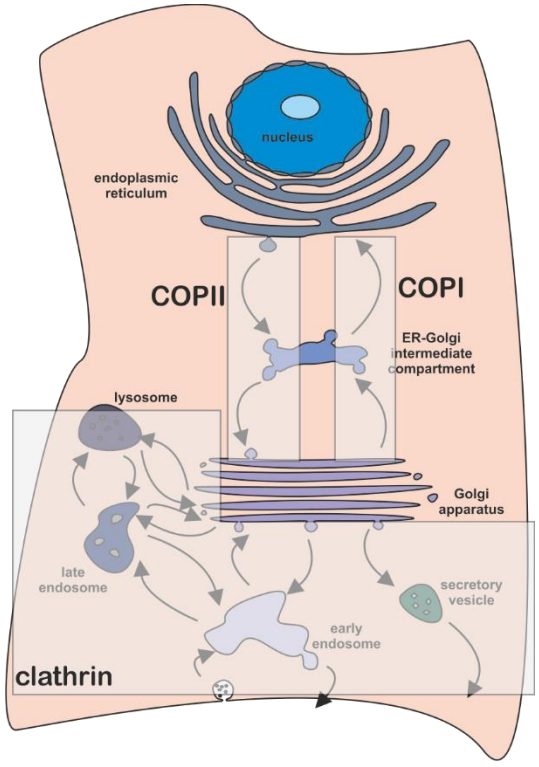

Figure 1.3-1: Vesicular membrane trafficking pathways. The anterograde ER to Golgi transport is mediated by COPII and the retrograde transport by COPI vesicles. Post-Golgi transport is mediated by clathrin-coated vesicles.

1.3.1 Fundamentals

COPII vesicle budding takes place at ER exit sites (ERES). The regions of ERES formation, also called the transitional ER (tER), is defined by the presence of the peripheral membrane protein Sec16 (Watson *et al.*, 2006). Sec16 has a scaffolding function and is thought to constitute a protein-interaction surface for COPII components (Hughes *et al.*, 2009; Sprangers and Rabouille, 2015). Proteins are loaded into COPII vesicles that assemble in a stepwise manner at the tER. The vesicle itself consists of a Sec23/Sec24 inner coat and a Sec13/Sec31 outer coat (Antonny and Schekman, 2001; D'Arcangelo, Stahmer and Miller, 2013; McCaughey and Stephens, 2018). The composition of the coat is somewhat flexible to accommodate cell-specific requirements, as multiple protein paralogs are present for these components. It was shown that Sec24a, Sec24b, Sec24c and Sec24d have different interaction partners (Adolf *et al.*, 2016) and that knock-out (KO) of Sec24c – but not Sec24a/Sec24b/Sec24d – leads to a tissue-specific, neurological phenotype in mice (Wang *et al.*, 2018). COPII vesicles travel from the ER in the direction of the Golgi. On this way, the vesicles fuse with the ERGIC, bud again and then finally reach the *cis*-Golgi (Lee *et al.*, 2004). Fusion of the vesicles is mediated by soluble N-ethylmaleimide-sensitive factor attachment receptor (SNARE) proteins. SNAREs at the vesicle (v-SNAREs) interact with SNAREs at the target membrane (t-SNAREs) to form an alpha-helical coil and forcibly pull the two membranes closer together (Mossessova, Bickford and Goldberg, 2003; Lee *et al.*, 2004). As an example, Sec22 was described as a v-SNARE responsible for both proper anterograde and retrograde vesicle transport with a potential additional t-SNARE function at the ER and Golgi apparatus (Adnan *et al.*, 2019). The early anterograde transport mechanism is summarised in Figure 1.3-2.

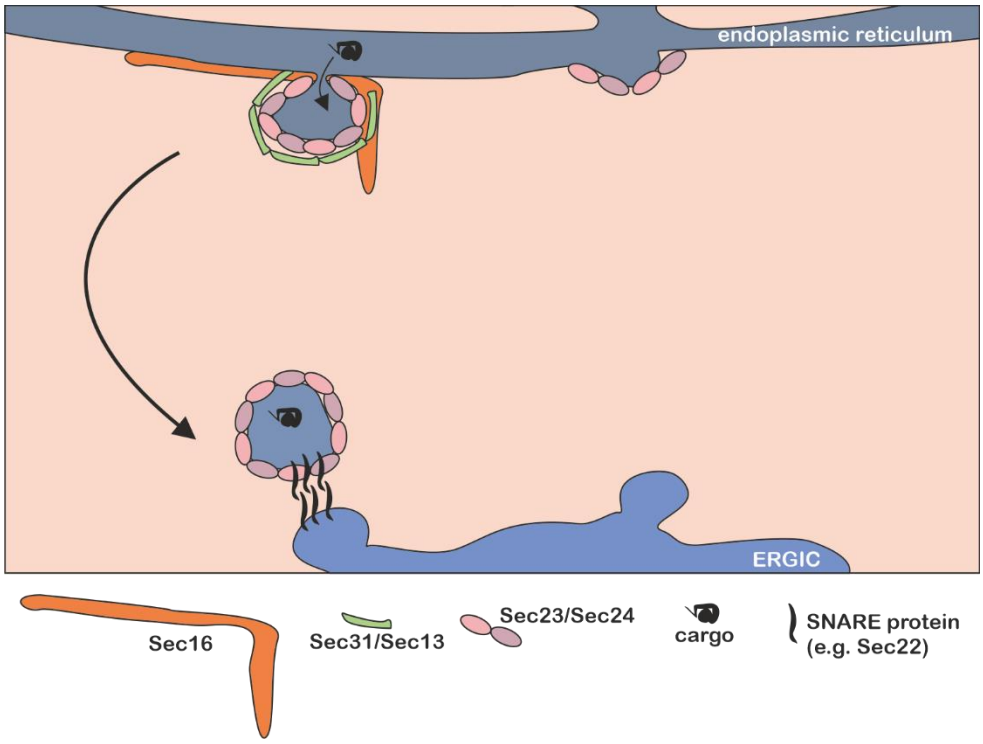

Figure 1.3-2: Schematic overview of ER to ERGIC transport via COPII vesicles.

After fusion with the *cis*-Golgi, cargo can either be cycled back via COPI vesicles or transported towards the *trans*-Golgi through the Golgi cisternae (a layered network of flat membrane sacks) (Jackson and Munro, 2009). While moving through the cisternae, cargo proteins are altered by glycosylation, proteolytic processing, sialylation and other modifications (Glick and Nakano, 2009; Nilsson, Au and Bergeron, 2009). At the *trans*-Golgi, cargo is sorted and packaged depending on its final destination (Guo, Sirkis and Schekman, 2014). Proteins destined for secretion are packaged into secretory vesicles, which are transported to the plasma membrane (Keller and Simons, 1997; Mostov, Verges and Altschuler, 2000). The exocyst complex mediates targeting and tethering of these vesicles to specific parts of the PM where exocytosis happens (Kee *et al.*, 1997).

Finally, it should be emphasised that the cytoskeleton has a vital role in membrane trafficking. Membrane vesicles travel along microtubules (Hehnly and Stamnes, 2007), in case of COPII vesicles via the interaction of Sec23 with Dynactin (Watson *et al.*, 2005; Gurel, Hatch and Higgs, 2014). Furthermore, the cytoskeleton plays a role in localization and organization of compartments that are vital for the secretory pathway. Myosin 18A links cytoskeletal proteins to the Golgi

apparatus to enable vesicle budding (Ng *et al.*, 2013). On a side note, this interaction is thought to lead to the typical flat cisternae arrangement of the Golgi (Dippold *et al.*, 2009).

1.3.2 Dynamic regulation

Secretory processes are highly flexible and able to quickly adapt to new requirements. To adapt to changing cargo loads, three major mechanisms have been described: regulation of gene expression (Dunne, Kondylis and Rabouille, 2002; Coutinho *et al.*, 2004; Schotman, Karhinen and Rabouille, 2009), changes in membrane dynamics and morphology (Forster *et al.*, 2006; Guo and Linstedt, 2006; Farhan *et al.*, 2008) and altered activity of kinases and phosphatases (Farhan *et al.*, 2010) (Figure 1.3-3).

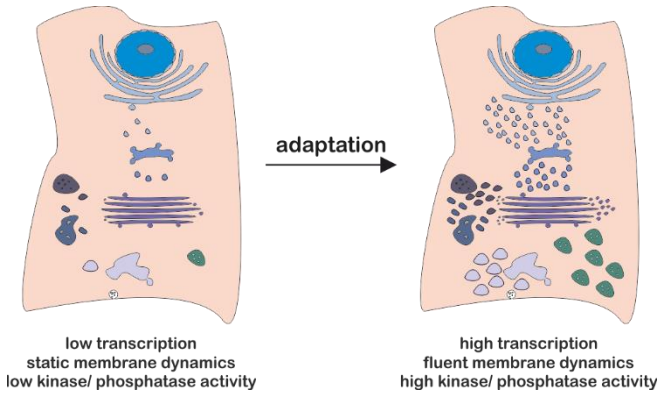

Figure 1.3-3: Modes of adapting the secretory pathway to higher secretory cargo.

For instance, transcription of sneezy, which encodes for the alpha subunit of the zebrafish coatomer complex, is regulated to match activity with cell-type and tissue specific trafficking requirements (Schotman, Karhinen and Rabouille, 2009). This process is relatively slow (in the order of days). To yield more immediate responses (within minutes), membrane dynamics can play a role. Farhan *et al.*, 2008 could show that acute cargo stress leads to a rearrangement of ERES components. This results in fewer, but larger ERES that can cope with the more challenging requirements. Finally, over 120 kinases and phosphatases were identified which control organization and trafficking of the secretory pathway, including players in the MAPK/ERK pathway (Farhan *et al.*, 2010).

Membrane trafficking processes need to be especially flexible during activation and differentiation processes (Farhan and Rabouille, 2011; McCaughey and Stephens, 2018). Naïve T cells have relatively low trafficking capability. When these cells are activated, production and export of cytokines is drastically upregulated in a short time frame (Huang *et al.*, 2013). Similarly, pre-adipocytes dynamically upregulate their membrane trafficking capabilities during differentiation into adipocytes (Kuryszko, Sławuta and Sapikowski, 2016). Although the mechanisms described above potentially play a role during these activation and differentiation processes, it remains largely unknown how exactly the upregulation of membrane trafficking is achieved.

1.3.3 Regulation by alternative splicing

The secretory pathway is dynamically regulated, often adapting cells to changing requirements in short time frames. It is thus very likely modulated by AS. Still, there have been only few reports where AS has been implicated in controlling transport processes. Blue *et al.*, 2018 recently summarised their view on how AS affects membrane trafficking. This review and its underlying studies will be discussed in the following paragraph.

The authors performed a meta-analysis of several publications about tissue-specific AS. They found that within the published lists of genes that exhibit tissue-specific splicing patterns, several are associated with transport processes (Dillman *et al.*, 2013; Giudice *et al.*, 2014; Irimia *et al.*, 2014; Brinegar *et al.*, 2017; Hannigan, Zagore and Licatalosi, 2017). Tissue-specific exons often encode for disordered protein regions that tend to be protein-protein interaction surfaces (Buljan *et al.*, 2012; Ellis *et al.*, 2012). The authors' conclusion was that these transport-associated genes could be involved in tissue-specific adaptations of membrane trafficking via AS.

They furthermore described AS of genes involved in clathrin-mediated endocytosis, encoding clathrin heavy and light chains, dynamin and the adapter protein DAB2: There are two human genes that encode for the clathrin heavy chain, which is involved in forming clathrin vesicles (Kedra *et al.*, 1996). Their AS is regulated in a tissue-specific manner in cardiomyocytes and skeletal muscle cells in a developmentally-regulated fashion (Giudice *et al.*, 2014, 2016; Brinegar *et al.*, 2017). Genes encoding for the clathrin light chain exhibit developmentally-regulated AS as well (Giudice *et al.*, 2014). No function of the implicated isoforms is known. Different endocytosis-associated phenotypes of dynamin KO cell lines have been described (Liu *et al.*, 2008).

Additionally, there is a disease-associated splice-altering mutation that leads to exclusion of an alternative exon, which is thought to have an effect on endocytic recycling (Boumil *et al.*, 2010). DAB2 exhibits an isoform-specific localization (Morris and Cooper, 2001).

Blue *et al.* next described implications of AS on SNARE proteins: SNAP25 is alternatively spliced, leading to two potential isoforms (Bark and Wilson, 1994). Exclusive expression of one or the other isoform leads to different sizes of vesicles destined for exocytosis (Sørensen *et al.*, 2003). A developmentally regulated switch in these isoforms exists (Bark *et al.*, 1995) and mis-regulation is linked to several neuronal and metabolic diseases (Johansson *et al.*, 2008; Valladolid-Acebes *et al.*, 2015; Daraio *et al.*, 2017). They also pointed out multiple AS isoforms for SNAP23, several syntaxins and the v-SNARE VAMP7 and isoform-specific localization patterns for some of these proteins (Shukla *et al.*, 2001; Martinez-Arca *et al.*, 2003; Vacca *et al.*, 2011). None of them have yet been reported to have an isoform-specific function in membrane trafficking.

Finally, they mentioned tissue-specific AS of the BAR-domain protein TRIP10 and the bridging integrator protein BIN1. TRIP10 AS leads to differential interactions (based on a two-hybrid screen, Chang, Adams and Saltiel, 2002; Wang *et al.*, 2002), while a certain isoform of BIN1 promotes transferrin endocytosis (Ellis *et al.*, 2012). The presented findings are summarised in

Lastly, the authors illustrated that several RBPs are involved in regulating AS of trafficking genes. In summary, Blue *et al.*, 2018 described how several RBPs regulate AS of numerous targets in tissue-, differentiation- and development-dependent fashion. Within these AS targets are genes that are involved in membrane trafficking processes. They also pointed out that mis-regulation of RBP activity can lead to disease manifestation, which potentially could be a secondary effect due to a mis-regulation of AS in transport-related genes. They however do not show that AS generally affects membrane-trafficking dynamics – neither on single-target nor on a genome-wide level – but mostly describe indicative data that allows for speculation in that direction.

Table 1.3-1: Summary of how AS affects membrane-trafficking dynamics based on Blue *et al.,* 2018. Shown are the described targets of AS and the resulting implications of the different isoforms. Implications directly associated with transport dynamics are marked with an asterisk

target	**described implications of AS**
clathrin heavy chain CLTC	tissue-specific, suggested to be important for muscle structure
clathrin light chain CLTA	brain-specific
clathrin light chain CLTB	developmentally regulated
adaptor protein DAB2	tissue-specific, *leads to differential number of clathrin binding sites
dynamin DNM1	*might alter endocytosis
dynamin DNM2	differential localization, *different abilities to export neutrophin receptor p75
SNARE protein SNAP25	*different sizes of primed vesicle pools
SNARE protein SNAP23	differential localization, change in protein domains
Syntaxin UNC-64	neuronal-specific, role in locomotion processes
Syntaxin STX3	tissue-specific, changes protein domains, role in axonal mRNA translation (mouse retinal cells)
SNARE VAMP7	change in protein domains, loss of interaction with adaptor protein AP3, differential localization
BAR-domain protein TRIP10	change in protein domains, differential interactions (based on two-hybrid screening), tissue-specific
Bridging integrator protein BIN1	muscle-specific, mis-splicing occurs in disease contexts, *promotion of transferrin endocytosis

1.4 Thesis Objective

Aim of this thesis was to leverage RNA-sequencing data and combine *in silico* findings with wet lab methods to explore how splicing is impacted by different stimuli and how in turn splicing affects physiological systems. More specifically, the following questions were investigated:

1) To what extent is alternative splicing controlled in a circadian-like fashion? What are the exogenous cues for this regulation and what is the physiological consequence of it?
2) What impact does alternative splicing have on the secretory pathway? How does alternative splicing regulate membrane trafficking in a tissue-specific or dynamic differentiation- and activation-dependent manner?
3) How do (disease-associated) mutations affect splicing? What is the physiological consequence of this mis-regulation?

To answer these questions, a combination of wet-lab and *in silico* techniques was applied. Generally, initial findings or mechanisms identified in biochemical experiments were further elucidated using bioinformatics methods. These global approaches then yielded data to make broader assumptions. Finally, the *in silico* findings were used for further wet-lab studies to validate the results and show physiological effects and molecular functions. The bioinformatics analysis often revolved around RNA-sequencing analyses, quantifying alternative splicing and gene expression. Furthermore, variant calling was conducted to identify genomic mutations. Obtained data from these analyses was then used for in-depth meta-analysis to identify overarching patterns in the data. Biochemical assays were usually cell-based, often manipulating splicing patterns of cells using Morpholinos, the CRISPR/Cas9 system or external signals like temperature, stimulating reagents or inhibitors. Aim of these assays was to gain further biological insight, which was mainly obtained either by extracting RNA from the manipulated cells for further investigation of gene expression levels and splicing patterns, or pursuing fluorescence-based read-outs, for example to quantify protein transport efficiencies.

Chapter 2. Results

2.1 Alternative splicing is globally regulated in a circadian-like manner by temperature, which leads to cycling protein function and abundance

---

This subchapter refers to the following publications:

Preußner M, Goldammer G, **Neumann A**, Haltenhof T, Rautenstrauch P, Müller-McNicoll M, Heyd F. Body Temperature Cycles Control Rhythmic Alternative Splicing in Mammals. Mol Cell. 2017 Aug 3;67(3):433-446.e4. doi: 10.1016/j.molcel.2017.06.006

Goldammer G, **Neumann A**, Strauch M, Müller-McNicoll M, Heyd F, Preußner M. Characterization of cis-acting elements that control oscillating alternative splicing. RNA Biol. 2018;15(8):1081-1092. doi: 10.1080/15476286.2018.1502587

* **Neumann A**, Meinke S, Goldammer G, Strauch M, Timmermann B, Heyd F, Preußner M. Rhythmic gene expression is controlled by evolutionary conserved temperature regulated alternative splicing triggering nonsense mediated decay. In preparation.

Based on a previous publication, we knew that exclusion of the mouse U2af26 alternative exons 6 and 7 happens in a light-inducible manner with a natural 24-hour rhythm in mice, which leads to drastically altered protein function (Preußner *et al.*, 2014). Next, we sought to investigate how this alternative splicing event is regulated and furthermore whether there is a global regulation of AS events in a circadian-like manner. We identified temperature to be both necessary and sufficient for regulation of U2af26 exon 6-7 alternative splicing in cell culture and *in vivo*. This event is so sensitive, that differences of only 1°C could be measured on mRNA level (Figure 2.1-1A), leading to circadian-like inclusion levels in mammals as their body temperature oscillates in a time of the

day-dependent manner in that range. We then identified the *cis*-regulatory elements and the *trans*-acting factors (Srsf2 and Srsf7) responsible for the splicing regulation (Figure 2.1-1B). We furthermore showed that phosphorylation – and thus the activity – of these SR proteins is regulated by temperature in a CDC-like kinase (Clk)-dependent manner (Figure 2.1-1C, D). Finally, we used publicly available RNA-seq data from mouse embryonic fibroblasts cultured at 32°C and 37°C, respectively, to identify additional alternative splicing events that are regulated by temperature. This analysis yielded over 200 events (amongst them U2af26), many of which we could show to be extremely temperature sensitive via RT-PCRs. In addition, we extracted and sequenced RNA of P19 cells treated with square-wave temperature cycles at two different time points to identify temperature-dependent oscillating AS events. This yielded about 100 events, a quarter of which overlapped with the list of previously generated events (Figure 2.1-1E), F. As one example of how this splicing-based thermometer impacts biological function, we demonstrated how a temperature-dependent alternative splicing event in the 5' untranslated region (UTR) of the transcription factor TATA-binding protein (Tbp) leads to cycling transcription of genes with a TATA box (Figure 2.1-1G).

We next investigated whether temperature-dependent AS generates NMD isoforms (AS-NMD) and if this leads to rhythmic gene expression patterns. To this end we sequenced temperature-entrained primary mouse hepatocytes (34°C and 38°C) that were treated with either cycloheximide (CHX) or dimethylsulfoxid (DMSO) (Figure 2.1-2A). CHX blocks translation elongation and thereby the NMD pathway which requires the first round of translation (Hurt et al. 2013). DMSO was used as a solvent control. From this sequencing approach, we were able to identify AS-NMD events by comparing the DMSO with the CHX conditions (Figure 2.1-2B, C). We could additionally investigate their temperature-sensitivity by comparing the CHX samples at different temperatures (as NMD isoforms are unstable in normal conditions, the temperature effect is less prominent in the DMSO samples). We indeed identified almost 4000 genes with AS-NMD events, of which almost 40% exhibited a temperature-dependence (Figure 2.1-2D).

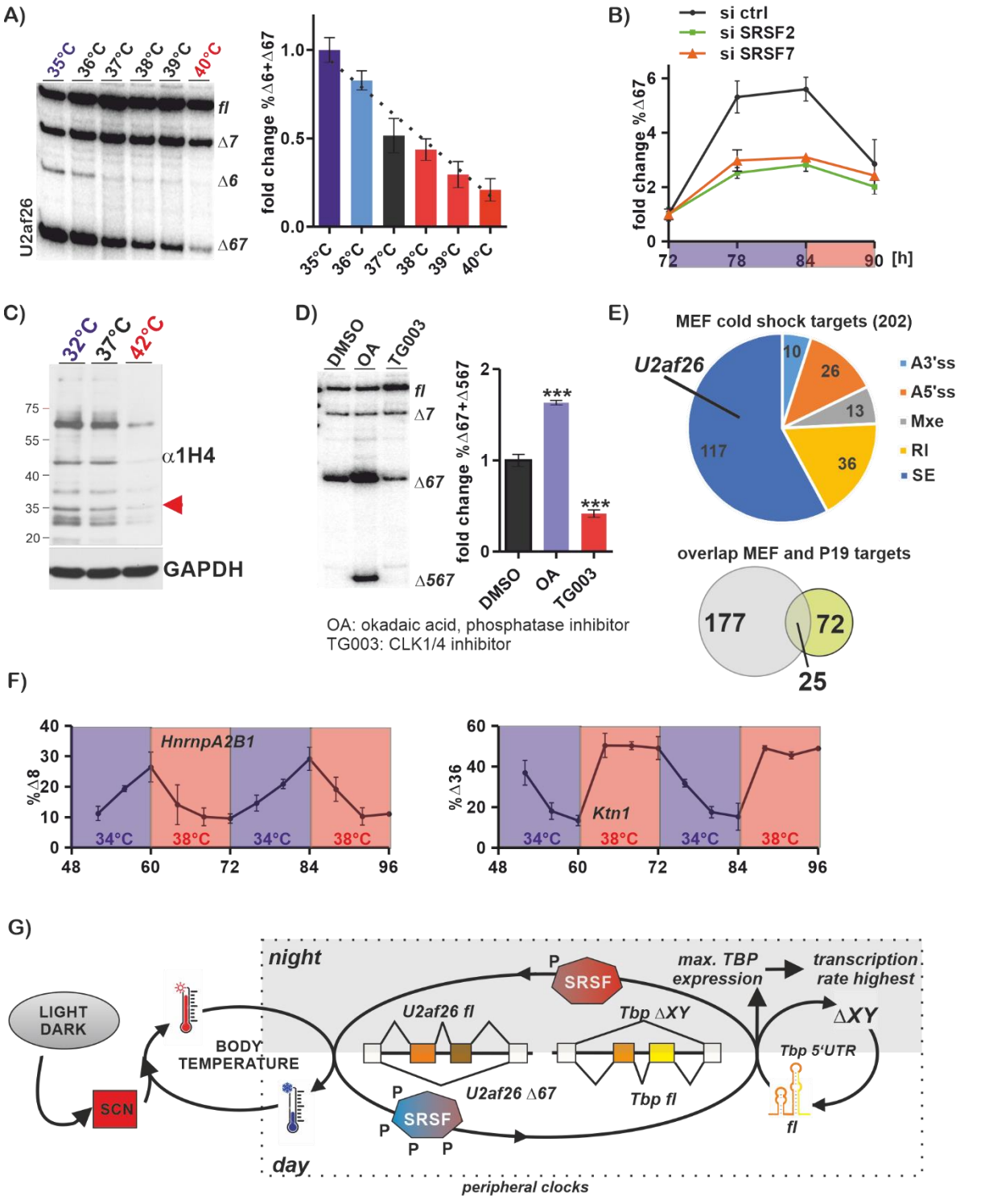

Figure 2.1-1: Summary of Preußner *et al.*, 2017; Goldammer *et al.*, 2018. A) Temperature sensitivity of U2af26 AS. B) Effect of SRSF2/7 KD on U2af26 AS. C) Temperature dependence of SR protein phosphorylation. D) Regulation of U2af26 AS by SR protein phosphorylation. E) Global identification of temperature sensitive AS in MEF and P19 cells. F) Exemplary validation of two identified targets. G) Model how AS is regulated by body temperature cycles. AN performed bioinformatical analyses shown in E. For further information, see Appendix E and Appendix G.

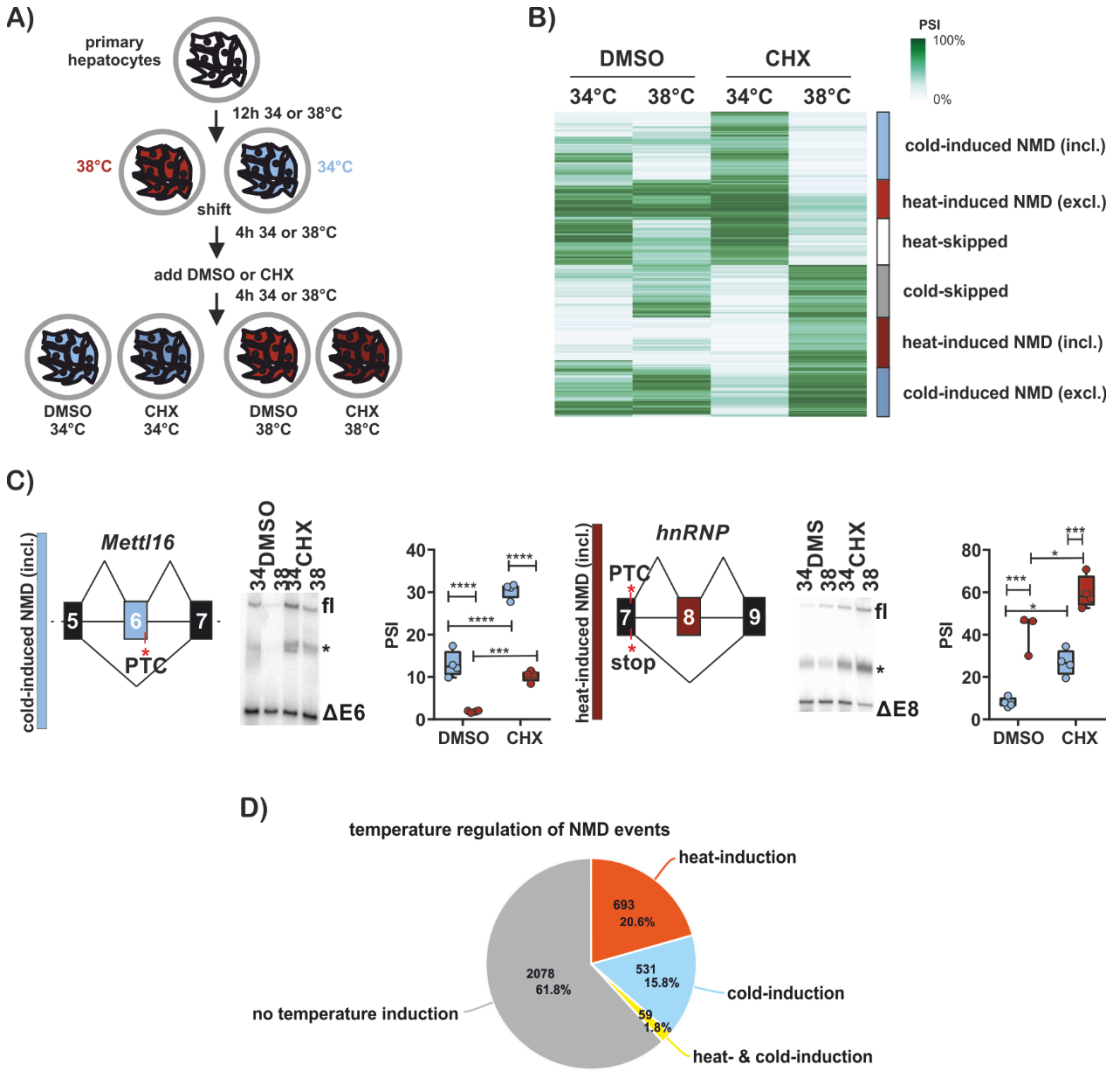

Figure 2.1-2: Identification of AS-NMD events from RNA-seq data of primary hepatocytes. A) Experimental design for identifying AS-NMD. B) Heatmap depicting the most regulated AS events between CHX treated cells cultured at 34 and 38°C. C) Exemplary validations of AS-NMD events. D) Temperature regulation of identified AS-NMD events on gene level. AN co-designed the experimental design in A and performed bioinformatical analyses shown in B and D. See Publication Appendix I for further information.

We found temperature-dependent AS-NMD events to be enriched in RBPs (Figure 2.1-3A, B). Intriguingly, the NMD-inducing exons exhibit highly conserved intronic regions adjacent to them (Figure 2.1-3A, C). Furthermore, AS-NMD regulates GE as NMD isoform inclusion anticorrelated with expression levels of the corresponding genes in the DMSO samples (Figure 2.1-3D, left). This effect is lost in the CHX samples, where NMD isoforms are not degraded and therefore cannot regulate GE (Figure 2.1-3D, right). This regulation was also observed in young mice with

artificially decreased temperature in comparison to young mice kept at warm temperatures (compare Preußner *et al.*, 2017, not shown).

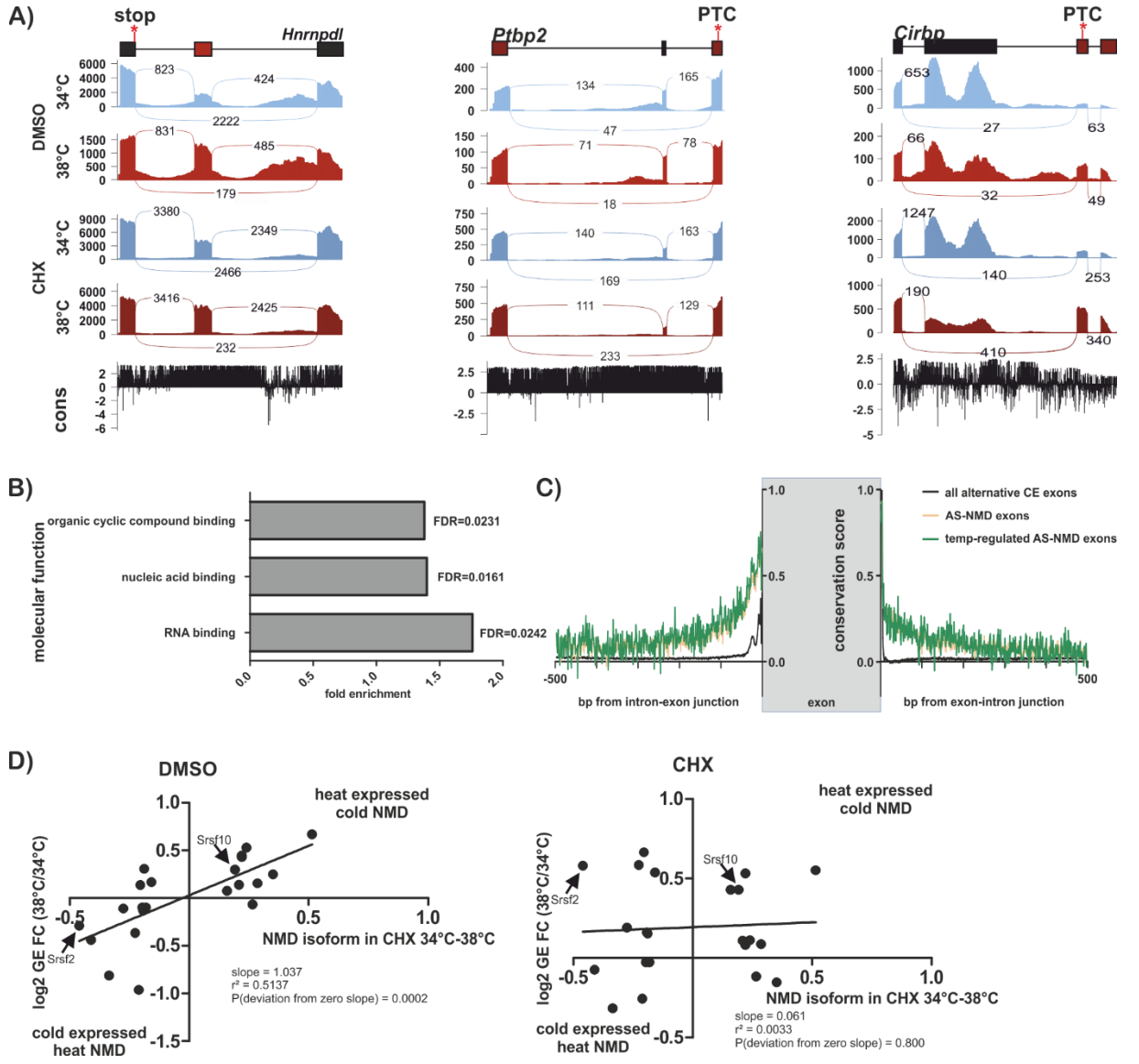

Figure 2.1-3: AS-NMD events are enriched in RBPs, exhibit high levels of conservation and regulate GE. A) Sashimi plots of AS-NMD events in Hnrnpdl, Ptbp2 and Cirbp. B) Molecular function analyses of identified AS-NMD genes. C) Placental conservation score of introns adjacent to AS-NMD events. D) Correlation of changes in NMD exon exclusion (in CHX samples) and corresponding GE (in DMSO, left, or CHX, right) between 34 and 38°C. AN performed all analyses shown in the figure. See Publication Appendix I for further information.

In a next step, we investigated AS-NMD isoforms of SR proteins in detail. These isoforms have been previously described and are known for their high conservation among mammals (see chapter 1.1.2 and (Lareau et al. 2007)), but no temperature regulation has yet been shown. Strikingly, it seems like temperature-regulated AS-NMD in SR proteins is the norm rather than an exception (Figure 2.1-4A). Two extreme examples are Srsf2, which has its NMD isoform strongly upregulated in warm conditions, and Srsf10, which exhibits elevated NMD isoform inclusion levels at cold temperatures (Figure 2.1-4B). Consistent with the previous data, inclusion of the NMD isoform leads to reduced GE levels. Furthermore, these events are again highly conserved as we have found the temperature-controlled AS-NMD event in human, mouse, rabbit, hamster and even chicken (Figure 2.1-4C).

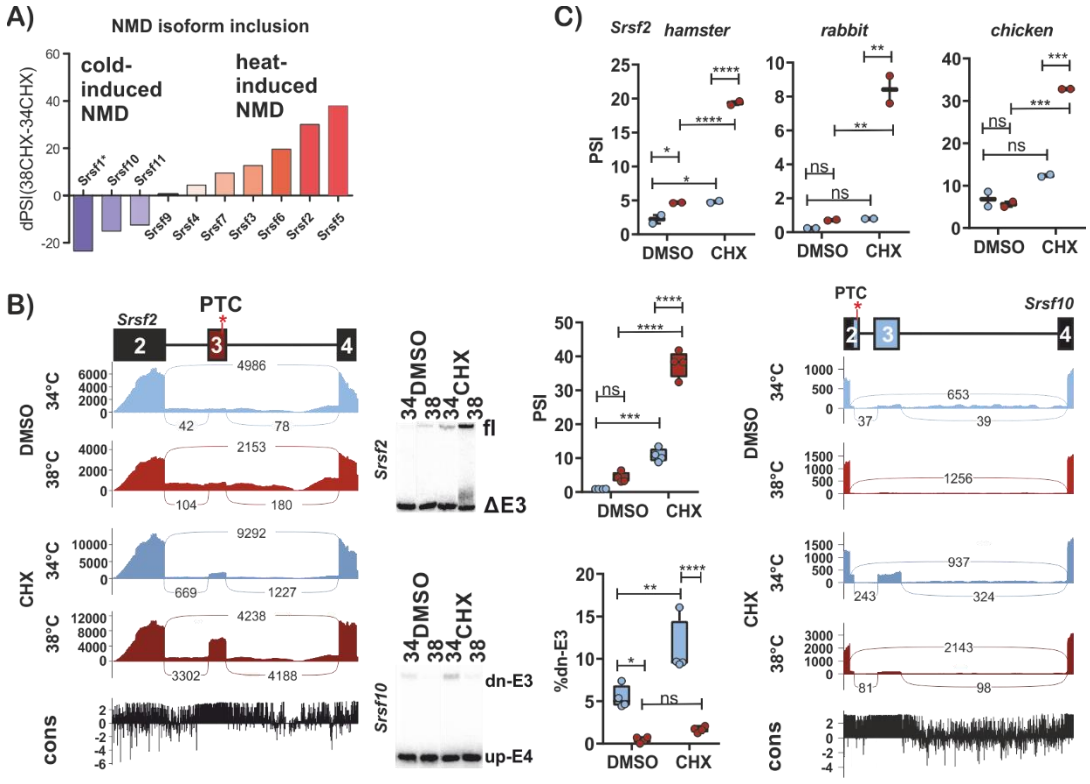

Figure 2.1-4: SR proteins frequently have temperature-dependent NMD splice events which are highly conserved. A) Cold- and heat-induced NMD isoform inclusion in SR proteins. B) Sashimi plots and corresponding validations of AS-NMD events in Srsf2 and Srsf10. C) Srsf2 AS-NMD conservation in hamster, rabbit and chicken. AN performed bioinformatical analyses shown in A and B. See Publication Appendix I for further information.

We investigated the example of Srsf10 further, showcasing in mechanistic detail that and how Srsf10 auto-regulates its own splicing in a temperature-dependent manner, including an identification of the *cis*-regulatory element and elaboration of the role of phosphorylation levels (Figure 2.1-5A, B). Moreover, rhythmic GE of Srsf10 is lost in cells lacking the NMD exon (Figure 2.1-5C). Lastly, the circadian-like inclusion of the Srsf10 NMD isoform leads to 24 hour rhythms of Srsf10 GE in mice (Figure 2.1-5D, E).

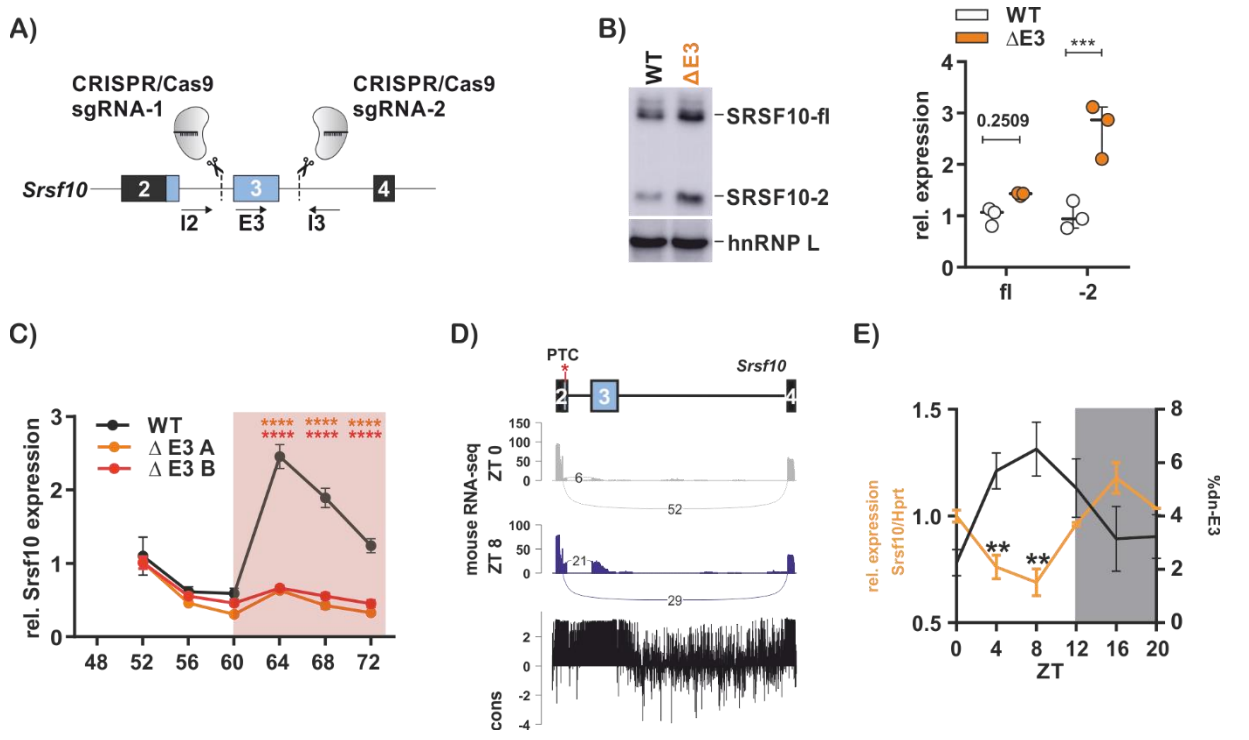

Figure 2.1-5: Srsf10 exon 3 is responsible for regulating Srsf10 GE in cells and *in vivo*. A) CRISPR approach for excising the Srsf10 NMD exon. B) Western Blot and quantification validating higher protein levels upon Srsf10 exon 3 excision. C) Cycling Srsf10 expression in wild-type, but not Srsf10 exon 3 KO cells upon square-wave temperature treatment. D) Sashimi plot of mouse RNA-seq data showing the NMD isoform inclusion at zeitgeber time 0 and 8. E) Correlation of Srsf10 exon 3 inclusion and Srsf10 GE *in vivo*. AN performed the bioinformatical analysis shown in D. See Publication Appendix I for further information.

Finally, we could show that the mechanism of AS-NMD regulating GE is not only present in placental organisms, but also in plants. Here, we used a publicly available time course dataset of *A. thaliana* plants kept at 20°C and then at 4°C for 24 hours each. Every 12 hours, the light condition was switched, starting with darkness. This allowed us to differentiate light- and temperature-dependent effects. Strikingly, most SR proteins in *A. thaliana* show a clear

temperature-regulation on GE level (Figure 2.1-6A). By inspecting Sashimi plots, we identified AS isoforms that anticorrelate with these GE patterns, which is highly indicative of AS-NMD (Figure 2.1-6B). We then used another set of public data where *A. thaliana* was exposed to NMD inhibiting agents – either CHX or knock-down (KD) of the critical NMD proteins Upf1 or Upf3 – with the respective controls included. We then *de-novo* identified AS-NMD events using these datasets. Using the newly discovered events, we checked their temperature-dependence in the time course data and correlated AS-NMD with GE of the respective genes. This approach bears two downsides: First, the AS-NMD events were identified without temperature changes present. This leads to exclusion of events that are only present at another temperature (4°C in this case). Second, the splicing ratios of the AS-NMD events were compared between temperatures without NMD inhibition. This results in a much lower detection rate and simultaneously in an under-estimation of AS-NMD amplitude, as there will be a fast degradation of strong NMD isoforms. Remarkably, we still observed a highly significant anti-correlation between NMD isoform generation and GE levels of the same gene (Figure 2.1-6C).

In summary, the following model can be deducted from the data presented: Temperature-regulated Clk proteins phosphorylate SR proteins leading to variable activity of these SR proteins (either higher or lower activity upon phosphorylation). This change in activity goes in hand with a change in numerous AS targets, including AS of SR protein transcripts. Many of these regulated AS events lead to promotion or repression of NMD-isoform generation. For SR proteins, the splicing regulation is part of an auto-regulatory feedback loop: higher activity leads to more of its NMD isoform and therefore less protein, lower activity leads to less NMD isoform and higher protein levels. In total, these AS changes behave in a circadian-like manner (in mammals) and lead to cycling and time of the day-dependent gene and protein expression patterns.

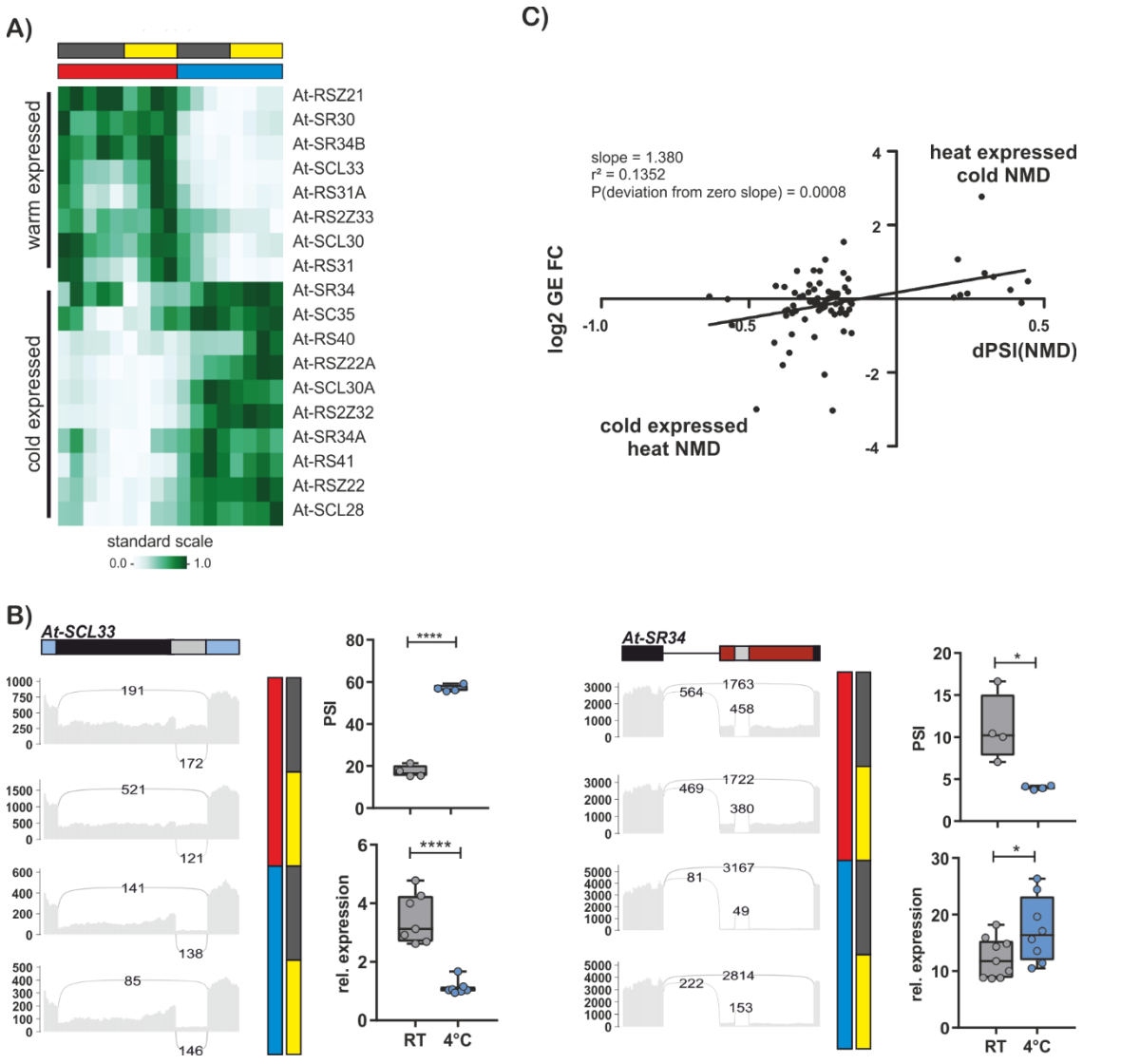

Figure 2.1-6: Temperature-dependent AS-NMD is present in *A. thaliana* SR proteins and is a general regulator of GE. A) Heatmap of *A. thaliana* SR protein GE during a dark-light and warm-cold time course. B) Sashimi plots and validations (RT-PCR and quantitative real-time PCR) of two exemplary SR proteins that exhibit cold- or heat-induced AS-NMD (left and right, respectively). C) Global correlation of the changes in NMD isoform exclusion and expression of the respective gene between warm and cold temperatures. AN performed all bioinformatical analyses shown in the figure. See Publication Appendix I for further information.

2.2 Alternative isoforms globally regulate membrane trafficking at all stages of the secretory pathway

This subchapter refers to the following publication:

Wilhelmi I, Kanski R, **Neumann A**, Herdt O, Hoff F, Jacob R, Preußner M, Heyd F. Sec16 alternative splicing dynamically controls COPII transport efficiency. Nat Commun. 2016 Aug 5;7:12347. doi: 10.1038/ncomms12347.

*** Neumann A**, Schindler M, Olofsson D, Wilhelmi I, Schürmann A, Heyd F. Genome-wide identification of alternative splicing events that regulate protein transport across the secretory pathway. JCS. 2019 Apr 25;132(8). pii: jcs230201. doi: 10.1242/jcs.230201.

In a previous study published by the Lynch lab, exons which are alternatively spliced upon T-cell activation were identified using an RNA-seq approach (Martinez *et al.*, 2012). This analysis led to the identification of a splicing switch in SEC16A, where the exon 29 isoform is predominantly formed upon activation. As SEC16A is known to be involved in COPII vesicle formation (see chapter 1.3.1) and since a T-cell needs to prime its secretory pathway for an increased cargo load during activation (see chapter 1.3.2), we speculated that the exon 29 isoform is required for more efficient COPII vesicle formation. We could indeed show that inclusion of this isoform is necessary for the increase in ERES observed during T-cell activation. In accordance with these findings, a CRISPR/Cas9-mediated knock-out of exon 29 in HEK 293T cells lead to reduced ER exit site numbers. Additionally, we could show that the different SEC16A isoforms have distinct interaction abilities with COPII components and therefore suggest that the protein acts as an isoform-specific interaction hub for recruiting COPII components (summarised in Figure 2.2-1).

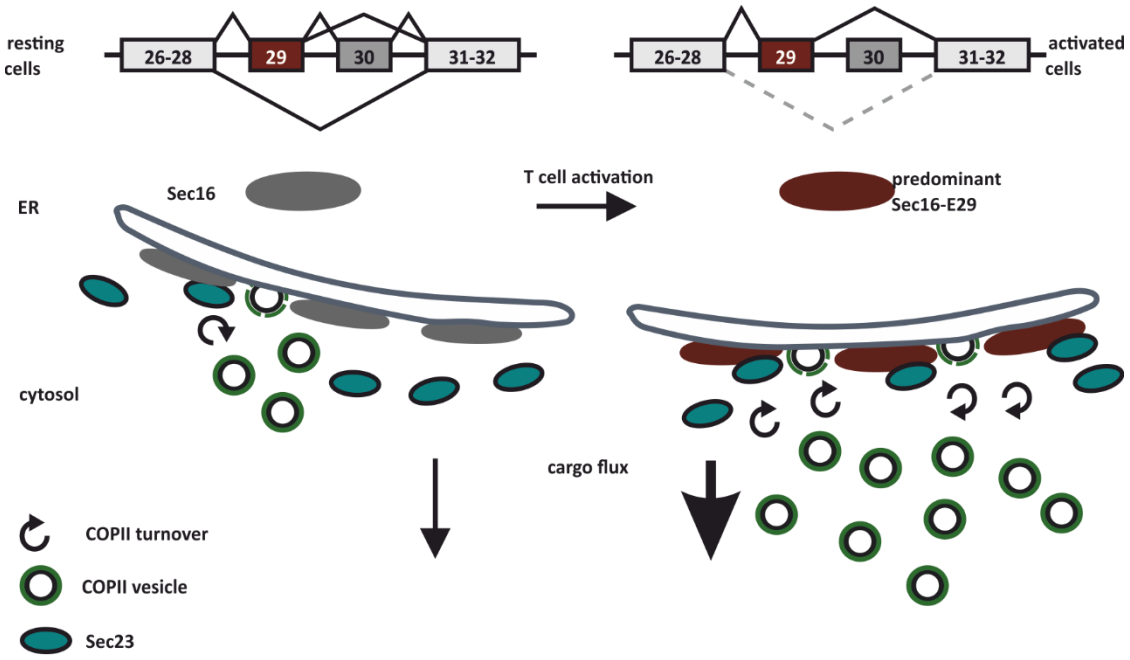

Figure 2.2-1: Sec16 dynamically controls COPII efficiency. Summary of Wilhelmi *et al.*, 2016, see Appendix D for further information. AN performed αSEC24C stainings, imaging and analysis during revision of the publication (not shown).

We thus found the first example of AS-dependent regulation of the early secretory pathway. Although our study and a few others implicated single AS events in the control of the secretory pathway (see chapter 1.3.3), no systematic approach had been taken to elucidate the impact of AS on the secretory pathway in a global manner. To investigate this in detail, we used KD RNA-seq data from four RBPs that were previously implicated in regulating protein secretion (Figure 2.2-2A). We argued that these RBPs would not have a direct effect on trafficking, but rather indirect by regulating AS of secretion-associated targets (Figure 2.2-2B). Using the RNA-seq data, we analysed differential alternative splicing between control and KD and then extracted events that were significantly differential in at least three of the analyses. This yielded over 200 events which we termed secretion-related AS events (Figure 2.2-2A, C).

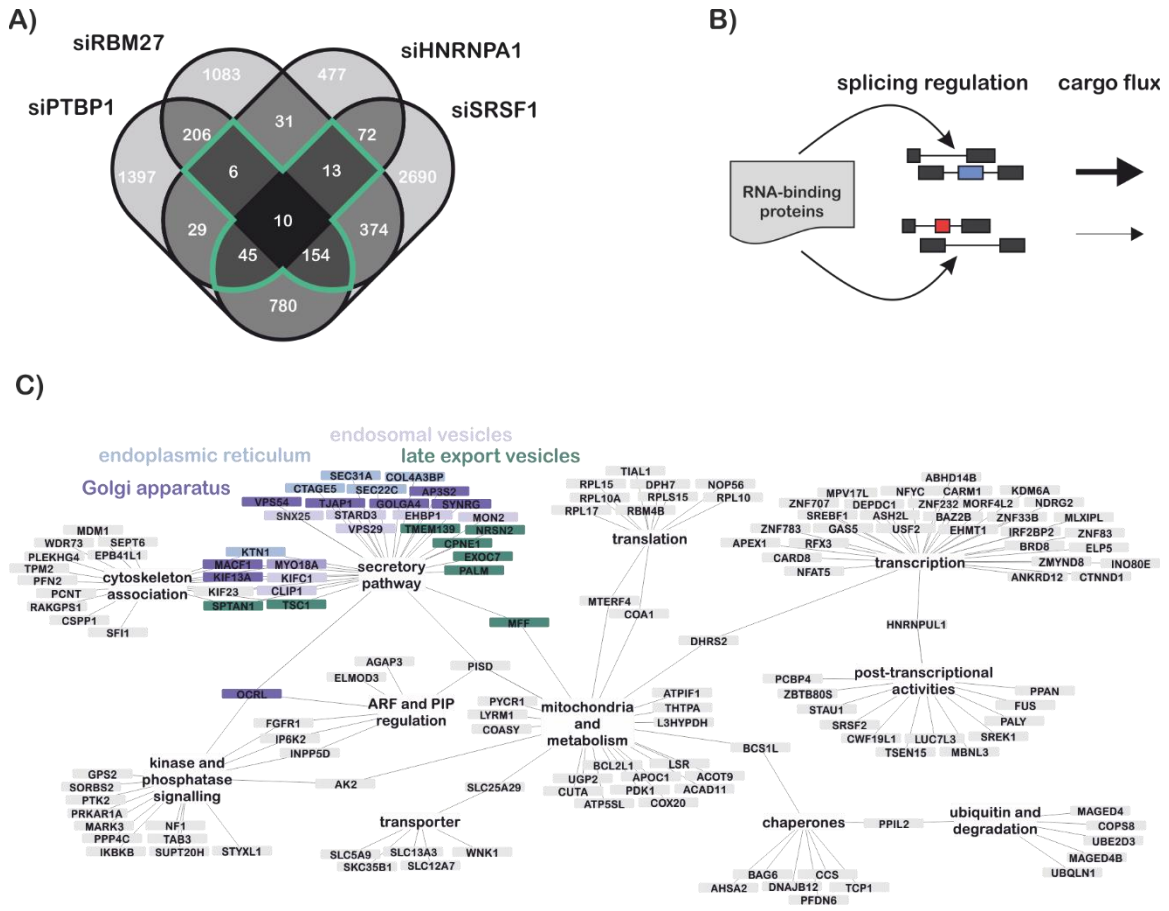

Figure 2.2-2: Genome-wide identification of secretion-related AS events. A) Genome-wide identification of secretion-related AS events. B) Model how RBPs indirectly regulate cargo flux. C) Classification of the secretion-related AS events. AN performed all analyses shown in the figure. See Appendix H for further information.

After establishing the retention using selective hooks (RUSH) system (Boncompain *et al.*, 2012) to reliably quantify protein transport capacities of cells (Figure 2.2-3A), we manipulated AS of four implicated secretion-related AS events (SEC31A exon 24, SEC22C exon 7, OCRL exon 19 and EXOC7 exon 7) using Morpholinos (MOs [ABBR]) and CRISPR/Cas9-mediated exon KO analysis (Figure 2.2-3B, C). We could validate a reduced ER-to-PM trafficking of a glycosyl-phosphatidyl-inositol – green fluorescent protein (GPI-GFP) reporter for all the tested cases, thereby validating the *in-silico* analysis (Figure 2.2-3D-F).

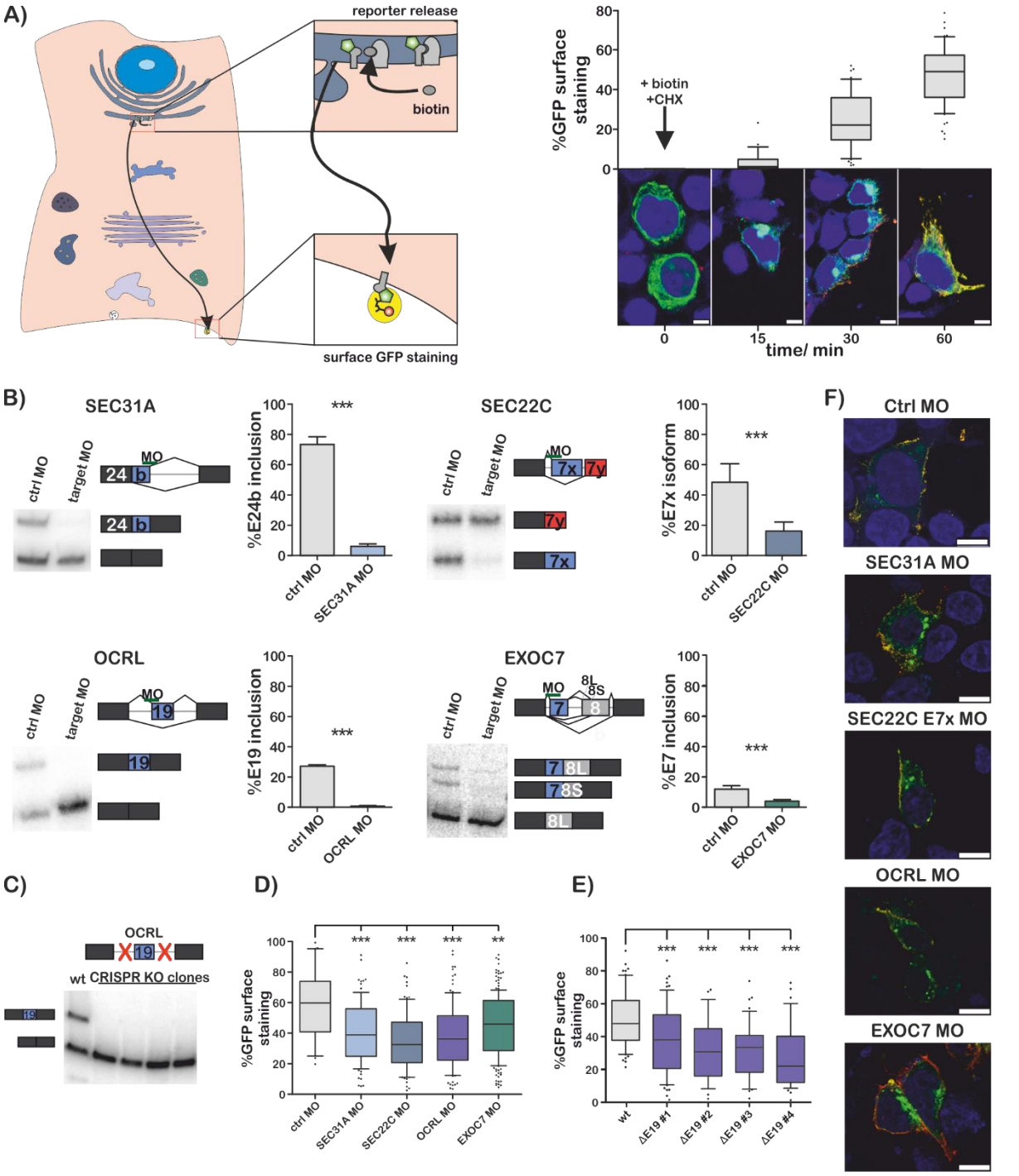

Figure 2.2-3: Validation of an isoform-specific transport phenotype for all tested targets. A) Model explaining the RUSH system (left) with an exemplary time course experiment (right). B) Manipulation of AS using MOs. C) Manipulation of AS using CRISPR. D) RUSH qualifications after MO treatment. E) RUSH quantification of CRISPR cells. F) Representative images of the RUSH assay. AN performed all experiments shown in the figure with support from MS. See Appendix H for further information.

We furthermore investigated the tissue-specificity and could show that these secretion-related AS events are regulated in a highly tissue-specific manner (Figure 2.2-4A, B). Lastly, we used T-cell activation and adipocyte differentiation as model systems for cells that transform from a state with low secretory potential to a secretion-heavy state (Figure 2.2-4C). We identified differential AS events in naïve versus activated T cells as well as SGBS adipocyte cells pre- and post-differentiation using publicly available RNA-seq datasets. In both systems, a highly significant number of secretion-related AS events were differentially regulated during activation and differentiation, showcasing the biological importance of these isoforms (Figure 2.2-4D, E). Additionally, we found that while T cells modulated secretion-associated splicing events of the whole secretory pathway during their activation, the SGBS adipocytes mainly adapted events in targets that are connected to post-Golgi trafficking (Figure 2.2-4E). At the same time, adipocytes exhibited an upregulation of COPII component expression (not shown), potentially explaining the absence of a splicing-dependent regulation in this part of the secretory pathway.

This might indicate that splicing-dependent modulation of membrane trafficking is especially crucial in dynamic regulation settings: On the one hand, activated T-cells have extreme requirements to their complete secretory pathway, as they transport large amounts of cytokines from the ER out of the cell. In adipocytes on the other hand, while exporting adipokines from the ER is also of importance, a crucial task is the insulin-dependent shuttling of the glucose transporter GLUT4 from post-Golgi vesicles to the PM and back. This happens in a highly dynamic fashion (minutes to hours), while the pre-Golgi transport machinery can be adapted to higher cargo loads during the relatively long time of differentiation (weeks).

Together, these data show that AS controls the secretory pathway in all of its stages. Moreover, this regulation is highly tissue-, activation- and differentiation-specific. The data also indicate that AS-mediated adaptations of membrane trafficking might be particularly effective in an intermediate time frame, supplementing the short-term regulation by kinases and phosphatases and the long-term regulation by transcriptional changes.

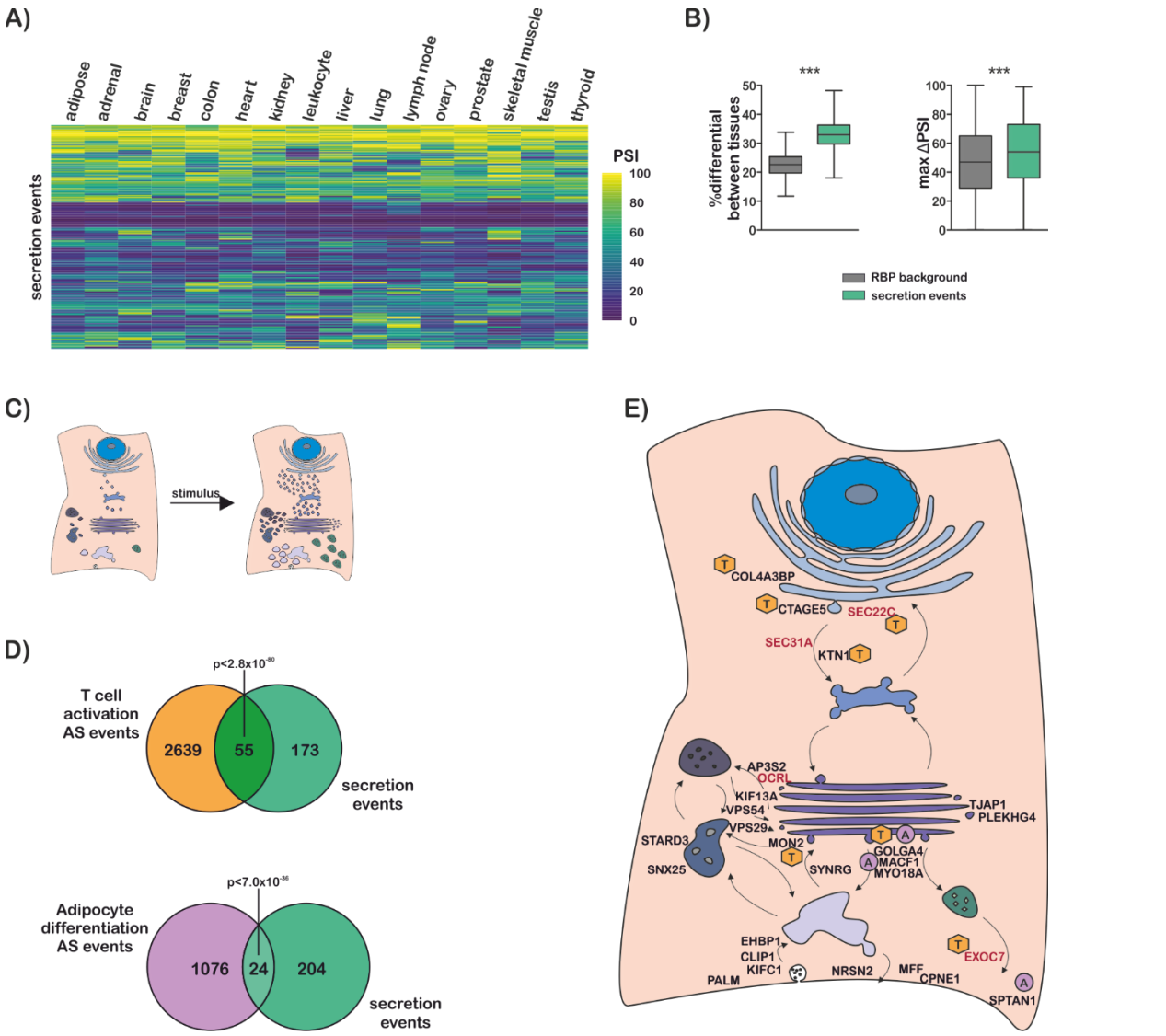

Figure 2.2-4: The secretion-related AS events are regulated in a highly tissue-, activation- and differentiation-specific manner. A) Inclusion levels of the secretion-related AS events in different tissues. B) Variability and specificity measures of the secretion-related AS events compared to background events. C) Model of a cell that upregulates its secretory capacity upon stimulus. D) Overlap of differential isoform expression upon T cell activation (top) or adipocyte differentiation (bottom) with the secretion-related AS events. E) Model how AS regulates protein transport across the secretory pathway. AN performed all analyses shown in the figure. DO performed primary analysis for figures A and B. See Appendix H for further information.

2.3 Discovery of disease-associated genomic mutations that lead to mis-splicing or differential alternative splicing

This subchapter refers to the following publication:

* Herdt O[#], **Neumann A[#]**, Timmermann B, Heyd F. The cancer-associated U2AF35 470A>G (Q157R) mutation creates an in-frame alternative 5' splice site that impacts splicing regulation in Q157R patients. RNA. 2017 Dec;23(12):1796-1806. doi: 10.1261/rna.061432.117

[#] These authors contributed equally to this work.

So far, this dissertation revolved around endogenous factors (temperature or stimulation/ differentiation triggers), that lead to an adjustment of AS. However, it has been described that disease-associated genomic mutations can also impact both constitutive and alternative splicing, especially when spliceosomal components are affected (Maciejewski and Padgett, 2012; Keightley *et al.*, 2013; Yoshida and Ogawa, 2014). In this case, we investigated two cancer-associated mutations in the splicing factor U2AF35 (also called U2AF1) in the second zinc finger of the protein. Both were previously classified as missense mutations, leading to substitution of the glutamine by arginine (c.470A>G, Q157R) and proline (c.470A>C, Q157P), respectively. While this classification is true for the latter mutation, the c.470A>G mutation actually leads to the creation of an in-frame alternative 5’ splice site (Figure 2.3-1A). Usage of this splice site causes deletion of four amino acids in addition to the glutamine-to-arginine substitution (Figure 2.3-1B).

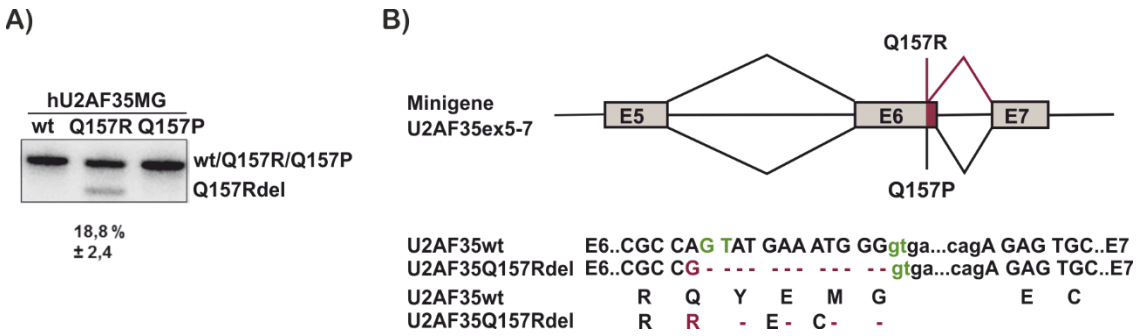

Figure 2.3-1: The U2AF35 Q157R mutation leads to creation of a cryptic splice site. A) Identification of cryptic splicing upon U2AF35 Q157R mutation. B) Implications of the U2AF35 Q157R deletion variant on mRNA and protein level. Experiments were performed by OH. See Appendix F for further information.

As this deletion lies within the second zinc finger domain which is involved in 3' splice site recognition of target exons, we investigated the effect of these mutant proteins (Q157P, Q157R and Q157R deletion variant) on splicing regulation. To this end, we knocked-down endogenous U2AF35 in HEK 293T cells and rescued with expression constructs for either the wild-type or one of the mutant proteins (Figure 2.3-2A). Using the wild-type rescue, we identified U2AF35-specific target exons and then compared the rescue abilities of the mutant proteins using both RT-PCR and RNA-seq analyses (Figure 2.3-2B, C). Of the 535 exons that showed differential inclusion upon knock-down and rescue by wild-type U2AF35, the mutants could rescue between 238 (Q157R deletion) and 354 (Q157R). While about 100 exons could be universally rescued by all the variants, there were between 19 (Q157P) and 111 (Q157R deletion) targets unique to their specific mutant protein. Of note, the deletion variant showed the most distinct rescue behaviour of the mutants, while Q157P and Q157R exhibited more similar splicing patterns. We next retrieved the 3' splice site sequences of the exons which were uniquely rescued by only one mutant to obtain individual consensus motifs for them. In this way, we identified striking binding preferences at the +1 position, validating that these three mutants regulate AS of distinct exons via differential splice site specificities (Figure 2.3-2B).

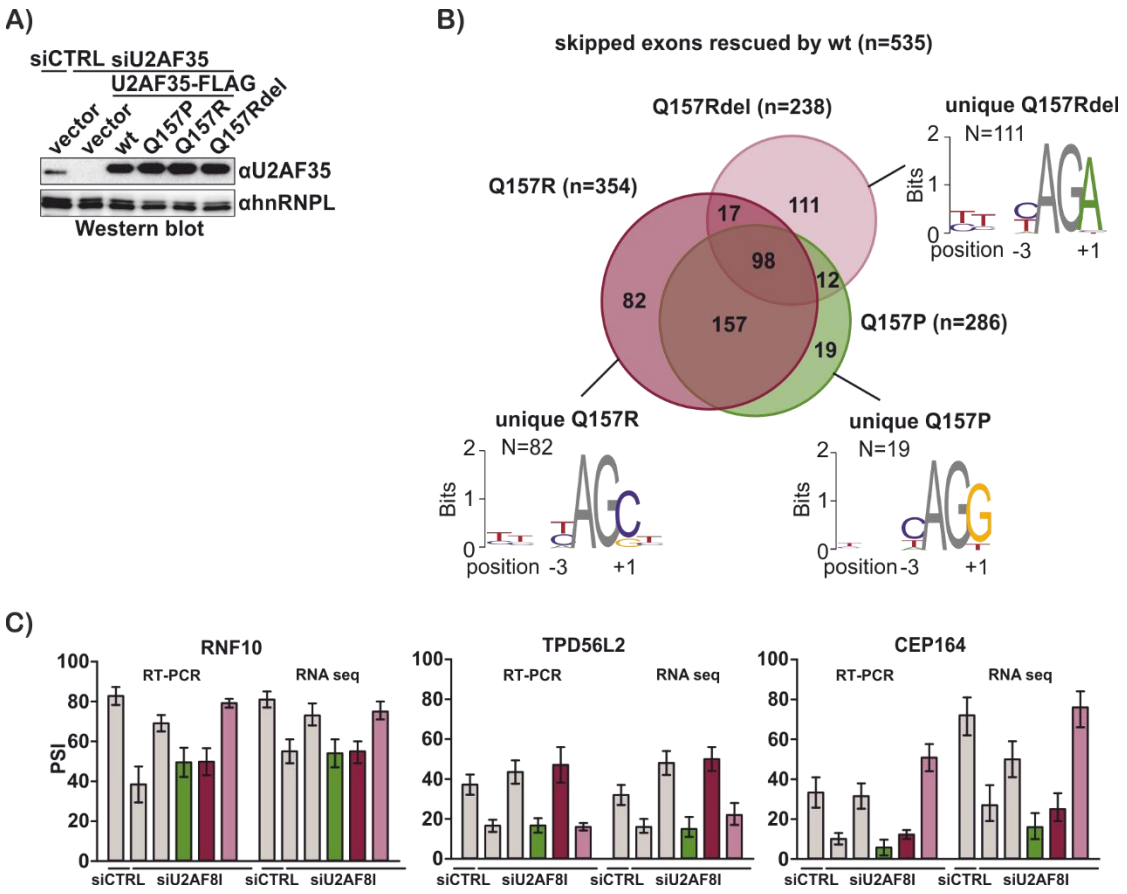

Figure 2.3-2: Identification of U2AF35 mutant-specific splice site preferences. A) Western Blot validating the KD-complementation assay. B) Identification of unique binding preferences of the individual mutant proteins. C) Comparison of AS ratios obtained from RT-PCR and RNA-seq. AN performed bioinformatical analyses shown in B and C. See Appendix F for further information.

Finally, we addressed the biological impact of these findings. To this end, we queried 533 acute myeloid leukemia (AML) patient RNA-seq datasets and identified patients with a c.470A>G (Q157R) or c.470A>C (Q157P) mutation. We initially revealed distinct splicing patterns between the two mutant groups (Figure 2.3-3A) – an analysis that had been neglected in the literature so far (Qiu *et al.*, 2016). We then compared splicing of alternative exons between the mutant patients and patients without a mutation in U2AF35 at that position and could largely recapitulate the findings we observed in the KD-complementation assay (Figure 2.3-3B-D). Lastly, we detected the presence of the Q157R deletion variant at RNA level in the c.470A>G patients as predicted, although at low levels (Figure 2.3-3E). This variant however seems to have an effect, which we demonstrated for several individual targets (Figure 2.3-3F). In these cases, the c.470A>G patients exhibit some target exons whose splicing is more similar to the cells complemented with the

U2AF35 Q157R deletion protein variant, instead of the Q157R substitution variant. In most of these examples, we observed an A at the +1 position of the targets' exon splice site, which – as previously determined – corresponds to the preferred binding sequence for the deletion variant.

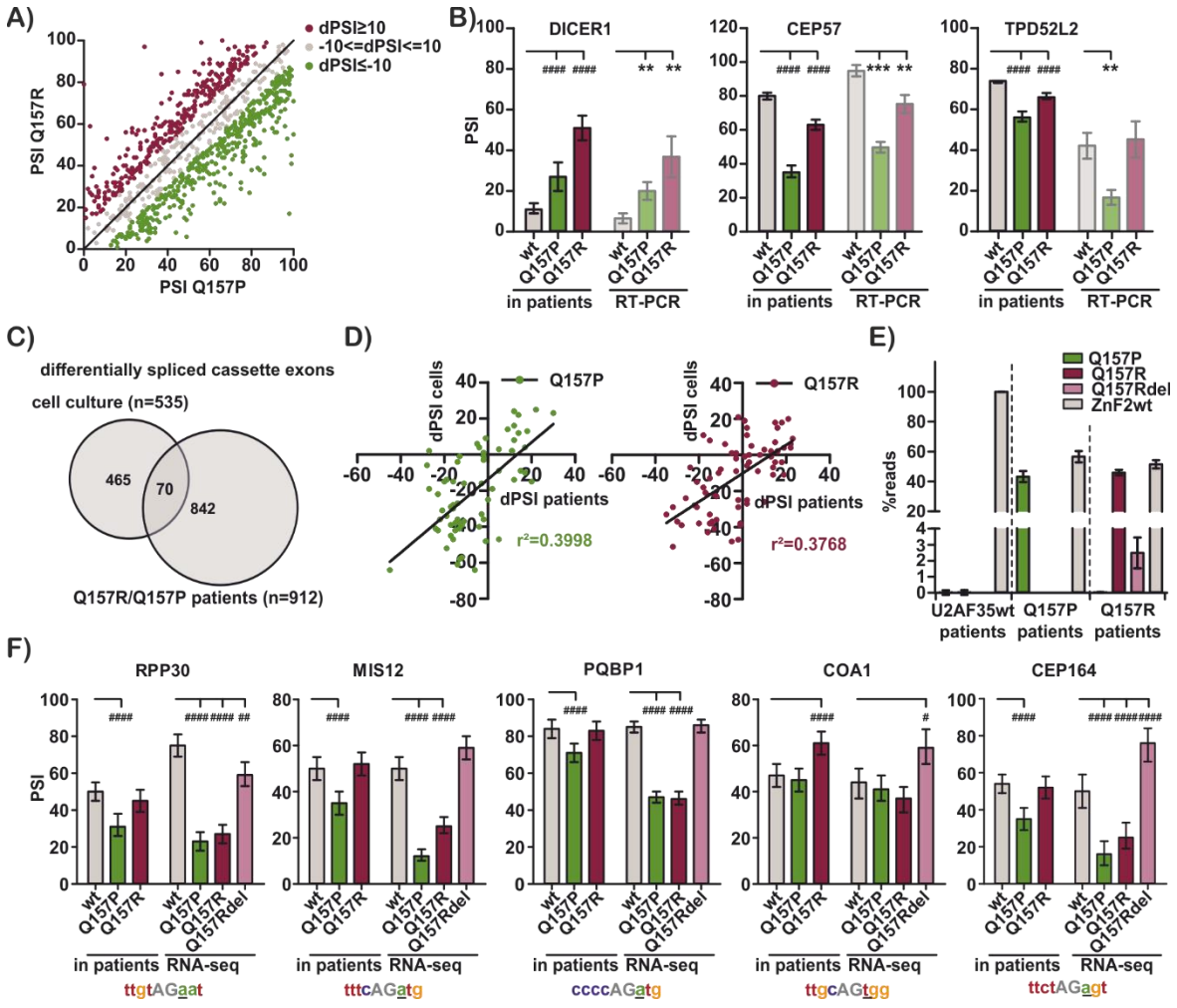

Figure 2.3-3: The KD-complementation assay recapitulates findings from patient data. A) Comparison of AS patterns between patients with the Q157R and Q157P mutation. B) Splicing ratios from patient RNA-seq and KD-complementation assay RT-PCR. C) Overlap between exons that were identified in the KD-complementation assay and exons that are differential between U2AF35 wt and U2AF35 Q157R/P mutant patients. D) Correlation of mutant patient inclusion levels and inclusion levels upon KD and complementation with the respective mutant protein. E) Identification of mutant reads in patients. F) Comparison of patient and KD-complementation inclusion levels for exemplary targets. AN performed bioinformatical analyses shown in A-F. See Appendix F for further information.

In summary, this study characterised two cancer-associated mutations in U2AF35 gene regarding their differential splice site binding preferences and the resulting differential splicing patterns. In

addition, we described an example of an exonic missense mutation that leads to the creation of a novel splice site, therefore deleting parts of the resulting protein instead of just substituting one amino acid. Such a mechanism has been reported, but our work stresses once more how important it is to consider changes on RNA level (splicing, mRNA stability, translation efficiency) when investigating supposed missense mutations.

Chapter 3. Discussion

3.1 Alternative splicing is regulated in highly dynamic settings to achieve rapid changes in biological function

In the works summarised above, we describe how rhythmic, circadian-like alternative splicing patterns are obtained via the Clk-dependent phosphorylation of SR proteins (for a differentiation between real circadian rhythms and circadian like, temperature controlled rhythms, see Preußner and Heyd, 2018). We additionally showcase how Tbp alternative splicing in the 5' UTR leads to cycling transcription levels of its target genes. Furthermore, we identified temperature-dependent AS of NMD isoforms as a mechanism to generate cycling GE patterns. The upregulation of NMD-inducing isoforms functions as autoregulatory feedback loop in SR proteins and potentially many other RNA-binding proteins. Strikingly and contrary to our findings, such autoregulatory feedback loops are usually thought to lead to steady-state levels instead of cycling patterns (Lareau *et al.*, 2007), a paradigm that needs to be revisited. Taken together, we describe a highly interconnected network of kinases, RBPs and hundreds of splicing targets. Regulation of a vast amount of cellular processes in a time of the day-dependent manner clearly has immense potential and the biological implications of this network remain to be investigated. Temperature-dependent AS, especially the governance of NMD isoform levels, is extremely conserved across not only mammals and plants (as shown in Neumann *et al.*, 2019), but also insects and reptilians. Strikingly, the temperature range in which splicing is regulated corresponds to the temperature ranges that the organism experiences (Haltenhof *et al.*, in preparation). We can therefore speculate that temperature-controlled AS is an ancient mechanism, potentially evolved to adapt cells to changing ambient temperatures. It has since been adopted in higher organisms to enable the adaptation to daily rhythms.

Other highly dynamic settings in which AS was shown to have a large impact are activation and differentiation processes, for example T-cell activation (Heyd and Lynch, 2011). The presented works identified hundreds of AS events that are involved in the secretory pathway and showed how these events are adapted during T-cell activation and adipocyte differentiation, in which cells need

to adapt their membrane trafficking machinery to higher cargo load. Interestingly, this regulation does not seem to happen during B-cell activation, in which only minor changes in AS were globally observed despite drastically increased cytokine and antibody export (based on analysis of publicly available RNA-seq datasets, not shown). These findings and the highly tissue-specific usage of the identified secretion-related AS events leads to the question how and why these events are regulated. Integration of AS and GE data from further RNA-seq datasets, together with analyses of sequence motifs and potentially crosslink immunoprecipitation (CLIP)-sequencing data could give further insights into *cis*-regulatory elements and *trans*-acting factors of the AS events. This however was beyond the scope of the current dissertation. Further research approaches should go both deeper and wider: Many of the identified events could be explored in mechanistic detail to understand the unique capabilities of the alternative isoforms. In the case of SEC22C, it has been shown that the isoforms differ in the number of transmembrane domains, which leads to differential localization (Yamamoto, Yurugi and Sakisaka, 2017). A wider approach would be to systematically investigate all or at least a majority of secretion-related AS events to globally validate and quantify their involvement in membrane trafficking. To this end, a CRISPR-based screening method could be used in combination with a high-throughput RUSH assay.

Changes in secretion-related AS are dynamically controlled and a connection with the daily regulation of splicing is to be expected. There are several studies in which time of the day-dependent secretion has been shown, for example in cortisol secretion (Cervantes *et al.*, 2001), melatonin (Foulkes *et al.*, 1996), the intestinal hormone GLP-1 (Gil-Lozano *et al.*, 2014) or adrenal glucocorticoid (Chung, Son and Kim, 2011). A splicing-based mechanism should be considered for these examples and remains to be investigated.

3.2 Genomic mutations are implicated in splicing regulation and cryptic splicing

We investigated two cancer-associated mutations in U2AF35 and characterised their distinct 3' splice site binding preferences. Furthermore, we identified a novel ss that is created by one of the mutations and caused exclusion of 12 nucleotides in the mature mRNA and therefore a protein with a four amino acid deletion. This ss was shown to be used in patients with that specific mutation and to have an impact on the regulation of U2AF35 target exons.

The effect of genomic mutations on splicing has been reported and there are several recent studies which try to globally address the question what proportion of currently annotated missense-mutations are in fact mutations that lead to aberrant splicing (Xiong *et al.*, 2015; Lee *et al.*, 2017; Baeza-Centurion *et al.*, 2019; Jaganathan *et al.*, 2019). These efforts culminated in a collaboration of groups from the Illumina Artificial Intelligence Laboratory, University of California, Stanford University and the Broad Institute (Harvard) that developed a tool called SpliceAI. The authors trained a deep neural network to classify splice sites and calculate a "usage probability". Using this network, it is possible to find and differentiate between constitutive and alternative splice sites solely with information about the primary mRNA sequence (Jaganathan *et al.*, 2019). If SpliceAI works as described, it has the potential to identify genomic mutations that alter ss usage or lead to creation of a novel ss, which is thought to be a frequent outcome of disease-causing mutations (Scotti and Swanson, 2016).

Before publication of these recent papers, I have started a project to globally assess the impact of genomic mutations on cryptic splice site usage. The computational work in this project was largely performed by Felix Peppert, while I operated as supervisor and contributed in the wet-lab part of the project. We improved the method that was used to identify patients with the c.470A>G mutations in Herdt *et al.*, 2017 and to test for usage of the new ss. Our generalised approach was to query human patient RNA-seq data, align these to the human genome using the STAR aligner (Dobin *et al.*, 2013) and then a) perform variant calling to identify genomic mutations and b) query for splice junctions that were previously not annotated. Novel splice junctions were only accepted when at least one of the splice sites used was previously annotated. We then associated the identified mutations with the novel splice junctions if they occurred in proximity of one another. If such associations were found in several patients in reciprocal fashion (the mutation is always

associated to the same and only this novel ss and this novel ss is always associated to only this specific mutation), the mutation was accepted as an effector of the aberrant splicing pattern. We continuously analysed RNA-seq data and parsed the results into a database, together with information about the usage of this novel ss and further meta-data. To validate the approach, we generated wild-type and mutant minigene constructs for some of the examples, transfected them separately into HEK 293T cells and then performed RT-PCR analysis (similar as in Herdt *et al.*, 2017). One example was a disease-associated mutation in SURF1, which mediates cytochrome C oxidase assembly (Williams *et al.*, 2004; Stiburek *et al.*, 2005). The intronic mutation leads to usage of a cryptic 5' ss and a drastically altered C terminus, which is essential for its protein function (Zhu *et al.*, 1998). The new splice junction was used in 23% of cases. We tested the effect of the mutation using the validation approach described above and could indeed show the predicted novel splice isoform present in cells transfected with the mutant minigene, but not in the wild type transfected cells.

Unexpectedly, we found many associations where a mutation was several kilobases distant from the novel splice junction. This was not in concordance with the current model, where splice site strength and splice site recognition is thought to be mainly influenced by the sequence of a few hundred nucleotides around the splice site (Barash *et al.*, 2010). However, our finding has been substantiated recently, as Jaganathan *et al.*, 2019 reported that elements multiple kilobases distant from a splice site influenced its strength.

Although our approach worked in principle, the bottleneck clearly was the limited amount of computing power we could apply to the task. With the current analysis pipeline and hardware, we would have needed years to compile a comprehensive database of mutations that could be associated with usage of novel or cryptic splice sites. In addition, the recent publications mentioned above used similar or more sophisticated approaches coupled to substantially higher computational resources. We therefore halted the project at this stage, but still could show the immense potential of using the plethora of available RNA-seq data for addressing such global questions.

3.3 Leveraging RNA-sequencing data enables biological insight

This work shines light on the changes of alternative mRNA splicing upon induction of exogen or endogen factors. It clearly displays the potential of RNA-seq analyses both using internally generated and publicly available data. During my time in the Heyd lab, I have tested and established numerous NGS analysis and meta-analysis tools and pipelines and experienced their advantages and disadvantages: I initially used the "true" read-mappers TopHat (Trapnell, Pachter and Salzberg, 2009) (slow, with medium-high requirements and inefficient memory usage) and later STAR (Dobin *et al.*, 2013) (very fast, but with extremely high memory requirements). With the advent of quasi-alignment, I also established mapping with Whippet (Sterne-Weiler *et al.*, 2018), Salmon (Patro *et al.*, 2017) and Kallisto (Bray *et al.*, 2016) (fast, with low requirements, but with specialised output). Read-mapping tools have been independently evaluated and it was found that the STAR aligner is currently the superior "true" alignment software. Whippet is a very recent tool and its alignment ability needs to be tested more thoroughly. From initial tests it produces slightly different results in comparison to STAR, but whether these are better or worse needs to be evaluated. Salmon and Kallisto can effectively only be used for GE analyses, as they lack the option to output alignment tracks. These are needed for many secondary analyses, visualizations and usually also for AS analysis.

Gene expression analysis was initially performed using the Cufflinks suite (Trapnell *et al.*, 2012), later a combination of STAR gene quantification and DESeq2 (Dobin *et al.*, 2013; Love, Huber and Anders, 2014) or the Whippet (Sterne-Weiler *et al.*, 2018) gene quantification option together with custom scripts. Additionally, I tested Salmon (Patro *et al.*, 2017) for quasi-alignment with immediate quantification. Currently, STAR-DESeq2 seems to be the gold-standard, but quasi-aligners like Salmon (and Kallisto) claim to produce very accurate results for transcript quantification (Bray *et al.*, 2016; Patro *et al.*, 2017). These can be used instead of the STAR quantification to feed into the DESeq2 software. As mentioned, a drawback of Salmon and Kallisto is that they cannot be used for downstream analysis other than transcript or GE for which they are designed. This means that for a pipeline that uses Salmon for GE quantification, the reads still need to be aligned separately to perform other analyses. Whippet is not restricted in this case and indeed produces alignment files for downstream analyses and at the same time outputs files for transcript and GE levels. It should however be mentioned that this output drastically increases time requirements.

Regarding AS analysis, I initially used the mixture of isoforms (MISO) tool (Katz *et al.*, 2010) which seems to produce reliable results, but has relatively high computational and time requirements. MISO also does not inherently handle replicates, which requires the user to build workarounds. One of the possibilities is to compare each replicate of one condition to each replicate of the other. In my experience, this leads to highly valid results but also a high false-negative rate. If the investigator is interested in only the most significant changes, this approach is completely respectable. If, however the number of true positive hits should be maximised, a different mode of analysis needs to be used. Another possibility is to just merge all replicate alignments before running MISO, which leads to very inclusive results with higher false-positive rates. After its release I also tested Whippet (Sterne-Weiler *et al.*, 2018) for splicing quantifications. This tool runs extremely fast with low requirements. Additionally, it needs to be stressed that it relieves many obstacles a bioinformatician needs to overcome when using MISO (e.g. replicate handling, general "clunkiness" of the program). Furthermore, Whippet is capable of true *de-novo* identification of AS events, which is not possible with MISO. Unfortunately, Whippet tends to over-predict transcription start and transcription end sites. These two categories usually make up the great majority of identified differential AS events. When investigating these further, they usually seem to be artefacts (sometimes they are only a few base pairs apart and often they are not visible at all in the alignment tracks). This is not always the case however - the Cirbp NMD isoform identified in Neumann *et al.*, 2019 was for example classified as transcription end site. This leads to an unpleasant situation where these events cannot be filtered out to not lose important information but leaving them in leads to a high number of false-positive events. It should be noted that these findings are not validated on large scale and should therefore be considered my personal opinion. Didrik Olofsson and I are currently evaluating different AS analysis tools and investigating how to improve the output of the tools or even develop a new tool that more accurately calculates AS ratios.

As shown in this dissertation, combining AS and GE analyses from several datasets can be a first step towards gaining a deeper biological understanding. Another step could be to include further analyses that can be applied to the same datasets (for example about alternative poly-adenylation, see Ha, Blencowe and Morris, 2018). Furthermore, different types of RNA-seq protocols can be applied to research questions. For AS analysis especially, it makes sense to incorporate CLIP-seq data that already is available for many RBPs (Van Nostrand *et al.*, 2016) to identify *trans*-acting

factors. Integrating the plethora of publicly available data and available post-analysis tools enables researchers to gain biological insights that were unimaginable a decade ago.

The use of NGS drastically increases in nearly all biological research settings. With the decrease in cost, sequencing is feasible even for groups with limited financial capabilities. In addition, public data can be re-used by anyone who is able to work with NGS data. For these reasons, the computational analysis is becoming a bottleneck in many projects. There is a large need for skilled bioinformaticians that can reliably perform these analyses. Moreover, existing and new tools need to be evaluated and integrated into the computational pipelines if they prove valuable. Lastly, meta-analyses of the results are vital for generating biologically meaningful results.

In short, this study clearly demonstrates the power of analysing RNA-seq datasets by uncovering new insights into RNA splicing mechanisms and proves the high potential of NGS for virtually any research project in the field of biology.

References

Adnan, M. *et al.* (2019) 'Diverse Role of SNARE Protein Sec22 in Vesicle Trafficking, Membrane Fusion, and Autophagy', *Cells 2019, Vol. 8, Page 337*. Multidisciplinary Digital Publishing Institute, 8(4), p. 337. doi: 10.3390/CELLS8040337.

Adolf, F. *et al.* (2016) 'Sec24C/D-isoform-specific sorting of the preassembled ER-Golgi Q-SNARE complex', *Molecular Biology of the Cell*, 27(17), pp. 2697–2707. doi: 10.1091/mbc.E16-04-0229.

Antonny, B. and Schekman, R. (2001) 'ER export: Public transportation by the COPII coach', *Current Opinion in Cell Biology*. doi: 10.1016/S0955-0674(00)00234-9.

Ashburner, M. *et al.* (2000) 'Gene ontology: tool for the unification of biology. The Gene Ontology Consortium.', *Nature genetics*. NIH Public Access, 25(1), pp. 25–9. doi: 10.1038/75556.

Baeza-Centurion, P. *et al.* (2019) 'Combinatorial Genetics Reveals a Scaling Law for the Effects of Mutations on Splicing.', *Cell*. Elsevier, 176(3), pp. 549-563.e23. doi: 10.1016/j.cell.2018.12.010.

Barash, Y. *et al.* (2010) 'Deciphering the splicing code.', *Nature*. Nature Publishing Group, 465(7294), pp. 53–59. doi: 10.1038/nature09000.

Barbosa-Morais, N. L. *et al.* (2012) 'The evolutionary landscape of alternative splicing in vertebrate species.', *Science (New York, N.Y.)*. American Association for the Advancement of Science, 338(6114), pp. 1587–93. doi: 10.1126/science.1230612.

Bark, I. C. *et al.* (1995) 'Differential expression of SNAP-25 protein isoforms during divergent vesicle fusion events of neural development.', *Proceedings of the National Academy of Sciences of the United States of America*. National Academy of Sciences, 92(5), pp. 1510–4. doi: 10.1073/pnas.92.5.1510.

Bark, I. C. and Wilson, M. C. (1994) 'Human cDNA clones encoding two different isoforms of the nerve terminal protein SNAP-25', *Gene*. Elsevier, 139(2), pp. 291–292. doi: 10.1016/0378-

1119(94)90773-0.

Bell-Pedersen, D. *et al.* (2005) ‘Circadian rhythms from multiple oscillators: lessons from diverse organisms.’, *Nature reviews. Genetics*. NIH Public Access, 6(7), pp. 544–56. doi: 10.1038/nrg1633.

Bhadra, U. *et al.* (2017) ‘Evolution of circadian rhythms: from bacteria to human’, *Sleep Medicine*. Elsevier, 35, pp. 49–61. doi: 10.1016/J.SLEEP.2017.04.008.

Black, D. L. (2003) ‘Mechanisms of Alternative Pre-Messenger RNA Splicing’, *Annual Review of Biochemistry*. Annual Reviews 4139 El Camino Way, P.O. Box 10139, Palo Alto, CA 94303-0139, USA, 72(1), pp. 291–336. doi: 10.1146/annurev.biochem.72.121801.161720.

Blau, J. and Young, M. W. (1999) ‘Cycling vrille Expression Is Required for a Functional Drosophila Clock’, *Cell*. Cell Press, 99(6), pp. 661–671. doi: 10.1016/S0092-8674(00)81554-8.

Blue, R. E. *et al.* (2018) ‘How alternative splicing affects membrane-trafficking dynamics’, *Journal of Cell Science*, 131(10), p. jcs216465. doi: 10.1242/jcs.216465.

Bodenstein, C., Heiland, I. and Schuster, S. (2012) ‘Temperature compensation and entrainment in circadian rhythms’, *Physical Biology*. IOP Publishing, 9(3), p. 036011. doi: 10.1088/1478-3975/9/3/036011.

Boncompain, G. *et al.* (2012) ‘Synchronization of secretory protein traffic in populations of cells’, *Nature Methods*, 9(5), pp. 493–498. doi: 10.1038/nmeth.1928.

Borgese, N. (2016) ‘Getting membrane proteins on and off the shuttle bus between the endoplasmic reticulum and the Golgi complex’, *Journal of Cell Science*, 0, pp. 1–9. doi: 10.1242/jcs.183335.

Boumil, R. M. *et al.* (2010) ‘A Missense Mutation in a Highly Conserved Alternate Exon of Dynamin-1 Causes Epilepsy in Fitful Mice’, *PLoS Genetics*. Edited by G. S. Barsh. Public Library of Science, 6(8), p. e1001046. doi: 10.1371/journal.pgen.1001046.

Bray, N. L. *et al.* (2016) ‘Near-optimal probabilistic RNA-seq quantification’, *Nature Biotechnology*. Nature Publishing Group, 34(5), pp. 525–527. doi: 10.1038/nbt.3519.

Brinegar, A. E. *et al.* (2017) ‘Extensive alternative splicing transitions during postnatal skeletal muscle development are required for calcium handling functions’, *eLife*, 6. doi:

10.7554/eLife.27192.

Brunner, M. and Schafmeier, T. (2006) ‘Transcriptional and post-transcriptional regulation of the circadian clock of cyanobacteria and Neurospora.’, *Genes & development*. Cold Spring Harbor Laboratory Press, 20(9), pp. 1061–74. doi: 10.1101/gad.1410406.

Buljan, M. *et al.* (2012) ‘Tissue-Specific Splicing of Disordered Segments that Embed Binding Motifs Rewires Protein Interaction Networks’, *Molecular Cell*. Cell Press, 46(6), pp. 871–883. doi: 10.1016/J.MOLCEL.2012.05.039.

Busch, A. and Hertel, K. J. (2012) ‘Evolution of SR protein and hnRNP splicing regulatory factors’, *Wiley Interdisciplinary Reviews: RNA*. John Wiley & Sons, Ltd, 3(1), pp. 1–12. doi: 10.1002/wrna.100.

Cervantes, P. *et al.* (2001) ‘Circadian secretion of cortisol in bipolar disorder.’, *Journal of psychiatry & neuroscience : JPN*. Canadian Medical Association, 26(5), pp. 411–6. Available at: http://www.ncbi.nlm.nih.gov/pubmed/11762208 (Accessed: 6 August 2019).

Chang, L., Adams, R. D. and Saltiel, A. R. (2002) ‘The TC10-interacting protein CIP4/2 is required for insulin-stimulated Glut4 translocation in 3T3L1 adipocytes.’, *Proceedings of the National Academy of Sciences of the United States of America*. National Academy of Sciences, 99(20), pp. 12835–40. doi: 10.1073/pnas.202495599.

Chatterjee, A. *et al.* (2010) ‘Regulation of gustatory physiology and appetitive behavior by the Drosophila circadian clock.’, *Current biology : CB*. Elsevier, 20(4), pp. 300–9. doi: 10.1016/j.cub.2009.12.055.

Chung, S., Son, G. H. and Kim, K. (2011) ‘Adrenal peripheral oscillator in generating the circadian glucocorticoid rhythm’, *Annals of the New York Academy of Sciences*. John Wiley & Sons, Ltd (10.1111), 1220(1), pp. 71–81. doi: 10.1111/j.1749-6632.2010.05923.x.

Colgan, D. F. and Manley, J. L. (1997) ‘Mechanism and regulation of mRNA polyadenylation.’, *Genes & development*. Cold Spring Harbor Laboratory Press, 11(21), pp. 2755–66. doi: 10.1101/GAD.11.21.2755.

Cortijo, S. *et al.* (2017) ‘Transcriptional Regulation of the Ambient Temperature Response by H2A.Z Nucleosomes and HSF1 Transcription Factors in Arabidopsis’, *Molecular Plant*. Cell Press,

10(10), pp. 1258–1273. doi: 10.1016/J.MOLP.2017.08.014.

Coutinho, P. *et al.* (2004) 'Differential requirements for COPI transport during vertebrate early development', *Developmental Cell*, 7(4), pp. 547–558. doi: 10.1016/j.devcel.2004.07.020.

CRICK, F. H. (1958) 'On protein synthesis.', *Symposia of the Society for Experimental Biology*, 12, pp. 138–63. Available at: http://www.ncbi.nlm.nih.gov/pubmed/13580867 (Accessed: 12 February 2019).

Cumming, B. G. and Wagner, E. (1968) 'Rhythmic Processes in Plants', *Annual Review of Plant Physiology*. Annual Reviews 4139 El Camino Way, P.O. Box 10139, Palo Alto, CA 94303-0139, USA , 19(1), pp. 381–416. doi: 10.1146/annurev.pp.19.060168.002121.

D'Arcangelo, J. G., Stahmer, K. R. and Miller, E. a. (2013) 'Vesicle-mediated export from the ER: COPII coat function and regulation', *Biochimica et Biophysica Acta - Molecular Cell Research*. Elsevier B.V., 1833(11), pp. 2464–2472. doi: 10.1016/j.bbamcr.2013.02.003.

Daraio, T. *et al.* (2017) 'SNAP-25b-deficiency increases insulin secretion and changes spatiotemporal profile of Ca2+oscillations in β cell networks', *Scientific Reports*. Nature Publishing Group, 7(1), p. 7744. doi: 10.1038/s41598-017-08082-y.

Darlington, T. K. *et al.* (1998) 'Closing the circadian loop: CLOCK-induced transcription of its own inhibitors per and tim.', *Science (New York, N.Y.)*. American Association for the Advancement of Science, 280(5369), pp. 1599–603. doi: 10.1126/science.280.5369.1599.

Di Giammartino, D. C., Nishida, K. and Manley, J. L. (2011) 'Mechanisms and Consequences of Alternative Polyadenylation', *Molecular Cell*. Cell Press, 43(6), pp. 853–866. doi: 10.1016/J.MOLCEL.2011.08.017.

Dibner, C., Schibler, U. and Albrecht, U. (2010) 'The Mammalian Circadian Timing System: Organization and Coordination of Central and Peripheral Clocks', *Annual Review of Physiology*. Annual Reviews , 72(1), pp. 517–549. doi: 10.1146/annurev-physiol-021909-135821.

Diernfellner, A. C. R. *et al.* (2005) 'Molecular mechanism of temperature sensing by the circadian clock of Neurospora crassa.', *Genes & development*. Cold Spring Harbor Laboratory Press, 19(17), pp. 1968–73. doi: 10.1101/gad.345905.

Dillman, A. A. *et al.* (2013) 'mRNA expression, splicing and editing in the embryonic and adult

mouse cerebral cortex', *Nature Neuroscience*. Nature Publishing Group, 16(4), pp. 499–506. doi: 10.1038/nn.3332.

Dippold, H. C. *et al.* (2009) 'GOLPH3 Bridges Phosphatidylinositol-4- Phosphate and Actomyosin to Stretch and Shape the Golgi to Promote Budding', *Cell*. Cell Press, 139(2), pp. 337–351. doi: 10.1016/J.CELL.2009.07.052.

Dobin, A. *et al.* (2013) 'STAR: Ultrafast universal RNA-seq aligner', *Bioinformatics*, 29(1), pp. 15–21. doi: 10.1093/bioinformatics/bts635.

Dunlap, J. C. and Loros, J. J. (2017) 'Making Time: Conservation of Biological Clocks from Fungi to Animals.', *Microbiology spectrum*. NIH Public Access, 5(3). doi: 10.1128/microbiolspec.FUNK-0039-2016.

Dunne, J. C., Kondylis, V. and Rabouille, C. (2002) 'Ecdysone triggers the expression of Golgi genes in Drosophila imaginal discs via Broad-complex', *Developmental Biology*, 245(1), pp. 172–186. doi: 10.1006/dbio.2002.0632.

Edgar, R. S. *et al.* (2012) 'Peroxiredoxins are conserved markers of circadian rhythms', *Nature*. Nature Publishing Group, 485(7399), pp. 459–464. doi: 10.1038/nature11088.

Ellis, J. D. *et al.* (2012) 'Tissue-Specific Alternative Splicing Remodels Protein-Protein Interaction Networks', *Molecular Cell*. Cell Press, 46(6), pp. 884–892. doi: 10.1016/J.MOLCEL.2012.05.037.

Farhan, H. *et al.* (2008) 'Adaptation of endoplasmic reticulum exit sites to acute and chronic increases in cargo load.', *The EMBO journal*. doi: 10.1038/emboj.2008.136.

Farhan, H. *et al.* (2010) 'MAPK signaling to the early secretory pathway revealed by kinase/phosphatase functional screening', *Journal of Cell Biology*, 189(6), pp. 997–1011. doi: 10.1083/jcb.200912082.

Farhan, H. and Rabouille, C. (2011) 'Signalling to and from the secretory pathway', *Journal of Cell Science*, 124(4), pp. 669–669. doi: 10.1242/jcs.086991.

Farré, E. M. *et al.* (2005) 'Overlapping and Distinct Roles of PRR7 and PRR9 in the Arabidopsis Circadian Clock', *Current Biology*. Cell Press, 15(1), pp. 47–54. doi: 10.1016/J.CUB.2004.12.067.

Forster, R. *et al.* (2006) 'Secretory Cargo Regulates the Turnover of COPII Subunits at Single ER

Exit Sites', *Current Biology*, 16(2), pp. 173–179. doi: 10.1016/j.cub.2005.11.076.

Foulkes, N. S. *et al.* (1996) 'Transcriptional control of circadian hormone synthesis via the CREM feedback loop.', *Proceedings of the National Academy of Sciences of the United States of America*. National Academy of Sciences, 93(24), pp. 14140–5. doi: 10.1073/pnas.93.24.14140.

Fu, X.-D. and Ares, M. (2014) 'Context-dependent control of alternative splicing by RNA-binding proteins', *Nature Reviews Genetics*. Nature Publishing Group, 15(10), pp. 689–701. doi: 10.1038/nrg3778.

Gil-Lozano, M. *et al.* (2014) 'Circadian secretion of the intestinal hormone GLP-1 by the rodent L cell.', *Diabetes*. American Diabetes Association, 63(11), pp. 3674–85. doi: 10.2337/db13-1501.

Giudice, J. *et al.* (2014) 'Alternative splicing regulates vesicular trafficking genes in cardiomyocytes during postnatal heart development', *Nature Communications*. Nature Publishing Group, 5(1), p. 3603. doi: 10.1038/ncomms4603.

Giudice, J. *et al.* (2016) 'Alternative Splicing of Four Trafficking Genes Regulates Myofiber Structure and Skeletal Muscle Physiology.', *Cell reports*. Elsevier, 17(8), pp. 1923–1933. doi: 10.1016/j.celrep.2016.10.072.

Glansdorff, N., Xu, Y. and Labedan, B. (2008) 'The Last Universal Common Ancestor: emergence, constitution and genetic legacy of an elusive forerunner', *Biology Direct*. BioMed Central, 3(1), p. 29. doi: 10.1186/1745-6150-3-29.

Glick, B. S. and Nakano, A. (2009) 'Membrane Traffic Within the Golgi Apparatus', *Annual Review of Cell and Developmental Biology*. Annual Reviews , 25(1), pp. 113–132. doi: 10.1146/annurev.cellbio.24.110707.175421.

Glossop, N. R. *et al.* (1999) 'Interlocked Feedback Loops Within the Drosophila Circadian Oscillator', *Science*. American Association for the Advancement of Science, 286(5440), pp. 766–768. doi: 10.1126/science.286.5440.766.

Glossop, N. R., Lyons, L. C. and Hardin, P. E. (1999) 'Interlocked feedback loops within the Drosophila circadian oscillator.', *Science (New York, N.Y.)*. American Association for the Advancement of Science, 286(5440), pp. 766–8. doi: 10.1126/science.286.5440.766.

Goldammer, G. *et al.* (2018) 'Characterization of *cis* -acting elements that control oscillating

alternative splicing', *RNA Biology*. Taylor & Francis, pp. 1–12. doi: 10.1080/15476286.2018.1502587.

Gotter, A. L. *et al.* (2000) 'A time-less function for mouse Timeless', *Nature Neuroscience*. Nature Publishing Group, 3(8), pp. 755–756. doi: 10.1038/77653.

Gotter, A. L. (2006) 'A Timeless debate: resolving TIM's noncircadian roles with possible clock function.', *Neuroreport*, 17(12), pp. 1229–33. doi: 10.1097/01.wnr.0000233092.90160.92.

Guo, Y. and Linstedt, A. D. (2006) 'COPII-Golgi protein interactions regulate COPII coat assembly and Golgi size', *Journal of Cell Biology*, 174(1), pp. 53–63. doi: 10.1083/jcb.200604058.

Guo, Y., Sirkis, D. W. and Schekman, R. (2014) 'Protein Sorting at the *trans* -Golgi Network', *Annual Review of Cell and Developmental Biology*. Annual Reviews , 30(1), pp. 169–206. doi: 10.1146/annurev-cellbio-100913-013012.

Gurel, P. S., Hatch, A. L. and Higgs, H. N. (2014) 'Connecting the Cytoskeleton to the Endoplasmic Reticulum and Golgi', *Current Biology*. Cell Press, 24(14), pp. R660–R672. doi: 10.1016/J.CUB.2014.05.033.

Ha, K. C. H., Blencowe, B. J. and Morris, Q. (2018) 'QAPA: a new method for the systematic analysis of alternative polyadenylation from RNA-seq data', *Genome Biology*. BioMed Central, 19(1), p. 45. doi: 10.1186/s13059-018-1414-4.

Hamid, F. M. and Makeyev, E. V. (2017) 'A mechanism underlying position-specific regulation of alternative splicing', *Nucleic Acids Research*. Narnia, 45(21), pp. 12455–12468. doi: 10.1093/nar/gkx901.

Hannigan, M. M., Zagore, L. L. and Licatalosi, D. D. (2017) 'Ptbp2 Controls an Alternative Splicing Network Required for Cell Communication during Spermatogenesis.', *Cell reports*. Elsevier, 19(12), pp. 2598–2612. doi: 10.1016/j.celrep.2017.05.089.

Hao, H., Allen, D. L. and Hardin, P. E. (1997) 'A circadian enhancer mediates PER-dependent mRNA cycling in Drosophila melanogaster.', *Molecular and cellular biology*. American Society for Microbiology Journals, 17(7), pp. 3687–93. doi: 10.1128/mcb.17.7.3687.

Harmer, S. L. *et al.* (2000) 'Orchestrated transcription of key pathways in Arabidopsis by the circadian clock.', *Science (New York, N.Y.)*. American Association for the Advancement of

Science, 290(5499), pp. 2110–3. doi: 10.1126/science.290.5499.2110.

Harmer, S. L. (2009) 'The Circadian System in Higher Plants', *Annual Review of Plant Biology*. Annual Reviews , 60(1), pp. 357–377. doi: 10.1146/annurev.arplant.043008.092054.

Haupt, M., Bennett, N. C. and Oosthuizen, M. K. (2017) 'Locomotor Activity and Body Temperature Patterns over a Temperature Gradient in the Highveld Mole-Rat (Cryptomys hottentotus pretoriae)', *PLOS ONE*. Edited by E. M. Mintz. Public Library of Science, 12(1), p. e0169644. doi: 10.1371/journal.pone.0169644.

Hehnly, H. and Stamnes, M. (2007) 'Regulating cytoskeleton-based vesicle motility', *FEBS letters*. NIH Public Access, 581(11), p. 2112. doi: 10.1016/J.FEBSLET.2007.01.094.

Helfrich-Förster, C. *et al.* (2001) 'The circadian clock of fruit flies is blind after elimination of all known photoreceptors.', *Neuron*. Elsevier, 30(1), pp. 249–61. doi: 10.1016/s0896-6273(01)00277-x.

Herdt, O. *et al.* (2017) 'The cancer-associated U2AF35 470A>G (Q157R) mutation creates an in-frame alternative 5' splice site that impacts splicing regulation in Q157R patients', *RNA Journal*, 23, pp. 1796–1806. doi: 10.1261/rna.061432.117.3.

Heyd, F. and Lynch, K. W. (2011) 'DEGRADE, MOVE, REGROUP: Signaling control of splicing proteins', *Trends in Biochemical Sciences*. Elsevier Ltd, 36(8), pp. 397–404. doi: 10.1016/j.tibs.2011.04.003.

Huang, J. *et al.* (2013) 'A Single peptide-major histocompatibility complex ligand triggers digital cytokine secretion in CD4+T Cells', *Immunity*. Elsevier Inc., 39(5), pp. 846–857. doi: 10.1016/j.immuni.2013.08.036.

Hughes, H. *et al.* (2009) 'Organisation of human ER-exit sites: requirements for the localisation of Sec16 to transitional ER.', *Journal of cell science*, 122(Pt 16), pp. 2924–2934. doi: 10.1242/jcs.044032.

Irimia, M. *et al.* (2014) 'A Highly Conserved Program of Neuronal Microexons Is Misregulated in Autistic Brains', *Cell*. Cell Press, 159(7), pp. 1511–1523. doi: 10.1016/J.CELL.2014.11.035.

Ishiura, M. *et al.* (1998) 'Expression of a gene cluster kaiABC as a circadian feedback process in cyanobacteria.', *Science (New York, N.Y.)*. American Association for the Advancement of Science,

281(5382), pp. 1519–23. doi: 10.1126/science.281.5382.1519.

Jackson, C. L. and Munro, S. (2009) ‘Mechanisms of transport through the Golgi complex.’, *Journal of cell science*. The Company of Biologists Ltd, 122(Pt 4), pp. 443–52. doi: 10.1242/jcs.032581.

Jaganathan, K. *et al.* (2019) ‘Predicting Splicing from Primary Sequence with Deep Learning.’, *Cell*. Elsevier, 176(3), pp. 535-548.e24. doi: 10.1016/j.cell.2018.12.015.

Johansson, J. U. *et al.* (2008) ‘An Ancient Duplication of Exon 5 in the Snap25 Gene Is Required for Complex Neuronal Development/Function’, *PLoS Genetics*. Edited by W. N. Frankel. Public Library of Science, 4(11), p. e1000278. doi: 10.1371/journal.pgen.1000278.

Jung, J.-H. *et al.* (2016) ‘Phytochromes function as thermosensors in Arabidopsis.’, *Science (New York, N.Y.)*. American Association for the Advancement of Science, 354(6314), pp. 886–889. doi: 10.1126/science.aaf6005.

Kaiser, T. S. *et al.* (2016) ‘The genomic basis of circadian and circalunar timing adaptations in a midge’, *Nature*. Nature Publishing Group, 540(7631), pp. 69–73. doi: 10.1038/nature20151.

Katz, Y. *et al.* (2010) ‘Analysis and design of RNA sequencing experiments for identifying isoform regulation.’, *Nature methods*, 7(12), pp. 1009–15. doi: 10.1038/nmeth.1528.

Katz, Y. *et al.* (2014) ‘Sashimi plots: Quantitative visualization of alternative isoform expression from RNA-seq data’, *bioRxiv*, (January), pp. 1–3. doi: 10.1101/002576.

Kedra, D. *et al.* (1996) ‘Characterization of a second human clathrin heavy chain polypeptide gene (CLH-22) from chromosome 22q11’, *Human Molecular Genetics*. Narnia, 5(5), pp. 625–631. doi: 10.1093/hmg/5.5.625.

Kee, Y. *et al.* (1997) ‘Subunit structure of the mammalian exocyst complex.’, *Proceedings of the National Academy of Sciences of the United States of America*. National Academy of Sciences, 94(26), pp. 14438–43. doi: 10.1073/pnas.94.26.14438.

Keightley, M.-C. *et al.* (2013) ‘In vivo mutation of pre-mRNA processing factor 8 (Prpf8) affects transcript splicing, cell survival and myeloid differentiation’, *FEBS Letters*, 587(14), pp. 2150–2157. doi: 10.1016/j.febslet.2013.05.030.

Keller, P. and Simons, K. (1997) ‘Post-Golgi biosynthetic trafficking’, *Journal of Cell Science*, 110(24).

Kidd, P. B., Young, M. W. and Siggia, E. D. (2015) ‘Temperature compensation and temperature sensation in the circadian clock’, *Proceedings of the National Academy of Sciences of the United States of America*. National Academy of Sciences, 112(46), p. E6284. doi: 10.1073/PNAS.1511215112.

Kirchhausen, T., Owen, D. and Harrison, S. C. (2014) ‘Molecular structure, function, and dynamics of clathrin-mediated membrane traffic.’, *Cold Spring Harbor perspectives in biology*. Cold Spring Harbor Laboratory Press, 6(5), p. a016725. doi: 10.1101/cshperspect.a016725.

Kloss, B. *et al.* (2001) ‘Phosphorylation of period is influenced by cycling physical associations of double-time, period, and timeless in the Drosophila clock.’, *Neuron*. Elsevier, 30(3), pp. 699–706. doi: 10.1016/s0896-6273(01)00320-8.

Koike, N. *et al.* (2012) ‘Transcriptional Architecture and Chromatin Landscape of the Core Circadian Clock in Mammals’, *Science*, 338(6105), pp. 349–354. doi: 10.1126/science.1226339.

Kornblihtt, A. R. (2015) ‘Transcriptional control of alternative splicing along time: Ideas change, experiments remain’, *RNA*. Cold Spring Harbor Laboratory Press, 21(4), pp. 670–672. doi: 10.1261/RNA.051151.115.

Krämer, A. (1996) ‘The Structure and Function of Proteins Involved in Mammalian Pre-mRNA Splicing’, *Annual Review of Biochemistry*. Annual Reviews 4139 El Camino Way, P.O. Box 10139, Palo Alto, CA 94303-0139, USA , 65(1), pp. 367–409. doi: 10.1146/annurev.bi.65.070196.002055.

Kuryszko, J., Sławuta, P. and Sapikowski, G. (2016) ‘Secretory function of adipose tissue’, *Polish Journal of Veterinary Sciences*, 19(2), pp. 441–446. doi: 10.1515/pjvs-2016-0056.

Lareau, L. F. *et al.* (2007) ‘Unproductive splicing of SR genes associated with highly conserved and ultraconserved DNA elements’, *Nature*, 446(7138), pp. 926–929. doi: 10.1038/nature05676.

Lee, C., Bae, K. and Edery, I. (1998) ‘The Drosophila CLOCK Protein Undergoes Daily Rhythms in Abundance, Phosphorylation, and Interactions with the PER–TIM Complex’, *Neuron*. Cell Press, 21(4), pp. 857–867. doi: 10.1016/S0896-6273(00)80601-7.

Lee, M. *et al.* (2017) 'Systematic Computational Identification of Variants That Activate Exonic and Intronic Cryptic Splice Sites', *The American Journal of Human Genetics*. Cell Press, 100(5), pp. 751–765. doi: 10.1016/J.AJHG.2017.04.001.

Lee, M. C. S. *et al.* (2004) 'BI-DIRECTIONAL PROTEIN TRANSPORT BETWEEN THE ER AND GOLGI', *Annual Review of Cell and Developmental Biology*. Annual Reviews, 20(1), pp. 87–123. doi: 10.1146/annurev.cellbio.20.010403.105307.

Levy, S. E. and Myers, R. M. (2016) 'Advancements in Next-Generation Sequencing', *Annual Review of Genomics and Human Genetics*. Annual Reviews , 17(1), pp. 95–115. doi: 10.1146/annurev-genom-083115-022413.

Lippincott-Schwartz, J., Roberts, T. H. and Hirschberg, K. (2000) 'Secretory protein trafficking and organelle dynamics in living cells.', *Annual review of cell and developmental biology*. National Center for Biotechnology Information (US), 16, pp. 557–89. doi: 10.1146/annurev.cellbio.16.1.557.

Liu, Y.-W. *et al.* (2008) 'Isoform and Splice-Variant Specific Functions of Dynamin-2 Revealed by Analysis of Conditional Knock-Out Cells', *Molecular Biology of the Cell*. Edited by D. G. Drubin, 19(12), pp. 5347–5359. doi: 10.1091/mbc.e08-08-0890.

Liu, Y. *et al.* (2017) 'Impact of Alternative Splicing on the Human Proteome', *Cell Reports*, 20(5), pp. 1229–1241. doi: 10.1016/j.celrep.2017.07.025.

Love, M. I., Huber, W. and Anders, S. (2014) 'Moderated estimation of fold change and dispersion for RNA-seq data with DESeq2', *Genome Biology*. BioMed Central, 15(12), p. 550. doi: 10.1186/s13059-014-0550-8.

Low, K. H. *et al.* (2008) 'Natural Variation in the Splice Site Strength of a Clock Gene and Species-Specific Thermal Adaptation', *Neuron*. Cell Press, 60(6), pp. 1054–1067. doi: 10.1016/J.NEURON.2008.10.048.

Maciejewski, J. P. and Padgett, R. A. (2012) 'Defects in spliceosomal machinery: a new pathway of leukaemogenesis', *British Journal of Haematology*, 158(2), pp. 165–173. doi: 10.1111/j.1365-2141.2012.09158.x.

Mardis, E. R. (2011) 'A decade's perspective on DNA sequencing technology', *Nature*. Nature

Publishing Group, 470(7333), pp. 198–203. doi: 10.1038/nature09796.

Mardis, E. R. (2013) 'Next-generation sequencing platforms.', *Annual review of analytical chemistry (Palo Alto, Calif.)*, 6, pp. 287–303. doi: 10.1146/annurev-anchem-062012-092628.

Martinez-Arca, S. *et al.* (2003) 'A dual mechanism controlling the localization and function of exocytic v-SNAREs.', *Proceedings of the National Academy of Sciences of the United States of America*. National Academy of Sciences, 100(15), pp. 9011–6. doi: 10.1073/pnas.1431910100.

Martinez, N. M. *et al.* (2012) 'Alternative splicing networks regulated by signaling in human T cells', *RNA*, 18(5), pp. 1029–1040. doi: 10.1261/rna.032243.112.

Más, P. and Yanovsky, M. J. (2009) 'Time for circadian rhythms: plants get synchronized', *Current Opinion in Plant Biology*. Elsevier Current Trends, 12(5), pp. 574–579. doi: 10.1016/J.PBI.2009.07.010.

McCaughey, J. and Stephens, D. J. (2018) 'COPII-dependent ER export in animal cells: adaptation and control for diverse cargo', *Histochemistry and Cell Biology*. Springer Berlin Heidelberg, 150(2), pp. 119–131. doi: 10.1007/s00418-018-1689-2.

McManus, C. J. and Graveley, B. R. (2011) 'RNA structure and the mechanisms of alternative splicing', *Current Opinion in Genetics & Development*. Elsevier Current Trends, 21(4), pp. 373–379. doi: 10.1016/J.GDE.2011.04.001.

Merkin, J. *et al.* (2012) 'Evolutionary dynamics of gene and isoform regulation in Mammalian tissues.', *Science (New York, N.Y.)*. American Association for the Advancement of Science, 338(6114), pp. 1593–9. doi: 10.1126/science.1228186.

Mi, H., Muruganujan, A. and Thomas, P. D. (2013) 'PANTHER in 2013: Modeling the evolution of gene function, and other gene attributes, in the context of phylogenetic trees', *Nucleic Acids Research*, 41(D1), pp. 377–386. doi: 10.1093/nar/gks1118.

Mockenhaupt, S. and Makeyev, E. V (2015) 'Non-coding functions of alternative pre-mRNA splicing in development.', *Seminars in cell & developmental biology*. Elsevier, 47–48, pp. 32–9. doi: 10.1016/j.semcdb.2015.10.018.

Morris, S. M. and Cooper, J. A. (2001) 'Disabled-2 Colocalizes with the LDLR in Clathrin-Coated Pits and Interacts with AP-2', *Traffic*. John Wiley & Sons, Ltd (10.1111), 2(2), pp. 111–123. doi:

10.1034/j.1600-0854.2001.020206.x.

Mossessova, E., Bickford, L. C. and Goldberg, J. (2003) ‘SNARE Selectivity of the COPII Coat’, *Cell*. Cell Press, 114(4), pp. 483–495. doi: 10.1016/S0092-8674(03)00608-1.

Mostov, K. E., Verges, M. and Altschuler, Y. (2000) ‘Membrane traffic in polarized epithelial cells’, *Current Opinion in Cell Biology*. Elsevier Current Trends, 12(4), pp. 483–490. doi: 10.1016/S0955-0674(00)00120-4.

Nabenishi, H. and Yamazaki, A. (2017) ‘Decrease in body surface temperature before parturition in ewes.’, *The Journal of reproduction and development*. Japanese Society of Animal Reproduction, 63(2), pp. 185–190. doi: 10.1262/jrd.2016-097.

Naftelberg, S. *et al.* (2015) ‘Regulation of Alternative Splicing Through Coupling with Transcription and Chromatin Structure’, *Annual Review of Biochemistry*. Annual Reviews , 84(1), pp. 165–198. doi: 10.1146/annurev-biochem-060614-034242.

Nakamichi, N. *et al.* (2010) ‘PSEUDO-RESPONSE REGULATORS 9, 7, and 5 are transcriptional repressors in the Arabidopsis circadian clock.’, *The Plant cell*. American Society of Plant Biologists, 22(3), pp. 594–605. doi: 10.1105/tpc.109.072892.

Neumann, A. *et al.* (2019) ‘Rhythmic gene expression is controlled by evolutionary conserved temperature regulated alternative splicing triggering nonsense mediated decay’, *in preparation*.

Neumann, D. (1966) ‘Die lunare und tägliche Schlüpfperiodik der Mücke Clunio’, *Zeitschrift für Vergleichende Physiologie*. Springer-Verlag, 53(1), pp. 1–61. doi: 10.1007/BF00343045.

Ng, M. M. *et al.* (2013) ‘GOLPH3L antagonizes GOLPH3 to determine Golgi morphology’, *Molecular Biology of the Cell*. Edited by B. S. Glick, 24(6), pp. 796–808. doi: 10.1091/mbc.e12-07-0525.

Ni, J. D. *et al.* (2017) ‘A rhodopsin in the brain functions in circadian photoentrainment in Drosophila’, *Nature*. Nature Publishing Group, 545(7654), pp. 340–344. doi: 10.1038/nature22325.

Nilsson, T., Au, C. E. and Bergeron, J. J. M. (2009) ‘Sorting out glycosylation enzymes in the Golgi apparatus’, *FEBS Letters*. John Wiley & Sons, Ltd, 583(23), pp. 3764–3769. doi: 10.1016/j.febslet.2009.10.064.

Nishiyama, H. *et al.* (1997) ‘A glycine-rich RNA-binding protein mediating cold-inducible suppression of mammalian cell growth.’, *The Journal of cell biology*. The Rockefeller University Press, 137(4), pp. 899–908. doi: 10.1083/jcb.137.4.899.

Van Nostrand, E. L. *et al.* (2016) ‘Robust transcriptome-wide discovery of RNA-binding protein binding sites with enhanced CLIP (eCLIP)’, *Nature Methods*. Nature Publishing Group, 13(6), pp. 508–514. doi: 10.1038/nmeth.3810.

Oakenfull, R. J. and Davis, S. J. (2017) ‘Shining a light on the Arabidopsis circadian clock’, *Plant, Cell & Environment*. John Wiley & Sons, Ltd (10.1111), 40(11), pp. 2571–2585. doi: 10.1111/pce.13033.

Ozturk, N. *et al.* (2011) ‘Reaction mechanism of Drosophila cryptochrome’, *Proceedings of the National Academy of Sciences*, 108(2), pp. 516–521. doi: 10.1073/pnas.1017093108.

Pan, Q. *et al.* (2008) ‘Deep surveying of alternative splicing complexity in the human transcriptome by high-throughput sequencing.’, *Nature genetics*, 40(12), pp. 1413–5. doi: 10.1038/ng.259.

Panda, S., Hogenesch, J. B. and Kay, S. A. (2002) ‘Circadian rhythms from flies to human’, *Nature*. Nature Publishing Group, 417(6886), pp. 329–335. doi: 10.1038/417329a.

Patro, R. *et al.* (2017) ‘Salmon provides fast and bias-aware quantification of transcript expression’, *Nature Methods*. Nature Publishing Group, 14(4), pp. 417–419. doi: 10.1038/nmeth.4197.

Pokhilko, A. *et al.* (2012) ‘The clock gene circuit in Arabidopsis includes a repressilator with additional feedback loops.’, *Molecular systems biology*. European Molecular Biology Organization, 8, p. 574. doi: 10.1038/msb.2012.6.

Preußner, M. *et al.* (2014) ‘Rhythmic U2af26 Alternative Splicing Controls PERIOD1 Stability and the Circadian Clock in Mice’, *Molecular Cell*. Cell Press, 54(4), pp. 651–662. doi: 10.1016/J.MOLCEL.2014.04.015.

Preußner, M. *et al.* (2017) ‘Body Temperature Cycles Control Rhythmic Alternative Splicing in Mammals’, *Molecular Cell*, pp. 1–14. doi: 10.1016/j.molcel.2017.06.006.

Preußner, M. and Heyd, F. (2018) ‘Temperature-controlled Rhythmic Gene Expression in Endothermic Mammals: All Diurnal Rhythms are Equal, but Some are Circadian’, *BioEssays*. John

Wiley & Sons, Ltd, 40(7), p. 1700216. doi: 10.1002/bies.201700216.

Qiu, J. *et al.* (2016) 'Distinct splicing signatures affect converged pathways in myelodysplastic syndrome patients carrying mutations in different splicing regulators.', *RNA (New York, N.Y.)*. Cold Spring Harbor Laboratory Press, 22(10), pp. 1535–49. doi: 10.1261/rna.056101.116.

Refinetti, R. and Menaker, M. (1992) 'The circadian rhythm of body temperature', *Physiology & Behavior*. Elsevier, 51(3), pp. 613–637. doi: 10.1016/0031-9384(92)90188-8.

Reppert, S. M. and Weaver, D. R. (1997) 'Forward Genetic Approach Strikes Gold: Cloning of a Mammalian Clock Gene', *Cell*. Cell Press, 89(4), pp. 487–490. doi: 10.1016/S0092-8674(00)80229-9.

Salomé, P. A., Weigel, D. and McClung, C. R. (2010) 'The role of the Arabidopsis morning loop components CCA1, LHY, PRR7, and PRR9 in temperature compensation.', *The Plant cell*. American Society of Plant Biologists, 22(11), pp. 3650–61. doi: 10.1105/tpc.110.079087.

Schotman, H., Karhinen, L. and Rabouille, C. (2009) 'Integrins mediate their unconventional, mechanical-stress-induced secretion via RhoA and PINCH in Drosophila', *Journal of Cell Science*, 122(15), pp. 2662–2672. doi: 10.1242/jcs.039347.

Scotti, M. M. and Swanson, M. S. (2016) 'RNA mis-splicing in disease', *Nature Reviews Genetics*. Nature Publishing Group, 17(1), pp. 19–32. doi: 10.1038/nrg.2015.3.

Shatkin, A. J. (1976) 'Capping of eucaryotic mRNAs', *Cell*. Cell Press, 9(4), pp. 645–653. doi: 10.1016/0092-8674(76)90128-8.

Shaw, P. J. *et al.* (2000) 'Correlates of sleep and waking in Drosophila melanogaster.', *Science (New York, N.Y.)*. American Association for the Advancement of Science, 287(5459), pp. 1834–7. doi: 10.1126/science.287.5459.1834.

Shen, S. *et al.* (2014) 'rMATS: robust and flexible detection of differential alternative splicing from replicate RNA-Seq data.', *Proceedings of the National Academy of Sciences of the United States of America*. National Academy of Sciences, 111(51), pp. E5593-601. doi: 10.1073/pnas.1419161111.

Shinohara, Y. *et al.* (2017) 'Temperature-Sensitive Substrate and Product Binding Underlie Temperature-Compensated Phosphorylation in the Clock.', *Molecular cell*. Elsevier, 67(5), pp.

783-798.e20. doi: 10.1016/j.molcel.2017.08.009.

Shukla, A. *et al.* (2001) 'Identification of Three New Splice Variants of the SNARE Protein SNAP-23', *Biochemical and Biophysical Research Communications*. Academic Press, 285(2), pp. 320–327. doi: 10.1006/BBRC.2001.5144.

Sørensen, J. B. *et al.* (2003) 'Differential Control of the Releasable Vesicle Pools by SNAP-25 Splice Variants and SNAP-23', *Cell*. Cell Press, 114(1), pp. 75–86. doi: 10.1016/S0092-8674(03)00477-X.

Sprangers, J. and Rabouille, C. (2015) 'SEC16 in COPII coat dynamics at ER exit sites.', *Biochemical Society transactions*, 43(1), pp. 97–103. doi: 10.1042/BST20140283.

Srivastava, A. *et al.* (2016) 'RapMap: a rapid, sensitive and accurate tool for mapping RNA-seq reads to transcriptomes', *Bioinformatics*. Narnia, 32(12), pp. i192–i200. doi: 10.1093/bioinformatics/btw277.

Stanewsky, R. *et al.* (1998) 'The cryb mutation identifies cryptochrome as a circadian photoreceptor in Drosophila.', *Cell*. Elsevier, 95(5), pp. 681–92. doi: 10.1016/s0092-8674(00)81638-4.

Sterne-Weiler, T. *et al.* (2018) 'Efficient and Accurate Quantitative Profiling of Alternative Splicing Patterns of Any Complexity on a Laptop', *Molecular Cell*. Cell Press, 72(1), pp. 187-200.e6. doi: 10.1016/J.MOLCEL.2018.08.018.

Stiburek, L. *et al.* (2005) 'Tissue-specific cytochrome c oxidase assembly defects due to mutations in SCO2 and SURF1.', *The Biochemical journal*. Portland Press Limited, 392(Pt 3), pp. 625–32. doi: 10.1042/BJ20050807.

Subramanian, A. *et al.* (2005) 'Gene set enrichment analysis: a knowledge-based approach for interpreting genome-wide expression profiles.', *Proceedings of the National Academy of Sciences of the United States of America*. National Academy of Sciences, 102(43), pp. 15545–50. doi: 10.1073/pnas.0506580102.

Szul, T. and Sztul, E. (2011) 'COPII and COPI Traffic at the ER-Golgi Interface', *Physiology*. American Physiological Society Bethesda, MD, 26(5), pp. 348–364. doi: 10.1152/physiol.00017.2011.

Taliaferro, J. M. *et al.* (2016) 'RNA Sequence Context Effects Measured In Vitro Predict In Vivo Protein Binding and Regulation.', *Molecular cell*. NIH Public Access, 64(2), pp. 294–306. doi: 10.1016/j.molcel.2016.08.035.

Temin, H. M. and Mizutani, S. (1970) 'Viral RNA-dependent DNA Polymerase: RNA-dependent DNA Polymerase in Virions of Rous Sarcoma Virus', *Nature*, 226(5252), pp. 1211–1213. doi: 10.1038/2261211a0.

Tian, B. and Manley, J. L. (2017) 'Alternative polyadenylation of mRNA precursors', *Nature Reviews Molecular Cell Biology*. Nature Publishing Group, 18(1), pp. 18–30. doi: 10.1038/nrm.2016.116.

Trapnell, C. *et al.* (2012) 'Differential gene and transcript expression analysis of RNA-seq experiments with TopHat and Cufflinks.', *Nature protocols*, 7(3), pp. 562–78. doi: 10.1038/nprot.2012.016.

Trapnell, C., Pachter, L. and Salzberg, S. L. (2009) 'TopHat: discovering splice junctions with RNA-Seq', *Bioinformatics*. Narnia, 25(9), pp. 1105–1111. doi: 10.1093/bioinformatics/btp120.

Vacca, M. *et al.* (2011) 'Alternative splicing of the human gene SYBL1 modulates protein domain architecture of longin VAMP7/TI-VAMP, showing both non-SNARE and synaptobrevin-like isoforms', *BMC Molecular Biology*. BioMed Central, 12(1), p. 26. doi: 10.1186/1471-2199-12-26.

Valladolid-Acebes, I. *et al.* (2015) 'Replacing SNAP-25b with SNAP-25a expression results in metabolic disease', *Proceedings of the National Academy of Sciences*, 112(31), pp. E4326–E4335. doi: 10.1073/pnas.1511951112.

Wahl, M. C., Will, C. L. and Lührmann, R. (2009) 'The Spliceosome: Design Principles of a Dynamic RNP Machine', *Cell*. doi: 10.1016/j.cell.2009.02.009.

Wang, B. *et al.* (2018) 'The COPII cargo adapter SEC24C is essential for neuronal homeostasis', *Journal of Clinical Investigation*, 128(8), pp. 3319–3332. doi: 10.1172/JCI98194.

Wang, L. *et al.* (2002) 'Identification and genetic analysis of human and mouse activated Cdc42 interacting protein-4 isoforms', *Biochemical and Biophysical Research Communications*. Academic Press, 293(5), pp. 1426–1430. doi: 10.1016/S0006-291X(02)00398-4.

Watson, P. *et al.* (2005) 'Coupling of ER exit to microtubules through direct interaction of COPII

with dynactin.', *Nature cell biology*, 7(1), pp. 48–55. doi: 10.1038/ncb1206.

Watson, P. *et al.* (2006) 'Sec16 defines endoplasmic reticulum exit sites and is required for secretory cargo export in mammalian cells', *Traffic*, 7(12), pp. 1678–1687. doi: 10.1111/j.1600-0854.2006.00493.x.

Webb, A. A. R. *et al.* (2019) 'Continuous dynamic adjustment of the plant circadian oscillator', *Nature Communications*. Nature Publishing Group, 10(1), p. 550. doi: 10.1038/s41467-019-08398-5.

Wilhelmi, I. *et al.* (2016) 'Sec16 alternative splicing dynamically controls COPII transport efficiency', *Nature Communications*, 7, p. 12347. doi: 10.1038/ncomms12347.

Will, C. L. and Lührmann, R. (2011) 'Spliceosome structure and function.', *Cold Spring Harbor perspectives in biology*. Cold Spring Harbor Laboratory Press, 3(7), p. a003707. doi: 10.1101/cshperspect.a003707.

Williams, S. L. *et al.* (2004) 'Cytochrome c oxidase subassemblies in fibroblast cultures from patients carrying mutations in COX10, SCO1, or SURF1.', *The Journal of biological chemistry*. American Society for Biochemistry and Molecular Biology, 279(9), pp. 7462–9. doi: 10.1074/jbc.M309232200.

Wilusz, C. J., Wormington, M. and Peltz, S. W. (2001) 'The cap-to-tail guide to mRNA turnover', *Nature Reviews Molecular Cell Biology*. Nature Publishing Group, 2(4), pp. 237–246. doi: 10.1038/35067025.

Xiong, H. Y. *et al.* (2015) 'RNA splicing. The human splicing code reveals new insights into the genetic determinants of disease.', *Science (New York, N.Y.)*. NIH Public Access, 347(6218), p. 1254806. doi: 10.1126/science.1254806.

Yamamoto, Y., Yurugi, C. and Sakisaka, T. (2017) 'The number of the C-terminal transmembrane domains has the potency to specify subcellular localization of Sec22c', *Biochemical and Biophysical Research Communications*. Elsevier Ltd. doi: 10.1016/j.bbrc.2017.04.071.

Yang, G. *et al.* (2016) 'Timing of expression of the core clock gene Bmal1 influences its effects on aging and survival.', *Science translational medicine*. American Association for the Advancement of Science, 8(324), p. 324ra16. doi: 10.1126/scitranslmed.aad3305.

Yang, X. *et al.* (2016) 'Widespread Expansion of Protein Interaction Capabilities by Alternative Splicing', *Cell*. Elsevier Inc., 164(4), pp. 805–817. doi: 10.1016/j.cell.2016.01.029.

Yanovsky, M. J. and Kay, S. A. (2002) 'Molecular basis of seasonal time measurement in Arabidopsis', *Nature*. Nature Publishing Group, 419(6904), pp. 308–312. doi: 10.1038/nature00996.

Yoshida, K. and Ogawa, S. (2014) 'Splicing factor mutations and cancer', *Wiley Interdisciplinary Reviews: RNA*. John Wiley & Sons, Ltd, 5(4), pp. 445–459. doi: 10.1002/wrna.1222.

Zhu, Z. *et al.* (1998) 'SURF1, encoding a factor involved in the biogenesis of cytochrome c oxidase, is mutated in Leigh syndrome', *Nature Genetics*. Nature Publishing Group, 20(4), pp. 337–343. doi: 10.1038/3804.

Curriculum vitae Alexander Neumann

For reasons of data protection, the curriculum vitae is not published in the electronic version.

This page is intentionally left blank.

Appendices

Appendix A Abbreviations

A. thaliana	*Arabidopsis thaliana*
A3ss	Alternative 3'splice site
A5ss	Alternative 5' splice site
APA	Alternative polyadenylation
ARNT	Aryl hydrocarbon receptor nuclear translocator
AS	Alternative splicing
AML	Acute myeloid leukemia
AS-NMD	Alternative splicing coupled to nonsense-mediated decay
Bmal1	Brain and muscle ARNT like 1
BP	Branch point
CCA1	CIRCADIAN AND CLOCK ASSOCIATED1
CHX	Cycloheximide
Cirbp	Cold induced RNA binding protein
CKIε	Casein kinase Iε
CLIP	Cross-link immunoprecipitation
Clk	CDC-like kinase
Clock	Circadian locomotor output cycle kaput
COP	Coatomer protein (complex)
CRISPR	Clustered regularly interspaced short palindromic repeats
Cry	Cryptochrome
Cyc	Cycle
D. melanogaster	*Drosophila melanogaster*
Dbt	Double-time
dClk	Drosophila clock
DMSO	Dimethylsulfoxide

DNA	Desoxyribonucleic acid
ER	Endoplasmic reticulum
ERES	Endoplasmic reticulum exit site(s)
ERGIC	Endoplasmic reticulum – Golgi intermediate compartment
ESE	Exonic splicing enhancer
ESS	Exonic splicing silencer
GE	Gene expression
GFP	Green fluorescent protein
GJA1	Gap junction alpha-1, connexin 43
GLUT4	Glucose transporter 4
GPI	Glycosyl-phosphatidyl-inositol
hnRNP	Heterogenous nuclear ribonucleoprotein particle
ISE	Intronic splicing enhancer
ISS	Intronic splicing silencer
KD	Knock down
KO	Knock out
LHY	LATE ELONGATED HYPCOTYL
MAPK	Mitogen-activated protein kinase
MISO	Mixture of isoforms
MO	Morpholino
mRNA	Messenger ribonucleic acid
MXE	Mutually exclusive exons
Nfil3	Nuclear factor, interleukin 3 regulated
NGS	Next-Generation Sequencing
NMD	Nonsense-mediated decay
PCR	Polymerase chain reaction
Per	Period
PM	Plasma membrane
Poly-A	Poly-adenosine
Pre-mRNA	Precursor messenger ribonucleic acid
PRR	PSEUDO-RESPONSE REGULATOR

Q157P	Glutamine to proline mutation at amino acid position 157
Q157R	Glutamine to arginine mutation at amino acid position 157
Q157R deletion	Glutamine to arginine and deletion mutation at amino acid position 157
Rbm3	RNA binding motif protein 3
RBP	Ribonucleic acid binding protein
RI	Retained intron
RNA	Ribonucleic acid
RNA-seq	Ribonucleic acid sequencing
RT	Reverse transcription
RUSH	Retention using selective hooks
SCN	Suprachiasmatic nucleus
SE	Skipped (cassette) exon
SF1	Splicing factor 1
Sgg	Shaggy
SNARE	Soluble N-ethylmaleimide-sensitive factor attachment receptor
snRNP	Small nuclear ribonucleoprotein particle
SR protein	Serine-arginine rich protein
ss	Splice site
Tbp	TATA binding protein
tER	Transitional endoplasmic reticulum
Tim	Timeless
TOC1	TIMING OF CAB EXPRESSION
t-SNARE	Target membrane soluble N-ethylmaleimide-sensitive factor attachment receptor
U2AF	U2 auxiliary factor
UTR	Untranslated region
v-SNARE	Vesicular soluble N-ethylmaleimide-sensitive factor attachment receptor

Appendix B List of Figures

Appendix C List of Tables

Appendix D Publication 1

Wilhelmi I, Kanski R, **Neumann A**, Herdt O, Hoff F, Jacob R, Preußner M, Heyd F. Sec16 alternative splicing dynamically controls COPII transport efficiency. Nat Commun. 2016 Aug 5;7:12347. doi: 10.1038/ncomms12347.

http://dx.doi.org/10.1038/ncomms12347

AN performed microscopy assays during revision of the manuscript. He performed αSEC24C stainings of HEK293 wild-type and HEK293 SEC16A ΔE29 cells, imaged the slides and analysed the obtained images.

nature COMMUNICATIONS

ARTICLE

Received 22 Jan 2016 | Accepted 24 Jun 2016 | Published 5 Aug 2016

DOI: 10.1038/ncomms12347 OPEN

Sec16 alternative splicing dynamically controls COPII transport efficiency

Ilka Wilhelmi[1,†], Regina Kanski[1], Alexander Neumann[1], Olga Herdt[1], Florian Hoff[2], Ralf Jacob[2], Marco Preußner[1] & Florian Heyd[1]

The transport of secretory proteins from the endoplasmic reticulum (ER) to the Golgi depends on COPII-coated vesicles. While the basic principles of the COPII machinery have been identified, it remains largely unknown how COPII transport is regulated to accommodate tissue- or activation-specific differences in cargo load and identity. Here we show that activation-induced alternative splicing of *Sec16* controls adaptation of COPII transport to increased secretory cargo upon T-cell activation. Using splice-site blocking morpholinos and CRISPR/Cas9-mediated genome engineering, we show that the number of ER exit sites, COPII dynamics and transport efficiency depend on *Sec16* alternative splicing. As the mechanistic basis, we suggest the C-terminal Sec16 domain to be a splicing-controlled protein interaction platform, with individual isoforms showing differential abilities to recruit COPII components. Our work connects the COPII pathway with alternative splicing, adding a new regulatory layer to protein secretion and its adaptation to changing cellular environments.

[1] Department of Biology, Chemistry, Pharmacy, Freie Universität Berlin, Institute of Chemistry and Biochemistry, Laboratory of RNA Biochemistry, Takustrasse 6, 14195 Berlin, Germany. [2] Department of Cell Biology and Cell Pathology, Philipps-University Marburg, Robert Koch Strae 6, 35037 Marburg, Germany. † Present addresses: Department of Experimental Diabetology, German Institute of Human Nutrition Potsdam-Rehbruecke, Arthur-Scheunert-Allee 114-116, D-14558 Nuthetal, Germany (I.W.). Correspondence and requests for materials should be addressed to F.He. (email: florian.heyd@fu-berlin.de).

The early secretory pathway, the transport from the endoplasmic reticulum (ER) to the Golgi, is initially mediated by COPII-coated vesicles[1]. The COPII coat consists of an inner and an outer layer that are made up of Sec23–Sec24 heterodimers and Sec13–Sec31 heterotetramers, respectively[2]. The formation of COPII-coated vesicles is initiated by the ER membrane located guanine-nucleotide-exchange factor Sec12, which activates the small GTPase Sar1. In the GTP-bound state, Sar1 is membrane-associated and recruits Sec23–24 to concentrate cargo and form a pre-budding complex. Binding of Sec13–31 then leads to cage formation and finally vesicle budding. Eventually, the GTPase-activating protein (GAP) activity of Sec23, which is stimulated by Sec31, leads to hydrolysis of the Sar1-bound GTP[2]. GTP hydrolysis has been suggested to control cargo sorting[3], coat disassembly[4] and vesicle release[5]. The latter has been called into question, as a recent study finds vesicle scission independent of GTP hydrolysis[6].

COPII vesicles form at specialized sites of the ER, the transitional ER (tER), more generally termed ER exit sites (ERESs)[7]. Sec16 is a peripheral membrane protein that localizes to and defines tER/ERES[8–11]. Although vesicle budding can be reconstituted in the absence of Sec16 *in vitro*[4], the loss of Sec16 in cells leads to disruption of the early secretory pathway and growth arrest[8,12,13]. In humans, a Sec16 paralogue, Sec16B, has been suggested to fulfil specialized, non-redundant functions[14,15]. Human Sec16 is a protein of 2,357 amino acids that displays a central conserved domain involved in ERES localization[10,13], as well as a C-terminal conserved region (CTR) (Fig. 1a). The CTR was shown to interact with several COPII components such as Sec12 and Sec23, and is essential for COPII vesicle formation[13,16] (also see below). In addition, Sec16 interacts with Sec13, Sec31 and Sar1, and was suggested to play a scaffolding role for COPII coat formation without becoming part of the budding vesicle itself[8–10,17]. Later reports also find a direct regulatory role of Sec16 as it interferes with the Sec31-mediated increase in the GAP activity of Sec23. This results in increased Sar1-GTP stability and may influence formation and turnover of the COPII coat[5,18–20].

Upon T-cell activation, the expression and secretion of effector molecules such as cytokines, chemokines and cytotoxins is strongly increased. Accordingly, T cells have evolved an elaborate system that allows regulated and directed secretion of effector proteins[21,22]. However, research aiming at understanding protein secretion upon T-cell activation almost exclusively focuses on post-Golgi compartments. In contrast, it remains elusive how the early secretory pathway copes with the increased secretory cargo load upon T-cell activation. In experimental settings, an increase of secretory cargo led to different adaptive mechanisms, possibly controlled by phosphorylation of Sec16 (refs 23–25); however, this has not been investigated in endogenous settings. Another currently discussed mechanism to regulate the COPII machinery is the expression of different variants of COPII components[26]. In humans, two paralogues of *Sec16*, *Sar1*, *Sec23* and *Sec31*, respectively, and four *Sec24* paralogues exist. These variants are expressed in a tissue-specific manner[27,28] and mutations in a single gene, for example, *Sar1B* or *Sec23A*, are associated with metabolic and developmental diseases[29]. While the role of different paralogues of COPII components is a subject of intense research[28], a potential role of alternative splicing in controlling functionality of individual members of the COPII machinery has not yet been addressed.

Alternative splicing is a mechanism that multiplies the genome's coding capacity and that has an enormous, yet largely unexplored, regulatory potential. In addition, signal-induced alternative splicing dynamically controls protein expression in different cell types under diverse conditions[30,31]. In recent work, RNA sequencing was used to identify exons that are alternatively spliced upon T-cell activation[32]. Among these are two exons in the C-terminal region of Sec16, exons 29 and 30 (Fig. 1). Here we show that an increased expression of the *Sec16* isoform containing only exon 29 leads to an increase in the number of ERES and more efficient COPII transport in activated T cells, thus allowing an adaptation to higher secretory cargo flux. We furthermore show that the different *Sec16* splice variants have altered abilities to interact with COPII components and that *Sec16* exon 29 controls COPII dynamics. Together, our data suggest that the C-terminal domain of Sec16 represents a platform for protein–protein interactions that is controlled by alternative splicing to regulate COPII vesicle formation. By linking dynamic changes in alternative splicing to the efficiency of COPII transport, we add a new regulatory layer to the early secretory pathway and provide evidence for an adaptive mechanism to increased endogenous secretory cargo.

Results

Sec16 is alternatively spliced upon T-cell activation. A recent RNA sequencing approach identified over 100 exons that show activation-induced alternative splicing upon activation of the Jurkat-derived human Jsl1 T-cell line[32,33]. Among the alternatively spliced exons are exons 29 and 30 of *Sec16* (Fig. 1; ref. 32) that make up a part of the CTR of the protein (Fig. 1a, left site shows domain organization of the Sec16 protein, right site shows exons that make up the Sec16 CTR and main splicing isoforms found in Jsl1 T cells). We first used splicing-sensitive RT-PCR to confirm these results. These experiments show an increase of the isoform containing only exon 29 (E29) and a concomitant decrease in the full-length (Fl) and the exon 30 (E30) containing isoforms in activated T cells (Fig. 1b,c). We confirmed that changed isoform expression was due to a splicing switch and not due to selective stabilization by showing similar stabilities of the different messenger RNA (mRNA) isoforms in resting and activated conditions (Supplementary Fig. 1a). While we observe a switch in *Sec16* isoform expression at the mRNA level, the overall protein expression remained constant after T-cell activation (Fig. 1d, left). In a standard minigel SDS–polyacrylamide gel electrophoresis (PAGE), we do not observe a change in the electrophoretic mobility of Sec16 protein, which runs as a single band under these conditions. This is likely due to the small size difference of the different isoforms, as the alternative exons account for only 1–2% of the total protein. However, using a 4–12% gradient gel, we do detect at least two Sec16 bands the ratio of which is altered upon T-cell activation (Fig. 1d, right, we interpret the slower migrating isoform increased upon activation as being the E29 isoform; also see below). In agreement with altered *Sec16* isoform expression at the protein level 48 h post stimulation, we observe a substantial increase in the E29 mRNA isoform already 24 h after activation (Supplementary Fig. 1b). In addition, we used Cycloheximide to block *de novo* protein synthesis to determine Sec16 protein stability and turnover in resting and stimulated T cells. In both conditions, we observed a rather short Sec16 protein half-life of $\sim$10 h (Supplementary Fig. 1c), which is in the same range as previously observed in HeLa cells[34]. Together, these observations strongly suggest that alternative splicing leads to altered *Sec16* isoform expression at the protein level 48 h post stimulation. Therefore, this time point was chosen for further investigation.

The Sec16 E29 CTR interferes with ER-to-Golgi transport. The alternatively spliced exons make up parts of the C-terminal domain of Sec16 (Fig. 1a) that has been shown to directly interact with Sec12 and Sec23, and to be essential for the function of Sec16

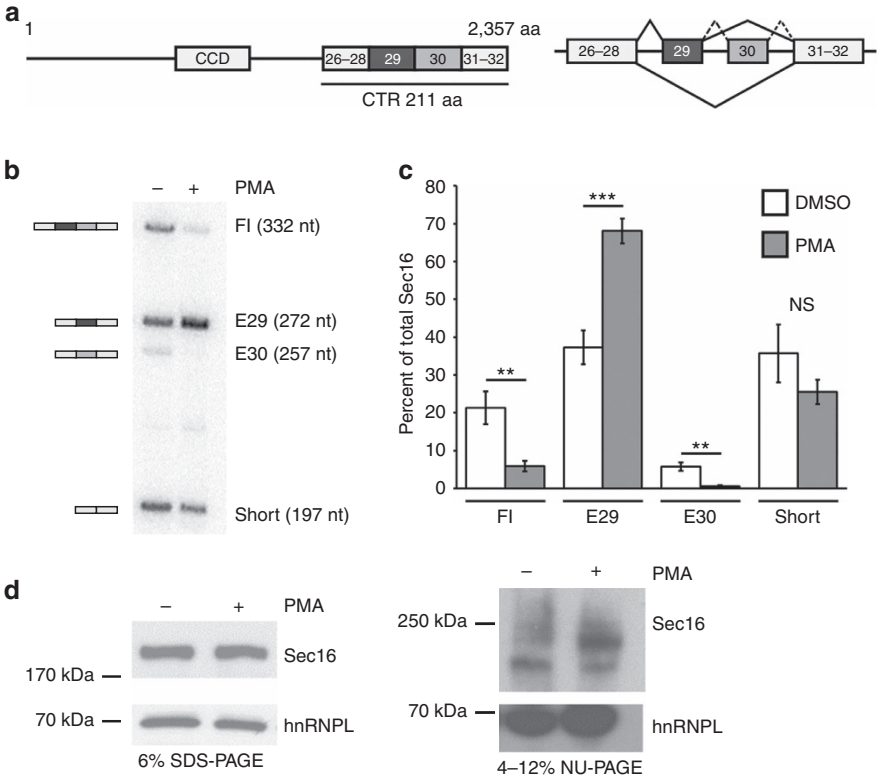

Figure 1 | *Sec16* exons 29 and 30 are alternatively spliced on T-cell activation. (**a**) Domain structure of the Sec16 protein (left) and schematic splicing pattern of the exons making up the CTR in Jsl1 T cells (right). CCD, central conserved domain; CTR, C-terminal region. The C-terminal region of Sec16 contains 211 amino acids in the isoform containing exons 26–32. Exons are not to scale. (**b**) Radioactive splicing-sensitive RT–PCR of resting (−) and stimulated (+) Jsl1 T cells detects four different splice isoforms. Schematic representation (left) and nomenclature used throughout the manuscript (right) of the four isoforms is shown. (**c**) Phosphorimager quantification of three independent experiments as shown in **b**. Shown is the mean amount of the individual splice isoforms as percentage of total *Sec16* ± s.d. *P* values (Student's *T*-Test) from left to right: 0,0041; 0,00067; 0,0015 and 0,099. (**d**) Western blot analysis comparing whole-cell extract of resting and stimulated Jsl1 T cells. Left panel shows separation on a standard 6% SDS-PAGE and right panel shows separation on a 4–12% gradient NuPAGE. hnRNPL served as a loading control.

to mediate COPII transport[13,16,18]. To elucidate potential functional differences of the four Sec16 isoforms, we over-expressed the different C-terminal domains in HeLa cells (Fig. 2a). When overexpressed, the C-terminal Sec16 domain is localized throughout the cytoplasm and disrupts ER-to-Golgi transport leading to Golgi breakdown, likely due to sequestering COPII components (Fig. 2b; ref. 13). Overexpressing similar amounts of the different Sec16 C-termini (Fig. 2c) revealed a particularly strong ability of the E29 isoform to interfere with ER-to-Golgi transport as evidenced by quantifying Golgi morphology (Fig. 2d; Supplementary Fig. 2). This could indicate an increased interaction of the E29 isoform with one of the COPII components, leading to the stronger dominant-negative effect. Conversely, it suggests that endogenous expression levels of the complete Sec16 E29 isoform, which is upregulated on T-cell activation, may regulate the efficiency of COPII transport.

T-cell activation increases ERES and ER export efficiency. We hypothesized that *Sec16* alternative splicing could be involved in an adaptation of the COPII machinery during T-cell activation. Although an adaptive mechanism to accommodate the strong increase in secretory cargo in activated T cells seems required, if and how such an adaptation takes place is unknown. To investigate this question and a potential connection to *Sec16* alternative splicing, we first compared the ER export capacity in resting and activated T cells using a fluorescence-activated cell sorting (FACS)-based modified vesicular-stomatitis-virus-glycoprotein (VSVG) export assay (Fig. 3a, left). To this end, a FLAG epitope was inserted into the extracellular domain of the VSVG-GFP reporter, which accumulates in the ER upon heat shock at 40 °C and is released at 32 °C (ref. 35). In intact cells, staining of the FLAG-tagged protein will only be possible, if VSVG was correctly exported after shifting the cells to the permissive temperature. We indeed observed more efficient VSVG export in stimulated cells (Fig. 3a, right), confirming increased secretory capacity in activated T cells. In addition, we generated Jsl1 T cells stably expressing the VSVG-GFP reporter and performed export assays using immunofluorescence (IF) as read-out (also see Fig. 5 and Methods for details). Culturing these T cells at 40 °C overnight and then switching the cells to 32 °C confirmed strongly increased ER export efficiency upon T-cell activation (Supplementary Fig. 3a–c).

Next, we assessed the morphology of compartments involved in the early secretory pathway. The ER (visualized by transfection with dsRed fused to an ER retention signal), tER (Sec16, see Discussion below and ref. 10), ERGIC (ERGIC53) and the Golgi (GM130) did not show differences between resting and activated T cells (Fig. 3b; Supplementary Fig. 4a). However, we did notice a substantial and significant increase in the number of COPII-positive structures as evidenced by staining for Sec31 (Fig. 3b,c). In addition, the localization of COPII structures changed, with staining in the nuclear periphery becoming apparent only in stimulated T cells. To confirm this finding with an independent COPII marker and to rule out a potential phorbol myristate acetate (PMA)-induced formation of Sec31 aggregates,

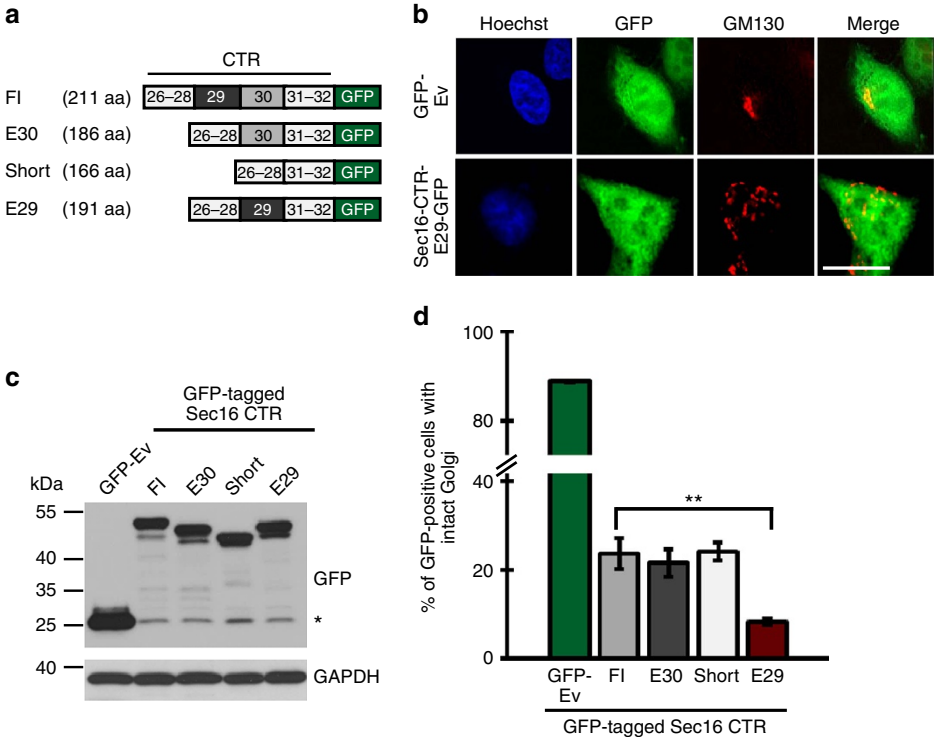

Figure 2 | Different Sec16 isoforms interfere differentially with COPII transport. (**a**) Schematic representation of the Sec16 CTR constructs fused to GFP. Exons are not to scale. (**b**) Expression of the Sec16 CTR leads to Golgi disruption. Immunofluorescence pictures of HeLa cells transfected and stained as indicated. Transfected cells were identified via GFP fluorescence and Golgi morphology was analysed using GM130 labelling. Control cells (top row) were transfected with a GFP empty vector (Ev) and show intact Golgi morphology, whereas cells overexpressing the GFP-tagged E29-CTR show a dispersed structure. (**c**) Western blot analysis of HeLa whole-cell extracts expressing the indicated constructs. GAPDH served as a loading control. * marks GFP alone. (**d**) The Sec16 E29 CTR leads to the strongest Golgi disruption. HeLa cells were transfected with either GFP control (Ev) or Sec16 CTRs fused to GFP. Golgi was labelled using GM130 antibody and morphology was analysed by fluorescence microscopy. At least 100 GFP-expressing cells were analysed in each of three independent experiments for each condition and evaluated for Golgi morphology. See Supplementary Fig. 2 for additional examples. Shown is the average percentage of counted cells showing an intact Golgi structure. $P = 0.0015$ (Student's *T*-Test).

we repeated the experiments with an antibody against Sec24C (ref. 36). As for Sec31, we observed a significant increase in the number of Sec24-positive structures upon PMA treatment (Supplementary Fig. 5), strongly suggesting that COPII-positive ERES or vesicles (see below) are indeed increased in activated T cells. The stronger effect we observe for Sec24C compared with Sec31 staining may be due to partial uncoating that mainly affects the outer COPII layer (Sec13/31), as the inner layer (Sec23/24) has been suggested to stay associated with vesicles after budding[37]. Notably, the activation of Jsl1 T cells with PMA did not induce ER stress, as the expression of two markers for ER stress remained unchanged between resting and activated conditions (Supplementary Fig. 6a). In addition, inducing ER stress did not lead to altered Sec16 alternative splicing (Supplementary Fig. 6b,c). We can thus rule out that the effect on *Sec16* alternative splicing and the COPII machinery is merely due to ER stress, suggesting an effect that is indeed due to T-cell activation (see below for the stimulation of primary cells). The majority of Sec24/31-positive structures, which do not costain with Sec16, has been suggested to represent COPII-coated vesicles with some nascent coats still associated with the ER stained as well[10,38]. This is consistent with our observation that Sec16- and Sec31-positive structures stain close to one another, but do not show a perfect co-localization (Fig. 3b; refs 10,39). Furthermore, Sec31-positive structures increase upon T-cell activation, but Sec16-positive tER does not (Fig. 3b,c), again suggesting that Sec16 and Sec31 stain (partially) non-overlapping structures. We thus consider it likely that we observe an increase in COPII-coated vesicles in activated T cells; we will, however, use the more general term ERES to describe Sec31-positive structures in the following.

These data raise the possibility that the efficiency of COPII coat recruitment/formation increases upon T-cell activation, as we observe constant Sec16 (tER) staining, but an increase in dot-like COPII staining without a substantial change in overall protein levels (Supplementary Fig. 4b). Furthermore, our data support a model, in which an increase in ERES allows T cells to adapt their early secretory pathway to increased secretory cargo in activated T cells.

Sec16 E29 controls ERES and ER export upon T-cell activation. Having established an increase in the *Sec16* E29 isoform upon T-cell activation (Fig. 1), a role of this isoform in controlling the efficiency of ER-to-Golgi transport (Fig. 2) and an increase in ERES and ER export efficiency in activated T cells (Fig. 3), we went on to provide a direct link between these observations. Transfection of a splice-site blocking morpholino (MO) against exon 29 induced efficient exon exclusion (Fig. 4a–c). In fact, the increase of the *Sec16* E29 isoform upon activation was completely blocked in these cells, and the E29 level in stimulated E29MO-treated cells was reduced to that observed in unstimulated control cells (Fig. 4a–c). While we observe a clear change in Sec16 isoform expression upon E29MO transfection at the RNA level, the overall Sec16 protein level was unchanged (Fig. 4d, upper panel). Using a 4–12% gradient gel, we observed a

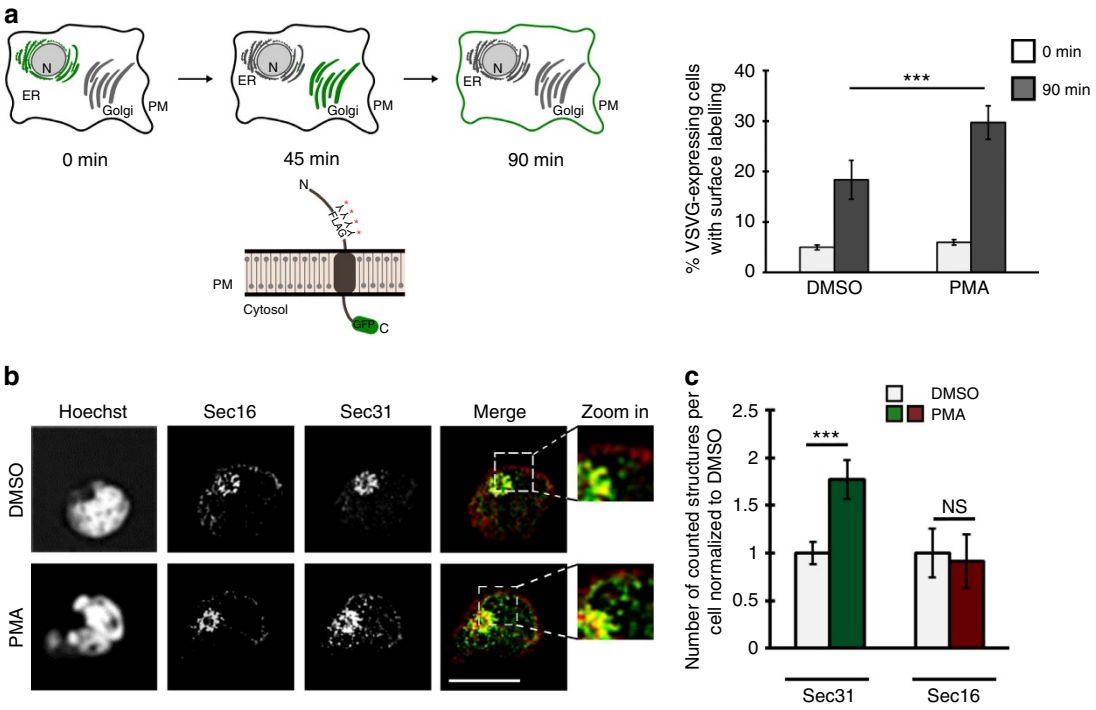

Figure 3 | The number of ERES and transport efficiency increase upon T-cell activation. (**a**) Schematic representation of a FACS-based export assay (left). The VSVG reporter remains in the ER upon 40 °C heat shock and is secreted after shifting the cells to 32 °C. Localization of the reporter at the different time points is indicated by green labelling of the corresponding cellular compartment. For surface labelling, a FLAG coding sequence was inserted in frame into the extracellular domain of the reporter (left, bottom). This assay was used to quantify ER export in resting (DMSO) and activated (PMA) Jsl1 T cells (right). Shown is the mean percentage of VSVG-expressing cells that showed FLAG surface labelling at the indicated time points. $N = 4$, error bars represent s.d. P value is 6.5×10^{-6}. See text and Methods for details. (**b**) Activated T cells show constant tER staining but an increase in ERES number. Fluorescence pictures of resting (DMSO) and stimulated (PMA) Jsl1 T cells. Cells were stained for tER (Sec16/red) and ERES (Sec31/green). (**c**) Cells as in **b** were quantified using the ImageJ particle counting tool as described in Methods. Shown is the average number of counted structures normalized to DMSO ± s.d. of three independent experiments including 15 cells each. Raw numbers for Sec31 DMSO: 39.3 ± 4.5; Sec31 PMA: 68.9 ± 3.7; Sec16 DMSO: 33.8 ± 8.6; Sec16 PMA: 29.3 ± 4.7. $P = 0.00094$ (Student's T-Test) for Sec31 and $P = 0.47$ (Student's T-Test) for Sec16. DMSO, dimethylsulphoxide.

slower migrating isoform as the main Sec16 isoform upon PMA treatment in CoMO-transfected cells. In contrast, the switch to the slower migrating Sec16 isoform was markedly reduced in E29MO-transfected cells, confirming the effect of the E29MO on the protein level (Fig. 4d lower panel). On the basis of these results, we interpret the slower migrating band as the exon 29 containing isoform and the faster migrating band to represent the short isoform lacking both exons; this is consistent with these isoforms representing the main isoforms on the RNA level (Fig. 1). Furthermore, as the Sec16 isoform ratio can be altered by a specific MO, the different bands are most likely not the result of post-translational modifications. Stimulation of the CoMO-transfected cells led to the expected increase in ERES, while, as in untransfected cells, the tER was unchanged (Fig. 4e,f). In contrast, transfection of the cells with the E29MO completely abolished the PMA-induced increase in ERES, whereas the MO had no influence on the tER (Fig. 4e,f). Our data showing that the E29MO reverses the increase in ERES upon PMA stimulation provide direct evidence that *Sec16* alternative splicing, likely the increase in the E29 isoform, mediates this process. To further validate this hypothesis, we used a MO against *Sec16* exon 30 and investigated the effect on Sec16 isoform expression and ERES number upon T-cell activation. The E30MO reduced the Fl and the E30 isoform, and led to a slight increase in the short *Sec16* isoform (Supplementary Fig. 7a). ERES number in these cells was only slightly reduced compared with CoMO-treated cells and this reduction was not statistically significant. Similarly, combining both MOs did not increase the effect on ERES number observed by transfecting the E29MO alone (Supplementary Fig. 7b). These data suggest that it is neither the Fl nor the E30 isoform that play the main role in controlling ERES number. Furthermore, the E30MO led to an increase of the short isoform without resulting in a significant change in ERES number. While this is consistent with the E29 isoform playing the predominant role in this process, we cannot rule out that parts of the effect observed in E29MO-treated cells is due to the strong increase of the short *Sec16* isoform (also see Discussion).

To directly connect *Sec16* alternative splicing with ER export efficiency upon T-cell activation, we performed the FACS-based ER export assay introduced above. As before, CoMO-transfected cells showed increased export efficiency upon PMA stimulation (Fig. 4g). Importantly, this PMA-induced increase in export efficiency was completely abolished in cells that were transfected with the E29MO (Fig. 4g). These data strongly suggest that Sec16 alternative splicing, by increasing ERES number (likely COPII-coated vesicles, see above), allows an adaptation of the early secretory pathway to higher cargo flux upon T-cell activation.

Sec16 exon 29 regulates the efficiency of ER export. To confirm an effect of *Sec16* alternative splicing on ER export efficiency in a more general system, we turned to HeLa cells. All four Sec16 isoforms were expressed in HeLa cells, and as in Jsl1 T cells, transfecting the E29MO resulted in a considerable decrease in the isoforms containing exon 29 (Fig. 5a,b). Consistent with the result in Jsl1 T cells, this was accompanied by a significant loss of ERES,

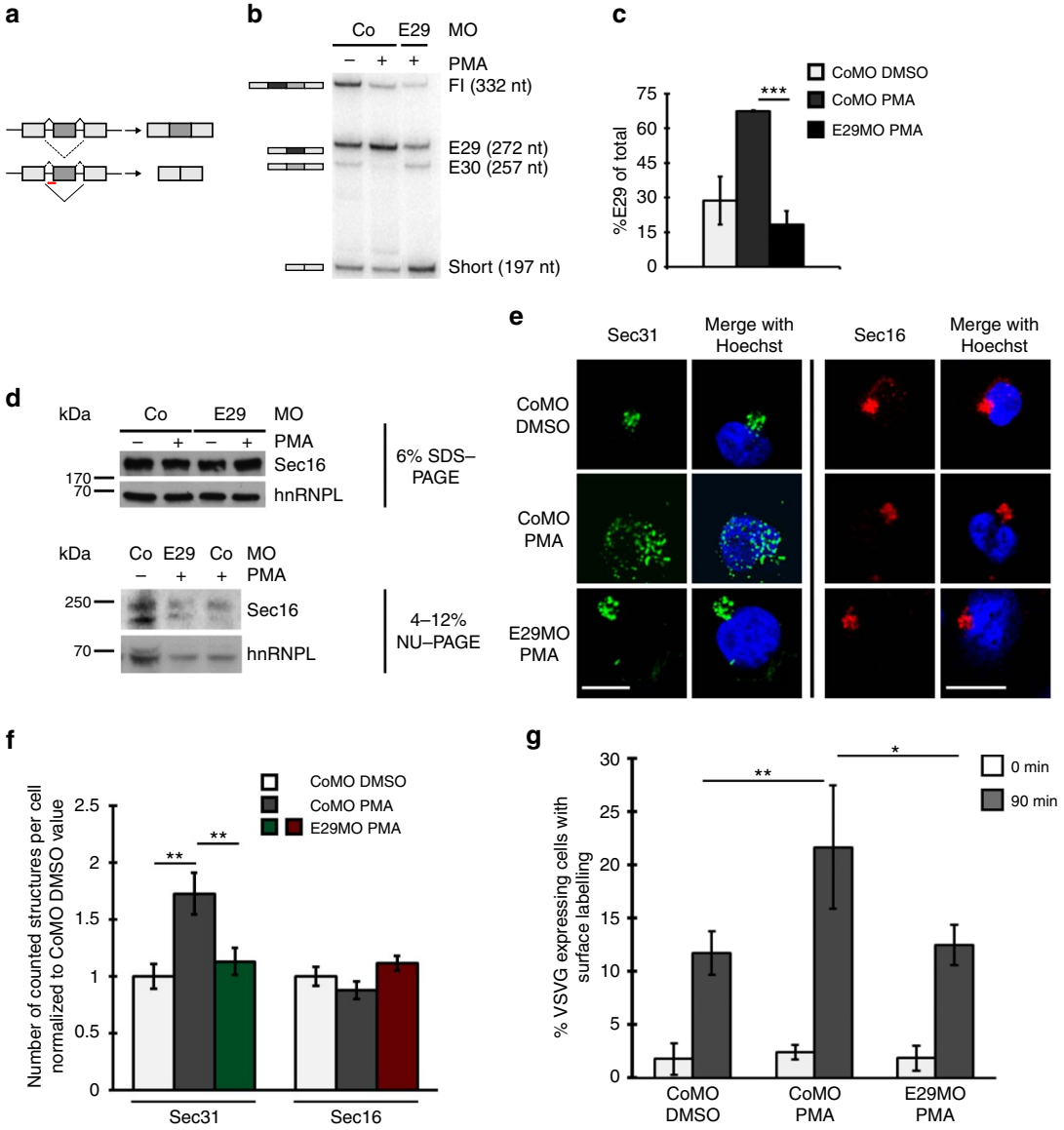

Figure 4 | *Sec16* alternative splicing is required for the increase in ERES upon T-cell activation. (**a**) Schematic view of the morpholino (MO) experiment. The exon in dark grey represents the exon targeted by the MO illustrated by the red bar. (**b**) Radioactive splicing-sensitive RT-PCR as in Fig. 1b of resting and stimulated Jsl1 T cells transfected with MOs as indicated and confirming a specific effect of the E29MO. (**c**) Phosphorimager quantification of the E29 isoform of three independent experiments as in **b**. Shown is the mean amount of the E29 isoform as percentage of total *Sec16* ± s.d. *P* value = 1.3×10^{-4}. (**d**) Total Sec16 protein level is not changed in MO-treated cells. Western blot analysis of whole-cell extract prepared from resting and stimulated Jsl1 cells transfected with either a control MO (CoMO) or a MO targeting Sec16 exon 29 (E29MO). Upper panel shows separation on a standard 6% SDS–PAGE and lower panel shows separation on a 4–12% gradient NuPAGE. hnRNPL served as loading control. (**e**) E29MO treatment prevents the increase of ERES on T-cell activation. Immunofluorescence pictures comparing Sec31 (green) and Sec16 (red) in MO-transfected cells ± PMA. Scale bar, 20 μm. (**f**) Cells described in **e** were analysed using the ImageJ particle counting tool (see Methods for details). Shown is the average number of counted structures normalized to CoMO DMSO ± s.d. of three independent experiments with 15 cells each. Raw numbers for Sec31: CoMO DMSO: 35.5 ± 3.9; CoMO PMA: 61.4 ± 6.5; E29MO PMA: 40.2 ± 4.2. Raw numbers for Sec16: CoMO DMSO: 39.4 ± 3.2; CoMO PMA: 34.6 ± 3.1; E29MO PMA: 40.4 ± 2.6. *P* values are 0.00409 (CoMO DMSO-PMA) and 0.00912 (PMA CoMO-E29MO). (**g**) FACS-based export assay using FLAG-VSVG-GFP as described in Methods. Shown is the percentage of VSVG-expressing cells with FLAG surface labelling after the indicated times at 32 °C under the conditions indicated. *N* = 3, error bar represents s.d. *P* values are: 0.004 and 0.048 (Student's *T*-Test). DMSO, dimethylsulphoxide.

whereas the tER remained unchanged (Fig. 5c,d). Notably, the magnitude of decrease in ERES upon E29MO treatment was similar to the effect observed by short interfering RNA (siRNA)-mediated knockdown of complete Sec16 in HeLa cells, which reduced ERES to 60–70% of control[23,34].

To confirm a direct influence of Sec16 isoform expression in controlling the efficiency of ER-to-Golgi transport, we used a VSVG-based export assay[35]. HeLa cells were sequentially transfected with the Sec16 E29MO and a VSVG-GFP reporter. Cells were then incubated at 40 °C overnight to retain VSVG-GFP in the ER, which was released by shifting the cells to 32 °C. We then quantified the distribution of VSVG-GFP in the ER or post-ER compartments at different time points upon shifting to the permissive temperature. In this assay, the MO-mediated decrease of exon 29 significantly reduced the efficiency of ER-to-Golgi transport (see Fig. 5e and Supplementary Fig. 8 for

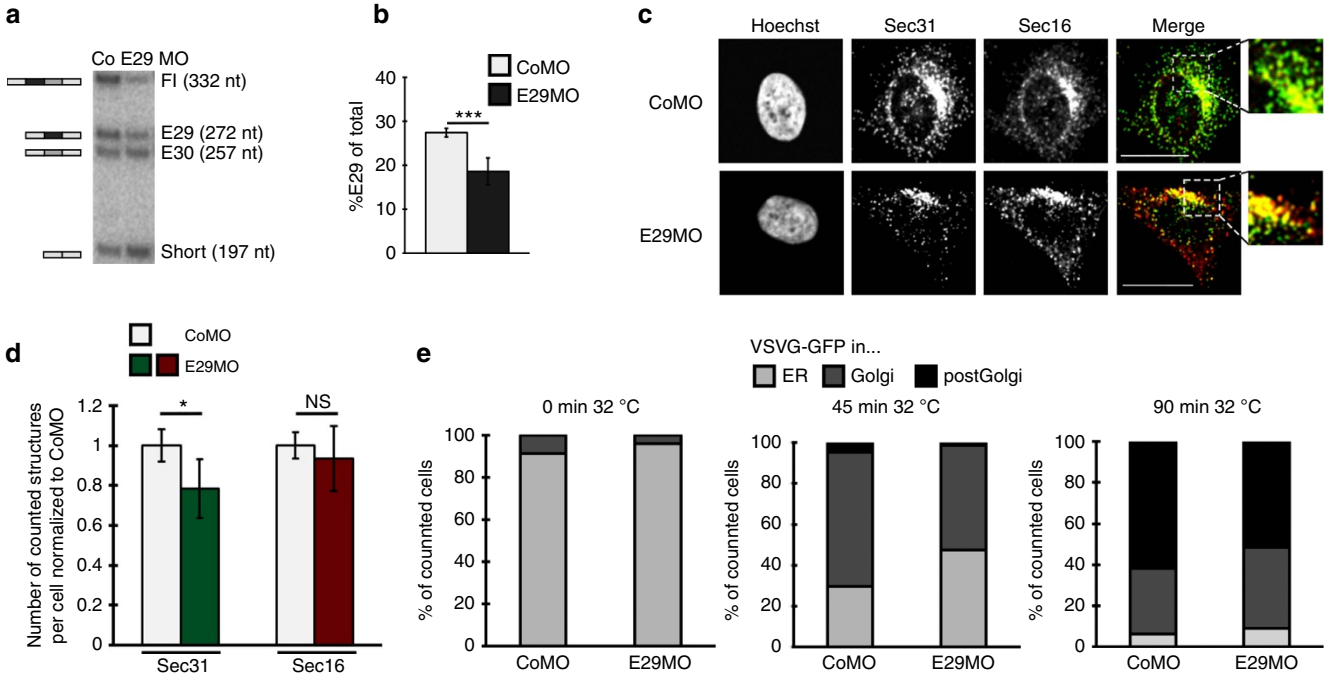

Figure 5 | *Sec16* alternative splicing regulates the efficiency of ER-to-Golgi transport in HeLa cells. (**a**) The *Sec16* E29MO works efficiently in HeLa cells. Radioactive splicing-sensitive RT–PCR as in Fig. 1b of HeLa cells transfected with either CoMO or *Sec16* E29MO. (**b**) Phosphorimager analysis of four independent experiments described in **a**. Shown is the mean amount of the E29 isoform as percentage of total *Sec16* ± s.d. *P* value 2.6×10^{-5}. (**c**) *Sec16* E29MO-treated cells show reduced ERES number and constant tER staining. Immunofluorescence pictures of HeLa cells transfected with either CoMO (top) or E29MO (bottom) stained for Sec16 (red) and Sec31 (green). Scale bar, 20 μm. (**d**) Cells as in **c** were analysed using the ImageJ particle counting tool. Shown is the mean number of counted structures of three independent experiments with 15 cells each normalized to CoMO cells ± s.d. Raw numbers for Sec31: CoMO: 183.7 ± 14.9; E29MO: 142.2 ± 21.7; $P = 0.037$. For Sec16: CoMO: 130.8 ± 8.7; E29MO: 122.7 ± 25.6. (**e**) The *Sec16* E29MO reduces ER export efficiency. VSVG-based export assay in MO-treated HeLa cells as described in Methods. At least 50 cells per condition were analysed per experiment in three independent experiments, shown is the average. Left (0 min): CoMO: cells with VSVG in: ER: 91.1 ± 2.8%; in Golgi: 8.9 ± 2.8%; E29MO: ER: 95.8 ± 1.3%; Golgi: 4.2 ± 1.3%. Middle (45 min): CoMO: ER: 29.8 ± 3.6%; Golgi: 65.7 ± 5.5%; post-Golgi: 4.5 ± 3.3%; E29MO: ER: 47.6 ± 3.7%; Golgi: 51.3 ± 2.7%; post-Golgi: 1.1 ± 1.1%; right (90 min): CoMO: ER: 6.1 ± 2.6%; Golgi: 31.9 ± 1.9%; post-Golgi: 61.9 ± 4.2%; E29MO: ER: 9.1 ± 3.5%; Golgi: 39.3 ± 0.6%; post-Golgi: 51.6 ± 2.9%. *P* values are $P = 0.016$ (Student's *T*-Test) for VSVG in Golgi after 45 min and $P = 0.024$ (Student's *T*-Test) for VSVG in post-Golgi structures after 90 min. For clarity, size marker have been omitted. Sar1A and B-GFP run around 50 kDa below the heavy chain; cytosolic Sec12-GFP runs between 75 and 100 kDa; Sec23-GFP has a predicted size of around 100 kDa and migrates with the corresponding marker band, the four Sec16-FLAG-tagged-CTRs migrate between the 25 and 15 kDa.

costaining of VSVG-GFP with ER and Golgi markers). As for the decrease in ERES number, the decrease in transport efficiency after E29MO treatment was comparable to the effect of siRNA-mediated *Sec16* knockdown[8]. These data directly confirm a regulatory role of *Sec16* isoform expression in the early secretory pathway and again suggest a particularly important role for *Sec16* exon 29 in this regulation.

Altered interaction of Sec16 isoforms with COPII components. To provide a mechanistic basis for our observations, we performed immunoprecipitations (IPs) with the different Sec16 isoforms. We used the four FLAG-tagged Sec16 C-terminal constructs that were expressed at equal levels (Fig. 6a, input). After FLAG-IP, we investigated an interaction with GFP-tagged Sar1A/B, Sec12 and Sec23 as the COPII components that were suggested to directly interact with the C-terminal part of Sec16. Interestingly, exons 29 and 30 seem to differentially influence the interaction with different COPII components: both exons are required for efficient interaction with Sec12, exon 29 alone is sufficient to interact with Sec23 and the interaction with Sar1 requires exon 30 (Fig. 6a). As the IPs with Sec23 suggested the strongest interaction with the E29 isoform, we aimed to test the functional importance of this interaction. To this end, we coexpressed the Sec16 E29 C terminus along with Sec23 and analysed Golgi disruption as in Fig. 2. While expression of Sec23 alone had no effect on Golgi morphology (Supplementary Fig. 9), the effect of the Sec16 E29 C terminus was completely rescued by coexpression of Sec23 (Fig. 6b,c). This indicates that the Sec16–Sec23 interaction is of crucial importance for the Sec16-mediated control of the early secretory pathway. Together, these experiments suggest a model, in which higher expression of the Sec16 E29 isoform and its increased interaction with Sec23 increase the efficiency of COPII transport in activated T cells.

Sec16 E29 controls protein export in primary human T cells. To investigate the physiological relevance of Sec16 exon 29, we analysed alternative splicing and its role in controlling protein secretion in primary human T cells. We used peripheral blood mononuclear cells (PBMCs) that were enriched for T cells and stimulated these cells with physiologically relevant stimuli, either α-CD3 or α-CD3/α-CD28. In both cases, we observed an increase in the exon 29 containing isoform and a concomitant decrease in the shortest isoform (Fig. 7a,b). This is consistent with the recent finding that PHA stimulation of primary human CD4+ T cells increases Sec16 exon 29 inclusion[32]. To test the functional impact of exon 29 in primary cells, we used MO-mediated exon exclusion

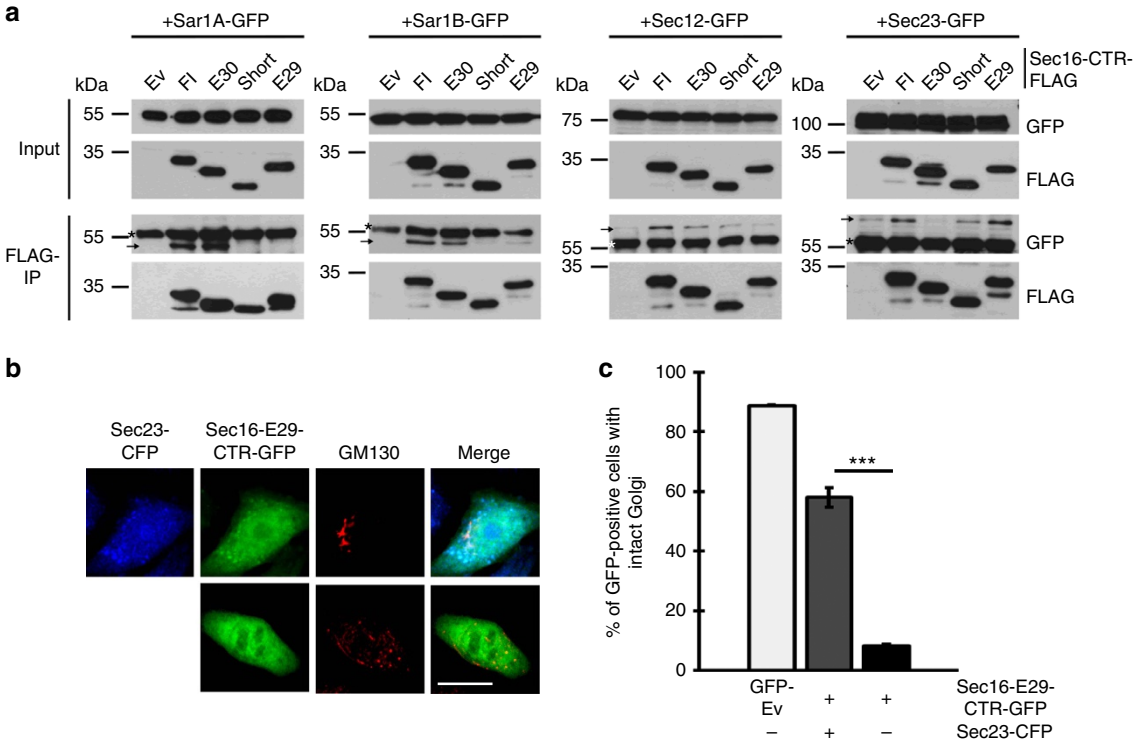

Figure 6 | Different Sec16 isoforms interact differentially with COPII components. (**a**) Coprecipitations of Sec16 isoforms with Sar1A, Sar1B, Sec12 and Sec23A show differential interactions. Hek293 cells were cotransfected with Sec16 CTRs fused to FLAG or FLAG-empty vector as control and COPII components fused to GFP. FLAG precipitates were analysed by western blot using FLAG and GFP antibodies. Top panels show 5% input and bottom panels show FLAG-IPs. → marks the coprecipitated protein and * marks the heavy chain. (**b**) Coexpressing Sec23 with the Sec16-E29-CTR-GFP rescues the effect on Golgi disruption. Fluorescence pictures of HeLa cells coexpressing Sec16-E29-CTR-GFP and Sec23A-CFP (top row) or Sec16-E29-CTR-GFP alone. Golgi is stained using GM130 antibody (red). Scale bar, 20 μm. (**c**) Cells as in **b** were analysed in three independent experiments with an average of 120 cells counted per experiment and compared with cells in Fig. 2c ($P = 0.00014$ (Student's *T*-Test)).

as in Fig. 4. Transfecting T-cell-enriched PBMCs with a Sec16 exon 29 splice-site blocking vivo-MO led to efficient exon exclusion as shown by RT–PCR (Fig. 7c). We used these cells, along with control vivo-MO-transfected cells, stimulated with α-CD3/α-CD28 and investigated secretion of interleukin (IL) 2 by enzyme-linked immunosorbent assay (ELISA). In this experiment, we observed a significantly reduced IL2 secretion in cells transfected with the E29MO (Fig. 7d). However, the amount of intracellular IL2 that was measured after inhibition of protein secretion was similar in E29MO- and CoMO-transfected cells, suggesting that Sec16 exon 29 exclusion does not alter total IL2 levels, but interferes with protein secretion (Fig. 7e). These data confirm our model in primary human T cells using a physiologically relevant stimulus. Altered export of an endogenous interleukin upon skipping of exon 29 emphasizes the relevance of *Sec16* splicing in the regulation of T-cell function.

Cells lacking Sec16 E29 show decreased ERES and ER export. Finally, we confirmed the crucial importance of *Sec16* exon 29 in the early secretory pathway using CRISPR/Cas9-mediated deletion of this exon in Hek293 cells. We obtained cells with homozygous deletion of exon 29 as assessed by genomic PCR and RT–PCR (see Fig. 8a and Supplementary Fig. 10a for targeting strategy). RT–PCR confirmed that deletion of exon 29 abolished formation of the full-length and E29 isoforms, whereas the E30 and short isoforms were still expressed (Fig. 8a). Western blots showed that deletion of exon 29 did not change overall protein levels, suggesting that the lack of exon 29 led to the increased formation of remaining isoforms (Fig. 8b). In line with MO experiments, staining of exon 29-deleted cells for Sec31 revealed a strongly reduced number and a more compact ERES localization when compared with wild-type (WT) Hek293 cells (Fig. 8c,d), while Sec16 staining itself (tER) showed no difference (Supplementary Fig. 10b). We then aimed to measure protein export in a VSVG-based export assay. However, as the exon 29-deleted cells showed reduced adherence, especially after the overnight incubation at 40 °C, we were unable to obtain enough cells for quantification after staining for IF. An EndoH assay qualitatively suggested a reduced efficiency of ER export in Hek293 cells lacking *Sec16* exon 29 (Fig. 8e), but was difficult to quantify due to the proximity of the two VSVG species in the SDS gel. To quantitatively measure protein export we turned to the FLAG-modified VSVG and FACS as read-out as described above. These experiments confirmed a strong export defect in *Sec16* exon 29-deleted cells, as the presence of the FLAG-tagged VSVG at the cell surface 90 min after shifting the cells to 32 °C was significantly reduced when compared to control cells (Fig. 8f).

The genome-engineered cells represent a well-suited model system to start addressing the mechanism of *Sec16* exon 29 mediated control of export efficiency. Our data would be consistent with exon 29 mediating more efficient COPII coat formation, probably through increased interaction with Sec23. We therefore used Sec23 fluorescence recovery after photobleaching (FRAP) to compare COPII dynamics in WT and exon 29-deleted cells. As predicted by our model, cells lacking *Sec16* exon 29 show a significantly increased Sec23 FRAP half-life (Fig. 8g), suggesting that COPII turnover is reduced in these cells. Together with the interaction studies in Fig. 6, these data suggest that Sec16 isoforms control

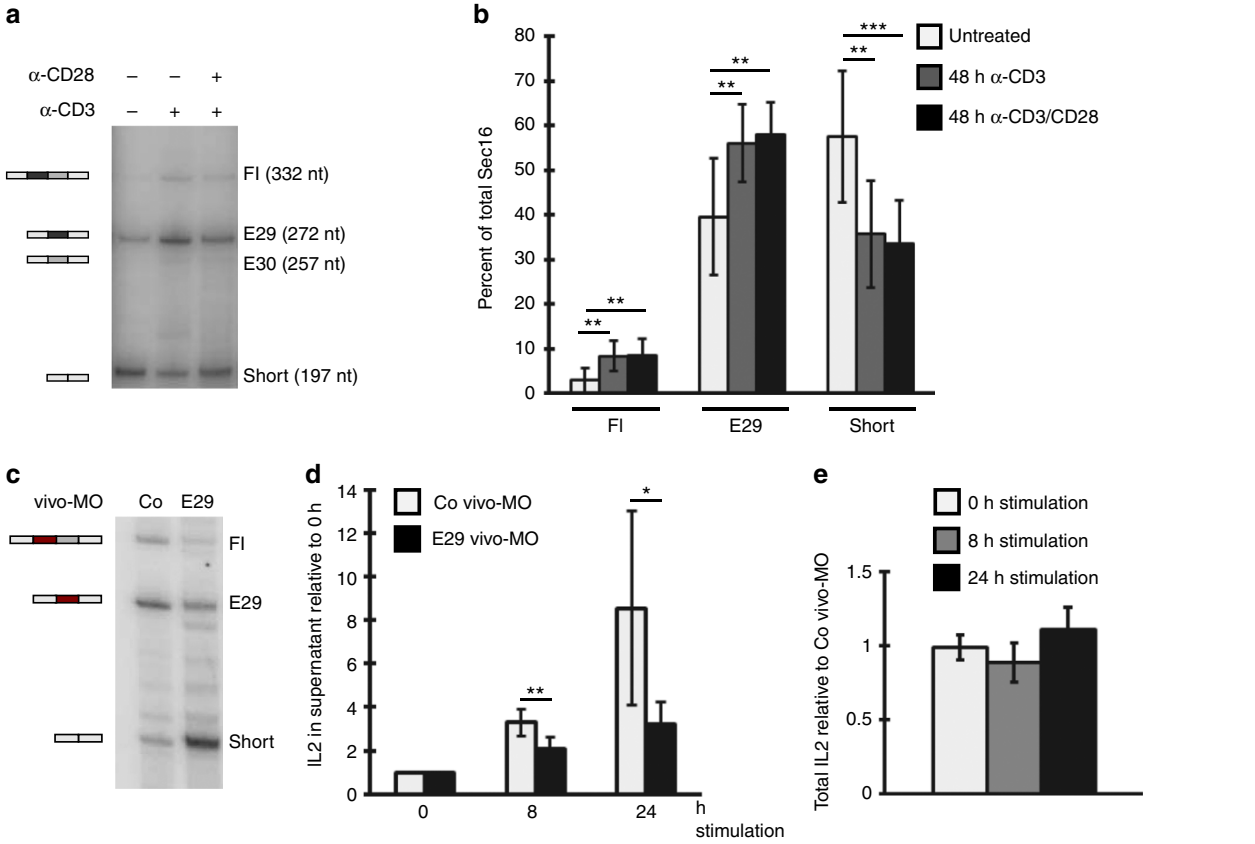

Figure 7 | *Sec16* is alternatively spliced upon activation of primary human PBMCs. (**a**) Primary human PBMCs were cultured and stimulated after lymphocyte enrichment (removing adherent cells) as described[33]. T-cell percentage was determined by FACS for three independent donors (66.9 ± 6.8% CD4 and 15.5 ± 4.7% CD8). RNA was prepared and *Sec16* isoform expression was analysed as in Fig. 1b. (**b**) Phosphorimager analysis shows the average percentage of *Sec16* isoforms. Shown is the average of four different donors measured in duplicates ± s.d. Note that E30 isoform is not reproducibly detectable in these primary cells. *P* values are for CD3: 0.002 (Fl); 0.006 (E29); 0.003 (short); for CD3/28: 0.0029 (Fl); 0.0018 (E29) and 8.7×10^{-4} (short) (Student's *T*-Test). (**c**) Cells as in **a** were transfected with vivo-MOs and *Sec16* isoform expression was analysed as in **a**. (**d**) T-cell-enriched PBMCs as in **a** were transfected with vivo-MOs, stimulated for the indicated time with α-CD3/α-CD28 and IL2 in the supernatant was measured by ELISA at the indicated time points. Data are normalized to unstimulated cells ($t = 0$) and represent means of four independent experiments each with two independent stimulations and assessed in duplicate ± s.d. *P* values are: 0.0098 and 0.031 (Student's *T*-Test). (**e**) PBMCs stimulated as in **d** were additionally treated with BFA for the last 40 min, cells were then lysed and total IL2 was measured as in **d**. Shown is the amount of IL2 in E29MO-transfected cells relative to CoMO-transfected cells at each time point ± s.d. ($n = 4$).

COPII dynamics through differential interaction with COPII members to regulate the efficiency of the early secretory pathway (see model in Fig. 9).

Discussion

Our data define the C terminus of Sec16 as a protein–protein interaction platform that is regulated by alternative splicing to control protein secretion upon T-cell activation. To our knowledge, this is the first example of an alternative splicing event that dynamically controls the early secretory pathway in response to changing cellular demands. Our data thus add a new regulatory layer to the control of COPII transport and describe an adaptive mechanism to increased endogenous secretory cargo.

Formation of COPII-coated vesicles has been investigated over the last decades, uncovering mechanistic and structural details. However, it remains largely unknown how the COPII machinery dynamically adapts to changes in secretory cargo load upon changing cellular conditions[34]. Similarly, it remains elusive how the COPII pathway adapts to tissue-specific differences in secretory cargo flux. The existence and tissue-specific expression of several paralogues of COPII components, for example, *Sar1A* and *Sar1B* or *Sec24A–D*[26] may be one mechanism to control the early secretory pathway. This idea is supported by mouse models[28] and human diseases linked to mutations in only one of several paralogues[29]. However, functional differences between paralogues are only beginning to emerge[40] and the regulation of individual COPII members, for example by alternative splicing, is even less well understood. It is interesting to note that we have observed *Sec16* alternative splicing also in mouse and find tissue-specific splicing patterns (unpublished observation). This suggests that *Sec16* alternative splicing not only controls dynamic adaptation of the COPII machinery but also contributes to tissue-specific differences in the early secretory pathway, probably acting together with selective expression of COPII paralogues.

Upon T-cell activation, a resting cell strongly increases the expression of many secreted effector molecules such as interleukins, cytokines and cytotoxins. However, the adaptation of ER-to-Golgi transport to this increase in cargo flux has, until now, not been investigated. Our work shows that indeed export efficiency is strongly increased in activated T cells and suggests that the underlying mechanism is an increase in the number of ERES, more specifically COPII-coated vesicles, mediated by Sec16 alternative splicing. We thus provide evidence for an adaptive mechanism to increased endogenous secretory cargo, also in primary human cells. Notably, Sec16 has been identified as a protein controlling ER

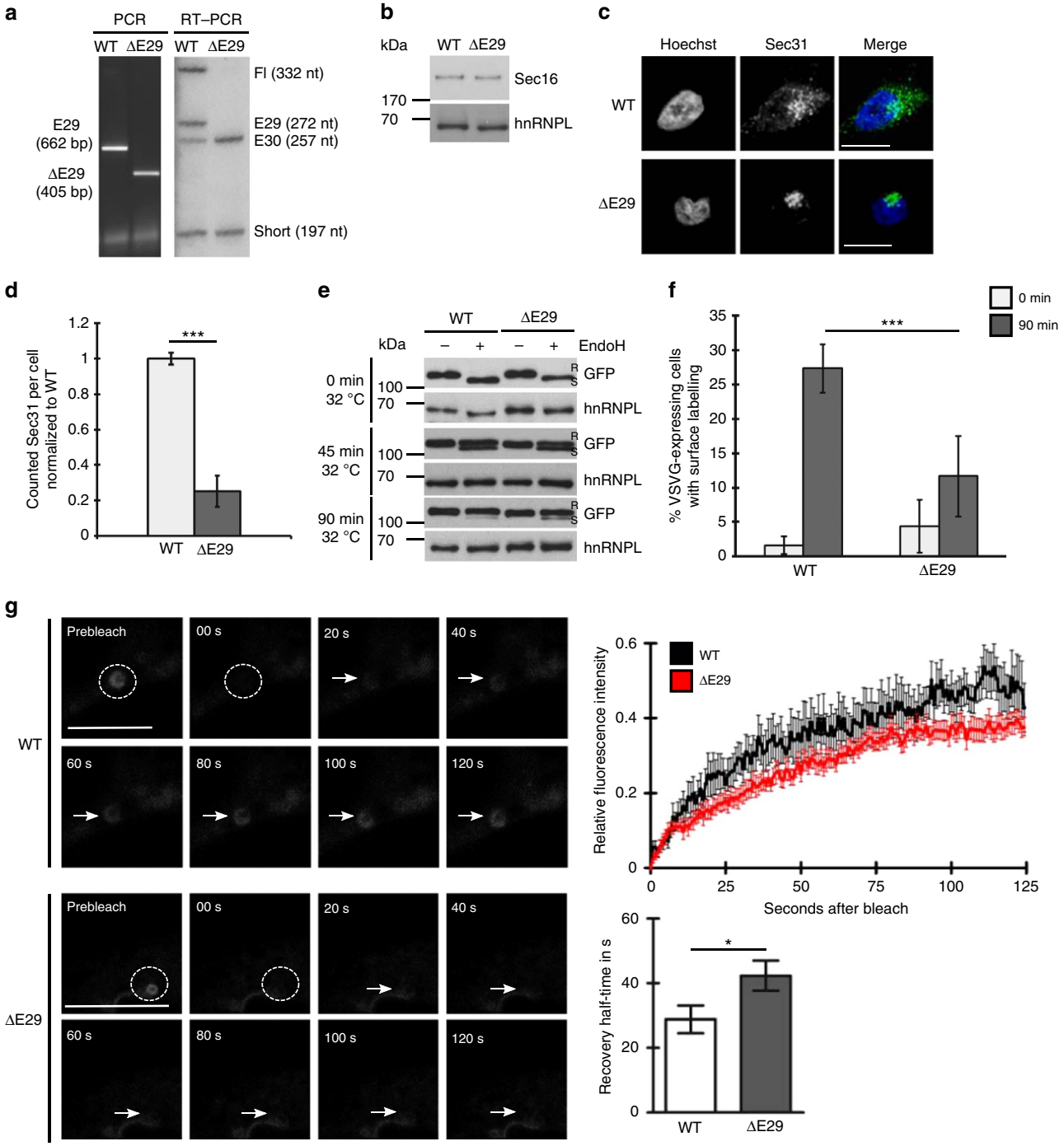

Figure 8 | *Sec16* exon 29 is necessary for efficient ERES formation and ER-to-Golgi transport. (**a**) CRISPR/Cas9-mediated deletion of *Sec16* exon 29 detected at the DNA and RNA level by genomic PCR (left) and RT-PCR (right). (**b**) Sec16 western blot of whole-cell extracts prepared from WT and ΔE29 Hek293 cell lines showing no difference of the total protein level. hnRNPL was used as a loading control. (**c**) Deletion of *Sec16* exon 29 strongly reduces ERES number. Immunofluorescence pictures of Hek293 WT and ΔE29 cells stained for Sec31. Scale bar, 20 μm. (**d**) Cells described in **c** were analysed using the ImageJ particle count tool. Shown is the mean number of counted Sec31-positive structures normalized to WT ± s.d. of three independent stainings with a total of 30 cells analysed. Raw numbers are for WT: 77.1 ± 2.6 for ΔE29: 19.5 ± 6.8. $P = 0.0002$ (Student's *T*-Test). (**e**) *Sec16* exon 29-deleted cells show a defect in ER export. Export assay performed in WT Hek293 and ΔE29 cells using the ts045-VSVG-GFP variant and EndoHf as described in Methods. VSVG was detected using GFP antibody. hnRNPL served as a loading control. R, resistant to EndoHf; S, sensitive to EndoHf. (**f**) Loss of *Sec16* exon 29 reduces protein secretion. Export assay performed in WT and ΔE29 Hek293 cells using a VSVG variant containing an internal FLAG-tag as a surface marker. Cells were stained with α-FLAG at the indicated time points after shifting the cells to 32 °C and secretion levels were measured via FACS. Shown is the average of three independent experiments. $P = 0.00014$. (**g**) COPII turnover rate is reduced in ΔE29 cells. WT and ΔE29 293Hek cells were transfected with a plasmid encoding Sec23 fused to a C-terminal GFP-tag. Sec23 turnover was analysed via FRAP. Left panel shows representative time laps pictures for each cell type. Scale bar, 10 μm. Upper right shows FRAP curves with slower recovery rate for Sec23 in ΔE29 cells and lower right shows a prolonged calculated half-life ± s.e.m. $n = 15$ from four independent experiments, $P = 0.0124$ (Student's *T*-Test).

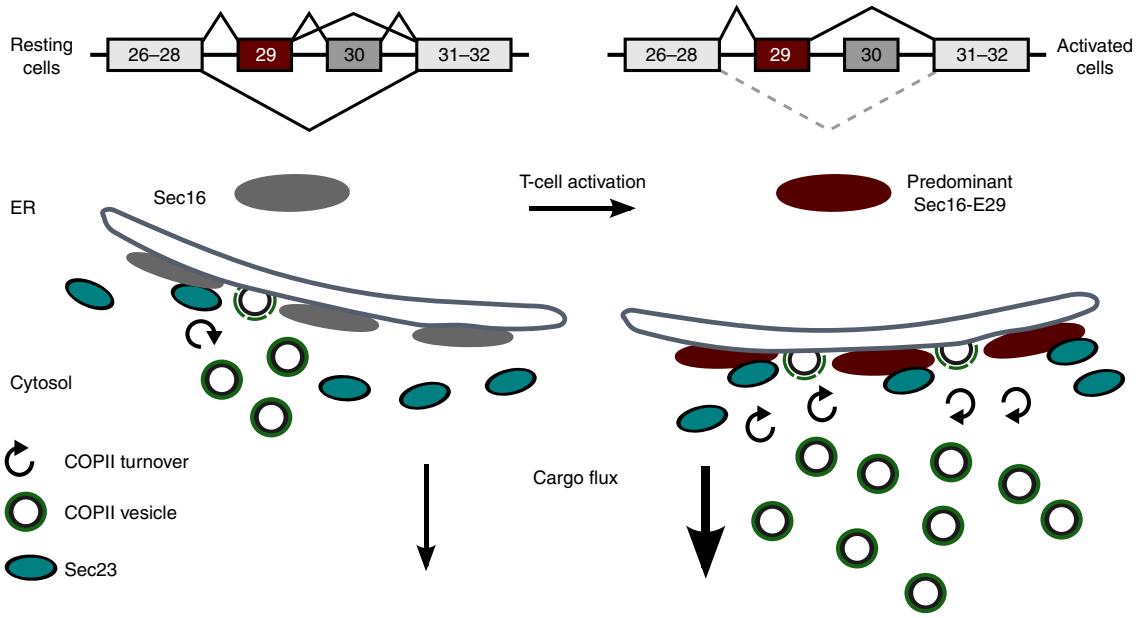

Figure 9 | Model summarizing the adaptation of the early secretory pathway upon T-cell activation. The main *Sec16* splice variants in resting and activated T cells are shown. The tER shape does not change upon T-cell activation, but Sec16 shows altered isoform expression (red). In activated T cells, Sec16 exon 29 containing isoforms show increased interaction with Sec23 and lead to an increase in COPII dynamics, COPII-positive structures (Sec31, green) and secretory cargo flux.

export in response to starvation[25], growth factor signalling and proliferation[24,34], and ectopic expression of secretory cargo[23]. In the latter study, a slight increase in the overall Sec16 expression level was observed[23] and changing Sec16 levels were also observed in response to growth factor signalling[34]. In addition, Sec16 phosphorylation has been shown to regulate its activity, for example by changing its intracellular localization in response to starvation[25]. These studies, together with our work, identify different levels of Sec16 modifications that, in response to changing cellular conditions, alter Sec16 functionality by distinct mechanisms. It is possible that Sec16 is modified by different mechanisms simultaneously, as we cannot rule out phosphorylation in addition to alternative splicing in activated T cells, and other studies have not investigated differential Sec16 isoform expression. Taken together, these studies show that several distinct signalling pathways converge on Sec16 to control ER export, suggesting Sec16 to play a central role in the dynamic adaptation of COPII transport in diverse cellular settings.

Our MO and CRISPR/Cas9 experiments clearly show an important role of *Sec16* alternative splicing, in particular exon 29, in regulating the COPII pathway. It is noteworthy that the MO-mediated change in *Sec16* alternative splicing has a similar effect on ERES number and export efficiency as siRNA-mediated knockdown of complete *Sec16* (refs 8,23,34). This is consistent with differential *Sec16* isoform expression playing a crucial role in controlling ERES formation and ER export. Our experimental conditions do lead to a reduction of the full-length and E29 isoform, and to an increase in the E30 and short isoforms with overall constant protein levels. These experiments do not distinguish whether it is the loss or gain of one of these isoforms that causes the observed phenotype. However, overexpression of the different C-termini and their effect on disrupting ER-to-Golgi transport provides additional information. In this experiment, the E29 C terminus clearly stands out as the isoform with a profound effect on the COPII pathway. These data together suggest that it is the loss of the E29 isoform that causes the defect in MO-treated and genome-engineered cells. This conclusion is further supported by experiments using a MO targeting *Sec16* exon 30, which did not result in a significant change of ERES number despite altered *Sec16* isoform expression. In addition, in the endogenous situation it is the E29 isoform that changes most strongly upon T-cell activation, again pointing to this isoform to mediate functional changes. However, given the differential interaction of the different Sec16 isoforms with COPII components, it appears possible that expression of the other Sec16 splice variants and ultimately the isoform ratio contribute to the regulation of ER export efficiency in the endogenous situation. A model is conceivable in which different Sec16 isoforms preferentially recruit particular components of the COPII machinery, which could then influence the efficiency of COPII coat generation and vesicle budding. Unfortunately, overexpressing full-length Sec16 isoforms interfered with the early secretory pathway (unpublished observation and refs 8,13), preventing us from testing whether expression of the E29 isoform alone would lead to more ERES and more efficient ER export or whether additional isoforms need to be coexpressed.

Interestingly, the defect caused by overexpressing the E29 C terminus can be completely rescued by coexpressing Sec23. Sec23 appeared to interact stronger with the E29 than with the other isoforms and has been suggested to fulfil a central role in the COPII pathway[37]. Consistently, our data suggest a crucial role of the Sec16–Sec23 interaction in controlling COPII transport. It furthermore points to a model, in which efficient recruitment of Sec23 by the Sec16 E29 isoform, potentially in combination with altered interaction with other COPII components, increase the efficiency of COPII vesicle formation and ER-to-Golgi transport. This model is supported by our FRAP experiments showing reduced COPII dynamics in cells lacking *Sec16* exon 29. The precise molecular mechanism for this regulation is so far unknown. A mere scaffolding function of Sec16 is conceivable and a more efficient interaction of the E29 isoform with Sec23 could explain the observed effects. However, Sec16 has

been shown to negatively regulate Sar1 activity by interfering with the Sec31-mediated increase in the GAP activity of Sec23 (refs 5,18,19). It is thus possible that in addition to the scaffolding function, Sar1 GTPase activity is differentially regulated by Sec16 isoforms, which interact differentially with Sar1, Sec12 (GEF) and Sec23 (GAP). This could allow a fine-tuning of Sar1-GTP hydrolysis, potentially depending on the Sec16 isoform ratio, which could be a decisive factor in controlling COPII vesicle formation.

In addition to Sec16, several other ER-localized proteins with known functions in ER export were shown to be alternatively spliced upon T-cell activation[32]. We therefore expect that our present work is only the first example of a connection between alternative splicing and the early secretory pathway, which may turn out to be a common regulatory principle.

Methods

Cell culture and transfection. Hek293 and HeLa cells were grown in DMEM supplemented with 10% fetal bovine serum and 1% penicillin/streptomycin (Invitrogen). Transfection of these cell lines was performed using Lipofectamine 2000 (Invitrogen) according to the manufacturer's instructions. For MO experiments, cells were seeded and transfected 1 day later using Endoporter following to the manufacturer's manual. MOs (Sec16 E29: ACCTGCCGAGGAAA AGAAGAATTGC and standard control) and Endoporter transfection reagent were purchased from Gene Tools.

Maintenance, transfection and stimulation of Jsl1 cells, and generation of stable cell lines were done essentially as described[32]. Stimulation was carried out using PMA (Sigma) at a final concentration of 20 ng ml^{-1} and an equal amount of dimethylsulfoxide as a vehicle control. Unless otherwise mentioned, experiments were performed 48 h post stimulation. For RNA stability assays, Jsl1 cells were treated with actinomycin D (Sigma) at a final concentration of 5 μg ml^{-1} for 0, 4 and 8 h, and cells were collected for RNA isolation. For the protein stability assay, cells were treated with cycloheximide at a final concentration of 40 μg ml^{-1} and cells were collected after 0, 6 and 10 h for further analysis.

For induction of ER stress, Jsl1 cells were treated with 1 μg ml^{-1} tunicamycin overnight. Stress induction was verified by quantitative RT–PCR (RT–qPCR) of marker genes.

For genome-engineering in Hek293 cells, intronic sequences flanking E29 of *Sec16* were analysed for single guide RNA (sgRNA) candidates *in silico*[41]. A pair of oligos for the highest ranked candidate sgRNAs (E29 5′-FW caccGAAGAGGGCG TTTGTAACCC, E29 5′Rev aaacGGGTTACAAACGCCCTCTTC, E29 3′-FW CaccgCTTTATGGAGGGGCGGTACT, E29 3′-Rev aaacAGTACCGCCCCTCCA TAAAGc) was synthesized and subcloned into the pSpCas9 (BB)-2A-Puro: PX459 vector (kindly provided by Stefan Mundlos). Hek293 cells were seeded on 24-well plates 24 h before transfection. Cells were transfected using Rotifect at 80–90% confluency following the manufacturer's protocol. For each well of a 24-well plate, a total of 500 ng Cas9 + sgRNA plasmid was used. Fourty-eight hours after transfection, the cells were treated with 1 μg ml^{-1} puromycin to select for cells expressing the sgRNAs. Genomic DNA was extracted using DNA extraction buffer (200 mM Tris (pH 8.3), 500 mM KCl, 5 mM $MgCl_2$ and 0.1% gelatine in H_2O) and a PCR was performed using gene-specific primers. First, the population of targeted cells was analysed and then clonal cell lines were isolated by dilution[41].

All cell lines were routinely tested and found negative for mycoplasma using a PCR-based method. Jsl1 cells were obtained from Kristen Lynch (UPenn), Hek293 and HeLa cells are lab stocks that have been extensively used over the past years and that show the expected morphological characteristics.

Constructs. ts045-VSVG-GFP was purchased from Addgene (#11912), GFP-Sec16 full-length expression plasmid was kindly provided by David Stephens (Bristol, UK). The Sec12 construct used for IPs corresponds to the cytoplasmic Sec12 used for a similar experiment before[16].

For all other expression constructs, open reading frames were PCR-amplified from complementary DNA using primers introducing restriction sites. Products were digested and ligated into pCMV-N3-FLAG or pCMV-N3-GFP expression vectors. All constructs were verified by sequencing.

For primer sequences see Supplementary Table 1.

RNA and RT–PCR and RT–qPCR. RNA was isolated using PeqGOLD RNApure (Peqlab) according to the manufacturer's instructions. RT–PCR was done as described[42]. Briefly, 1 μg RNA was used for RT–PCR using a gene-specific reverse primer for the RT reaction followed by a low-cycle PCR using a radioactive ^{32}P-labelled forward primer. PCR products were separated on a denaturing PAGE. Quantification was done after phosphorimaging using ImageQuant TL software. Quantifications are shown as mean of independent experiments ± s.d. For *Sec16* splice PCR, the following primer pair was used: forward: 5′-GATGGCCTCCTCGCTCTCTCATCCC-3′ and reverse: 5′-GCCAGCTGAGCAGGGTTGTAGAAGG-3′. For RT–qPCRs, the RT protocol described above was used combining up to four gene-specific reverse primers. qPCR was performed using the ABsolute qPCR SYBR green mastermix in a 96-well-plate in a Stratagene MX3005p system.

Western blotting and IP. Whole-cell extracts (WCEs) were prepared with lysis buffer (60 mM Tris (pH7.5), 30 mM NaCl, 1 mM EDTA and 1% TritonX-100) supplemented with protease inhibitors. Concentrations were determined using Bradford test. SDS–PAGE, NuPAGE and western blotting were performed using standard protocols. For IPs, 50 μg WCEs was incubated in 500 μl modified RIPA buffer (10 mM Tris (pH8.0), 1% NP40, 5 mg ml^{-1} sodium deoxycholate, 2 mM EDTA and 200 mM NaCl) supplemented with protease inhibitors and pre-cleaned by rotating 1 h at 4 °C with protein-A/G sepharose beads (Santa Cruz). Pre-cleaned WCE was then supplemented with equilibrated FLAG-M2 beads (Sigma) and rotation was continued overnight at 4 °C. Beads were then washed five times and eluted by boiling 5 min in 2 × SDS-loading buffer. Eluted samples were separated on SDS–PAGE and analysed by western blotting.

For all WBs where only the relevant part of the blot is shown in the main figure, full blots are presented in Supplementary Fig. 11.

Antibodies. The following primary antibodies were used: α-GFP (B2, sc9996, Santa Cruz, WB 1:500), α-FLAG (DYKDDDDK, 2368, Cell Signaling, WB 1:1,000), α-FLAG (M2, Sigma, FACS 1:400), α-hnRNPL (4D11, sc32317, Santa Cruz, WB loading control 1:5,000), α-GAPDH (GT239, GeneTex, WB loading control 1:5,000), α-Sec16 (KIAA0310, A300-648A-1, Bethyl laboratories, WB 1:1,000 and IF 1:200), α-Sec31A (sc-136233, Santa Cruz, WB 1:1,000 and IF 1:200), α-Sec24C (IF 1:100, kindly provided by David Stephens, ref. 36), α-GM130 (EP892Y, 1837-1, Epitomics, IF 1:400), α-ERGIC53 (E1031, Sigma, IF 1:400) and α-Sar1A (SAB1402607, Sigma, WB 1:500). The following conjugated secondary antibodies were used: α-mouse-HRP (7076S, Cell Signalling, WB 1:5,000), α-rabbit-HRP (7074S, Cell Signalling, WB 1:5,000), α-rabbit-Alexa647 (A21245, Life Technologies, IF 1:400), α-mouse-Alexa488 (A212002, Life Technologies, IF 1:400) and α-Mouse-Cy5 (Jackson Immuno Research, IF 1:400).

Export assay and EndoHf. Cells were transfected with the ts045-VSVG-GFP reporter construct and shifted to 40 °C overnight to retain the reporter protein in the ER. On the next day, cells were supplemented with cycloheximide at a final concentration of 100 μg ml^{-1} before they were shifted to the permissive temperature of 32 °C to allow refolding and secretion of the reporter protein. Cells were fixed at the indicated time points for IF or collected for EndoHf digestion. EndoHf was used according to the manufacturer's instructions. In brief, 10 μg WCE was incubated at 95 °C for 10 min to allow denaturing. Afterwards, the samples were incubated for 1 h at 32 °C with 1,000 U enzyme and separated for further analysis on SDS–PAGE. To analyse protein export by IF, cells transfected and treated as above were processed for IF 45 and 90 min post heat shock. To determine VSVG localization with respect to the Golgi, cells were stained with the *cis*-Golgi marker GM130. The level of secretion was defined according to the localization of VSVG in ER (pre-Golgi), Golgi or post-Golgi structures. Where indicated, a plasmid encoding dsRed fused to an ER retention signal was transfected.

FACS and ELISA. For secretion rate analysis by FACS, export assays were performed as described above using a ts045-VSVG-GFP variant expressing an internal FLAG-tag introduced in frame in the EcoNI site in the extracellular domain of the protein. Jsl1 cells were collected on shifting cells to 32 °C for 90 min and stained against the FLAG epitope for 30 min on ice in 3% bovine serum albumin in PBS. Cells were washed in PBS and stained with a Cy5 coupled α-mouse antibody for 30 min on ice in 3% bovine serum albumin in PBS. Cells were washed and resuspended in an adequate volume of PBS and analysed using a Guava easyCyte 8 FACS. Living cells were gated for GFP expression and analysed for FLAG surface staining.

Hek293 cells, WT and ΔE29, were seeded in 12-well plates and transfected with the VSVG variant described above. After the 40 °C heat shock, cells were trypsinized, kept at 32 °C for the indicated time, and then stained and analysed by FACS as described above.

IL2 sandwich ELISA was performed using the ELISA MAX Kit (BioLegend) according to the manufacturer's instructions. Primary human PBMCs were isolated as described[33] and T cells were enriched by removing adherent cells. Cells were then transfected with the *Sec16* E29 or control vivo-MO and stimulated with 1 μg precoated CD3 and 1 μg soluble CD28 for the indicated times. For total IL2 analysis, cells were treated with 5 μg ml^{-1} Brefeldin A (BFA) at 37 °C 40 min before collecting, washed in PBS and lysed in non-denaturing lysis buffer (20 mM Tris–HCl (pH 8.0), 137 mM NaCl, 10% glycerol, 1% NP40, 2 mM EDTA and proteinase inhibitors).

Fluorescence microscopy and FRAP. Cells were seeded on coverslips and transfected the following day. Fourty-eight hours later, cells were fixed in 4% paraformaldehyde, followed by equilibration with 0.1% Tx100/PBS and blocking in 5% goat serum/PBS. Primary antibody was incubated for 2 h at room temperature

and secondary antibody for 1 h at room temperature. After nucleus staining using Hoechst, the cells were mounted in Moviol and dried overnight before imaging. Jsl1 cells were collected and fixed in a 1.5 ml reaction tube followed by cytospin for 7 min at 200 r.p.m. Cells were then treated as described above. To study the impact of Sec16 CTR overexpression, HeLa cells were seeded on coverslips and transfected on the following day with plasmids encoding the four different Sec16 CTRs fused to a C-terminal GFP-tag. Fourty-eight hours post transfection, cells were fixed and stained with the *cis*-Golgi marker GM130. The Golgi morphology in untransfected cells appeared as one distinct structure close to the nucleus and was defined as 'intact'. Golgi stainings that showed a loose multimeric structure in the cell periphery were defined as a 'disrupted' Golgi. Dividing cells, as identified by Hoechst staining, were not considered as these cells showed a natural dispersed Golgi structure (see Supplementary Fig. 2 for examples).

Samples were imaged with either a Leica TC Sp2 or TC SP8 using a $\times 63$ magnification oil immersion objective. Images were processed using ImageJ free software. For Sec16 and Sec31, quantification images were analysed using the ImageJ particle count tool. For this purpose, images were converted into 8 bit images in grayscale applying uniform thresholding. A scale was set to each picture and particles with a diameter above 60 nm were counted corresponding to the lower size limit of a COPII vesicle[29].

For FRAP experiments, cells were seeded in 4 cm Willco dishes in DMEM medium with 10% fetal bovine serum and transfected 1 day later with a Sec23-GFP-expressing plasmid. Twenty-four hours after transfection, medium was replaced by DMEM without carbonate and phenol red, and supplemented with 20 mM HEPES. Imaging was performed with a Leica SP2 equipped with a preheated 37 °C chamber using a $\times 63$ oil immersion objective and the 488 nm Ar laser. Five prebleach images were acquired, followed by eight bleaching images with 100% laser intensity. After bleaching, 150 images were taken with a scanning speed of 400 Hz. FRAP recovery rate was determined after full-scale normalization, setting prebleach intensity to 1 and post-bleach intensity to 0. Calculation of half-life time was performed as previously described[43] using GraphPad Prism software.

Statistical analysis. The number of independent experiments is given in each figure. To test significance, Student's unpaired *T*-test was performed using standard office software. The following thresholds were used: $^{*}P<0.05$; $^{**}P<0.01$; $^{***}P<0.001$.

Data availability. The authors declare that the data supporting the findings of this study are either available within the article (and its Supplementary Information files) or available on request by emailing the corresponding author.

References

1. Antonny, B. & Schekman, R. ER export: public transportation by the COPII coach. *Curr. Opin. Cell Biol.* **13,** 438–443 (2001).
2. Gurkan, C., Stagg, S. M., Lapointe, P. & Balch, W. E. The COPII cage: unifying principles of vesicle coat assembly. *Nat. Rev. Mol. Cell Biol.* **7,** 727–738 (2006).
3. Sato, K. & Nakano, A. Dissection of COPII subunit-cargo assembly and disassembly kinetics during Sar1p-GTP hydrolysis. *Nat. Struct. Mol. Biol.* **12,** 167–174 (2005).
4. Supek, F., Madden, D. T., Hamamoto, S., Orci, L. & Schekman, R. Sec16p potentiates the action of COPII proteins to bud transport vesicles. *J. Cell Biol.* **158,** 1029–1038 (2002).
5. Kung, L. F. *et al.* Sec24p and Sec16p cooperate to regulate the GTP cycle of the COPII coat. *EMBO J.* **31,** 1014–1027 (2012).
6. Adolf, F. *et al.* Scission of COPI and COPII vesicles is independent of GTP hydrolysis. *Traffic* **14,** 922–932 (2013).
7. Budnik, A. & Stephens, D. J. ER exit sites--localization and control of COPII vesicle formation. *FEBS Lett.* **583,** 3796–3803 (2009).
8. Watson, P., Townley, A. K., Koka, P., Palmer, K. J. & Stephens, D. J. Sec16 defines endoplasmic reticulum exit sites and is required for secretory cargo export in mammalian cells. *Traffic* **7,** 1678–1687 (2006).
9. Ivan, V. *et al.* Drosophila Sec16 mediates the biogenesis of tER sites upstream of Sar1 through an arginine-rich motif. *Mol. Biol. Cell* **19,** 4352–4365 (2008).
10. Hughes, H. *et al.* Organisation of human ER-exit sites: requirements for the localisation of Sec16 to transitional ER. *J. Cell Sci.* **122,** 2924–2934 (2009).
11. Cho, H. J. *et al.* Leucine-rich repeat kinase 2 regulates Sec16A at ER exit sites to allow ER-Golgi export. *EMBO J.* **33,** 2314–2331 (2014).
12. Espenshade, P., Gimeno, R. E., Holzmacher, E., Teung, P. & Kaiser, C. A. Yeast SEC16 gene encodes a multidomain vesicle coat protein that interacts with Sec23p. *J. Cell Biol.* **131,** 311–324 (1995).
13. Bhattacharyya, D. & Glick, B. S. Two mammalian Sec16 homologues have nonredundant functions in endoplasmic reticulum (ER) export and transitional ER organization. *Mol. Biol. Cell* **18,** 839–849 (2007).
14. Budnik, A., Heesom, K. J. & Stephens, D. J. Characterization of human Sec16B: indications of specialized, non-redundant functions. *Sci. Rep.* **1,** 77 (2011).
15. Yonekawa, S. *et al.* Sec16B is involved in the endoplasmic reticulum export of the peroxisomal membrane biogenesis factor peroxin 16 (Pex16) in mammalian cells. *Proc. Natl Acad. Sci. USA* **108,** 12746–12751 (2011).
16. Montegna, E. A., Bhave, M., Liu, Y., Bhattacharyya, D. & Glick, B. S. Sec12 binds to Sec16 at transitional ER sites. *PLoS ONE* **7,** e31156 (2012).
17. Whittle, J. R. & Schwartz, T. U. Structure of the Sec13-Sec16 edge element, a template for assembly of the COPII vesicle coat. *J Cell Biol* **190,** 347–361 (2010).
18. Yorimitsu, T. & Sato, K. Insights into structural and regulatory roles of Sec16 in COPII vesicle formation at ER exit sites. *Mol. Biol. Cell* **23,** 2930–2942 (2012).
19. Bharucha, N. *et al.* Sec16 influences transitional ER sites by regulating rather than organizing COPII. *Mol. Biol. Cell* **24,** 3406–3419 (2013).
20. Sprangers, J. & Rabouille, C. SEC16 in COPII coat dynamics at ER exit sites. *Biochem. Soc. Trans.* **43,** 97–103 (2015).
21. Huse, M., Lillemeier, B. F., Kuhns, M. S., Chen, D. S. & Davis, M. M. T cells use two directionally distinct pathways for cytokine secretion. *Nat. Immunol.* **7,** 247–255 (2006).
22. Huse, M., Quann, E. J. & Davis, M. M. Shouts, whispers and the kiss of death: directional secretion in T cells. *Nat. Immunol.* **9,** 1105–1111 (2008).
23. Farhan, H., Weiss, M., Tani, K., Kaufman, R. J. & Hauri, H. P. Adaptation of endoplasmic reticulum exit sites to acute and chronic increases in cargo load. *EMBO J.* **27,** 2043–2054 (2008).
24. Farhan, H. *et al.* MAPK signaling to the early secretory pathway revealed by kinase/phosphatase functional screening. *J. Cell Biol.* **189,** 997–1011 (2010).
25. Zacharogianni, M. *et al.* ERK7 is a negative regulator of protein secretion in response to amino-acid starvation by modulating Sec16 membrane association. *EMBO J.* **30,** 3684–3700 (2011).
26. Miller, E. A. & Schekman, R. COPII - a flexible vesicle formation system. *Curr. Opin. Cell Biol.* **25,** 420–427 (2013).
27. Tao, J. *et al.* SEC23B is required for the maintenance of murine professional secretory tissues. *Proc. Natl Acad. Sci. USA* **109,** E2001–E2009 (2012).
28. Adams, E. J., Chen, X. W., O'Shea, K. S. & Ginsburg, D. Mammalian COPII coat component SEC24C is required for embryonic development in mice. *J. Biol. Chem.* **289,** 20858–20870 (2014).
29. Jensen, D. & Schekman, R. COPII-mediated vesicle formation at a glance. *J. Cell Sci.* **124,** 1–4 (2011).
30. Heyd, F. & Lynch, K. W. Degrade, move, regroup: signaling control of splicing proteins. *Trends Biochem. Sci.* **36,** 397–404 (2011).
31. Preussner, M. *et al.* Rhythmic U2af26 alternative splicing controls PERIOD1 stability and the circadian clock in mice. *Mol. Cell* **54,** 651–662 (2014).
32. Martinez, N. M. *et al.* Alternative splicing networks regulated by signaling in human T cells. *RNA* **18,** 1029–1040 (2012).
33. Michel, M., Wilhelmi, I., Schultz, A. S., Preussner, M. & Heyd, F. Activation-induced tumor necrosis factor receptor-associated factor 3 (Traf3) alternative splicing controls the noncanonical nuclear factor kappaB pathway and chemokine expression in human T cells. *J. Biol. Chem.* **289,** 13651–13660 (2014).
34. Tillmann, K. D. *et al.* Regulation of Sec16 levels and dynamics links proliferation and secretion. *J. Cell. Sci.* **128,** 670–682 (2015).
35. Presley, J. F. *et al.* ER-to-Golgi transport visualized in living cells. *Nature* **389,** 81–85 (1997).
36. Townley, A. K. *et al.* Efficient coupling of Sec23-Sec24 to Sec13-Sec31 drives COPII-dependent collagen secretion and is essential for normal craniofacial development. *J. Cell Sci.* **121,** 3025–3034 (2008).
37. Fromme, J. C., Orci, L. & Schekman, R. Coordination of COPII vesicle trafficking by Sec23. *Trends Cell. Biol.* **18,** 330–336 (2008).
38. Jin, L. *et al.* Ubiquitin-dependent regulation of COPII coat size and function. *Nature* **482,** 495–500 (2012).
39. Zeuschner, D. *et al.* Immuno-electron tomography of ER exit sites reveals the existence of free COPII-coated transport carriers. *Nat. Cell Biol.* **8,** 377–383 (2006).
40. Zanetti, G., Pahuja, K. B., Studer, S., Shim, S. & Schekman, R. COPII and the regulation of protein sorting in mammals. *Nat. Cell Biol.* **14,** 20–28 (2012).
41. Ran, F. A. *et al.* Genome engineering using the CRISPR-Cas9 system. *Nat. Protoc.* **8,** 2281–2308 (2013).
42. Heyd, F. & Lynch, K. W. Phosphorylation-dependent regulation of PSF by GSK3 controls CD45 alternative splicing. *Mol. Cell* **40,** 126–137 (2010).
43. Goodwin, J. S. & Kenworthy, A. K. Photobleaching approaches to investigate diffusional mobility and trafficking of Ras in living cells. *Methods* **37,** 154–164 (2005).

Acknowledgements

We thank David Stephens (Bristol, UK) for providing a GFP-Sec16 expression construct and the Sec24C antibody. Stefan Mundlos (Berlin, Germany) provided CRISPR/Cas9 plasmids. Sophie Veitinger (Marburg, Germany) initially helped with microscopy, Monika Michel (Marburg, Germany) provided technical assistance and Lara Kämmerer contributed as a rotation student. Funding was provided by an Emmy-Noether-Fellowship of the DFG to F.He. (HE 5398/3); additional support came from the DFG-funded SFB958/A21.

Author contributions

I.W. performed most of the experiments and was supported by M.P., A.N. and O.H. R.K. generated genome-engineered cell lines and performed initial phenotyping. R.J. and F.Ho. contributed essential equipment and expertize in microscopy studies, especially FRAP. F.He. and I.W. planned the experiments, analysed the data and wrote the manuscript. F.He. initiated and designed the study, and supervised the work.

Additional information

Supplementary Information accompanies this paper at http://www.nature.com/naturecommunications

Competing financial interests: The authors declare no conflict of interests.

Reprints and permission information is available online at http://npg.nature.com/reprintsandpermissions/

How to cite this article: Wilhelmi, I. *et al.* Sec16 alternative splicing dynamically controls COPII transport efficiency. *Nat. Commun.* 7:12347 doi: 10.1038/ncomms12347 (2016).

Appendix E Publication 2

Preußner M, Goldammer G, **Neumann A**, Haltenhof T, Rautenstrauch P, Müller-McNicoll M, Heyd F. Body Temperature Cycles Control Rhythmic Alternative Splicing in Mammals. Mol Cell. 2017 Aug 3;67(3):433-446.e4. doi: 10.1016/j.molcel.2017.06.006.

http://dx.doi.org/10.1016/j.molcel.2017.06.006

AN analysed RNA-sequencing data to identify cold-responsive alternative splicing events and performed meta-analysis on the resulting list of events.

Appendix F Publication 3

***** Herdt O, **Neumann A**, Timmermann B, Heyd F. The cancer-associated U2AF35 470A>G (Q157R) mutation creates an in-frame alternative 5' splice site that impacts splicing regulation in Q157R patients. RNA. 2017 Dec;23(12):1796-1806. doi: 10.1261/rna.061432.117.

http://dx.doi.org/10.1261/rna.061432.117

AN analysed RNA-sequencing data to elucidate the rescue capabilities and individual 3’ splice site binding preferences of different U2AF35 mutant proteins (corresponding to proteins potentially produced in patients with the U2AF35 Q157R or Q157P mutations). This included the creation of a custom annotation to incorporate novel splicing targets in the MISO analysis. Furthermore, AN queried public datasets to find RNA-sequencing data of patients with these mutations and quantified mutation-induced mis-splicing, verifying production of a deleterious protein formed in the Q157R patients. AN compared alternative splicing in these patients and 3’ splice site binding preferences, suggesting an effect of the deletion protein variant on splicing regulation.

Appendix G Publication 4

Goldammer G, **Neumann A**, Strauch M, Müller-McNicoll M, Heyd F, Preußner M. Characterization of cis-acting elements that control oscillating alternative splicing. RNA Biol. 2018;15(8):1081-1092. doi: 10.1080/15476286.2018.1502587.

http://dx.doi.org/10.1080/15476286.2018.1502587

AN analysed RNA-sequencing data to identify temperature-responsive, circadian-like alternative splicing events and performed meta-analysis on the resulting list of events.

Appendix H Publication 5

*** Neumann A**, Schindler M, Olofsson D, Wilhelmi I, Schürmann A, Heyd F. Genome-wide identification of alternative splicing events that regulate protein transport across the secretory pathway. JCS. 2019 Apr 25;132(8). pii: jcs230201. doi: 10.1242/jcs.230201.

http://dx.doi.org/10.1242/jcs.230201

AN analysed RNA-sequencing data to identify secretion-related alternative splicing events and performed meta-analyses on the resulting set. AN established the RUSH system to quantify transport efficiencies, including a custom tool for semi-automated analysis. AN and MS performed experiments to manipulate alternative splicing (using Morpholinos and CRISPR/Cas9) and validate a transport deficiency for four of the secretion-related alternative splicing events. AN showed a global tissue-, differentiation- and activation-specificity of the events using public RNA-sequencing data of human tissues, T cells and adipocytes. AN and FH conceptualised the work and wrote the manuscript.

Appendix I Publication 6

* **Neumann A**, Meinke S, Goldammer G, Strauch M, Timmermann B, Heyd F, Preußner M. Rhythmic gene expression is controlled by evolutionary conserved temperature regulated alternative splicing triggering nonsense mediated decay. In preparation.

AN analysed mouse hepatocyte and liver RNA-sequencing data to *de-novo* identify alternative splicing events that trigger the nonsense-mediated decay pathway. To this end, published analysis tools were combined with custom scripts and analysis pipelines. AN characterised these events using several meta-analysis methods (molecular function, sequence conservation) and compared the findings with previous studies. AN also analysed public RNA-sequencing data from *Arabidopsis thaliana* in different temperature conditions to transfer the findings in mouse to plants. AN and MP designed the study, planned experiments, analysed data and wrote the manuscript with help from SM and FH.

Rhythmic gene expression is controlled by evolutionary conserved temperature regulated alternative splicing triggering nonsense mediated decay

Alexander Neumann[1], Stefan Meinke[1], Gesine Goldammer[1], Miriam Strauch[1], Bernd Timmermann[2], Florian Heyd [1*], Marco Preußner [1*]

[1]Freie Universität Berlin, Institute of Chemistry and Biochemistry, Laboratory of RNA Biochemistry, Takustrasse 6, 14195 Berlin, Germany.

*Co-corresponding Authors: florian.heyd@fu-berlin.de, mpreussner@zedat.fu-berlin.de
Phone: +49 30 83870703
FAX: +49 30 838-4-62938

Summary

Mammalian body temperature oscillates with the time of the day, is altered in diverse pathological conditions and can be influenced by the ambient temperature. We have recently identified a thermometer-like kinase, which alters SR protein phosphorylation and thereby globally controls alternative splicing (AS). AS can generate mRNA variants containing premature termination codons, which are then degraded by nonsense mediated decay (NMD). Here we investigate if AS-NMD is regulated by temperature and how this mechanism globally regulates gene expression (GE). RNA-seq reveals that temperature-controlled NMD-inducing splicing events are frequent, evolutionarily conserved and pervasively found within RNA binding proteins – including most SR proteins. NMD-inducing exons are essential for rhythmic GE, supporting a global role of AS-NMD in establishing temperature-dependent GE profiles. Within SR proteins, generation of the NMD isoform is under autoregulatory control and anti-correlates with GE – both, in mammals under circadian body temperature cycles and in plants in response to ambient temperature changes.

Keywords

Alternative splicing, NMD, SR proteins, temperature, circadian clock, Cirbp

Highlights

- Frequent temperature-controlled generation of splicing variants triggering NMD
- Temperature-regulated AS-NMD can generate 24-hour rhythms in gene expression
- SR-proteins autoregulate their own expression in response to temperature changes
- SR-proteins from evolutionary distinct species show temperature-controlled AS-NMD

Introduction

Circadian clocks act as cell autonomous time-measuring devices, which anticipate daytime and coordinate behavior and physiology accordingly. The mammalian circadian timing system is organized in a hierarchical manner: The central pacemaker in the brain's suprachiasmatic nucleus (SCN) serves as a master regulator to coordinate circadian clocks throughout the body (Dibner et al., 2010). Therefore, information on the geophysical time (light-dark) is transferred from the retina to the SCN, which then uses diverse neuronal and humoral cues to synchronize circadian clocks in other 'light-blind' parts of the brain and in other organs of the body (Gerber et al., 2015). Although the mechanisms of synchronization are different in the various organs, the conventional perception is that the majority of 24-hour rhythms depend on an identical transcription translation feedback loop in each cell of the body (Ko and Takahashi, 2006). Only 50% of circadian mRNA rhythms depend on *de novo* transcription (Koike et al., 2012; Menet et al., 2012), strongly arguing for an involvement of other posttranscriptional mechanisms in generating rhythms (Preussner and Heyd, 2016). Additionally, there is evidence for 24-hour rhythms which cycle independent of this central oscillator (Kornmann et al., 2007). This central clock independent 24-hour rhythms in GE are difficult to discriminate from real circadian oscillations *in vivo* (reviewed in (Preussner and Heyd, 2018)) and our mechanistic understanding of most of these rhythms is limited.

Here we focus on the systemic signal 'body temperature cycles' (Refinetti and Menaker, 1992), which can synchronize the central oscillator in peripheral clocks (Brown et al., 2002; Buhr et al., 2010; Saini et al., 2012), but can also directly result in rhythmic changes in GE. Examples include rhythmic expression of cold induced RNA-binding proteins (RBPs) – such as *Cirbp* and *Rbm3* (Liu et al., 2013; Morf et al., 2012) – or rhythmic changes in the ratio of alternative splicing (AS) isoforms of *U2af26* (Goldammer et al., 2018; Preussner et al., 2014). In all of these examples, gene or alternative isoform expression of RBPs depends on post-transcriptional mechanisms (Gotic et al., 2016; Preussner et al., 2017), which have to be sensitive enough to respond to 1-2°C changes in temperature. In our previous work we revealed key components regulating temperature-dependent AS. The phosphorylation level of SR proteins serves as a fast and extremely sensitive molecular thermometer transferring the signal body temperature into global changes in AS. Colder temperatures result in hyper-phosphorylation of SR proteins – mediated via temperature-controlled CDC-like kinase activity (CLKs, {Haltenhof, 2019}) – and SRSF2 and SRSF7 are inactivated by hyper-phosphorylation resulting in target exon skipping (Goldammer et al., 2018; Preussner et al., 2017). The protein family of SR proteins (13 canonical members in human) is characterized by a domain rich in serine and arginine residues, known as the RS domain (Manley and Krainer, 2010). SR proteins have multiple roles in eukaryotic GE with a key function

in splicing regulation (Long and Caceres, 2009). In general, SR proteins are nuclear sequence-specific activators of splicing, but their activity as well as their subcellular localization can be modulated through reversible phosphorylation of the RS domain (Huang et al., 2004). Western blots with an antibody detecting all phosphorylated SR proteins identified a general correlation of temperature and SR protein phosphorylation (Preussner et al., 2017), but it remained elusive which SR protein is regulated by temperature to what extent. SR proteins contain ultraconserved elements, allowing autoregulation of their own expression level (Lareau et al., 2007). Autoregulatory mechanisms involve SR protein promoted inclusion of an exon containing a premature translation termination codon (PTC; (Sureau et al., 2001)), or SR protein promoted splicing results in the normal stop codon becoming a PTC (Goncalves and Jordan, 2015; Lareau et al., 2007). PTC-containing mRNAs are recognized and degraded by the nonsense mediated decay (NMD) surveillance pathway and for SR proteins this is understood as a mechanism associated with homeostatic control (Ni et al., 2007). AS-NMD is not restricted to SR proteins and is thus understood as a dynamic modulator of global GE (Braunschweig et al., 2013; Lykke-Andersen and Jensen, 2015), and several thousand genes are affected by inhibition of the NMD pathway (Hurt et al., 2013).

Here we investigated to which extend AS-NMD is regulated by temperature and how this mechanism globally regulates temperature dependent GE. We find that NMD isoforms of different RBPs, especially SR proteins are differentially affected by temperature and that temperature-controlled autoregulation of an SR protein is sufficient to *de novo* generate 24-hour rhythms in GE. Temperature-dependent AS-NMD is evolutionary conserved, not restricted to SR proteins and represents a novel global mechanism for the generation of rhythmic GE *in vivo*.

Results

Temperature-dependent AS-NMD occurs frequently in mammalian cells

The detection of temperature dependent PTC containing isoforms is quite challenging as these isoforms are quickly degraded by NMD. It therefore requires depletion or pharmacological inhibition of the NMD pathway (Rehwinkel et al., 2006). NMD occurs co-translational, so that blocking translation (e.g. via cycloheximide (CHX)) represents a fast and reliable way of blocking the NMD pathway (Hurt et al., 2013). To investigate temperature-controlled AS-NMD we use freshly isolated hepatocytes incubated at 34 or 38°C for 12h and then shifted to 38 and 34°C, respectively. After 4h cells were treated with CHX (or DMSO as solvent control), to block NMD mediated degradation, incubated for further 4h, and harvested. Isolated RNA was then investigated by RNA-Seq (Figure 1A). A principal component analysis reveals clear clustering of the biological triplicates and comparably strong effects of temperature and CHX on AS (Figure

1B). Using Whippet (Sterne-Weiler et al., 2018), we identify 4740 temperature-controlled splicing events in CHX treated cells (Figure S1A and Table S1). Only one 3rd of the strongest events respond only to temperature but not to CHX treatment, indicating non-NMD events (Figure 1C, heat-skipped or cold-skipped). Temperature-dependent AS-NMD events, responding to temperature and CHX, are found enriched in genes previously associated with NMD (Figure S1B) and the majority can be categorized into four groups: (I) cold-induced NMD via inclusion; (II) heat-induced NMD via inclusion; (III) cold-induced NMD via exclusion; and (IV) heat-induced NMD via exclusion. Examples for each of these categories were confirmed by radioactive RT-PCRs with RNAs from independently generated hepatocytes (Figure 1D, see also S1C and S1D) and are further clarified in the following: In *Mettl16* exon 6 encodes a PTC, and the full length (fl) isoform – containing exon 6 – is therefore stabilized via CHX. Exon 6 inclusion is strongly promoted at 34°C, representing a cold-induced NMD event. In *hnRNP DL* exon 8 inclusion generates a second splice-site after the canonical stop in exon 7, turning this stop into a PTC. The fl isoform is stabilized by CHX and, as it predominates at 38°C, represents a heat induced NMD event. In *hnRNP H1* and *Slc9a8* skipping of an exon (length not divisible by 3) generates a frameshift and a PTC in a downstream exon. The NMD inducing skipping isoforms are stabilized by CHX and found either in cold or in heat. In addition to skipped exon events, we also find temperature-dependent AS-NMD in the form of alternative 3' or 5' splice sites, intron retention, mutually exclusive exons, transcription starts and transcription ends (Table S1 and below).

Overall, PSI values predicted by Whippet and determined by RT-PCR from independent biological samples show strong correlation, allowing us to draw reliable conclusions from our bioinformatics analysis (Figure S1E). In all presented examples, as well as globally, PSI changes in DMSO correlate with PSI changes in CHX, confirming that these variants are present also in DMSO but are stabilized after CHX treatment (Figure S1F). When analyzing all genes with NMD events (all isoforms stabilized by CHX at 34 or 38°C) we find that almost 40% of these genes present temperature-regulated NMD isoforms (Figure 1E and S1G), pointing to a global role in shaping temperature-controlled GE. Interestingly, we find temperature-controlled NMD events enriched in RBPs (Figure 1F and below). In summary, temperature controlled AS coupled to NMD represents a frequent mode of posttranscriptional GE, with wide implications for temperature-controlled GE levels – especially of RBPs.

Conserved AS-NMD globally regulates temperature dependent GE

Our bioinformatics analysis finds over 60 RBPs with temperature-regulated NMD exons of different types (Figure 2A and S2A for examples, see also Table S1). Note, in the Sashimi plots, that higher NMD isoform inclusion correlates with decreased GE in the DMSO samples (see also below).

Using radioactive RT-PCR we confirm the usage of an alternative last exon in *Cirbp*, which is strongly stabilized after addition of CHX and much more abundant at higher temperatures (exon 7b, Figure 2B). The heat-induced NMD isoform of *Cirbp* – and also of *Rbm3* (see Figure S2A) – is likely responsible for the cold-induced expression. In line with that we find that young mice exposed to a lower ambient temperature, resulting in decreased body temperature (see (Preussner et al., 2017)), show increased *Cirbp* GE levels anti-correlating with NMD exon inclusion (Figure 2C). Rhythmic *Cirbp* expression was also observed in the liver of mice lacking a functional liver clock (Kornmann et al., 2007), consistent with the idea that temperature-controlled AS-NMD can generate core clock independent rhythms in GE. Furthermore, we could independently validate the emergence of a temperature-dependent NMD isoform for *hnRNP DL*, *Ptbp2*, *Cirbp*, *Rbm3* and *hnRNP H3* in temperature-entrained human Hek293 cells (Figure 2D and S2B). In line with that, we find that all temperature controlled AS-NMD exons as well as their surrounding introns (as all AS-NMD exons) are highly conserved across mammals (Figure 2E and 'conservation' in Sashimi plots in Figures 2A, S2A, 3B, 3C and S3D), arguing for an evolutionary conserved function.

Using RT-qPCRs we confirm that temperature-dependent GE in DMSO-treated cells anti-correlates with the heat-induced NMD isoform generation of *Cirbp* in mouse and human cells (Figure 2F). This is abolished in CHX-treated cells, as CHX blocks the translation coupled degradation of NMD-inducing isoforms. Consistently, when considering all RBPs with temperature-dependent AS-NMD skipped exon events in our list, we see a highly significant global correlation of temperature-dependent NMD-isoform generation and reduced GE levels in DMSO (slope of 1), while this correlation is completely lost in the CHX samples (slope of 0, Figure 2G). This strongly argues for AS-NMD being the cause of temperature dependent GE. Looking at all genes with skipped exon temperature-dependent AS-NMD events, this global trend still is present, although to a lesser extent (Figure S2C). This indicates that temperature-dependent GE of several of these genes is additionally controlled by other mechanisms. In summary, these data point to an evolutionary conserved mechanism of controlling GE in a temperature-dependent manner via the NMD pathway in mammals.

AS-NMD events within SR proteins are differentially affected by temperature

We next elucidated the role of temperature-regulated AS-NMD in SR proteins, as it was previously described that these have NMD-inducing exons with ultraconserved regions (Lareau et al., 2007) and as certain SR proteins were identified as regulators of temperature controlled AS (Preussner et al., 2017). We detected AS-NMD variants for most SR proteins ranging from temperature-

insensitive to strongly temperature-dependent (Figure 3A and S3A). Again, PSI changes in DMSO correlate with PSI changes in CHX, confirming a stabilizing effect of the CHX treatment (Figure S3B). For *Srsf2* we observed strong heat-induced NMD exon inclusion (Figure 3B), which was confirmed with the NMD-specific inhibitor NMDI14 ((Martin et al., 2014), see Figure S3C). In contrast, we observed strong cold-induced generation of the NMD isoform for *Srsf10* (Figure 3C), indicating antagonistic effects of temperature on different SR proteins. Again, the heat-induced NMD exon inclusion of *Srsf2* correlates with decreased GE in heat and vice versa for *Srsf10* (Figure 3B and 3C, also highlighted in Figure 2G). Further examples include heat induced inclusion of *Srsf7* exon 4 (Figure S3D) and cold induced splicing in the 3'UTR of *Srsf1* (Figure S3E). AS-NMD in *Srsf2*, *Srsf10* and *Srsf7* responds with the same directionality to 24h square-wave 34/38°C temperature-rhythms in human Hek293 (Figure 3D, 3E, and S3F), confirming a cell-type independent and evolutionary conserved function in adapting SR proteins to (circadian) temperature changes. We also note that exon inclusion changes within 4-8h at one temperature and is often reverted already within this temperature, which is indicative for an autoregulatory feedback loop (see below). In summary, we find SR protein specific differences in temperature dependent NMD exon inclusion, which could serve as evolutionary-conserved thermometers.

SRSF10 autoregulates its own splicing in a temperature dependent manner

Mechanistically we propose that temperature dependent AS-NMD in SR proteins depends on autoregulatory feedback loops. Autoregulation is known for many RBPs including *Srsf2*/*7* (Lejeune et al., 2001; Sureau et al., 2001), but not for *Srsf10*. To obtain further evidence that temperature dependent AS-NMD within SR proteins is more general a result of autoregulation, we test this hypothesis using *Srsf10*. *Srsf10* contains two competing 5' splice-sites (ss) in exon 2 (E2), which are recognized either by the minor or the major spliceosome (Turunen et al., 2013): The upstream (up) minor-ss is coupled to E4 inclusion, while usage of the downstream (dn) major-ss is coupled to E3 inclusion and usage of an alternative polyadenylation site in E3 (Figure S4A). The dn-E3 variant is not an ideal NMD target as the stop codon in E2 is close to the exon junction complex connecting E2/3 (<50 nucleotides, (Nagy and Maquat, 1998)) and results in a hypothetical short protein variant (SRSF10-s). To investigate, whether temperature driven changes in *Srsf10* AS depend on an autoregulatory feedback loop, we use a *Srsf10* minigene containing mouse exons 2-4 (Figure 4A, wt) and investigate AS of the minigene after knockdown of endogenous *Srsf10*. This identifies SRSF10 as a strong activator of E3 inclusion as knockdown decreases dn-E3 inclusion (Figure 4B lanes 1 and 2, and Figure S4B). We confirm knockdown of *Srsf10* via Western Blot and qPCR (Figure 4B top and S4C) and observe a reduced E3/E4 ratio also for endogenous *Srsf10* mRNA (Figure S4C), consistent with SRSF10 activating E3 inclusion. In contrast,

knockdown of *Srsf2* or *Srsf7* does not affect *Srsf10* AS (Figure S4D). Next we perform rescue experiments with the different *Srsf10* splicing isoforms: SRSF10-fl and SRSF10-2 (resulting from different last exons (Shin and Manley, 2002)) rescue E3 inclusion, while the hypothetical protein SRSF10-s does not affect splicing (Figure 4B lanes 3-5, and Figure S4B). Finally, titration experiments show that *Srsf10* autoregulation is responsive to small changes in SRSF10 levels, with SRSF10-fl being a more potent activator than SRSF10-2 (Figure S4E). To investigate whether the phosphorylation state of SRSF10 has an impact on autoregulation we applied a 2-hour heat shock. This dephosphorylates SRSF10 (Shin et al., 2004) and consistent with SRSF10 being a splicing-activator only in the phosphorylated state (Feng et al., 2008), heat shock reduces dn-E3 formation (Figure 4C, lanes 1 and 2) as observed for endogenous splicing (see Figure 3C and 3E). Additionally, SRSF10 was reported to be quickly re-phosphorylated after shifting cells back to 37°C (Ninomiya et al., 2011) and consistently formation of dn-E3 is restored within hours (Figure S4F and S4G). To prove that temperature dependent changes in *Srsf10* AS-NMD require SRSF10, we combine knockdown and heat shock, which clearly demonstrates the requirement of SRSF10 for heat responsive splicing regulation (Figure 4C).

To identify the cis-regulatory element required for autoregulation we apply systematic mutational analysis of the *Srsf10* minigene (Figure 4A). This identifies a GA-rich enhancer element (consistent with the previously-identified consensus binding site (Shin and Manley, 2002; Zhou et al., 2014)) at the 5'-end of exon 3 necessary for autoregulation (Figure 4D). To confirm our minigene analysis on endogenous *Srsf10*, we applied CRISPR/Cas9 to delete exon 3 (Figure 4E). In absence of the autoregulatory exon 3, SRSF10 cannot downregulate its own expression resulting in increased *Srsf10* mRNA and protein levels (Figure 4F and 4G), and consequently we detect changes in AS of SRSF10-target exons antagonizing *Srsf10* knockdown (Figure 4H). In summary, the example of SRSF10 demonstrates that temperature dependent AS-NMD within SR proteins could be more generally the result of autoregulatory feedback loops involving ultraconserved elements and temperature-controlled SR protein phosphorylation-based activity (Figure 4I).

AS-NMD generates 24-hour rhythms in *Srsf10* GE *in vivo*

Next we address the question whether AS-NMD within SR proteins is also regulated *in vivo* by natural occurring body temperature cycles. We focus on *Srsf10*, since dn-E3 inclusion reflects a weak NMD target, which can be detected in the absence of NMD inhibitors. Comparison of RNA sequencing data from Zeitgeber Time (ZT) 0 (warm) and ZT8 (cold) in mouse cerebellum (Preussner et al., 2014), reveals stronger formation of the dn-E3 isoform at ZT8 (Figure 5A). Validation PCRs throughout a circadian cycle confirm maximal usage of dn-E3 during the cold day

(Figure 5B). Similar to *U2af26* AS (Preussner et al., 2014), *Srsf10* AS persists in constant darkness and is entrainable to a new light-dark regime (Figure S5A and S5B), and we find an almost perfect correlation of *U2af26* E6/7 skipping and *Srsf10* dn-E3 inclusion in 17 mice from different ZTs (Figure 5C). This suggests antagonistic effects of temperature on SRSF2/7 and SRSF10: SRSF2/7 are stronger activators during the night, while SRSF10 is a stronger activator during the day. Consistent with reduced stability of the NMD-inducing dn-E3 isoform, we find rhythmic GE of *Srsf10* in circadian cerebellum samples, which anti-correlates with the generation of the dn-E3 isoform (Figure 5D). As a result of the rhythmic mRNA levels, we also observe day-time dependent rhythms in SRSF10 protein expression (SRSF10-fl and -2) in liver and cerebellum (Figure 5E and S5C). Interestingly, we also detect an SRSF10 isoform (SRSF10-fl-P) – likely representing hyperphosphorylated SRSF10 (Figure S5D) – which anti-correlates with overall expression levels (Figure 5E and 5F). We therefore propose the following model for a core-clock independent autoregulatory 24-hour rhythm in GE: Body temperature-controlled kinase activity {Haltenhof, 2019} controls phosphorylation of SR proteins, resulting in higher phosphorylation during the colder day phase in mice. While increased phosphorylation of SRSF2 and SRSF7 reduced their activity in mediating U2af26 exon 6/7 inclusion (Preussner et al., 2017), we find for *Srsf10* that phosphorylation activates SRSF10 which then promotes inclusion of the dn-E3 isoform. Consequently, NMD of the dn-E3 variant results in reduced mRNA and protein levels during the colder day. We assume, that in the absence of further temperature changes a new stable steady-state level with less but more active SRSF10 would be reached. However, as body temperature rises with beginning of the night, SRSF10 becomes dephosphorylated resulting in formation of the up-E4 isoform and more mRNA/protein. In summary, these data demonstrate that an autoregulatory NMD event can generate rhythms in GE *in vivo*.

Autoregulation *de novo* generates rhythms in SR protein GE

To confirm that changes in GE depend on AS-NMD, we use our cell line lacking SRSF10 E3. While external temperature cycles are sufficient to generate rhythms in full length *Srsf10* mRNA (up-E4, WT in Figure 6A, S6A and 6B), these rhythms are absent in cells lacking the autoregulatory E3, as shown by radioactive RT-PCR (Figure 6A and S6A) and in two independently generated cell lines by qPCR (Figure 6B). To prove generality, we generated CRISPR/Cas9 modified cell lines lacking the autoregulatory ultraconserved exons of *Srsf2* and *Srsf7* (Figure 6C). As for *Srsf10*, loss of autoregulation results in increased GE (Figure S6C), and lost or altered rhythms in temperature-dependent GE (Figure 6D and 6E). For *Srsf10* and *Srsf2* GE clearly anti-correlates with the appearance of the NMD isoform, while *Srsf7* expression seems

to be influenced by additional mechanisms. Together, these cell culture data confirm that autoregulatory feedback loops can generate autonomous rhythms in GE.

Temperature-dependent AS-NMD regulates expression levels of SR proteins in *A. thaliana*

AS-NMD in SR genes arose independently, evolutionary rapid and in an SR protein specific manner during mammalian evolution (Lareau and Brenner, 2015). The pervasive identification of temperature controlled AS-NMD in distinct SR proteins (and other RBPs) therefore indicates an evolutionary advantage in homoeothermic mammals. But is a similar mechanism also in place for poikilotherms, which experience much greater differences in body temperature? To investigate whether temperature-dependent AS-NMD also arose in poikilotherms, we next examine SR protein splicing and expression in plants. Also in *A. thaliana* SR proteins contain evolutionary conserved regions triggering AS-NMD (Palusa and Reddy, 2010; Rauch et al., 2014; Richardson et al., 2011) and cold-induced GE changes with a potential connection to NMD isoforms has been suggested (Calixto et al., 2018; Filichkin et al., 2010; Staiger and Brown, 2013). We analyze a publicly-available time course RNA-seq dataset from plants kept at 20°C for 24 hours and then shifted to 4°C for the next 24 hours, while being under a 12-hour dark-light regime (Calixto et al., 2018), allowing us to distinguish between light- and temperature-dependent effects. When looking at GE, we indeed find that all 18 SR proteins (based on (Barta et al., 2010)) show a clear temperature-dependent regulation (Figure 7A). Some of the genes additionally show a light-dependent expression pattern, but temperature is in general the dominant signal. About half of the regulated SR proteins show higher GE at RT, while the other half is cold-induced. Interestingly, we find at least one examples for both warm- and cold-expressed SR genes in almost all SR protein subfamilies (Figure 7B), which suggests complementing functions. Within the RNA-Seq data we additionally find clear evidence for an antagonistically regulated splicing event in At-SR34 and At-SCL33 (Figure 7C), and more globally in ~50% of temperature regulated SR proteins (Figure S7A). In this dataset – without inhibition of the NMD pathway – the identification of NMD isoforms was challenging. Nevertheless, we found all antagonistically regulated temperature-dependent splicing events stabilized in CHX conditions (based on another RNA-Seq dataset, see Table S1), and therefore likely NMD-inducing (Figure S7B). In all tested examples, splicing and GE changes could be confirmed by PCR from independently generated plant samples (Figure 7C, right, and S7C). Furthermore, we obtained evidence for an autoregulatory feedback loop in At-RS2Z33, in which overexpression lead to higher inclusion levels of the NMD isoform (Figure S7D), further pointing to a mechanism similar as described for mammalian *Srsf10*.

Using the RNA-seq data of CHX-treated plants we next aim to globally identify temperature dependent AS-NMD events. The dataset is not optimal, as there is no additional temperature

treatment and we therefore need to first identify NMD events and then quantify temperature regulation in samples without NMD inhibition. Nevertheless, we identify 65 NMD isoforms clearly affected by temperature (Table S1). In concordance with our findings in mouse, there is a highly significant anti-correlation between NMD isoform inclusion and GE (Figure 7D). This includes a temperature controlled AS-NMD event in the snRNP assembly factor At-GEMIN2, which was previously identified as a key regulator of downstream temperature-dependent splicing events (Schlaen et al., 2015). In conclusion, these data expand our findings from the mammalian to the plant system, showcasing the evolutionary ancient mechanism of generating rhythmic GE by temperature-regulated AS-NMD.

Discussion

Here we report that temperature-regulated AS coupled to NMD occurs frequently in diverse genes from evolutionary distinct species. We furthermore show that these splicing events are sufficient to generate temperature-dependent GE changes and to induce rhythms in GE. Under constant 24-hour temperature cycles, these rhythms also follow the light-dark cycle (e.g. *Srsf10* in Figure 5) and are therefore hard to distinguish from classical circadian rhythms (Preussner and Heyd, 2018). At first sight the existence of two independent 24-hour rhythms appears puzzling, but these two rhythms are fundamentally different: While classical circadian rhythms depend on transcription-translation feedback loops and are robust to minor ambient changes (Gonze et al., 2002), temperature-induced rhythms are generated post-transcriptionally and can quickly adapt gene expression in response to changing temperatures. Therefore, temperature-induced rhythms can stabilize circadian rhythms under circadian temperature cycles (Morf et al., 2012) but can additionally adapt GE in response to sudden temperature changes; i.e. under stress conditions. Furthermore, the interplay of these two mechanisms could be involved in seasonal control of gene expression by integrating light and temperature signals i.e. At-RS40 exhibits an intriguing upregulation of GE in cold light conditions, representing winter days (Figure 7A).

The presence of temperature-regulated AS-NMD isoforms in many RBPs is indicative for an interlocked network of RBPs to adapt GE to temperature post-transcriptionally. In mammals, this network requires sensors and modulators that are sensitive enough to respond to temperature differentials of ~1°C, to be able to respond to daily changes in body temperature. In independent work we characterized CLK kinases as the direct molecular sensor of temperature changes and here we describe how AS-NMD shapes expression of the modulating SR proteins. Interestingly we find in evolutionary distinct species, that groups of SR proteins are antagonistically affected by temperature. Assuming that NMD exon inclusion is generally autoregulated in SR proteins (as for *Srsf10*, Figure 4), these data indicate cold-induced activity of SRSF10/1/11 (At-SR34 and others

in plants) and heat-induced activity of most other SR proteins including SRSF2/7 (At-SCL33 and others in plants); which is consistent with stronger activity at higher temperatures for SRSF2/7 as suggested for *U2af26* AS regulation (Preussner et al., 2017). These data are further consistent with AS of target gene splicing: colder temperature resembled *Srsf2* knockdown while heat rather resembled *Srsf11* knockdown (Goldammer et al., 2018). SR protein phosphorylation appeared generally controlled by temperature (Preussner et al., 2017), but it remains to be investigated whether different SR proteins are differentially phosphorylated or whether phosphorylation changes differentially affect SR protein activity.

Autoregulatory feedback loops were initially characterized as a mechanism allowing homeostatic regulation of SR proteins (Lareau et al., 2007; Ni et al., 2007). Here we report – for the first time – that the same autoregulatory feedback loop is capable of producing rhythms in gene expression. An input signal controlling SR protein activity is therein sufficient to change SR protein GE. This has also interesting consequences for SR protein target genes, as activation of a protein reduces total levels of the same protein. Target genes with high affinity binding sites might therefore be bound and activated while target genes with low affinity binding sites are not bound, due to the reduced total protein levels, and therefore rather repressed. Overall this mechanism would allow dynamic and highly gene-specific control of posttranscriptional gene expression. In addition to SR proteins, we identified temperature controlled NMD-inducing splicing isoforms in many other RBPs. Mechanistically, it will be interesting to investigate, whether these splicing events are directly controlled by SR proteins or whether temperature also controls the activity of other RBPs (e.g. by phosphorylation or other post-translational modifications). Especially the identification of heat-induced NMD isoforms in *Rbm3* and *Cirbp* is interesting, as it shows that these genes are actually not cold-induced but rather heat-degraded via a heat-induced NMD isoform. Several diseases are associated with altered expression levels of *Rbm3* and *Cirbp* – e.g. neurodegenerative diseases for *Rbm3* (Peretti et al., 2015) and cancer for *Cirbp* (Lujan et al., 2018) – and the identification of NMD inducing exons could allow the therapeutic control of their expression level via splicing-changing antisense oligonucleotides (Bennett et al., 2019). Furthermore, characterizing NMD isoforms at different temperatures allowed us to identify several unannotated NMD variants (as in *Rbm3* and *Cirbp*) and could therefore provide further target exons in disease associated genes.

Homoeothermic and poikilothermic organisms experience quite different differentials in body temperature and it is therefore a striking finding that in mouse/human (1-2°C) and plants (>20°C) an almost identical mechanism controls SR protein levels. Our knowledge on the evolution of AS-NMD in SR proteins (Lareau and Brenner, 2015) indicates an evolutionary independent origin of the temperature-controlled exons/introns. Mechanistically it will therefore be interesting to

investigate how cis-regulatory elements, SR proteins and kinases are evolutionary adapted to allow control of SR protein expression in the body temperature range of diverse organisms. We believe that the evolutionary pervasive identification of temperature-controlled AS-NMD in SR proteins is indicative for an important function in temperature adaptation. Additionally, the fact that ultraconserved elements within SR proteins have evolved rapidly and are effectively 'frozen' in mammals and birds (Bejerano et al., 2004), which are all endothermic homeoetherms, represents a strong connection to endothermy. Because of the high sensitivity of temperature controlled AS-NMD we suggest that this mechanism could be involved in setting or maintaining a constant body temperature. Finally, our data are consistent with a model were CLK kinases and SR proteins represent a dynamic module that directly and quickly responds to temperature changes. In line with this model changes in gene expression are rather a secondary effect of change in SR protein activity i.e. through a temperature controlled NMD-inducing isoform.

Author Contributions

SM, GG, MS and MP performed experiments. AN performed the bioinformatics analysis. AN and MP designed the study, planned experiments, analyzed data and wrote the manuscript with help from SM and FH. MP and FH conceived and supervised the work.

Acknowledgments

The authors would like to thank Jessica Stock, Alena Lohnert, Kevin Huolt and Hoonsung Cho for their contribution to this work as rotation students. Furthermore, we would like to thank Dirk Hincha and Daniel Schubert for discussing AS-NMD in plants, Tom Haltenhof for the isolation of primary hepatocytes, the SeqCore facility for generation of RNA Sequencing data and the HPC Service of ZEDAT, Freie Universität Berlin, for computing time. This work was founded through DFG grants HE5398/3 and HE5398/4 to FH. MP is founded by a stipend from the Peter Traudl Engelhorn Foundation.

References

Barta, A., Kalyna, M., and Reddy, A.S. (2010). Implementing a rational and consistent nomenclature for serine/arginine-rich protein splicing factors (SR proteins) in plants. The Plant cell *22*, 2926-2929.

Bejerano, G., Pheasant, M., Makunin, I., Stephen, S., Kent, W.J., Mattick, J.S., and Haussler, D. (2004). Ultraconserved elements in the human genome. Science (New York, NY) *304*, 1321-1325.

Bennett, C.F., Krainer, A.R., and Cleveland, D.W. (2019). Antisense Oligonucleotide Therapies for Neurodegenerative Diseases. Annual review of neuroscience *42*, 385-406.

Braunschweig, U., Gueroussov, S., Plocik, A.M., Graveley, Brenton R., and Blencowe, Benjamin J. (2013). Dynamic Integration of Splicing within Gene Regulatory Pathways. Cell *152*, 1252-1269.

Brown, S.A., Zumbrunn, G., Fleury-Olela, F., Preitner, N., and Schibler, U. (2002). Rhythms of mammalian body temperature can sustain peripheral circadian clocks. Current biology : CB *12*, 1574-1583.
Buhr, E.D., Yoo, S.H., and Takahashi, J.S. (2010). Temperature as a universal resetting cue for mammalian circadian oscillators. Science (New York, NY) *330*, 379-385.
Calixto, C.P.G., Guo, W., James, A.B., Tzioutziou, N.A., Entizne, J.C., Panter, P.E., Knight, H., Nimmo, H.G., Zhang, R., and Brown, J.W.S. (2018). Rapid and Dynamic Alternative Splicing Impacts the Arabidopsis Cold Response Transcriptome. The Plant cell *30*, 1424-1444.
Dibner, C., Schibler, U., and Albrecht, U. (2010). The mammalian circadian timing system: organization and coordination of central and peripheral clocks. Annual review of physiology *72*, 517-549.
Dobin, A., Davis, C.A., Schlesinger, F., Drenkow, J., Zaleski, C., Jha, S., Batut, P., Chaisson, M., and Gingeras, T.R. (2012). STAR: ultrafast universal RNA-seq aligner. Bioinformatics *29*, 15-21.
Feng, Y., Chen, M., and Manley, J.L. (2008). Phosphorylation switches the general splicing repressor SRp38 to a sequence-specific activator. Nature Structural &Amp; Molecular Biology *15*, 1040.
Filichkin, S.A., Priest, H.D., Givan, S.A., Shen, R., Bryant, D.W., Fox, S.E., Wong, W.K., and Mockler, T.C. (2010). Genome-wide mapping of alternative splicing in Arabidopsis thaliana. Genome research *20*, 45-58.
Garrido-Martin, D., Palumbo, E., Guigo, R., and Breschi, A. (2018). ggsashimi: Sashimi plot revised for browser- and annotation-independent splicing visualization. PLoS computational biology *14*, e1006360.
Gerber, A., Saini, C., Curie, T., Emmenegger, Y., Rando, G., Gosselin, P., Gotic, I., Gos, P., Franken, P., and Schibler, U. (2015). The systemic control of circadian gene expression. Diabetes, obesity & metabolism *17 Suppl 1*, 23-32.
Goldammer, G., Neumann, A., Strauch, M., Muller-McNicoll, M., Heyd, F., and Preussner, M. (2018). Characterization of cis-acting elements that control oscillating alternative splicing. RNA biology *15*, 1081-1092.
Goncalves, V., and Jordan, P. (2015). Posttranscriptional Regulation of Splicing Factor SRSF1 and Its Role in Cancer Cell Biology. BioMed research international *2015*, 287048.
Gonze, D., Halloy, J., and Goldbeter, A. (2002). Robustness of circadian rhythms with respect to molecular noise. Proceedings of the National Academy of Sciences of the United States of America *99*, 673-678.
Gotic, I., Omidi, S., Fleury-Olela, F., Molina, N., Naef, F., and Schibler, U. (2016). Temperature regulates splicing efficiency of the cold-inducible RNA-binding protein gene Cirbp. Genes & development *30*, 2005-2017.
Heyd, F., and Lynch, K.W. (2010). Phosphorylation-dependent regulation of PSF by GSK3 controls CD45 alternative splicing. Molecular cell *40*, 126-137.
Huang, Y., Yario, T.A., and Steitz, J.A. (2004). A molecular link between SR protein dephosphorylation and mRNA export. Proceedings of the National Academy of Sciences of the United States of America *101*, 9666-9670.
Hunter, J.D. (2007). Matplotlib: A 2D Graphics Environment. Computing in Science & Engineering *9*, 90-95.
Hurt, J.A., Robertson, A.D., and Burge, C.B. (2013). Global analyses of UPF1 binding and function reveal expanded scope of nonsense-mediated mRNA decay. Genome research *23*, 1636-1650.
Ko, C.H., and Takahashi, J.S. (2006). Molecular components of the mammalian circadian clock. Human molecular genetics *15 Spec No 2*, R271-277.
Koike, N., Yoo, S.H., Huang, H.C., Kumar, V., Lee, C., Kim, T.K., and Takahashi, J.S. (2012). Transcriptional architecture and chromatin landscape of the core circadian clock in mammals. Science (New York, NY) *338*, 349-354.
Kornmann, B., Schaad, O., Bujard, H., Takahashi, J.S., and Schibler, U. (2007). System-Driven and Oscillator-Dependent Circadian Transcription in Mice with a Conditionally Active Liver Clock. PLoS biology *5*, e34.
Lareau, L.F., and Brenner, S.E. (2015). Regulation of splicing factors by alternative splicing and NMD is conserved between kingdoms yet evolutionarily flexible. Molecular biology and evolution *32*, 1072-1079.
Lareau, L.F., Inada, M., Green, R.E., Wengrod, J.C., and Brenner, S.E. (2007). Unproductive splicing of SR genes associated with highly conserved and ultraconserved DNA elements. Nature *446*, 926-929.

Lejeune, F., Cavaloc, Y., and Stevenin, J. (2001). Alternative splicing of intron 3 of the serine/arginine-rich protein 9G8 gene. Identification of flanking exonic splicing enhancers and involvement of 9G8 as a trans-acting factor. The Journal of biological chemistry *276*, 7850-7858.
Liu, Y., Hu, W., Murakawa, Y., Yin, J., Wang, G., Landthaler, M., and Yan, J. (2013). Cold-induced RNA-binding proteins regulate circadian gene expression by controlling alternative polyadenylation. Scientific reports *3*, 2054.
Long, J.C., and Caceres, J.F. (2009). The SR protein family of splicing factors: master regulators of gene expression. The Biochemical journal *417*, 15-27.
Lujan, D.A., Ochoa, J.L., and Hartley, R.S. (2018). Cold-inducible RNA binding protein in cancer and inflammation. Wiley Interdiscip Rev RNA *9*.
Lykke-Andersen, S., and Jensen, T.H. (2015). Nonsense-mediated mRNA decay: an intricate machinery that shapes transcriptomes. Nature Reviews Molecular Cell Biology *16*, 665.
Manley, J.L., and Krainer, A.R. (2010). A rational nomenclature for serine/arginine-rich protein splicing factors (SR proteins). Genes & development *24*, 1073-1074.
Martin, L., Grigoryan, A., Wang, D., Wang, J., Breda, L., Rivella, S., Cardozo, T., and Gardner, L.B. (2014). Identification and characterization of small molecules that inhibit nonsense-mediated RNA decay and suppress nonsense p53 mutations. Cancer research *74*, 3104-3113.
McKinney, W.T. (2010). Data Structures for Statistical Computing in Python. Proceedings of the 9th Python in Science Conference *51-56*.
Menet, J.S., Rodriguez, J., Abruzzi, K.C., and Rosbash, M. (2012). Nascent-Seq reveals novel features of mouse circadian transcriptional regulation. eLife *1*, e00011.
Mi, H., Muruganujan, A., and Thomas, P.D. (2013). PANTHER in 2013: modeling the evolution of gene function, and other gene attributes, in the context of phylogenetic trees. Nucleic acids research *41*, D377-386.
Morf, J., Rey, G., Schneider, K., Stratmann, M., Fujita, J., Naef, F., and Schibler, U. (2012). Cold-inducible RNA-binding protein modulates circadian gene expression posttranscriptionally. Science (New York, NY) *338*, 379-383.
Nagy, E., and Maquat, L.E. (1998). A rule for termination-codon position within intron-containing genes: when nonsense affects RNA abundance. Trends in biochemical sciences *23*, 198-199.
Neph, S., Kuehn, M.S., Reynolds, A.P., Haugen, E., Thurman, R.E., Johnson, A.K., Rynes, E., Maurano, M.T., Vierstra, J., Thomas, S.*, et al.* (2012). BEDOPS: high-performance genomic feature operations. Bioinformatics *28*, 1919-1920.
Ni, J.Z., Grate, L., Donohue, J.P., Preston, C., Nobida, N., O'Brien, G., Shiue, L., Clark, T.A., Blume, J.E., and Ares, M., Jr. (2007). Ultraconserved elements are associated with homeostatic control of splicing regulators by alternative splicing and nonsense-mediated decay. Genes & development *21*, 708-718.
Ninomiya, K., Kataoka, N., and Hagiwara, M. (2011). Stress-responsive maturation of Clk1/4 pre-mRNAs promotes phosphorylation of SR splicing factor. The Journal of cell biology *195*, 27-40.
Palusa, S.G., and Reddy, A.S. (2010). Extensive coupling of alternative splicing of pre-mRNAs of serine/arginine (SR) genes with nonsense-mediated decay. The New phytologist *185*, 83-89.
Pedregosa, F., Varoquaux, G., Gramfort, A., Michel, V., Thirion, B., Grisel, O., Blondel, M., Prettenhofer, P., Weiss, R., Dubourg, V.*, et al.* (2011). Scikit-learn: Machine Learning in Python. Journal of Machine Learning Research *12*, 2825-2830.
Peretti, D., Bastide, A., Radford, H., Verity, N., Molloy, C., Martin, M.G., Moreno, J.A., Steinert, J.R., Smith, T., Dinsdale, D.*, et al.* (2015). RBM3 mediates structural plasticity and protective effects of cooling in neurodegeneration. Nature *518*, 236-239.
Pollard, K.S., Hubisz, M.J., Rosenbloom, K.R., and Siepel, A. (2010). Detection of nonneutral substitution rates on mammalian phylogenies. Genome research *20*, 110-121.

Preussner, M., Goldammer, G., Neumann, A., Haltenhof, T., Rautenstrauch, P., Muller-McNicoll, M., and Heyd, F. (2017). Body Temperature Cycles Control Rhythmic Alternative Splicing in Mammals. Molecular cell *67*, 433-446.e434.
Preussner, M., and Heyd, F. (2016). Post-transcriptional control of the mammalian circadian clock: implications for health and disease. Pflugers Archiv : European journal of physiology *468*, 983-991.
Preussner, M., and Heyd, F. (2018). Temperature-controlled Rhythmic Gene Expression in Endothermic Mammals: All Diurnal Rhythms are Equal, but Some are Circadian. BioEssays : news and reviews in molecular, cellular and developmental biology *40*, e1700216.
Preussner, M., Wilhelmi, I., Schultz, A.S., Finkernagel, F., Michel, M., Moroy, T., and Heyd, F. (2014). Rhythmic U2af26 alternative splicing controls PERIOD1 stability and the circadian clock in mice. Molecular cell *54*, 651-662.
Quinlan, A.R., and Hall, I.M. (2010). BEDTools: a flexible suite of utilities for comparing genomic features. Bioinformatics *26*, 841-842.
Ran, F.A., Hsu, P.D., Wright, J., Agarwala, V., Scott, D.A., and Zhang, F. (2013). Genome engineering using the CRISPR-Cas9 system. Nature protocols *8*, 2281-2308.
Rauch, H.B., Patrick, T.L., Klusman, K.M., Battistuzzi, F.U., Mei, W., Brendel, V.P., and Lal, S.K. (2014). Discovery and expression analysis of alternative splicing events conserved among plant SR proteins. Molecular biology and evolution *31*, 605-613.
Refinetti, R., and Menaker, M. (1992). The circadian rhythm of body temperature. Physiology & behavior *51*, 613-637.
Rehwinkel, J., Raes, J., and Izaurralde, E. (2006). Nonsense-mediated mRNA decay: Target genes and functional diversification of effectors. Trends in biochemical sciences *31*, 639-646.
Richardson, D.N., Rogers, M.F., Labadorf, A., Ben-Hur, A., Guo, H., Paterson, A.H., and Reddy, A.S. (2011). Comparative analysis of serine/arginine-rich proteins across 27 eukaryotes: insights into sub-family classification and extent of alternative splicing. PloS one *6*, e24542.
Saini, C., Morf, J., Stratmann, M., Gos, P., and Schibler, U. (2012). Simulated body temperature rhythms reveal the phase-shifting behavior and plasticity of mammalian circadian oscillators. Genes & development *26*, 567-580.
Schlaen, R.G., Mancini, E., Sanchez, S.E., Perez-Santangelo, S., Rugnone, M.L., Simpson, C.G., Brown, J.W., Zhang, X., Chernomoretz, A., and Yanovsky, M.J. (2015). The spliceosome assembly factor GEMIN2 attenuates the effects of temperature on alternative splicing and circadian rhythms. Proceedings of the National Academy of Sciences of the United States of America *112*, 9382-9387.
Shin, C., Feng, Y., and Manley, J.L. (2004). Dephosphorylated SRp38 acts as a splicing repressor in response to heat shock. Nature *427*, 553-558.
Shin, C., and Manley, J.L. (2002). The SR protein SRp38 represses splicing in M phase cells. Cell *111*, 407-417.
Siepel, A., Bejerano, G., Pedersen, J.S., Hinrichs, A.S., Hou, M., Rosenbloom, K., Clawson, H., Spieth, J., Hillier, L.W., Richards, S.*, et al.* (2005). Evolutionarily conserved elements in vertebrate, insect, worm, and yeast genomes. Genome research *15*, 1034-1050.
Staiger, D., and Brown, J.W. (2013). Alternative splicing at the intersection of biological timing, development, and stress responses. The Plant cell *25*, 3640-3656.
Sterne-Weiler, T., Weatheritt, R.J., Best, A.J., Ha, K.C.H., and Blencowe, B.J. (2018). Efficient and Accurate Quantitative Profiling of Alternative Splicing Patterns of Any Complexity on a Laptop. Molecular cell *72*, 187-200.e186.
Sureau, A., Gattoni, R., Dooghe, Y., Stévenin, J., and Soret, J. (2001). SC35 autoregulates its expression by promoting splicing events that destabilize its mRNAs. The EMBO journal *20*, 1785-1796.
Turunen, J.J., Niemelä, E.H., Verma, B., and Frilander, M.J. (2013). The significant other: splicing by the minor spliceosome. Wiley Interdisciplinary Reviews RNA *4*, 61-76.

Walt, S.v.d., Colbert, S.C., and Varoquaux, G. (2011). The NumPy Array: A Structure for Efficient Numerical Computation. Computing in Science & Engineering *13*, 22-30.
Zhou, X., Wu, W., Li, H., Cheng, Y., Wei, N., Zong, J., Feng, X., Xie, Z., Chen, D., Manley, J.L.*, et al.* (2014). Transcriptome analysis of alternative splicing events regulated by SRSF10 reveals position-dependent splicing modulation. Nucleic acids research *42*, 4019-4030.

Figure legends

Figure 1. Characterization of temperature controlled AS-NMD in mammalian cells

(A) Generation of RNA samples from mouse primary hepatocytes for analysis of temperature-dependent AS-NMD.

(B) Principle component analysis of the investigated triplicate samples by RNA sequencing.

(C) Automatic cluster-mapping of the temperature-dependent splicing changes in CHX, based on changes in PSI (percent spliced in). Categories (right) were manually assigned. Here the top 1000 events are shown, see also Figure S1A for all events.

(D) Examples for cold-induced (blue) or heat-induced (red) AS-NMD via exon inclusion (top) or exon skipping (bottom). In each example, on the left a simplified exon-intron structure is given, PTCs and the length of frameshift inducing exons are highlighted. Predicted splicing changes were validated by radioactive RT-PCR with primers binding to the surrounding constitutive exons. A representative gel image is shown in the middle (asterisks indicate degradation products) and the PSI is quantified on the right. Boxplots represent mean +/- standard deviation (SD) of four different samples from at least two different mice. Individual data points are shown as circles. Statistical significance was determined by 2-way ANOVA and is indicated by asterisks: adjusted p values: not significant (ns), *p<0.05, ***p<0.001, ****p<0.0001.

(E) Classification of genes with NMD events.

(F) GO-term analysis of temperature-controlled AS-NMD genes. All genes with mean tpm > 0 served as background.

See also Figure S1.

Figure S1. Validation of temperature dependent AS in mammalian cells

(A) Automatic cluster-mapping of temperature-dependent splicing changes in CHX, based on PSI (percent spliced in). All events with dPSI>0.15 and p>0.85 between CHX 34 and 38°C are shown.

(B) Overlap of genes with NMD events identified in our study in primary mouse hepatocytes (34 and 38°C) and by Hurt et al., 2013 in embryonic stem cells (37°C).

(C) Examples for heat-skipped (white) or cold-skipped (grey) splicing events. Analysis as in Figure 1D, here only the quantifications are shown. Note that these splicing events are barely affected by CHX.

(D) Further examples for cold-induced (blue) or heat-induced (red) AS-NMD events. Analysis as in Figure 1D, here only the quantifications are shown.

(E) Comparison of temperature-regulated alternative splicing events predicted by Whippet RNA-Seq analysis and validated by RT-PCR from independent samples. The line depicts linear regression fit, goodness of fit is represented by R^2.

(F) Comparison of splicing changes in CHX (x-axis) and DMSO (y-axis) for all events presented in S1A. The line depicts linear regression fit, goodness of fit is represented by R^2. The slope significantly differs from zero (p=0).

(G) Temperature dependence of the strongest NMD events (top 500, largest dPSI in either 34 or 38°C comparison of DMSO vs CHX). Categories (right) were manually assigned. We assign four categories: (I) cold-induced NMD, (II) heat-induced NMD, (III) temperature independent NMD, and (IV) temperature dependent splicing events with one CHX-sensitive isoform (probably also temperature dependent NMD).

Figure 2. Conserved, temperature-dependent AS-NMD events globally regulate GE

(A) Temperature-dependent AS-NMD events in *hnRNP DL* (left, see also Figure 1D), *Ptbp2* (middle) and *Cirbp* (right). For each target, on top a simplified exon-intron structure is given and below Sashimi plots show the distribution of raw sequencing reads. Exon-Exon junction reads are indicated by the numbers connecting the exons. Below sequence conservation across placental species is given. *hnRNP DL* exhibits a heat-included exon that leads to a PTC, *Ptbp2* a heat-skipped exon that leads to a frameshift, and in *Cirbp*, heat leads to inclusion of an alternative transcript end, which leads to formation of a PTC.

(B) Validation PCR for alternative last exon usage in *Cirbp* by radioactive RT-PCR as described in Figure 1D. Statistical significance was determined by 2-way ANOVA and is indicated by asterisks: adjusted p values: not significant (ns), ***p<0.001, ****p<0.0001.

(C) *Cirbp* splicing and GE in the liver of young mice (12-13 days) kept at room temperature (RT) or at 18°C for 2 hours (cold, see (Preussner et al., 2014) for post mortem temperatures). Splicing was analyzed as in B, GE was analyzed by qRT-PCR and is shown normalized to *Hprt* and RT. Statistical significance was determined by unpaired t-tests, **p<0.01.

(D) AS-NMD in a 24h temperature-rhythm in human cells. Hek293 cells were pre-entrained with square-wave temperature cycles (12h 34°C/ 12h 38°C) for 48h, after 8 hours at 34°C (T56, blue) or 38°C (T68, red) are shown. Statistical significance was determined by 2-way ANOVA and is indicated by asterisks: adjusted p values: not significant (ns), ***p<0.001, ****p<0.0001.

(E) Intron conservation of alternative cassette exons. Shown are average placental conservation scores introns surrounding all alternative exons (black), AS-NMD exons (yellow) and temperature-regulated AS-NMD exons (green).

(F) Investigation of temperature-dependent GE of *Cirbp* in samples as in B (left, mouse hepatocytes) or D (right, Hek293). GE was analyzed by qRT-PCR and is shown normalized to *Gapdh* and for DMSO or CHX relative to 34°C (left) or T60 (right).

(G) Correlation of NMD isoform inclusion and GE levels for all RBPs with temperature-dependent AS-NMD skipped exon events. Shown are the log2 fold change (FC) in GE versus the dPSI of the NMD isoform between the CHX samples. Top shows the GE change between the DMSO samples and bottom between the CHX samples. Slope, R^2 and P (deviation from zero slope) are indicated. See also Figure S2.

Figure S2. Conserved, temperature-dependent AS-NMD events globally regulate GE

(A) Temperature-dependent AS-NMD events in *Rbm3* (left) and *hnrnph3* (right). Sashimi plots as shown in Figure 2A. *Rbm3* exhibits a heat-included exon encoding a PTC, *hnrnph3* a cold-skipped exon that leads to a frameshift. For *Rbm3* the exon inclusion level is below the detection threshold for significantly different splicing events.

(B) AS-NMD in a 24h temperature-rhythm in human cells. Hek293 cells were prepared as in Figure 2D, only 8 hours at 34°C (blue) or 38°C (red) are shown. Statistical significance was determined by 2-way ANOVA and is indicated by asterisks: adjusted p values: not significant (ns), **0.01, ***p<0.001, ****p<0.0001.

(C) Global correlation of NMD isoform inclusion and GE levels for all genes with temperature-dependent AS-NMD skipped exon events. Shown are the log2 fold change (FC) in GE versus the dPSI of the NMD isoform between the CHX samples. Left shows the GE change between the DMSO samples and right the between the CHX samples. Slope, R^2 and P(deviation from zero slope) are indicated.

Figure 3. Temperature dependent AS-NMD is regulated in an SR protein-specific manner

(A) Comparing temperature dependent AS-NMD (dPSI of 34 vs 38°C CHX) in SR proteins. dPSI values of DMSO vs CHX confirm that these are NMD events (see Figure S3A). The NMD event in *Srsf1* (*) escaped the computational analysis; data are derived from radioactive RT-PCR (Figure S3E).

(B, C) Temperature-dependent NMD exon inclusion in primary mouse hepatocytes (prepared as in Figure 1A). Heat-induced NMD exon inclusion is shown exemplarily for *Srsf2* (B) and cold-induced NMD isoform formation for *Srsf10* (C). In each example, on the left Sashimi plot is shown as in Figure 2A. On the right each splicing event was validated by radioactive RT-PCR as described in Figure 1D. Statistical significance was determined by 2-way ANOVA and is indicated by asterisks: adjusted p values: not significant (ns), *p<0.05, **p<0.01, ***p<0.001, ****p<0.0001.

(D, E) NMD exon inclusion for *Srsf2* (D) and *Srsf10* (E) in a 24h temperature-rhythm in human cells. Hek293 cells were pre-entrained with square-wave temperature cycles (12h 34°C/ 12h 38°C) for 48h. For the last 24h cells were treated with DMSO or CHX every 4h and harvested after 4h and analyzed as in B, C (n=3, mean ± SD). White area: 34°C; Read area: 38°C.

(F) Quantification of *Srsf2* AS-NMD in hamster, rabbit and chicken cells (n=2, mean ± SD). Statistical significance was determined by 2-way ANOVA, asterisks as in B, C.

See also Figure S3.

Figure S3. Temperature dependent AS-NMD is regulated in an SR protein-specific manner

(A) Comparison of CHX-dependent AS-NMD (dPSI of DMSO vs CHX samples) in SR proteins for the 34 (left) and 38°C samples (right), confirming the CHX-induction of the AS events. For Srsf1 see panel E.

(B) Comparison of splicing changes in CHX (x-axis) and DMSO (y-axis) for SR protein AS-NMD events presented in A. The line depicts linear regression fit, goodness of fit is represented by R^2. Note the strongly elevated amplitude in CHX (x-axis).

(C) Primary mouse hepatocytes were treated as in Figure 1A using the specific NMD inhibitor NMDI14 (NMDi) instead of CHX. Srsf2 AS was analyzed as in Figure 3B. Statistical significance was determined by 2-way ANOVA and is indicated by asterisks: adjusted p values: not significant (ns), **p<0.01, ****p<0.0001.

(D) Heat-induced NMD exon inclusion is *Srsf7* (samples as in Figure 1D). Sashimi plot on the left as shown in Figure 2A. On the right validation by radioactive RT-PCR as described in Figure 1D. Statistical significance was determined by 2-way ANOVA and is indicated by asterisks: adjusted p values: not significant (ns), ****p<0.0001.

(E) Cold temperature-promoted inclusion of the *Srsf1* NMD isoform. Presented is a representative radioactive PCR as described in Figure 1D. Statistical significance was determined by 2-way ANOVA and is indicated by asterisks: adjusted p values: *p<0.05, ****p<0.0001.

(F) NMD exon inclusion for *Srsf7* in a 24h temperature-rhythm in human Hek293 cells as described in Figure 3D (n=3, mean ± SD). White area: 34°C; Read area: 38°C.

Figure 4. AS-NMD in *Srsf10* is mediated via an autoregulatory feedback loop

(A) Exon/intron structure of *Srsf10* minigenes used for mutational analysis. The wt minigene reporter contains mouse exons 2 to 4 (and complete intervening introns) with indicated primer binding sites (arrows). Exon and intron sequences were replaced by sequences containing a minor intron from glia maturation factor beta (*Gmfb*, marked in grey).

(B) Western Blot of SRSF10 after siRNA-mediated knockdown and cotransfection with overexpression vectors for the different GFP-tagged SRSF10 isoforms and the wt minigene in HeLa cells (top). Vinculin was used as a loading control. Bottom: Exemplary gel of *Srsf10* minigene splicing. See Figure S4B for quantifications.

(C) Transfection and splicing analysis as described in B, followed by a 2-hour heat shock. For each condition, the dn-E3 isoform was quantified relative to 37°C (n=4). Statistical significance was determined by 2-way ANOVA and is indicated by asterisks: adjusted p values: not significant (ns), **p<0.01, ***p<0.001, ****p<0.0001.

(D) Minigenes from A were investigated as described in B using only SRSF10-fl for rescue. Splicing of mutants is shown relative to the wt from Figure S3B (shown again for comparison) and for each mutant to the ctrl siRNA (n=5, mean ± SD). Statistical significance was determined by 2-way ANOVA.

(E) Generation of clonal Hek293 cell lines lacking exon 3. Left: Schematic of CRISPR/Cas9-mediated deletion of Srsf10 exon 3. Arrows indicate primer binding sites. Right: genotyping PCR on genomic DNA.

(F, G) Srsf10 expression in cells lacking exon 3. In (F) qPCR for *Srsf10*-fl and *Srsf10*-2 in WT and CRISPR/Cas9-edited Hek293 cells (∆E3, orange). Isoform expression is shown normalized to *Gapdh* and WT. In (G) SRSF10 protein levels were analyzed by Western Blot and quantified relative to hnRNP L (n=3). Statistical significance was determined by 2-way ANOVA.

(H) SRSF10 target gene splicing (*Zfp207*, *Bclaf1*, *Ptbp2*) after depletion of *Srsf10* exon 3 (orange) compared to knockdown of *Srsf10* (grey; n>3). Statistical significance was determined by 2-way ANOVA.

(I) Autoregulation of *Srsf10* depends on phosphorylation and an ultraconserved binding site in exon 3.

See also Figure S4.

Figure S4. AS-NMD in *Srsf10* is mediated via an autoregulatory feedback loop

(A) Schematic of the *Srsf10* exon-intron structure with usage of the downstream (dn) major splice site (GT..AG) leading to inclusion of exon 3, which can be coupled to polyadenylation. Usage of the upstream (up) minor splice site (AT..AC) leads to inclusion of exon 4 and the canonical protein coding mRNA.

(B) Quantification of SRSF10 minigene splicing upon knockdown and rescue as shown in Figure 4B (n>3). Statistical significance was determined by 2-way ANOVA and is indicated by asterisks: adjusted p values: not significant (ns), **p<0.01, ***p<0.001, ****p<0.0001.

(C) Confirmation of the *Srsf10* knockdown on mRNA level. The expression of the different Srsf10 isoforms is shown relative to *Gapdh* and control siRNA (n>6). Note the reduced dn-E3/up-E4 ratio after knockdown of Srsf10. Statistical significance was determined by 1-way ANOVA.

(D) *Srsf10* exon 3 splicing upon *Srsf2* and *Srsf7* knockdown. N2A cells were transfected with the indicated siRNAs and *Srsf10* splicing was analyzed and quantified (n=2). Statistical significance was determined by 1-way ANOVA. In the same samples *U2af26* AS was strongly effected (Preussner et al., 2017).

(E) Dose dependent *Srsf10* autoregulation. HeLa cells were cotransfected with the minigene, decreasing amounts of SRSF10-fl or -2 (0.1, 0.05, or 0.025ug) and adjusted amounts of GFP. Expression was confirmed using an antibody against GFP (top). Note the higher expression levels of SRSF10-2. Vinculin served as a loading control. Bottom: Splicing analysis of cotransfected minigene (n=2).

(F, G) *Srsf10* AS upon heat shock recovery. Minigene transfected Hela (F) or N2A (G) cells were heat shocked for 2 hours following 6 or 4-hour incubation at 37°C. Splicing was investigated as in Figure 2A relative to 37°C (n=3). Statistical significance was determined by 1-way ANOVA.

Figure 5. AS-NMD generates rhythms in *Srsf10* expression *in vivo*

(A) RNA sequencing data of mouse cerebellum comparing inclusion of *Srsf10* exon 3 at ZT0 and ZT8 (Preussner et al., 2014). Sashimi plots are depicted below the *Srsf10* exon-intron structure.

(B) *Srsf10* exon 3 inclusion in mouse cerebellum samples from the indicated ZTs. Splicing was analyzed using radioactive RT-PCR of at least 3 mice per time point. Student's unpaired t test-derived p values **p<0.01, ***p<0.001.

(C) Correlation of *U2af26*%Δ67 and *Srsf10*%dn-E3 in 17 mice from different ZTs. The line depicts linear regression fit, goodness of fit is represented by R^2. The slope significantly differs from zero (p<0.0001).

(D) Correlation of rhythmic *Srsf10* expression (orange, left y-axis) and exon 3 splicing as depicted in B (black, right y-axis). Expression was determined by qRT-PCR and is shown relative to *Hprt* and ZT0 (mean of at least 3 mice ± SEM). Student's unpaired t test-derived p values **p<0.01.

(E) Representative Western blot of SRSF10 protein levels from mouse liver nuclear extracts (NX) from different ZTs. The different SRSF variants are highlighted on the right. The largest band probably represents hyperphosphorylated SRSF10 (SRSF10-fl-P, see also Figure S5D). hnRNP L was used as a loading control.

(F) Quantification of SRSF10-fl-P (orange, left y-axis) and SRSF10-fl + SRSF10-2 (black, right y-axis) relative to ZT0 and hnRNP L (mean of at least 3 mice ± SEM). Student's unpaired t test-derived p values *p<0.05, ***p<0.001.

See also Figure S5.

Figure S5. AS-NMD generates rhythms in *Srsf10* expression *in vivo*

(A) Rhythmic *Srsf10* AS persists in constant darkness. Mice were kept in constant darkness for 24h and sacrificed at the indicated circadian times (CTs) of the following subjective day. RT-PCR analysis as in Figure 5B (n=3, mean ± SD). Student's unpaired t test-derived p values *p<0.05.

(B) Entrained *Srsf10* AS. Mice were 8-hour phase delayed and on the 4th day sacrificed at the indicated ZTs. RT-PCR analysis as in Figure 5B (n=3, mean ± SD). Student's unpaired t test-derived p values *p<0.05.

(C) Representative Western blot of SRSF10 protein levels from mouse cerebellum nuclear extracts (NX) from different ZTs. The different SRSF variants are highlighted on the right. In brain the SRSF10-fl isoform predominates. hnRNP L was used as a loading control.

(D) Representative Western blot of SRSF10 protein levels from liver nuclear extracts (NX) from ZT12 after treatment with Antarctic phosphatase (AP). The different SRSF variants are highlighted on the right. After AP treatment we observe an increased signal at the approximate size of SRSF10-fl, which is probably to some cross-reactivity of the SRSF10 antibody with AP.

Figure 6. Temperature-dependent AS-NMD is necessary for rhythmic GE

(A, B) Hek293 WT and *Srsf10* ∆E3 cells were incubated and harvested at indicated temperatures and time points of a square-wave temperature rhythm. In A *Srsf10* AS was analyzed by RT-PCR as in Figure 2C. A *Gapdh* PCR was performed simultaneously and served as a loading control. A representative gel image is shown. The asterisk indicates an unspecific product. A quantification of the amount of up-E4 relative to *Gapdh* is shown in Figure S6B. In B *Srsf10* GE was analyzed by qRT-PCR. For each clone (WT and two independent ∆E3 clones) expression is shown relative to time point 52h and *Gapdh* (n=4, mean +/- SEM). Statistical significance was determined by 2-way ANOVA and is indicated by asterisks: adjusted p values: ****p<0.0001.

(C) Generation of cell lines lacking NMD exons for Srsf2 (top) and Srsf7 (bottom).

(D, E) Rhythmic *Srsf2* (D) and *Srsf7* (E) mRNA levels (relative to *Gapdh*) in WT and CRISPR/Cas9-edited cells (ΔNMD Exon) in a 24h temperature rhythm (n = 3, mean ± SEM).

See also Figure S6.

Figure S6. Temperature-dependent AS-NMD is necessary for rhythmic GE

(A) Quantification of gel images as in Figure 6B. The amount of up-E4 is shown relative to time point 52h and *Gapdh* (n=2). Statistical significance was determined by 2-way ANOVA and is indicated by asterisks: adjusted p values: *p<0.05, **p<0.01.

(B) Lack of NMD exons in clonal *Srsf2* (left) and *Srsf7* (right) CRISPR/Cas9-edited cell lines as indicated in Figure 6D. WT and mutant cell lines were treated with DMSO or CHX and inclusion of the NMD isoforms was investigated as in Figure 2.

(C) Increased *Srsf2* (left) and *Srsf7* (right) expression. Independent clonal cell lines were investigated by qRT-PCR. Expression is depicted relative to wt cells (set to 1) and *Gapdh*.

Figure 7. Temperature-dependent AS-NMD of SR proteins is conserved in plants

(A) Normalized GE values of plant SR proteins in a 48-hour time course. In the first day, plants were kept at 20°C (red) and shifted to 4°C (blue) for the second day. Plants were under a 12-hour dark/light regimen (gray/yellow bars). Warm- and cold-expressed genes are indicated.

(B) *A. thaliana* SR proteins divided in their subfamilies and classified as warm- or cold-expressed.

(C) Sashimi plots (left) as shown in Figure 2A (without conservation score) and PCR validations (top right) for NMD-inducing AS events upon RT (At-SR34, left) or cold treatment (At-SCL33). Data for time points 4, 8, 12 and 16 (12 and 24 hours RT or cold, respectively). Bottom right shows corresponding expression levels based on qPCR.

(D) Correlation of NMD isoform inclusion and GE levels for temperature-dependent AS-NMD skipped exon events. Shown are the log2 fold change (FC) in GE versus the dPSI of the NMD isoform between the CHX samples Slope, R^2 and P (deviation from zero slope) are indicated.

(E) Validation of an AS-NMD event in Gemin2, in which cold-induced inclusion of the NMD isoform correlates with lower GE.

See also Figure S7.

Figure S7. Temperature-dependent AS-NMD of SR proteins is conserved in plants

(A) Normalized NMD isoform expression of plant SR proteins as in Figure 7A. In three cases, a clear temperature-regulated alternative poly-adenylation (APA) event occurred but was not quantified. In two cases, no NMD event could be identified. Four times NMD seemed to be too efficient, as no events could be identified without CHX treatment (compare B).

(B) AS-NMD isoform inclusion in wt or CHX-treated plants for the same genes as in A.

(C) Validation RT-PCRs and qPCRs of NMD events in plant SR proteins. Only quantifications are shown. For each case, NMD isoform inclusion correlates with lower GE.

(D) Validation of an autoregulatory feedback loop in At-RS2Z33. Overexpression leads to higher inclusion levels of the NMD isoform.

STAR methods

Contact for Reagent and Resource Sharing

Please contact M.P. (mpreussner@zedat.fu-berlin.de) for reagents and resources generated in this study. Accession numbers to all RNA-seq datasets used in this study are noted in Table S1.

Experimental Model and Subject Details

Mouse maintenance

All animal experiments were performed with C57BL/6 mice in accordance with institutional and governmental recommendations and laws. Mice were kept under constant 12-hour light-dark conditions. To investigate the impact of the environmental temperature, we used samples from young mice previously described (Preussner et al., 2017). RNA samples across a circadian day, from constant darkness or after jet-lag were previously generated (Preussner et al., 2014) Mice of both genders were used. For preparation of RNA, tissues were quickly removed, frozen in liquid nitrogen and homogenized in RNATri (Bio&Sell). For preparation of nuclear extracts, we first prepared single cell suspensions of freshly isolated liver or cerebellum samples.

Tissue culture cells

HEK293T, HeLa and N2A cell lines have been present in the lab for over 5 years and are maintained in liquid nitrogen. Early passage aliquots are thawed periodically. Rabbit RK-13, Chinese hamster CHO and chicken enterocyte 8E11 cell lines were a kind gift from Dusan Kunec (FU Berlin). For all cell lines, cell morphology and growth is routinely assessed and corresponds to the expected phenotype. Cell cultures are tested for mycoplasma contamination monthly using a PCR-based assay. NIH3T3, HEK293T and 8E11 cell lines were maintained in DMEM medium containing 10% FBS and Pen/Strep (Invitrogen). N2A cells were maintained in 50% DMEM/ 50% OptiDMEM + GlutaMAX (life technologies) containing 10% FBS and Pen/Strep. RK13 cells were maintained in EMEM medium containing 10% FBS and Pen/Strep (Invitrogen). CHO cells in Ham's F12 medium containing 10% FBS and Pen/Strep. All cell lines were usually maintained at 37°C and 5% CO^2, except for 8E11 cells (39°C). For square-wave temperature cycles we used two incubators set to 34°C and 38°C and shifted the cells every 12 hours. See (Preussner et al., 2017) for an image of the square-wave temperature cycles with temperatures and time points. For chicken cells we used 34°C and 40°C (as 37°C degrees would already be a reduced temperature). Transfections of N2A, HeLa, and Hek293T using Rotifect (Roth) were performed according to the manufacturer's instructions. For knockdown of Srsf10 we used the following siRNA sequence 5'-

GCGUGAAUUUGGUUAUdTdT or si-ctrl 5'-UUUGUAAUCGUCGAUACCCdTdT (final concentration: 0.08 µM). Cycloheximide (Sigma) was used at 40µg/ml final concentration or DMSO as solvent control.

To isolate primary mouse hepatocytes, liver was perfused with PBS and digested using Collagen digestion solution. Liver was transferred into a Petri dish and cells were liberated by mechanical force. Cells were washed three time with Williams Medium E and 10% FCS and plated.

A. thaliana

To confirm temperature dependent alternative splicing and gene expression in *A. thaliana* we isolated RNA from 28-day old Col-0 plants kept only at RT or 31-day old Col-0 plants kept at 4°C for the last 3 days. For RNA isolation, using Trizol (see below) we used ~100mg material from leaves.

Method Details

RT-PCR and RT-qPCR

RT-PCRs were done as previously described (Preussner et al., 2014). Briefly, RNA was extracted using RNATri (Bio&Sell) and 1µg RNA was used in a gene specific RT-reaction. For analysis of minigene splicing the RNA was additionally digested with DNase I and re-purified. Low-cycle PCR with a ^{32}P-labeled forward primer was performed, products were separated by denaturing PAGE and quantified using a Phosphoimager and ImageQuantTL software. For qRT-PCR up to 4 gene-specific primers were combined in one RT reaction. qPCR was then performed in a 96 well format using the ABsolute QPCR SYBR Green Mix (Thermo Fisher) on Stratagene Mx3000P instruments. qPCRs were performed in duplicates, mean values were used to normalize expression to a housekeeping gene (mouse: *Hprt*, human: *Gapdh*, plants: *Ipp2*; ΔCT) and $\Delta(\Delta CT)$s were calculated for different conditions. See Table S2 for primer sequences.

RNA-Seq analysis

Mapping of reads to reference genomes was performed using STAR version 2.5.3a (Dobin et al., 2012). Reference genomes mm10 (mouse) and TAIR10 (*A.* thaliana) were applied. Whippet version 0.11 (Sterne-Weiler et al., 2018) was used to obtain splicing ratios and transcript per million GE quantifications. To obtain splicing quantifications of AS-NMD events, index creation was supplemented with mapped reads of NMD-inhibited sequencing samples (see Table S1 for plant accession numbers) and the low TSL flag was not set. A splice event was considered

significantly different between two conditions with a |dPSI| > 15%, probability > 85% and on average more than 10 junction reads. For AS-NMD events of SR proteins that could not be properly quantified by Whippet, PSI values were calculated based on junction read counts (e.g. Srsf7). Downstream analyses were performed using Python3, bash and R scripts. Most relevant Python packages used were pandas (general secondary data analysis, (McKinney, 2010)), numpy (numerical operations, (Walt et al., 2011)), Matplotlib (data visualization, (Hunter, 2007)) and scikit-learn (principle component analysis, (Pedregosa et al., 2011)). Molecular function analysis was performed using PANTHER version 14.1 (Mi et al., 2013) with all genes expressed above 1 TpM as background. Sashimi plots were generated using a customized version of ggsashimi (Garrido-Martin et al., 2018), which additionally displays conservation scores. Junction reads with low count numbers were removed for clarity. Phylogenetic p-value conservation score data of placental organisms was downloaded from UCSC (mm10 phyloP60way placental, (Pollard et al., 2010; Siepel et al., 2005)) and manipulated with BEDOPS version 2.4.26 and bedtools version 2.26.0 (Neph et al., 2012; Quinlan and Hall, 2010).

For mouse data, splicing events were classified into the following groups:

1) events that show differential splicing upon temperature (34°C vs 38°C between DMSO or CHX conditions)
2) events that show differential splicing upon CHX treatment (DMSO vs CHX in 34°C or 38°C conditions) and no temperature-dependent differential splicing (34°C vs 38°C in CHX)
3) events that show differential splicing upon CHX treatment (DMSO vs CHX in 34°C or 38°C conditions) and additional temperature-dependent differential splicing (34°C vs 38°C in CHX)
4) events that do not fall into any of the above categories

Splicing events in groups 2) and 3) were identified as AS-NMD events. The temperature-regulated events were further divided into cold-induced and heat-induced AS-NMD events (considering directionality of the CHX-induction). AS-NMD events that showed different directionality upon CHX treatment at the two temperatures were omitted from the analysis (these made up <2% of CHX-induced events).

For *A. thaliana*, AS-NMD events were identified by using independent RNA-seq data from CHX-treated plants. These data did not include a temperature shift and therefore the classification between temperature-dependent and -independent AS-NMD events was done using temperature shifted but not CHX treated data. Otherwise the classification was performed as for mouse.

Molecular cloning

For overexpression constructs of different SRSF10 variants inserts were amplified from mouse cDNA and cloned into the pEGFP-N3 (Clontech) backbone using XhoI and BamHI restriction sites. We used on forward primer including the start codon F:5'- ttCTCGAGATGTCCCGATACCTGC GCC and three different reverse primers for -2: 5'- ttGGATCCGATCTTTCTTGAAGTGTAGTAAG, fl: 5'- ttGGATCCgtggccactggacttggg and short: 5'-ttGGATCCACACCCCTCACTAATCATCC. For cloning of the Srsf10 minigene the region spanning exons 2 to 4 was amplified from mouse genomic DNA with the following primers F:5'-TTAAGGATCCGTCTGAAGATTTACGTCGGG and R:5'-TTAACTCGAGTCTTCCGATCCCCCTGTGC, thereby introducing restriction sites for BamHI and XhoI. The resulting 3.5 kBP long insert was afterwards cloned into pcDNA3.1(+) via conventional cloning. For mutational analysis *Srsf10* exons/introns were replaced by sequences from the human *Gmfb* gene: exons 4 to 5, intron 4 is a minor intron. New inserts were amplified by 1-step or 2-step PCR and cloned into pcDNA3.1(+) using BamHI and XhoI or into the wt minigene using internal restrictions sites for BsrGI (exon 3) and XbaI (intron 3). In the I3 mutant 356nt of *Srsf10* exon 3 were maintained, downstream sequence was replaced by the 5'ss of *Gmfb* exon 4 (TCGatatcc…) and downstream sequence. For the E3 mutant sequences downstream of the BsrGI site (+16 in exon 3) were replaced by *Gmfb* exons 4 to 5 (CACCAGA…). For the ESE mutant exon 3 nucleotids 17 to 60 were replaced by *Gmfb* exon 4 sequence. For the minigene containing only minor splice sites we replaced the major splice sites of Srsf10 intron 2 by minor splice sites of *Gmfb* intron 4 (5'ss:TCGatatcc; 3'ss: 5'-ttctttaacttgagaaaaacCTT). In the minigene containing only major splice sites the upstream 5'ss of exon 2 and the 3'ss of exon 4 were replaced by major splice sites from *Gmfb* intron 5 or 3, respectively (5'ss: TTGgtaagt; 3'ss: 5'-gcttttctctgtggtgccagGGC). All constructs were confirmed by sequencing.

Generation of CRISPR/Cas9 modified cell lines.

For genome-engineering in Hek293T cells or N2A cells, sequences flanking the conserved exons of Srsf2, Srsf7 or Srsf10 (human) and the alternative last exon 7b of Cirbp (mouse) were analyzed for sgRNA candidates *in silico* using the Benchling tool. Upstream and downstream of each exon at least one pair of oligos for the highest ranked candidate sgRNA (Ran et al., 2013) was synthesized and subcloned into the PX459 vector (kindly provided by Stefan Mundlos). sgRNA sequences are available on request. Cells were transfected in 6-well plates using Rotifect following the manufacturer's protocol. 48 hours after transfection, the transfected cells were selected with 1 µg/ml puromycin and clonal cell lines were isolated by dilution (Ran et al., 2013). Genomic DNA was extracted using DNA extraction buffer (200 mM Tris pH 8.3, 500 mM KCl, 5 mM MgCl2, 0.1% gelatin in H_2O) and a PCR was performed using gene-specific primers to confirm the exon

knockout on DNA level. In promising clones the exon knockout was additionally confirmed after RNA isolation by splicing sensitive PCR.

Western Blot

Lysates and nuclear/cytoplasmic fractionations (NX/CTX) were performed as previously described (Heyd and Lynch, 2010). For AP treatment 30µg of liver nuclear extracts were incubated for 15 minutes at 37°C with 2µl of FastAP (Thermo Scientific). SDS-PAGE and Western blotting followed standard procedures. Western blots were quantified using the ImageQuant TL software. The following antibodies were used for Western blotting: hnRNP L (4D11, Santa Cruz), SRSF10 (T-18, Santa Cruz), Vinculin (H-300, Santa Cruz), and GFP (B-2, Santa Cruz).

Quantification and statistical analysis

Figure legends contain information on repetitions and statistical tests used.

Data and Software Availability

Full gel images and raw data files will be deposited as Mendeley Data.

Supplemental information

Table S1. RNA Sequencing

Table S2. Primer sequences, Related to STAR methods

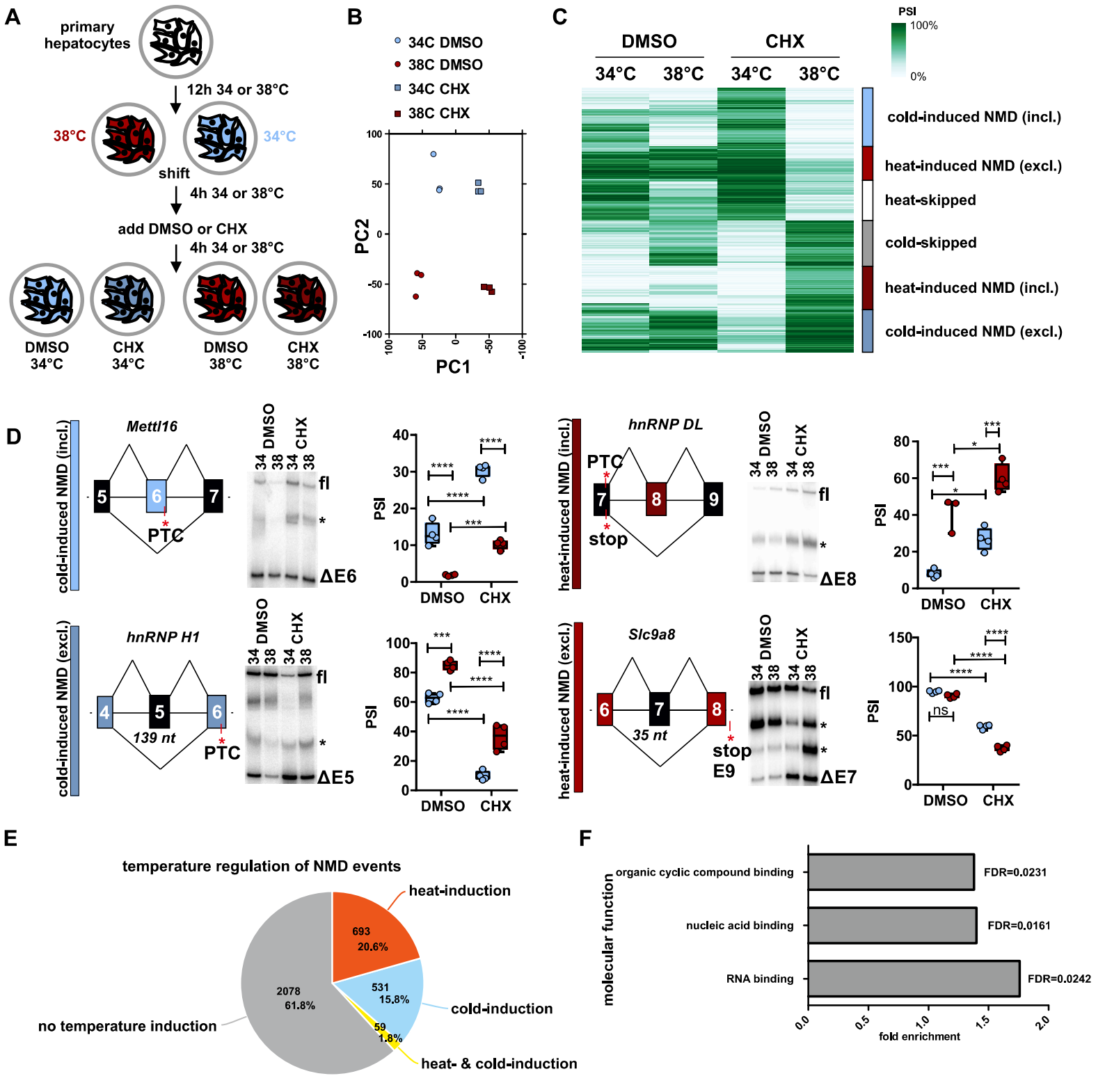
A
primary hepatocytes
12h 34 or 38°C
38°C
34°C
shift
4h 34 or 38°C
add DMSO or CHX
4h 34 or 38°C
DMSO 34°C
CHX 34°C
DMSO 38°C
CHX 38°C
B
34C DMSO
38C DMSO
34C CHX
38C CHX
PC2
PC1
C
DMSO
CHX
34°C
38°C
34°C
38°C
PSI
100%
0%
cold-induced NMD (incl.)
heat-induced NMD (excl.)
heat-skipped
cold-skipped
heat-induced NMD (incl.)
cold-induced NMD (excl.)
D
cold-induced NMD (incl.)
Mettl16
PTC
fl
ΔE6
PSI
DMSO
CHX
heat-induced NMD (incl.)
hnRNP DL
stop
ΔE8
cold-induced NMD (excl.)
hnRNP H1
139 nt
ΔE5
heat-induced NMD (excl.)
Slc9a8
35 nt
stop E9
ΔE7
ns
E
temperature regulation of NMD events
heat-induction
693
20.6%
cold-induction
531
15.8%
heat- & cold-induction
59
1.8%
no temperature induction
2078
61.8%
F
molecular function
organic cyclic compound binding
FDR=0.0231
nucleic acid binding
FDR=0.0161
RNA binding
FDR=0.0242
fold enrichment

Figure 1

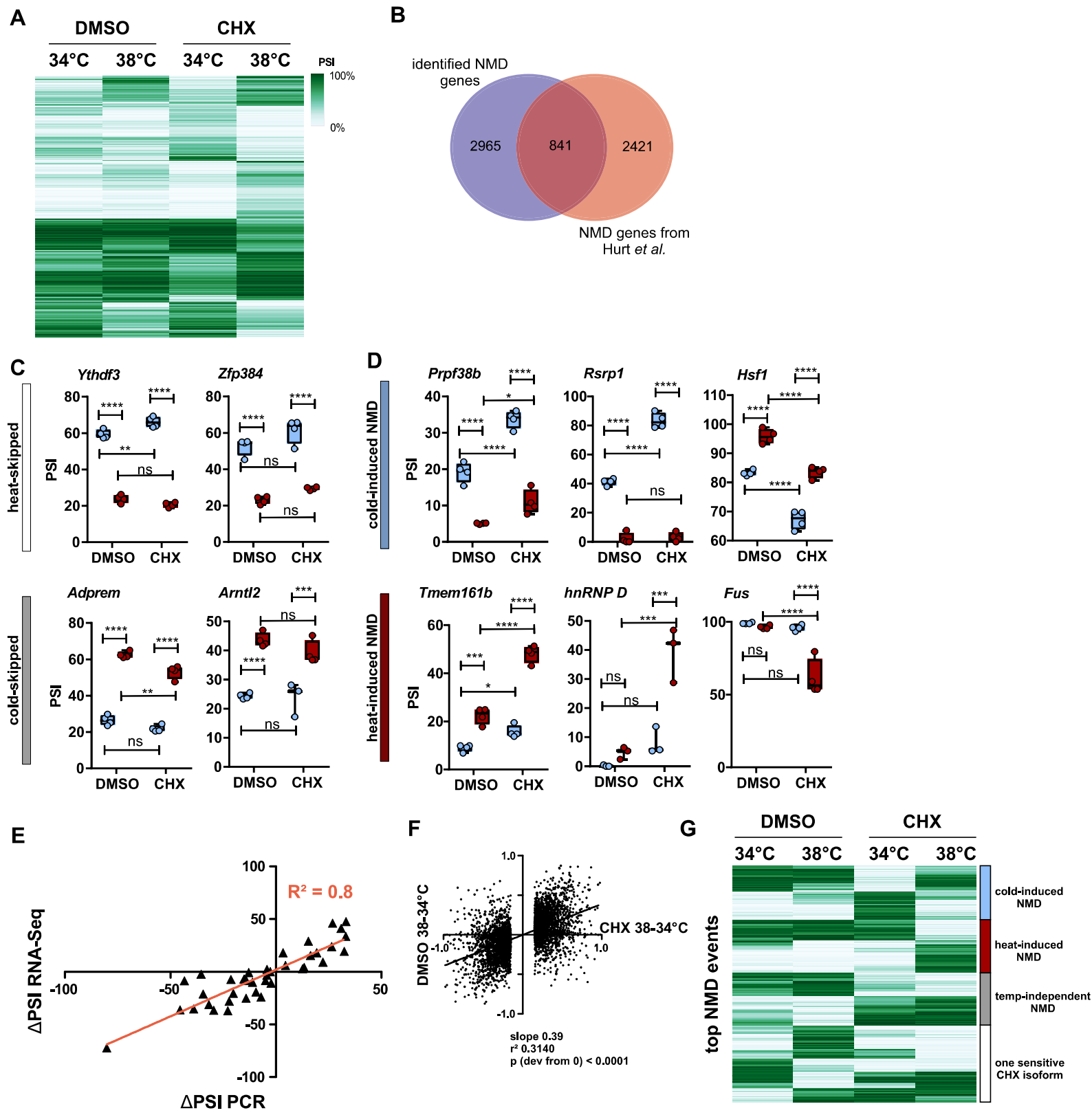
A
DMSO
CHX
34°C
38°C
34°C
38°C
PSI
100%
0%
B
identified NMD genes
2965
841
2421
NMD genes from Hurt et al.
C
heat-skipped
cold-skipped
Ythdf3
Zfp384
Adprem
Arntl2
PSI
DMSO
CHX
D
cold-induced NMD
heat-induced NMD
Prpf38b
Rsrp1
Hsf1
Tmem161b
hnRNP D
Fus
E
R² = 0.8
ΔPSI RNA-Seq
ΔPSI PCR
F
DMSO 38-34°C
CHX 38-34°C
slope 0.39
r² 0.3140
p (dev from 0) < 0.0001
G
top NMD events
cold-induced NMD
heat-induced NMD
temp-independent NMD
one sensitive CHX isoform

Figure S1

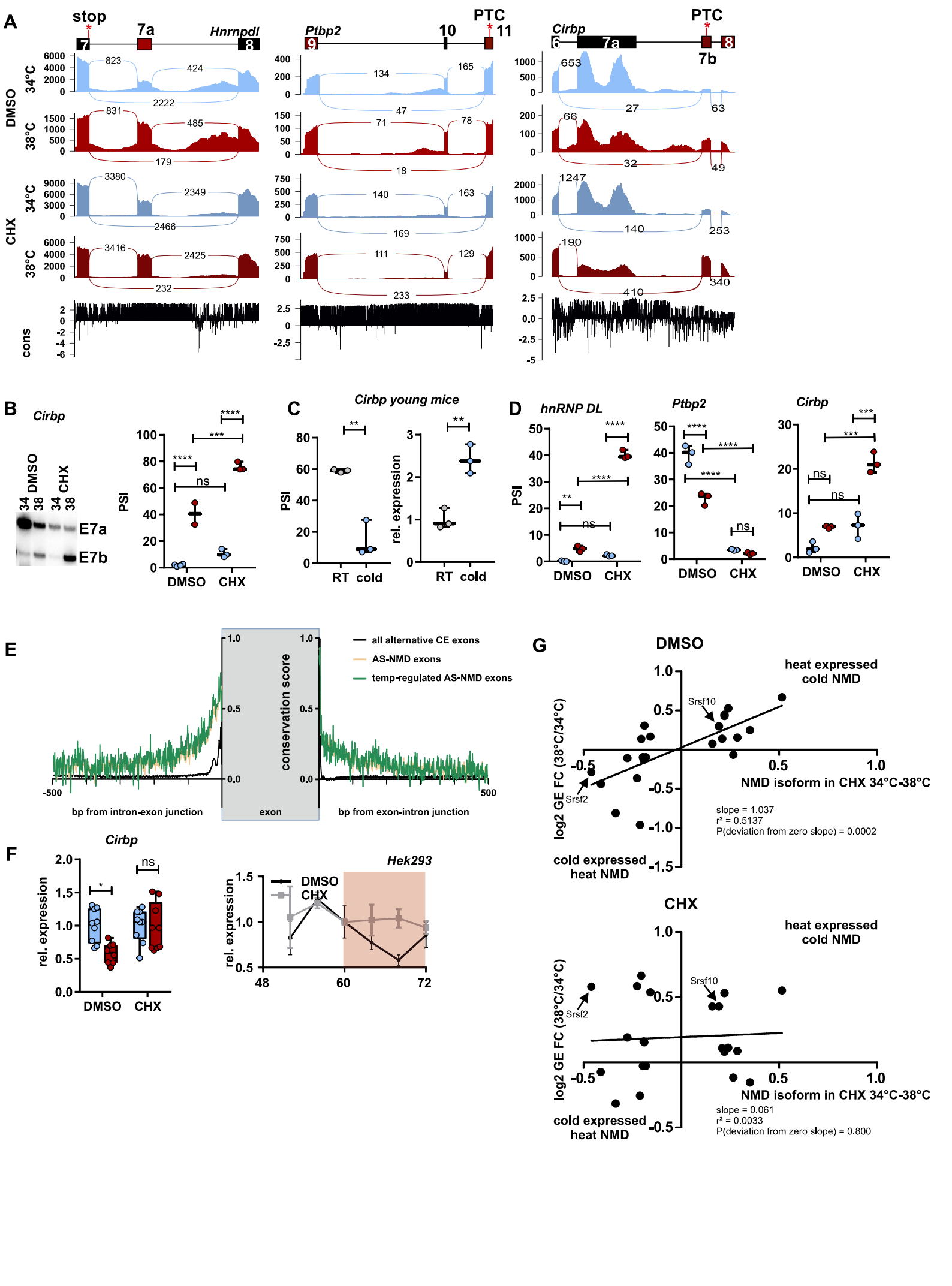
A
stop
7a
Hnrnpdl
Ptbp2
PTC
10
11
Cirbp
7b
DMSO
CHX
34°C
38°C
cons
B
Cirbp
DMSO
CHX
E7a
E7b
PSI
C
Cirbp young mice
PSI
rel. expression
RT
cold
D
hnRNP DL
Ptbp2
Cirbp
PSI
DMSO
CHX
E
all alternative CE exons
AS-NMD exons
temp-regulated AS-NMD exons
conservation score
bp from intron-exon junction
exon
bp from exon-intron junction
F
Cirbp
rel. expression
Hek293
DMSO
CHX
G
DMSO
heat expressed
cold NMD
Srsf10
Srsf2
log2 GE FC (38°C/34°C)
NMD isoform in CHX 34°C-38°C
slope = 1.037
r² = 0.5137
P(deviation from zero slope) = 0.0002
cold expressed
heat NMD
CHX
heat expressed
cold NMD
Srsf10
Srsf2
log2 GE FC (38°C/34°C)
NMD isoform in CHX 34°C-38°C
slope = 0.061
r² = 0.0033
P(deviation from zero slope) = 0.800
cold expressed
heat NMD

Figure 2

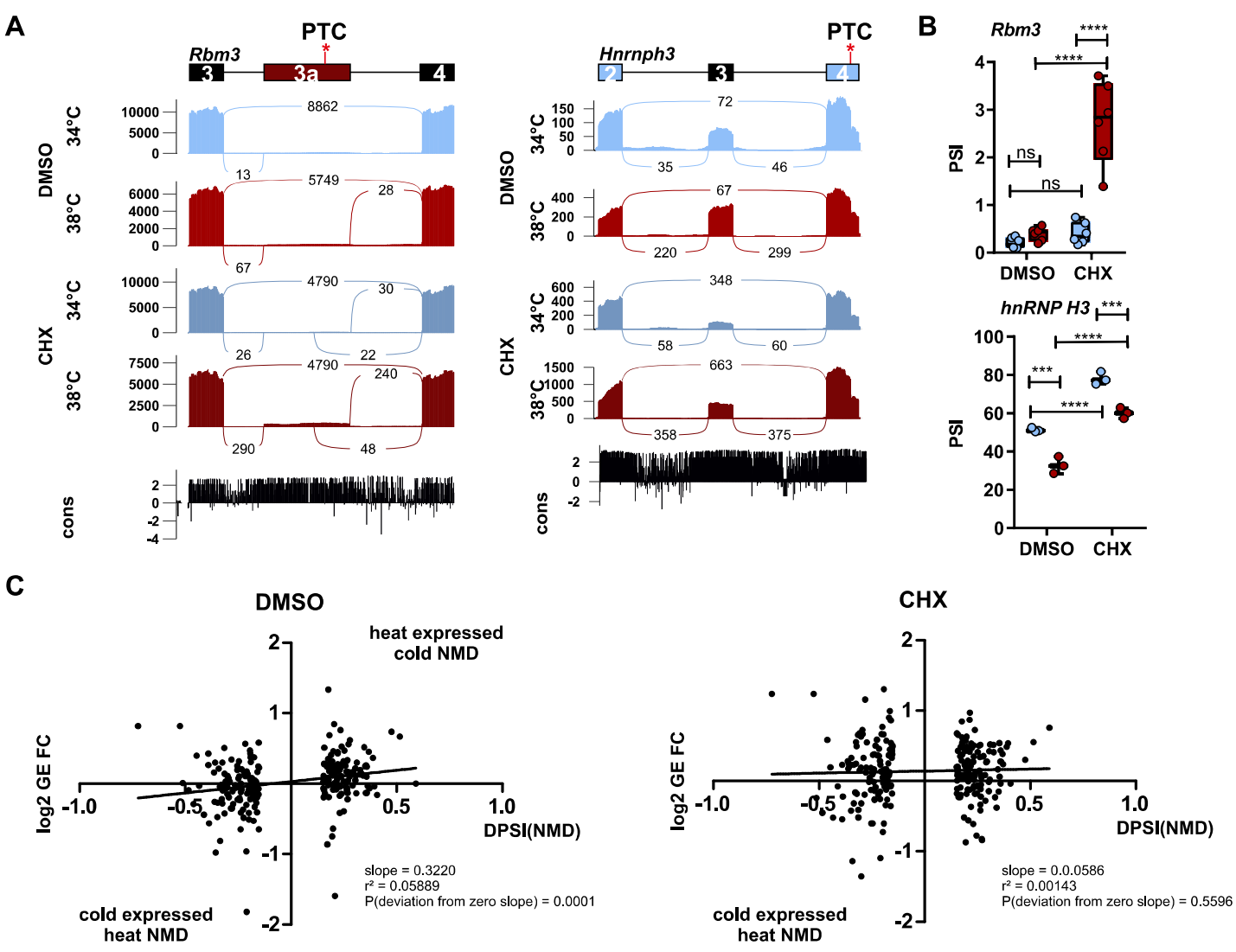
A
PTC
Rbm3
3
3a
4
Hnrnph3
2
3
4
DMSO
CHX
34°C
38°C
cons
8862
13
5749
28
67
4790
30
26
22
4790
240
290
48
72
35
46
67
220
299
348
58
60
663
358
375
B
Rbm3
hnRNP H3
PSI
ns
DMSO
CHX
C
DMSO
CHX
heat expressed
cold NMD
cold expressed
heat NMD
log2 GE FC
DPSI(NMD)
slope = 0.3220
r² = 0.05889
P(deviation from zero slope) = 0.0001
slope = 0.0.0586
r² = 0.00143
P(deviation from zero slope) = 0.5596

Figure S2

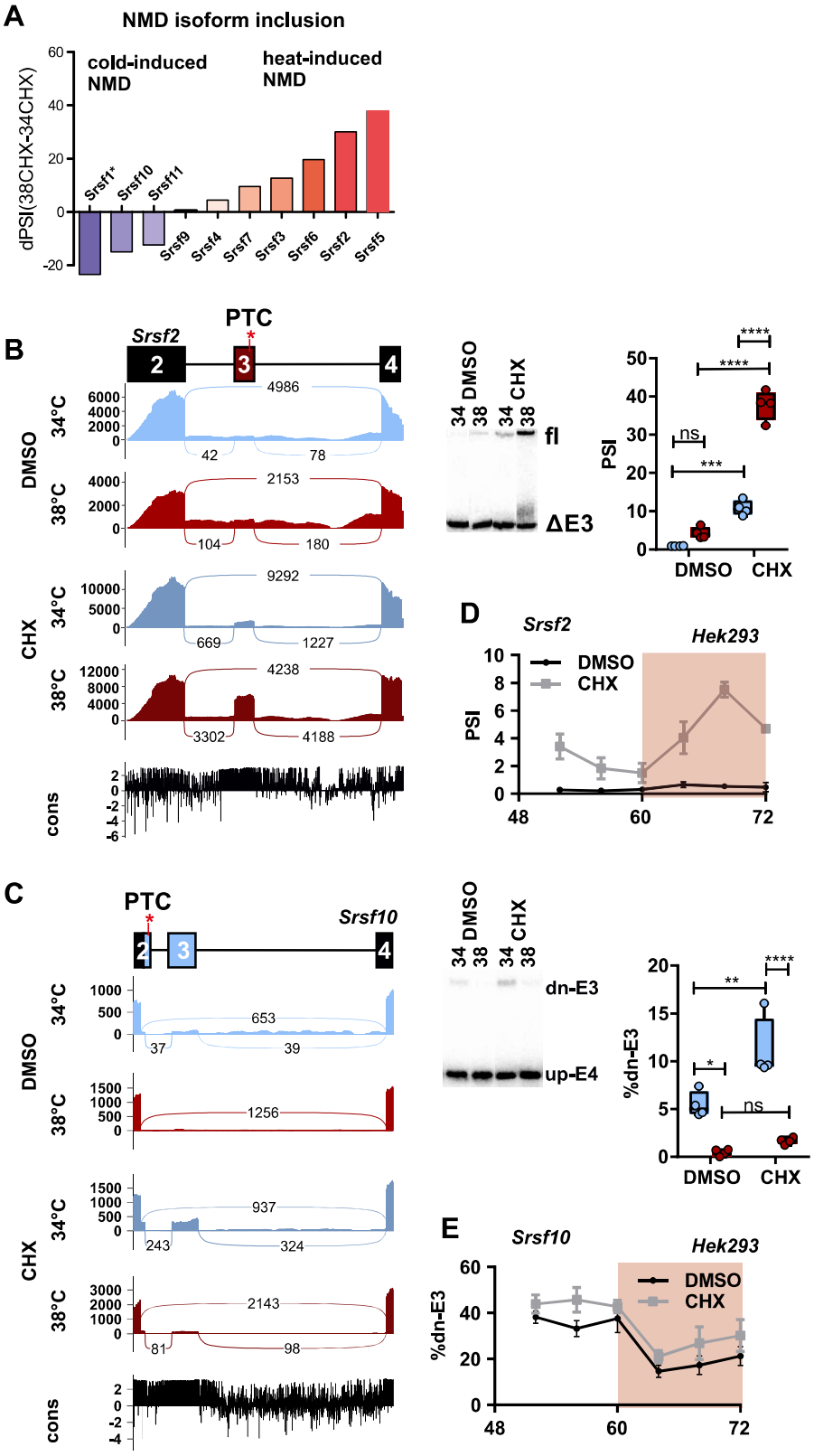
A
NMD isoform inclusion
cold-induced NMD
heat-induced NMD
dPSI(38CHX-34CHX)
Srsf1*
Srsf10
Srsf11
Srsf9
Srsf4
Srsf7
Srsf3
Srsf6
Srsf2
Srsf5
B
PTC
Srsf2
DMSO
CHX
34°C
38°C
cons
4986
42
78
2153
104
180
9292
669
1227
4238
3302
4188
fl
ΔE3
PSI
ns
***
****
C
PTC
Srsf10
653
37
39
1256
937
243
324
2143
81
98
dn-E3
up-E4
%dn-E3
*
**
D
Srsf2
Hek293
E
Srsf10
Hek293

Figure 3

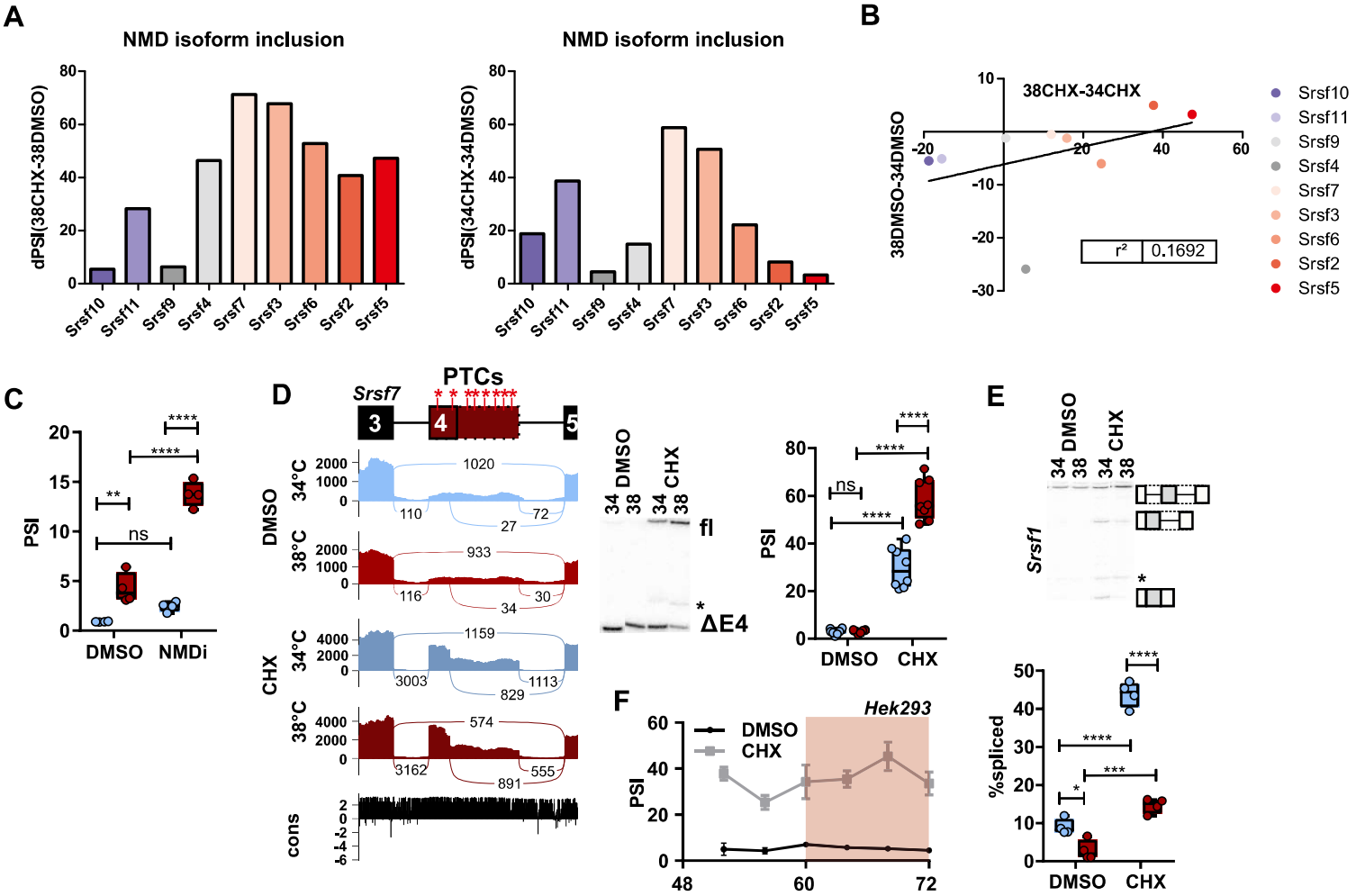
A
NMD isoform inclusion
dPSI(38CHX-38DMSO)
NMD isoform inclusion
dPSI(34CHX-34DMSO)
Srsf10
Srsf11
Srsf9
Srsf4
Srsf7
Srsf3
Srsf6
Srsf2
Srsf5
B
38CHX-34CHX
38DMSO-34DMSO
r²
0.1692
C
PSI
DMSO
NMDi
D
PTCs
Srsf7
DMSO
CHX
34°C
38°C
cons
fl
ΔE4
E
Srsf1
%spliced
F
Hek293
PSI

Figure S3

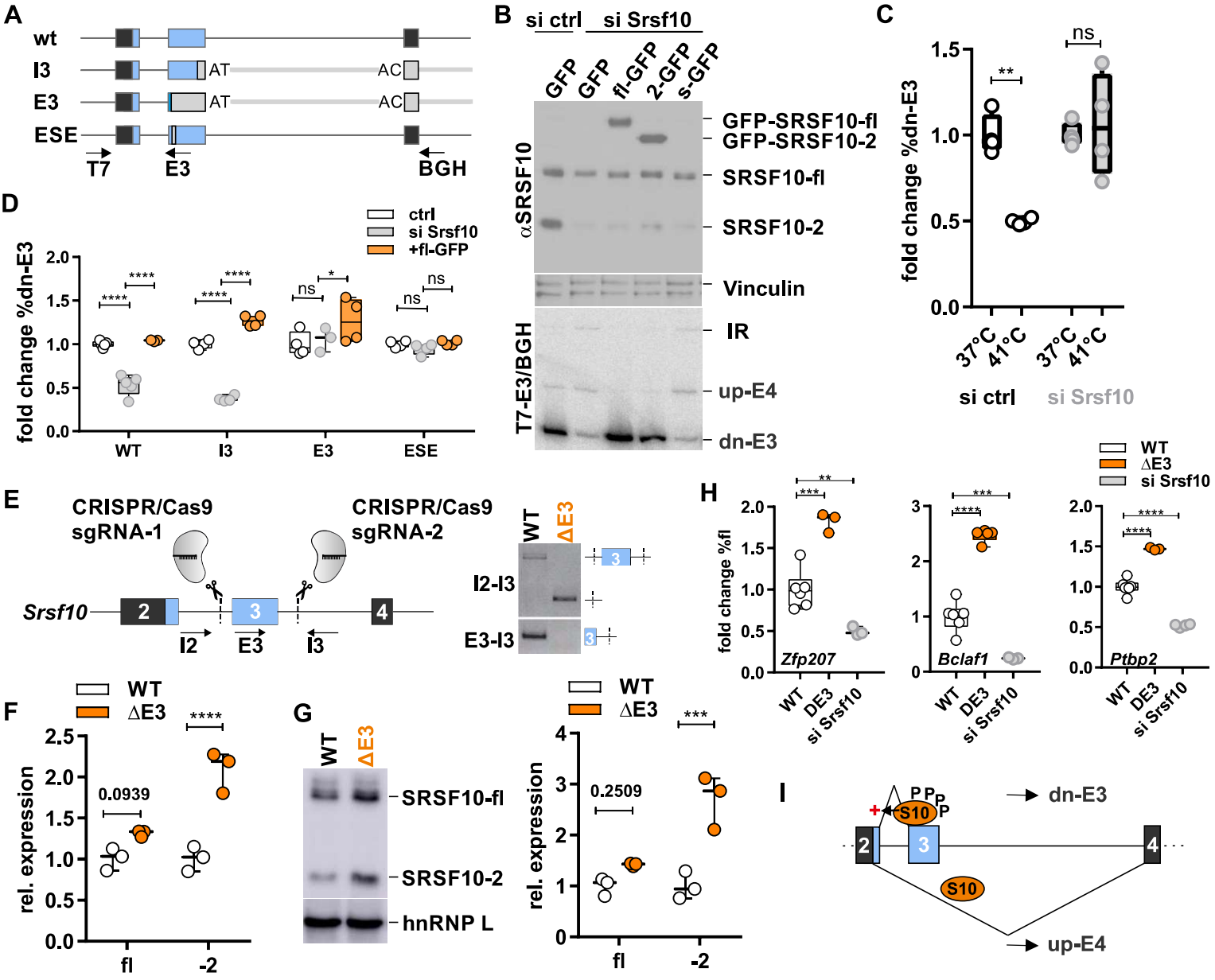
A
wt
I3
E3
ESE
AT
AC
T7
E3
BGH
B
si ctrl
si Srsf10
GFP
GFP
fl-GFP
2-GFP
s-GFP
αSRSF10
GFP-SRSF10-fl
GFP-SRSF10-2
SRSF10-fl
SRSF10-2
Vinculin
T7-E3/BGH
IR
up-E4
dn-E3
C
fold change %dn-E3
ns
**
37°C
41°C
37°C
41°C
si ctrl
si Srsf10
D
ctrl
si Srsf10
+fl-GFP
fold change %dn-E3
WT
I3
E3
ESE
E
CRISPR/Cas9
sgRNA-1
CRISPR/Cas9
sgRNA-2
Srsf10
2
3
4
I2
E3
I3
WT
ΔE3
I2-I3
E3-I3
H
WT
ΔE3
si Srsf10
fold change %fl
Zfp207
Bclaf1
Ptbp2
WT
DE3
si Srsf10
F
WT
ΔE3
rel. expression
0.0939
fl
-2
G
WT
ΔE3
SRSF10-fl
SRSF10-2
hnRNP L
rel. expression
0.2509
fl
-2
I
P
P
P
S10
dn-E3
2
3
4
S10
up-E4

Figure 4

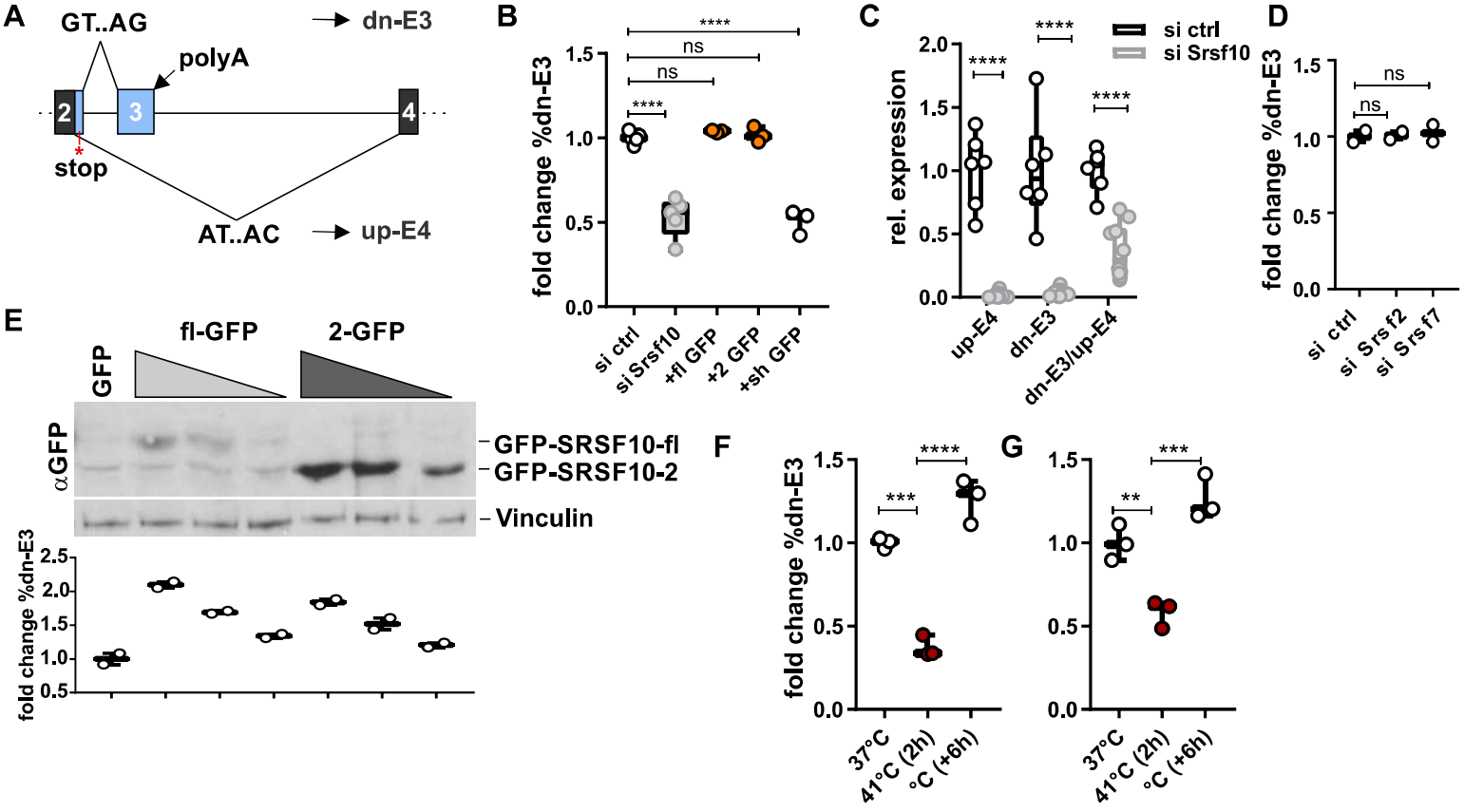
A
GT..AG
dn-E3
polyA
2
3
4
stop
AT..AC
up-E4
B
fold change %dn-E3
****
ns
ns
****
si ctrl
si Srsf10
+fl GFP
+2 GFP
+sh GFP
C
si ctrl
si Srsf10
rel. expression
****
****
****
up-E4
dn-E3
dn-E3/up-E4
D
fold change %dn-E3
ns
ns
si ctrl
si Srsf2
si Srsf7
E
fl-GFP
2-GFP
GFP
αGFP
GFP-SRSF10-fl
GFP-SRSF10-2
Vinculin
fold change %dn-E3
F
fold change %dn-E3
***
****
37°C
41°C (2h)
°C (+6h)
G
**
***
37°C
41°C (2h)
°C (+6h)

Figure S4

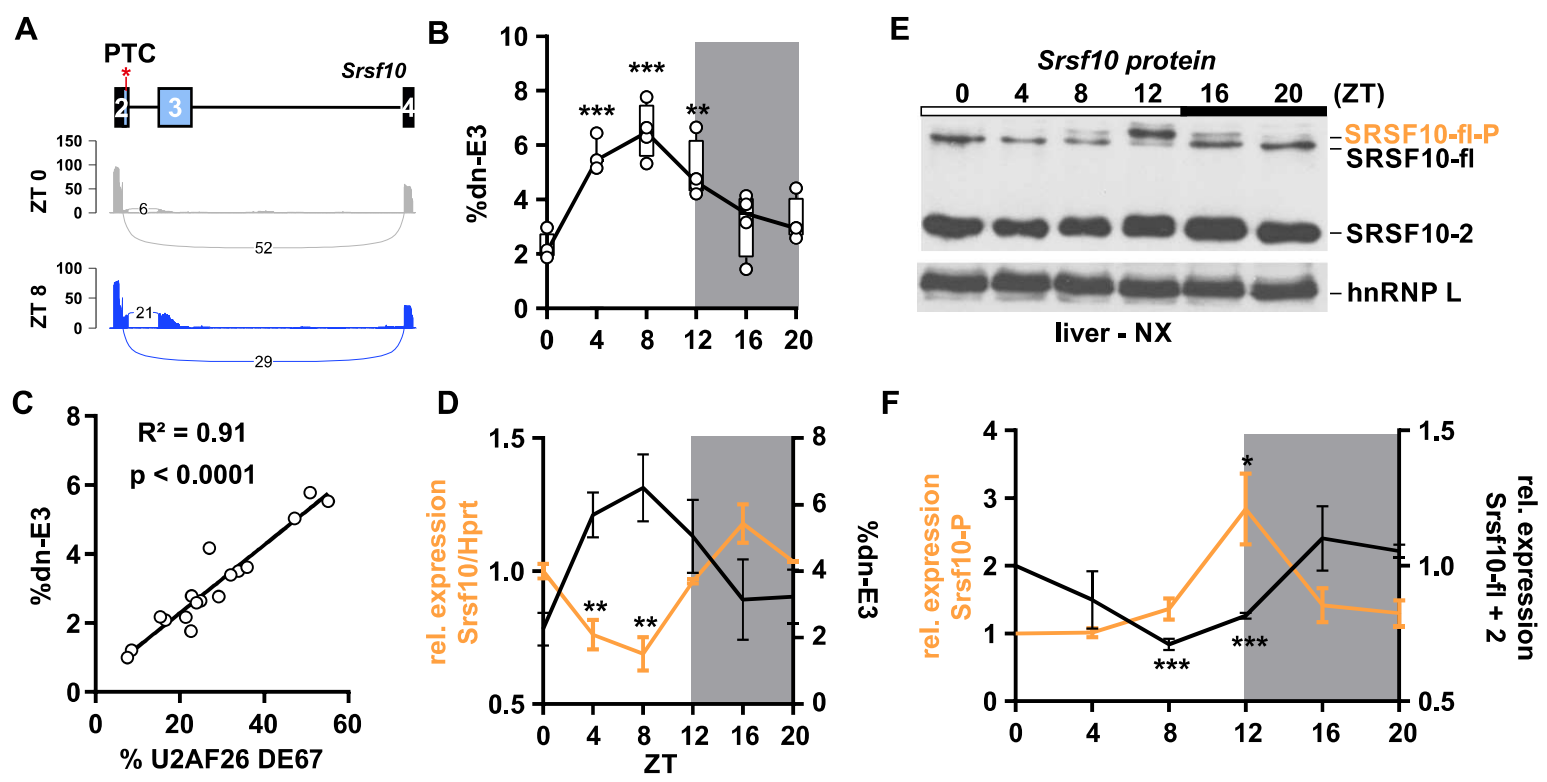
A
PTC
Srsf10
2
3
4
ZT 0
ZT 8
6
52
21
29
B
%dn-E3
***
***
**
ZT
C
R² = 0.91
p < 0.0001
%dn-E3
% U2AF26 DE67
D
rel. expression Srsf10/Hprt
%dn-E3
**
**
ZT
E
Srsf10 protein
0 4 8 12 16 20 (ZT)
SRSF10-fl-P
SRSF10-fl
SRSF10-2
hnRNP L
liver - NX
F
rel. expression Srsf10-P
rel. expression Srsf10-fl + 2
*
***
***

Figure 5

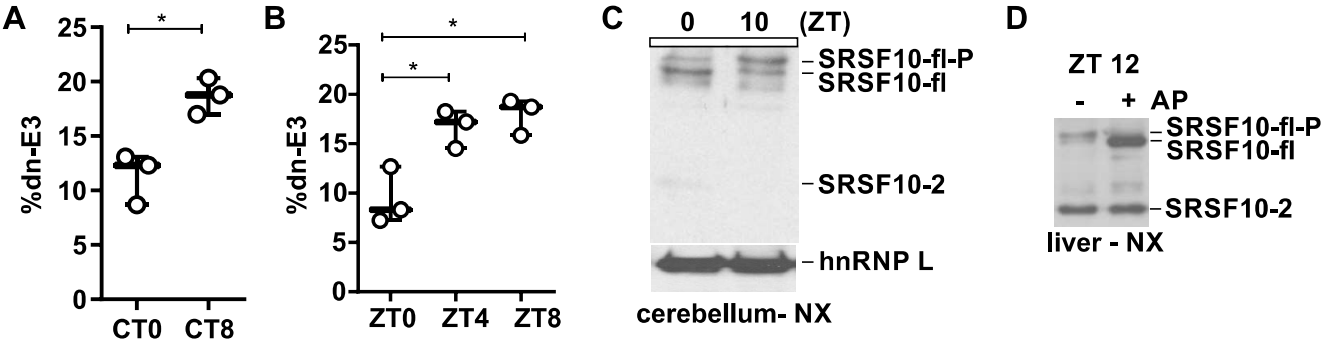
A
%dn-E3
25
20
15
10
5
0
*
CT0
CT8
B
%dn-E3
25
20
15
10
5
0
*
*
ZT0
ZT4
ZT8
C
0
10
(ZT)
SRSF10-fl-P
SRSF10-fl
SRSF10-2
hnRNP L
cerebellum- NX
D
ZT 12
-
+ AP
SRSF10-fl-P
SRSF10-fl
SRSF10-2
liver - NX

Figure S5

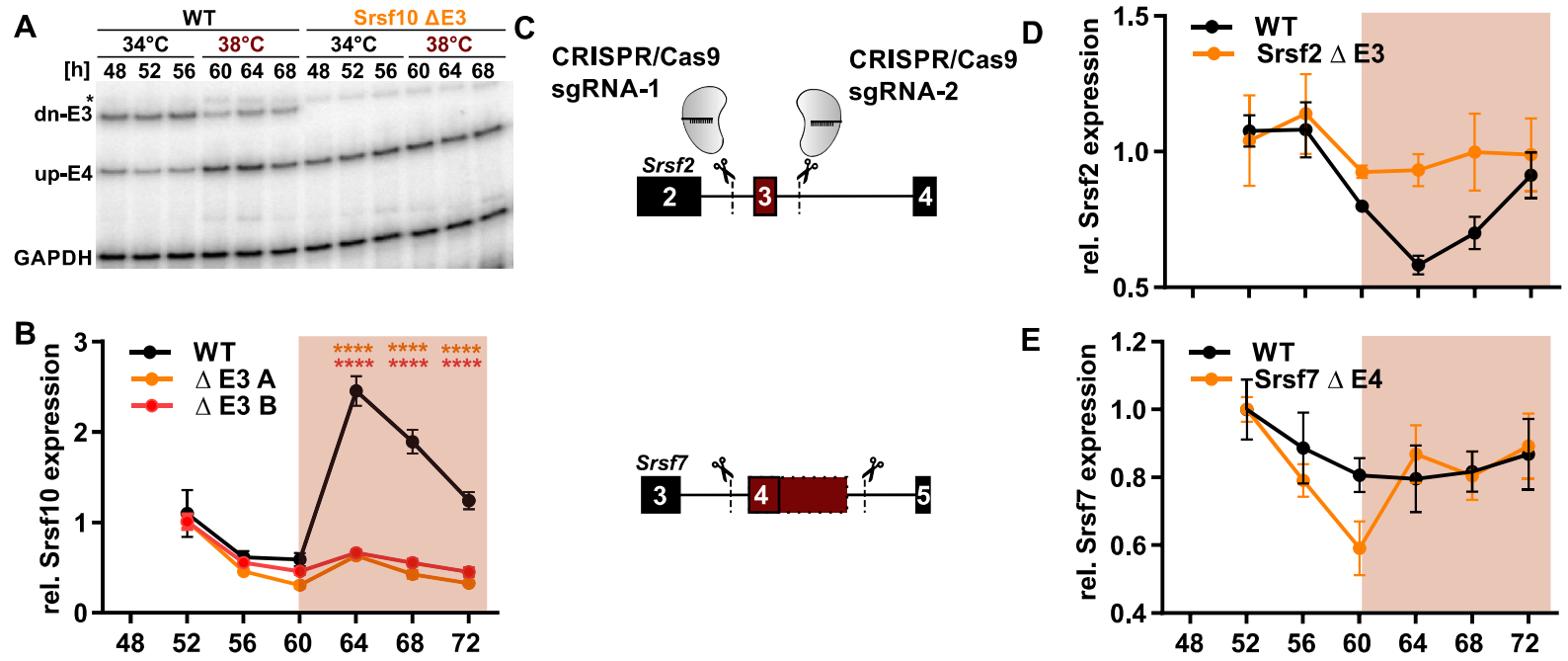
A
WT
Srsf10 ΔE3
34°C
38°C
34°C
38°C
[h] 48 52 56 60 64 68 48 52 56 60 64 68
dn-E3*
up-E4
GAPDH
C
CRISPR/Cas9 sgRNA-1
CRISPR/Cas9 sgRNA-2
Srsf2
2
3
4
D
rel. Srsf2 expression
WT
Srsf2 Δ E3
1.5
1.0
0.5
B
rel. Srsf10 expression
WT
Δ E3 A
Δ E3 B
3
2
1
0
48 52 56 60 64 68 72
Srsf7
3
4
5
E
rel. Srsf7 expression
WT
Srsf7 Δ E4
1.2
1.0
0.8
0.6
0.4
48 52 56 60 64 68 72

Figure 6

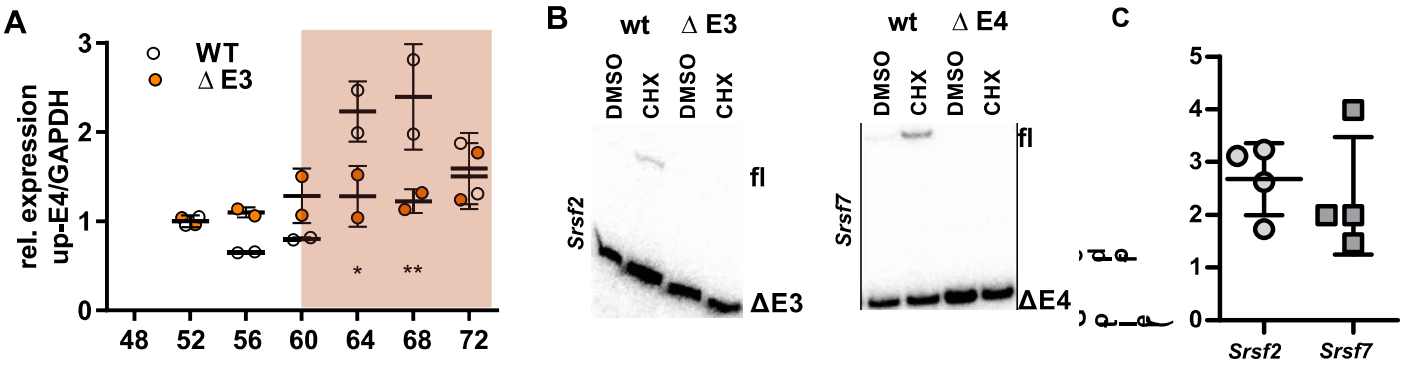
A
rel. expression
up-E4/GAPDH
WT
Δ E3
48
52
56
60
64
68
72
B
wt
Δ E3
DMSO
CHX
DMSO
CHX
Srsf2
fl
ΔE3
wt
Δ E4
DMSO
CHX
DMSO
CHX
Srsf7
fl
ΔE4
C
Srsf2
Srsf7

Figure S6

A

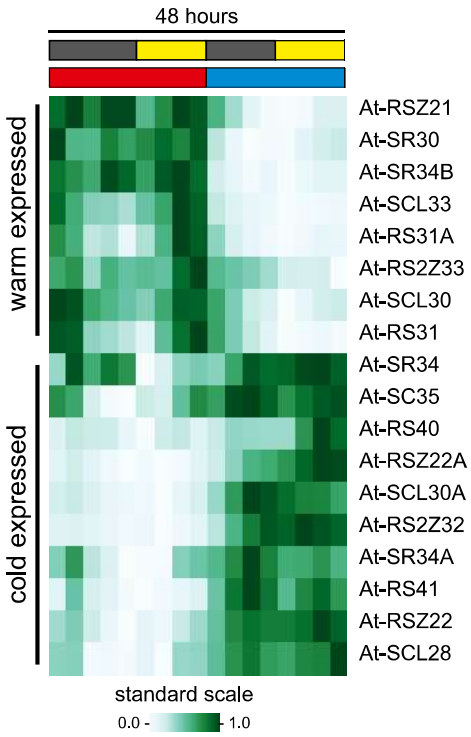

B

subfamily	heat-expressed	cold-expressed
SR	At-SR30, At-SR34b	At-SR34, At-SR34a
RSZ	At-RSZ21	At-RSZ22, At-RSZ22a
SC	At-SC35	-
SCL	At-SCL30, At-SCL33	At-SCL28, At-SCL30a
RS2Z	At-RS2Z33	At-RSZ2Z32
RS	At-RS31a, At-RS31	At-RS40, At-RS41

C

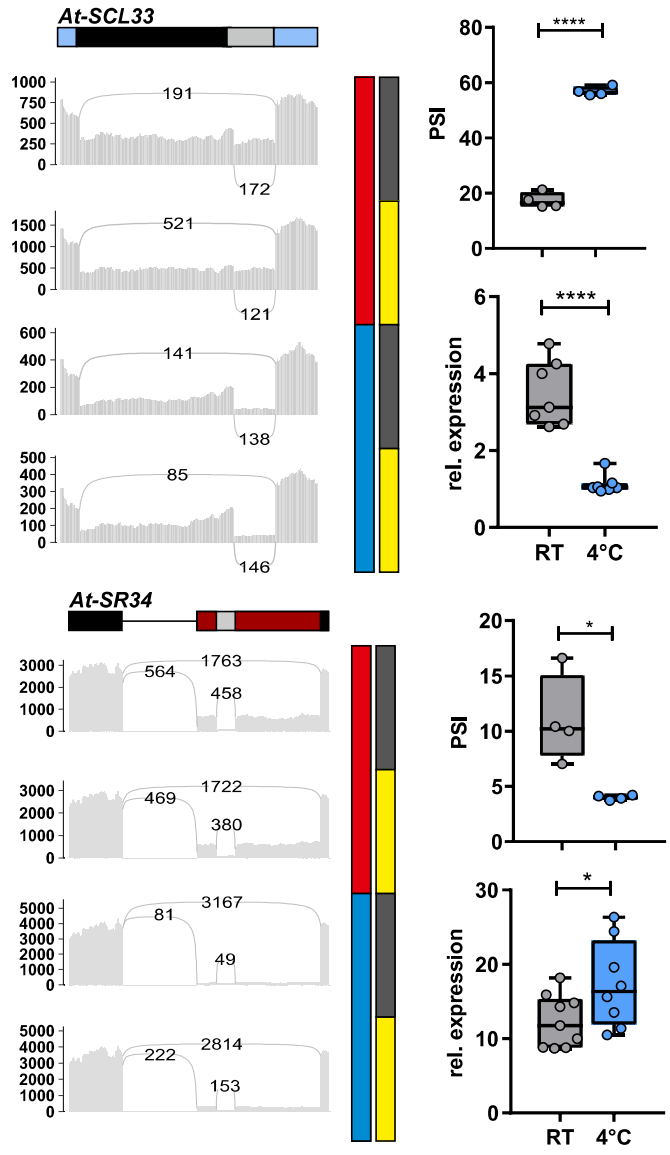

D

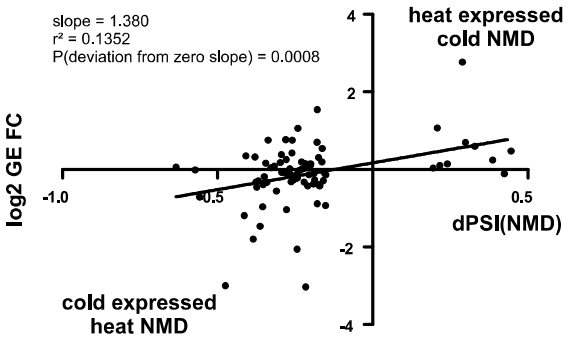

E

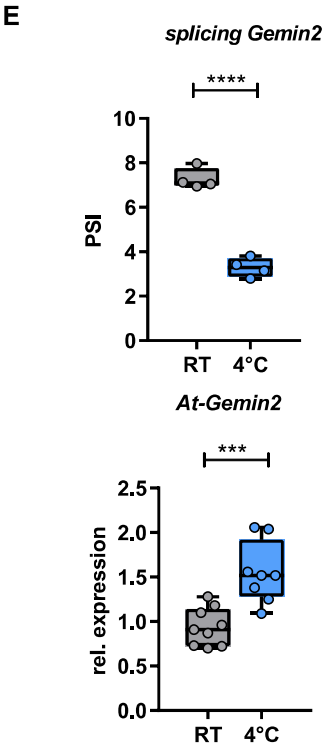

Figure 7

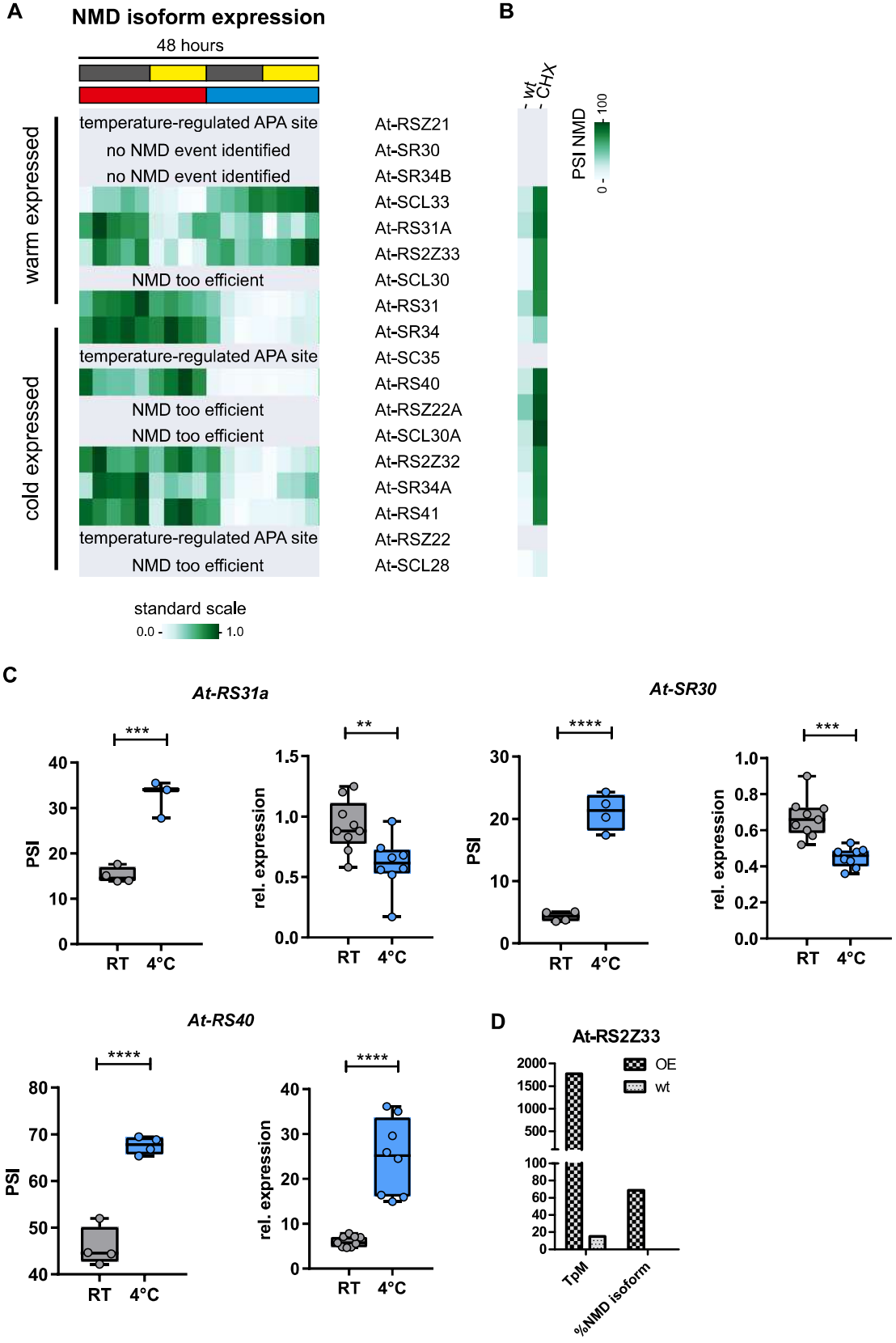
A
NMD isoform expression
48 hours
warm expressed
cold expressed
temperature-regulated APA site
no NMD event identified
no NMD event identified
NMD too efficient
NMD too efficient
temperature-regulated APA site
NMD too efficient
NMD too efficient
NMD too efficient
temperature-regulated APA site
NMD too efficient
At-RSZ21
At-SR30
At-SR34B
At-SCL33
At-RS31A
At-RS2Z33
At-SCL30
At-RS31
At-SR34
At-SC35
At-RS40
At-RSZ22A
At-SCL30A
At-RS2Z32
At-SR34A
At-RS41
At-RSZ22
At-SCL28
standard scale
0.0
1.0
B
wt
CHX
PSI NMD
100
0
C
At-RS31a
At-SR30
At-RS40
PSI
rel. expression
RT
4°C
***
**
****
D
At-RS2Z33
OE
wt
TpM
%NMD isoform

Figure S7